UNIVERSITÉ DE STRASBOURG

ÉCOLE DOCTORALE MATHEMATIQUES, SCIENCES DE L'INFORMATION ET L'INGENIEUR

Laboratoire des sciences de l'ingénieur, de l'informatique et de l'imagerie

THÈSE présentée par :

María Elena VALLE MEDINA

soutenue le : **25 novembre 2019**

pour obtenir le grade de : **Docteur de l'université de Strasbourg**

Discipline/ Spécialité : Génie des Procédés / Traitement des Eaux

---

Modélisation des décanteurs secondaires : Etude en mécanique des fluides numériques de la dynamique de la sédimentation des boues activées.

THÈSE dirigée par :
M. LAURENT Julien   Maître de Conférences, ENGEES

RAPPORTEURS :
M. COCKX Arnaud   Professeur, à l'Institut National de Sciences Appliquées de Toulouse
M. LIPEME KOUYI Gislain   Maître de Conférences, à l'Institut National de Sciences Appliquées de Lyon

---

AUTRES MEMBRES DU JURY :
Mme. CHARPENTIER Isabelle   Directrice de Recherches, CNRS
M. CHIVA Sergio   Professeur, à l'Université Jaume I
Mme. TORFS Elena   Docteure, à l'Université de Gand

Resume

Le procédé conventionnel des boues activées pour le traitement des eaux usées est la technique la plus répandue pour éliminer les polluants des eaux urbaines. Dans ce processus, les bactéries et les eaux usées sont en contact dans un réacteur afin de réduire la quantité de matière organique et d'autres nutriments comme l'azote et le phosphore.

Les clarificateurs secondaires constituent le goulot d'étranglement du processus des boues activées. Ils doivent respecter trois fonctions principales : la séparation boues-eau (clarification), le recyclage des boues activées et le stockage en cas de surcharge hydraulique. Par conséquent, la sédimentation des boues activées dans les clarificateurs régit directement la qualité de l'effluent en termes de matières en suspension (MES) et indirectement dans la biomasse du système (recyclage), affectant ainsi les processus biocinétiques se produisant dans le réacteur biologique (Torfs et al., 2015b).

Les particules de boue activée peuvent avoir différents comportements de décantation, selon leurs propriétés (densité, taille des particules, concentration...). On peut classer les comportements d'établissement dans un clarificateur en quatre mécanismes principaux:

1. Décantation discrète : les particules se déposent à des vitesses individuelles et sans interactions entre elles ; ce régime est limité par le seuil de floculation Mancell-Egala et al., 2016; Mancell-Egala et al., 2017. 2. Zone de floculation : les particules entrent en collision formant des flocs qui se déposent aussi à des vitesses individuelles. 3. Zone de sédimentation : au-dessus d'une certaine concentration de transition (Mancell-Egala et al., 2016; Mancell-Egala et al., 2017; Torfs et al., 2016), les particules sont considérées comme se déposant toutes à la même vitesse selon la concentration locale Kynch, 1952 (Kynch, 1952). Ce régime est limité par la concentration critique (Xcrit). 4. Zone de compression : une fois la concentration critique atteinte, les particules forment un réseau et les boues commencent à s'épaissir en raison de la forte interaction entre les particules. Ce réseau exerce une contrainte solide qui ralentit la vitesse de sédimentation. Néanmoins, des données récentes suggèrent que même pour des concentrations plus élevées, les propriétés individuelles des particules affectent également la vitesse de sédimentation Torfs et al., 2015a.

La modélisation des clarificateurs secondaires est utile pour comprendre le comportement de décantation des boues mais aussi pour la conception des réservoirs, le

dépannage, l'optimisation et le contrôle des procédés. Les approches de modélisation vont des modèles 0D et 1D (Bürger, Ruiz-Baier, and Torres, 2012) aux modèles 2D/3D CFD (Griborio, 2004; Samstag et al., 2016).

Les modèles 1D sont utilisés dans la plupart des logiciels commerciaux pour la simulation à l'échelle des stations d'épuration. Ils permettent par exemple d'évaluer les stratégies opérationnelles de SST et de répondre à la variabilité des débits entrants. Afin de bien comprendre les mécanismes de décantation des boues activées en combinaison avec l'hydrodynamique de la SST, la CFD est également devenue un outil bien accepté. La simulation des SST de boues activées est probablement le domaine d'application le plus développé de la CFD dans les eaux usées. (Samstag et al., 2016).

Ces travaux ont déjà conduit à l'ajout de la compression en tant que terme de second ordre dans l'équation différentielle aux dérivées partielles décrivant la sédimentation de la boue. (Bürger, Diehl, and Nopens, 2011; Plósz et al., 2007; ainsi qu'à l'analyse critique de la fonction de sédimentation de zone qui considère les fonctions puissance plutôt que les fonctions exponentielles (Torfs et al., 2017).

Torfs et al., 2016 ont proposé un modèle 1D unifié pour tous ces régimes de sédimentation. A ce jour, la plupart de ces améliorations n'ont pas été incluses dans les modèles CFD. En effet, la plupart des auteurs qui modélisent les clarificateurs secondaires à l'aide de la CFD, s'appuient encore sur une seule fonction qui relie la vitesse de sédimentation de particules et leur concentration (exprimés habituellement par des fonctions exponentielles) (Lakehal et al., 1999; Griborio, 2004; Flamant et al., 2004; Weiss et al., 2007). La décantation et la floculation discrètes sont généralement modélisées séparément au sein de différents types de décanteurs, par exemple dans les bassins de décantation primaires.

Certaines stations d'épuration fonctionnent souvent avec un débit intermittent, c'est-à-dire : le débit d'entrée est discontinu et il dépend de la période de la journée. C'est souvent le cas pour les petits STEU où le débit d'entrée est contrôlé par une station de pompage fonctionnant avec un contrôle marche/arrêt en fonction du niveau de l'eau dans le réservoir d'entrée. D'ailleurs, la pompe de recirculation fonctionne souvent de manière discontinue : le débit des boues activées de retour est constant mais la pompe ne fonctionne que quelques minutes (5 à 30 minutes) par heure en fonction du débit d'entrée au clarificateur. Ce phénomène est susceptible d'avoir un impact à la fois sur la hauteur du lit de boues et sur l'inventaire des boues dans le bassin de décantation.

Dans un avenir proche, le nombre de petites installations de traitement de l'eau augmentera et s'accompagnera d'une forte demande d'informations sur les technologies et les procédures d'optimisation. Dans les petits STEU, différentes conditions limites sont présentes, par exemple des fluctuations de charge, des problèmes d'exploitation

et de maintenance.... (Boller, 1997). En France, 95% des WRRRF CAS ont une capacité inférieure à 9000 EH, ce qui indique qu'un grand nombre de ces installations fonctionnent avec ces différentes conditions limites.

Le comportement de sédimentation des boues activées est un processus complexe impliquant plusieurs mécanismes (discrètes, zone, compression...) qui est également fortement influencée par l'hydrodynamique du clarificateur. La plupart des modèles CFD envisage l'optimisation de la géométrie et l'impact sur les conditions de l'effluent. Ces modèles incluent évidemment un haut niveau de représentation physique concernant l'hydrodynamique elle-même, le comportement rhéologique des boues, les turbulences, etc. Cependant, en ce qui concerne les modèles de vitesse de sédimentation eux-mêmes, la plupart des modèles publiés dans la littérature ne reposent encore que sur des relations empiriques établies il y a des décennies. À notre avis, la complexité des mécanismes de décantation des boues doit être considérée avec le même niveau de complexité que les autres composantes d'un modèle CFD.

L'objectif du présent travail est donc de développer un code CFD basé sur le cadre de Bürger-Diehl (Bürger, Diehl, and Nopens, 2011) et intégrant la fonction de compression de DeClercq (De Clercq, 2006). Pour réduire le temps de calcul, une approche axisymétrique d'un clarificateur circulaire sera utilisée. Puisque le code de base est basé sur l'approche du mélange pour la modélisation du transport des fluides, nous restons dans cette approche. Comme le suggère Brennan, 2001, le modèle k-epsilon (qui comprend un thérme flottabilité) est employé. Enfin, les résultats des simulations seront comparés aux données expérimentales obtenues directement sur le terrain et utilisées pour l'étude de certains scénarios, y compris les changements des paramètres du modèle et des conditions opérationnelles.

La simulation des clarificateurs secondaires de boues activées est probablement le domaine d'application le plus développé de la CFD dans le traitement des eaux usées (Samstag et al., 2016). Larsen, 1977 ont mené des expériences et ont trouvé un courant de densité (semblable à une chute d'eau) créé par la concentration de la boue. Kahane, Schwarz, and Johnston, 1997 et Kahane, Nguyen, and Schwarz, 2002 ont également modélisé ce phénomène en 3D en utilisant des épaississants industriels. Par conséquent, dans l'entrée des clarificateurs, l'écoulement tend à être en trois dimensions (Brennan, 2001).

Même si l'on considère que les particules se déposent et que le flux entrant est constant et uniforme, des régions à circulation élevée existent et le champ d'écoulement s'écarte de la distribution uniforme idéale (Tamayol, Firoozabadi, and Ashjari, 2010). Au cours de la dernière décennie, des efforts considérables ont été (et sont toujours) entrepris pour améliorer les modèles unidimensionnels.

Les décanteurs secondaires doivent être simulés en considérant les deux phases (solide et liquide). Ceci peut être réalisé à l'aide d'une approche Euler-Euler à deux

fluides comme celle de Kahane, Nguyen, and Schwarz, 2002. Dans cette approche, un ensemble d'équations de continuité et de momentum est résolu pour chaque phase. Ce calcul est intensif car de nombreux paramètres sont impliqués pour décrire les termes d'échange de moment d'inertie interphasique (par exemple, la traînée entre le liquide et les particules...).

Ainsi, la modélisation CFD des décanteurs secondaires est donc généralement réalisée par une approche transport scalaire actif pour décrire la phase dispersée (boues) (Lakehal et al., 1999 ; Griborio, 2004 ; Kim et al., 2005 ; Patziger, 2016). Les équations de continuité et quantité de mouvement de la phase continue sont résolues ; la phase dispersée suit l'écoulement advectif et est ensuite modélisée comme un scalaire. La diffusion, principalement liée à la turbulence, est également prise en compte dans l'équation de transport résultante. Cette approche nécessite un couplage de densité et de viscosité en fonction de la concentration scalaire (Ungarish, 1995).

Une approche moins courante pour modéliser la sédimentation des boues, consiste à utiliser un modèle de mélange dans lequel les phases sont traitées comme une seule phase continue (Wicklein et al., 2015). Un seul ensemble d'équations de continuité et de momentum est résolu pour le mélange. L'introduction du concept de vitesse glissante permet de décrire le mouvement relatif de la phase dispersée. Cette approche est actuellement unique dans les solveurs par défaut de la plate-forme OpenFOAM® de CFD open-source.

Pour considérer la compression dans un modèle CFD, il faut modifier la structure du modèle en y incluant la contrainte solide des boues qui implique une dépendance sur le gradient de concentration. Dans le chapitre 2 de cette thèse, on met en œuvre le modèle de Bürger-Diehl (Bürger, Diehl, and Nopens, 2011), dans un code numérique CFD basé sur l'approche mélange. Donc, la fonction phénoménologique de De Clercq (De Clercq et al., 2008) est utilisée, mais on peut sélectionner une autre expression de manière modulaire. En plus du modèle de Takacs (Takács, Patry, and Nolasco, 1991) et de Vesilind (Vesilind, 1968), l'expression de la loi de puissance de Diehl (Diehl, 2015) a également été ajoutée. Ces développements intègrent les connaissances les plus récentes sur les mécanismes de sédimentation des boues activées qui n'ont jamais été décrites sous leur forme actuelle dans un code CFD.

La simulation 2D d'un clarificateur axisymmetrique a montré que la vitesse de sédimentation est ralentie au-dessus d'une concentration critique lors de l'ajout de la fonction de compression, ce qui conduit à une prédiction plus précise du voile des boues. Une simulation transitoire avec des charges hydrauliques élevées a révélé que la hauteur du voile de boues variait davantage avec la compression. La concentration des boues activées de retour a été plus affectée malgré le fait que ces variations étaient moins importantes par rapport aux modèles 1D. Cependant, ces modèles 1D ne prennent évidemment pas en compte la géométrie du clarificateur (chicanes, recirculation, pente...).

Afin de construire un modèle de sédimentation des boues plus robuste, il est nécessaire de faire une estimation des valeurs des paramètres des fonctions qui décrivent la sédimentation de zone et de compression. Les essais de décantation batch sont la méthode la plus utilisée pour évaluer les vitesses de décantation (Ramin et al., 2014b; Griborio and McCorquodale, 2006. Pour ce faire, un algorithme mathématique fait l'évaluation d'une fonction objective.

Cette fonction mesure les résultats d'une certaine variable du modèle et la compare aux mesures physiques de la même variable. Etant donné que dans le modèle 1D Bürger-Diehl (Bürger, Diehl, and Nopens, 2011), on peut choisir entre différentes fonctions constitutives, le calage devient complexe, car on peut avoir un nombre différent de paramètres selon les fonctions choisies.

Ainsi, différents procédés d'optimisation peuvent être utilisés pour trouver le bon jeu de paramètres. La plupart d'entre eux sont des algorithmes d'optimisation globale. Torfs et al., 2013 ont réalisé une analyse de sensibilité globale (GSA en anglais) en utilisant une méthode de Monte Carlo à force brute pour calibrer 2 modèles de sédimentation de zone et 1 modèle de compression. Ils ont constaté que les paramètres de la fonction de Vesilind (Vesilind, 1968) sont identifiables alors que l'un des paramètres de l'équation de Takacs (Takács, Patry, and Nolasco, 1991) ne peut être identifiable. Ils ont vu que les paramètres de compression (Torfs et al., 2013) ne peuvent pas décrire différentes courbes de sédimentation Batch avec un ensemble unique de paramètres. En résumé, aucun ensemble unique de paramètres ne peut être trouvé pour les équations combinées pour la sédimentation de zone et la sédimentation de compression.

Locatelli, 2015 ont utilisé un outil de différenciation automatique pour modéliser la décantation des boues. Ils ont choisi un couplage Vesilind-DeClercq (les deux équations avec deux paramètres) pour la sédimentation de zone et de compression respectivement dans l'approche Bürger-Diehl (Bürger, Diehl, and Nopens, 2011). Ces quatre paramètres ont un effet important sur la prédiction de la hauteur du voile de boues simulé. Le modèle avec les paramètres calibrés ne peut être précis que dans les trois premières heures de décantation, au-delà de cette période, le SBH est surestimé. Sept jeux de paramètres différents ont été testés et la qualité de l'estimation a été mesurée en comparant visuellement la hauteur du voile des boues simulée et mesurée.

D'autres auteurs ont utilisé un modèle 1D appelé modèle HTC (Hindered, Transient and Compression décantation) (Ramin et al., 2014b), qui calcule le flux de solides dans un domaine de 60 couches horizontales pour représenter le comportement de décantation dans une colonne batch. Selon eux, dans un tel modèle, seuls 3 paramètres sont estimés. La méthode d'optimisation de l'étalonnage global choisie a été la méthode de Monte Carlo à chaîne de Markov (MCMC). Ils n'ont pas signalé

de problèmes d'identification pour les trois paramètres. Néanmoins, la méthode nécessite un grand nombre de simulations, ce qui en fait un outil de calcul intensif.

L'un des avantages de la plate-forme OpenFOAM est que le même solveur peut être utilisé pour effectuer des simulations 3D, 2D-axymétriques, 2D ou même 1D. Par conséquent, le même solveur et les mêmes méthodes numériques peuvent être utilisés pour l'estimation et la validation des paramètres dans une colonne de décompte des lots ainsi que pour la simulation d'un clarificateur réel. Cela rend le processus plus facile et plus fiable.

DAKOTA® (https://dakota.sandia.gov/) est un logiciel open-source (licence GNU LGPL) qui fournit une interface entre les codes de simulation et une variété de méthodes d'itérations pour l'analyse des systèmes, y compris l'optimisation, la quantification de l'incertitude.... DAKOTA® peut donc être couplé à OpenFOAM afin d'effectuer l'identification des paramètres pour le modèle de décantation.

Dans cette étude, une méthode d'optimisation locale a été utilisée puisque le coût de calcul est moindre, d'ailleurs il n'y avait pas suffisamment de points expérimentaux disponibles pour effectuer une analyse globale. Deux séries de données expérimentales ont été choisies en raison des caractéristiques extrêmement variables des boues dans l'installation étudiée. Chacun des ensembles de données expérimentales est modélisé selon une approche différente. Une méthode des moindres-carrés non linéaires est effectuée afin de minimiser la fonction objective. Dans cette méthode, l'équation du modèle est ajustée aux données expérimentales plutôt que de les transformer en une forme linéaire (Sagnella, 1985).

L'estimation consiste à trouver les valeurs optimales pour les paramètres qui peuvent minimiser une fonction de coût ou Quantité d'intérêt. La fonction de coût, souvent décrite comme la somme des erreurs quadratiques entre les données observées et les données simulées, est minimisée par rapport aux différents paramètres du modèle.

La qualité/précision des résultats du modèle est évaluée en introduisant une statistique appelée Nash Sutcliffe Efficiency (NSE). Le NSE peut être décomposée en trois composantes : la corrélation, le biais et la variabilité relative des valeurs simulées et observées pour montrer les problèmes systématiques inhérents à l'étalonnage (Gupta et al., 2009).

Le logiciel DAKOTA a été couplé avec succès à un modèle 1D réalisé en OpenFOAM®. DAKOTA constitue un outil puissant qui peut également être utilisé pour effectuer un processus global d'optimisation, ouvrant une nouvelle opportunité pour les développeurs d'étudier en profondeur les paramètres de compression dans le modèle OpenFOAM.

Les caractéristiques différentes des boues prélevées dans la STEU en différentes saisons a rendu difficile l'obtention d'une relation générale entre la concentration

et la vitesse de sédimentation. Plus la concentration de la boue est élevée, plus la vitesse de sédimentation est faible. La vitesse de sédimentation est fortement influencée par le contenu de matière minérale. Des vitesses de sédimentation plus rapides ont été observées lorsque le contenu de matière minérale est plus élevé. Ce comportement nous a mené à réaliser deux processus de calibrage/validation avec les boues de la STEU d'Achenheim.

Des problèmes d'identification peuvent survenir au sein du modèle, car les valeurs des paramètres optimisés dépendent de la supposition initiale de ces valeurs. En effet, une méthode basée sur le gradient tente de trouver une quantité minimale locale dans la fonction coût.

Cependant, les paramètres estimés ont montré une bonne précision, dont la qualité a été mesurée par le NSE pour les différentes zones de décantation et la courbe de décantation complète. L'utilisation d'une analyse globale n'entrait pas dans le cadre de cette étude. Le processus de calage et de validation a permis d'obtenir une bonne estimation des paramètres du modèle de sédimentation de zone. Toutefois, pour les paramètres du modèle de compression, la validation n'a été acceptable que dans la première heure de décantation, qui est du au fait que le modèle décrit la concentration critique comme une valeur constante dans le temps. Néanmoins, il n'y a pas d'évidence physique qui prouve cette affirmation.

L'état de floculation est un phénomène qui peut expliquer que les paramètres de compression soient en fonction du temps, ceci a été inclus dans un modèle de décantation 1D multi-classe par Torfs et al, 2016. Cependant, la modélisation de la floculation des boues n'entre pas dans le cadre du modèle CFD. Par conséquent, cette première affirmation et le fonctionnement intermittent de la STEU nous incitent à prendre la décision d'utiliser les paramètres estimés des essais de décantation des lots et des simulations 1D présentés ici.

Dans les stations d'épuration à culture libre, les bassins de décantation doivent permettre la séparation des boues et des eaux, le recyclage de la biomasse et le stockage en cas de surcharge hydraulique. La modélisation de ce procédé unitaire est donc essentielle pour obtenir un fonctionnement optimal d'un STEU.

Dans Torfs et al., 2015b, une simulation en flux continu 1D d'un procédé classique à boues activées est réalisée. Elle révèle que l'ajout de la compression comme fonction constitutive améliore la prédiction de la hauteur du voile de boues lorsque des charges hydrauliques élevées sont présentes dans le clarificateur. Cela permet de prédire une concentration de boues de recirculation plus réaliste dans le réacteur biologique.

Pour optimiser la géométrie et le fonctionnement des décanteurs secondaires, la modélisation CFD est d'un grand intérêt car elle permet de capturer l'hydrodynamique dans le clarificateur. Même si l'on considère que les particules se déposent et que le flux entrant est constant et uniforme, il existe des régions à forte circulation ou

l'écoulement n'est pas uniforme (Tamayol, Firoozabadi, and Ashjari, 2010). Certains STEU fonctionnent souvent avec un débit intermittent, c'est-à-dire que les débits d'entrée et de recirculation sont discontinus et dépendent de la période de la journée.

L'un des objectifs de cette étude est d'utiliser le solveur CFD décrit dans (Valle Medina and Laurent, 2020) pour simuler un décanteur à taille réelle en fonctionnement discontinue. Ainsi, la petite STEU d'Achenheim a un débit séquentiel, c'est-à-dire qu'en fonction du débit en amont provenant du réseau unitaire, des capteurs de niveau déclenchent une ou deux pompes pour alimenter les réservoirs.

Par conséquent, ce comportement intermittent peut affecter la prédiction de la hauteur du voile de boues ainsi que la concentration dans la recirculation et la qualité des MES de sortie. Pour cette simulation hydrodynamique, les conditions des campagnes expérimentales d'avril et octobre 2018 sont présentées. Ces campagnes expérimentales avaient pour but de recueillir des données sur la hauteur du voile de boues et la vitesse de sédimentation des particules.

Les simulations avec différentes concentrations de boues et conditions aux limites ont été effectuées pour valider les données obtenues en avril et octobre. Les modèles de turbulence et de viscosité restent les mêmes pour toutes les simulations. Les paramètres du modèle de décantation sont ceux obtenus à l'aide du test de décantation batch.

Les mesures en continu pendant 51 heures ont révélé que le voile de boues à l'intérieur du clarificateur a un comportement dynamique, avec des valeurs de hauteur entre 0,6 et 0,2m. Les mesures ponctuelles, effectuées pendant 20 minutes à différentes distances radiales, ont montré que la sédimentation des particules peut être perturbée par les courants de densité générés par le débit d'entrée. En effet, les particules montent et descendent dans le lit de boues toutes les 30 secondes, même à des distances éloignées de l'entrée.

Dans le cas de l'état stationnaire, nous avons observé que dans la zone externe du clarificateur, des conditions de repos sont créées. En effet, grâce aux profils verticaux de vitesse et de concentration, on obtient un comportement similaire à celui des profils de décantation des lots.

En comparant les vitesses de particules mesurées et les vitesses de convection et de sédimentation verticales simulées, nous avons pu observer que la vitesse de sédimentation des particules est négligeable par rapport à la vitesse verticale convective du fluide. Ainsi, la vitesse de convection du fluide entraîne le mouvement des particules à l'intérieur du voile de boues du clarificateur.

Les simulations CFD ont montré que la dynamique de la hauteur du voile des boues peut être représentée avec précision en mettant les mêmes conditions de fonctionnement du clarificateur de la STEU d'Achenheim. Même s'il y a une réponse plus

tardive dans la prédiction des pics plus élevés du SBH, on peut voir que les hauteurs moyennes simulées du lit de boues sont similaires à celles mesurées.

La teneur en matière minérale des boues activées produit des résultats différents dans la prédiction du voile de boues mesuré et simulé ainsi que dans la concentration de RAS. Avec des concentrations initiales similaires (5,54 kg.m-3 en avril et 4,54 kg.m-3 en octobre), l'épaississement du lit de boues est différent.

En résumé, en utilisant le solveur amélioré décrit dans Valle Medina et Laurent (2020) et les paramètres calibrés, différentes simulations CFD ont été réalisées et ont révélé des résultats satisfaisants dans la prédiction de l'épaisseur du voile de boues et du profil de vitesse des particules.

La CFD est devenue un outil puissant de prédiction, d'optimisation et d'analyse de l'hydrodynamique à l'intérieur d'une STEU. La CFD permet d'obtenir une vue d'ensemble du comportement de décantation, dans laquelle on peut étudier le comportement du fluide à l'intérieur du clarificateur.

Ainsi, différents scénarios sont présentés en modifiant certaines variables du modèle de décantation CFD. D'une part, il s'agit d'évaluer les réponses du modèle aux modifications des paramètres et/ou fonctions du modèle (paramètres de compression, rhéologie). D'autre part, la simulation d'une condition de temps de pluie permet d'évaluer si le modèle peut capturer la dynamique du voile des boues et de la concentration des boues à la recirculation, dans ces conditions.

Une modification dans les paramètres de compression a révélé une prédiction différente dans la hauteur, de voile de boues, dans la distribution des boues à l'intérieur du clarificateur et dans la concentration de la boue de recirculation. Il en a résulté une forte dispersion des boues à l'intérieur de la zone de couverture le long du clarificateur et des prédictions d'une boue peu concentrée. La STEU d'Achenheim peut fonctionner avec des charges hydrauliques élevées sans compromettre la qualité des effluents. Dans le cas d'un événement pluvieux, le modèle CFD a démontré que le clarificateur peut stocker les boues en excès et les épaissir sans trop affecter la qualité de l'eau traitée.

Les propriétés des boues sont une variable importante pour l'accumulation des boues dans le clarificateur. Une teneur élevée en minéraux entraîne une décantation rapide des particules et donc une couche de boues non épaissie avec une concentration élevée de boues au fond. Cela indiquerait que la fonction de compression n'est pas active.

Pour les boues d'Achenheim, le modèle rhéologique-plastique s'adapte mieux pour simuler son hydrodynamique. Les résultats expérimentaux ont montré qu'une surface uniforme du voile de boues peut être trouvée tout le long de l'axe, et que les vitesses de sédimentation sont plus élevées près de l'entrée et non dans le mur externe.

Il a été démontré qu'une boue plastique s'écoule mieux vers la recirculation, ce qui est un comportement attendu dans un clarificateur. Dans ce cas, les vitesses de décantation sont affectées par le type de modèle rhéologique utilisé, le modèle plastique de Bingham prévoit des vitesses de décantation plus faibles que le modèle plastique seul. L'effet de la fonction de compression est presque imperceptible lorsqu'un modèle plastique de Bingham est utilisé, en particulier dans les zones en repos. Les vitesses de sédimentation estimées sont très faibles au fond et dans les zones où il n'y a pas de gradient de concentration verticale. Ces simulations soulignent l'importance du calage et de la validation du modèle CFD appliqué aux décanteurs.

Grâce à cet exercice, nous pouvons remarquer l'importance d'utiliser les modèles de mécanique des fluides numériques comme un outil d'optimisation, prévision et contrôle. En changeant certaines variables, nous avons analysé les conséquences possibles dans la prédiction des boues au niveau de l'enlèvement, de la concentration des boues ou d'un éventuel court-circuit à l'intérieur du réservoir.

Le modèle CFD doit encore être amélioré. Plusieurs études ont montré que la concentration critique n'est pas constante dans le temps. Locatelli (2015) a décrit ce comportement par une équation exponentielle empirique. Toutefois, d'un point de vue physique, la concentration critique ne devrait pas dépendre de la concentration initiale des boues. Ainsi, des essais expérimentaux ont montré que les changements dans l'état de floculation des particules influencent la compression (Torfs et al., 2015b).

L'addition d'une équation pour chaque classe/taille de particules, comme celle décrite dans Torfs et al., 2016, améliorerait la prédiction de la hauteur du voile de boues et, par conséquent, la concentration de la boue de recirculation serait mieux estimée. La prédiction de la qualité de l'effluent serait prise en compte dans les résultats du modèle CFD et donnerait donc une estimation de la performance du clarificateur.

Le débit intermittent des petites STEU, montre qu'elles ont des conditions de fonctionnement très différentes de celles des plus grands (EH > 90 000). En effet, les périodes d'inactivité des pompes d'entrée influencent la recirculation et les performances du clarificateur. Les modélisateurs de CFD SST devraient également examiner ces petites STEU pour tester et améliorer les modèles existants.

Dans ce travail, nous avons couplé le logiciel DAKOTA à OpenFOAM pour l'estimation des paramètres. Cet outil offre des perspectives prometteuses pour de nombreux de domaines, comme par exemple :

- L'utilisation d'algorithmes d'analyse de sensibilité globale et d'estimation pour un processus de calage amélioré dans la décantation batch et la simulation des décanteurs secondaires ;

- L'amélioration de la conception géométrique des bassins. DAKOTA peut être utilisé pour l'optimisation automatique des formes. Plusieurs caractéristiques géométriques peuvent être modifiées afin d'optimiser les performances : taille des chicanes internes, distance des chicanes par rapport à l'entrée, rotation et configuration des racleurs ou encore taille du réservoir. Les possibilités sont illimitées pour optimiser les performances des SST.

Le solveur CFD peut également être amélioré en ajoutant de nouveaux modèles rhéologiques. Actuellement, dans le nouveau solveur, OpenFOAM ne prend en compte que les modèles plastiques et Bingham-Plastic pour décrire la viscosité des boues. D'autres modèles de type Cross, Herschel-Buckley, Carreau, devraient être inclus afin d'étudier également les effets de l'ajout du cisaillement (comportement pseudo-plastique) dans l'hydrodynamique de la boue activée.

Ceci ouvre des perspectives d'utilisation de ce solveur dans d'autres procédés unitaires où les gradients de densité et les propriétés rhéologiques peuvent affecter significativement l'hydrodynamique : comme le réacteur biologique, les digesteurs anaérobies, les procédés d'épaississement des boues, etc...

Abstract

The conventional activated sludge process is the most widely used process for treating urban wastewater. Biomass (activated sludge) grows and forms biological flocs that must be separated from the treated water. This is usually performed by gravity in a clarifier. Activated sludge particles are subject to different settling processes, depending on their properties. Clarifier simulation is probably the most developed field of application for computational fluid dynamics applied to wastewater treatment. However, all sedimentation mechanisms are not always fully represented. This work began by adding the compression mechanism as a second-order term in the partial differential equation describing sludge sedimentation in a CFD approach. The CFD model is based on the mixture approach, which considers that only one set of momentum and continuity equations is solved for the whole mixture. The parameters of the modified model were identified based on experimental data from a closed laboratory system. Model optimization was performed through the coupling of DAKOTA and OpenFOAM open-source softwares. Then, simulations of a full-scale clarifier allowed the model to be validated based on the field measurement of sludge blanket height and particle velocity profiles using acoustic Doppler velocimetry. Small treatment plants are characterized by very dynamic inlet conditions (flow variations, on/off cycles). Thus, the validated model was used to simulate these transient operating conditions.

Acknowledgements

First, I want to thank Arnaud Cockx, Gislain Lipeme, Isabelle Charpentier, Sergio Chiva and Elena Torfs for accepting and validating this thesis. Thanks for your scientific spirit to evaluate these results and to give positive feedback to improve the research.

Je poursuis en remerciant mon encadrant, Julien Laurent, qui a cru en moi pour commencer et finir cette thèse, même quand mes connaissances en CFD étaient inexistantes. Sa patience, sa motivation et son enthousiasme m'ont encouragée à continuer dans cette recherche.

Thanks Julien, to encourage me to participate at different international congresses, where I could meet prominent people, like, Ingmar Nopens, Stephan Diehl, Raymond Bürger, Alonso Griborio... and share our experiences in the clarifiers modeling field.

Encore je remercie Isabelle Charpentier pour partager tes connaissances sur l'optimisation des modèles mathématiques.

Merci à Pierre François pour le temps passé ensemble à faire les mesures dans la STEU et dans la colonne, ainsi que pour le traitement des données.

Merci, Fabrice, Abdel, et Martin pour votre support dans l'élaboration et la mise en place des équipements nécessaires aux expérimentations dans la STEU et aux autres démarches dans le laboratoire.

Je tiens également à remercier Ubertone et l'Eurometropole de Strasbourg pour me permettre d'utiliser leurs appareils sophistiqués et leurs installations qui m'ont permis de valider cette thèse.

A mes collègues du bureau, Adrien, Paul, Teddy, Eloise, Julie, Mamad, Le Ahn, Pulchérie, Milena, Florent, Yannick, Robert, Gilles, Mohammed ... pour tous les exchanges de connaissances et votre support dans le déroulement de cette thèse, ainsi que pour les bons moments passés ensemble.

Merci Marie et Carole pour votre support dans le suivi des protocoles de laboratoire pour mesurer mes échantillons.

xviii

Dedicated to. . .

This thesis is dedicated to my beloved Father, he inspired me to start and finish this project. Maybe your PhD project is finished now through my work. Nineteen years ago you've passed away, but you will be always present in my thoughts and heart.

Contents

List of Figures

List of Tables

Abreviations

CAS Conventional Activated Sludge.

CFD Computational Fluid Dynamics.

CFL Courant-Friedrichs-Lewy condition.

DNS Direct Numerical Simulation.

EPS Exo Polymeric Substances.

ESS Efluent Suspended Solids.

GSA Global Sensitivity Analysis.

HRAS High Rate Activated Sludge.

HRT Hydraulic Retention Time.

HTC Hindered, Transient and Compression settling.

LES Large Eddy Simulation.

LOSS Limit of Stockesian Settling.

MAE Mean Absolute Error.

MBR Membrane Bio Reactor.

MLSS Mixed Liquor Suspended Solids.

NLS Non-Linear Squares.

NSE Nash Sutcliffe Efficiency.

NVSS Non-Volatile Suspended Solids.

PBM Population Balance Model.

PDE Partial Differential Equation.

PRF Pulse Repetition Frequency.

RANS Reynolds Average Navier-Stokes.

RAS Return Activated Sludge.

RSM Reynolds Stress Model.

SBH Sludge Blanket Height.

SRT Sludge Retention Time.

SSE Sum of Squared Errors.

SST Secondary Settling Tanks.

TOF Threshold of Flocculation.

TSS Total Suspended Solids.

VSS Volatile Suspended Solids.

WRRF Wastewater Resource Recovery Facility.

Nomenclature

A_{in} Secondary Settling Tanks (SST) inlet surface area, m^2

A_{rec} Withdrawal section, m^2

$C\text{-}$ Turbulence model constant

D_m Molecular diffusion coefficient, $\text{m}^2\cdot\text{s}^{-1}$

G_k Buoyancy term, $\text{kg}\cdot\text{m}^{-1}\cdot\text{s}^{-2}$

P_{m} Pressure of the mixture, $\text{kg}\cdot\text{m}^{-1}\cdot\text{s}^{-2}$

Q wastewater treatment plant through flow rate, $\text{m}^3\cdot\text{s}^{-1}$

Q_{in} SST inlet flow rate, $\text{m}^3\cdot\text{s}^{-1}$

Q_{in} Clarifier incoming flow, $\text{m}^3\cdot\text{h}^{-1}$

Q_r Recirculation flow, $\text{m}^3\cdot\text{h}^{-1}$

R Recirculation factor, Dimensionless

Sc_t Turbulent Schmidt number, Unitless

T_{u} Turbulence intensity, Dimensionless

X Sludge concentration, $\text{kg}\cdot\text{m}^{-3}$

X_0 Initial Concentration, $\text{Kg}\cdot\text{m}^{-3}$

X_{crit} Critical concentration, $\text{kg}\cdot\text{m}^{-3}$

X_{in} Inlet sludge concentration, $\text{kg}\cdot\text{m}^{-3}$

$\bar{X}$ Diehl concentration parameter, $\text{kg}\cdot\text{m}^{-3}$

$\vec{M}_{\text{m}}$ Surface tension force on the mixture, $\text{kg}\cdot\text{m}^{-2}\cdot\text{s}^{-2}$

$\vec{v}_0$ Maximum settling velocity, $\text{m}\cdot\text{s}^{-1}$

$\vec{v}_{\text{conv}}$ Convective velocity (null when using a batch settling column), $\text{m}\cdot\text{s}^{-1}$

$\vec{v}_{\text{c}}$ Continuous phase (water) velocity, $\text{m}\cdot\text{s}^{-1}$

$\vec{v}_{\text{dj}}$ Drift velocity, $\text{m}\cdot\text{s}^{-1}$

$\vec{v}_{\mathrm{d}}$ Dispersed phase velocity, m·s^{-1}

$\vec{v}_{\mathrm{hse}}$ Experimental hindered settling velocity, m·s^{-1}

$\vec{v}_{\mathrm{hs}}$ Hindered settling velocity, m·s^{-1}

$\vec{v}_{\mathrm{mrec}}$ Mixture Velocity at the withdrawal boundary, m·s^{-1}

$\vec{v}_{\mathrm{m}}$ Mixture center of mass velocity (convective velocity), m·s^{-1}

$\vec{g}$ Gravity acceleration, 9.81 m·s^{-2}

$\vec{k}$ Unit vector, Dimensionless

a_1 Rheological parameter, kg·m^{-1}·s^{-2}

b_1 Rheological parameter, Dimensionless

d_{comp} Compression function, m^2·s^{-2}

d_{disp} Dispersion function to model the effects of turbulence in the inlet, m^2·s^{-2}

k Turbulent kinetic energy, m^2·s^{-2}

l_{u} Turbulence length scale, m

q Diehl exponent parameter, Dimensionless

r_{h} Hindered settling parameter, m^3·kg^{-1}

r_p Parameter for particles velocity within the discrete zone, m^3·Kg^{-1}

t Time, s

z Height, m

Greek letters

α_{c} Continuous phase (water) volume fraction, Dimensionless

α_{d} Dispersed phase (sludge) volume fraction, Dimensionless

δ Dirac delta distribution

ϵ Turbulent kinetic energy dissipation rate, m^2·s^{-3}

Γ Turbulent diffusion coefficient, m^2·s^{-2}

λ Effective solid stress parameter, kg·m^{-1}·s^{-2}

ν_{t} Turbulent viscosity, m^2·s^{-1}

ρ_{c} Continuous phase (water) density, kg·m^{-3}

ρ_{d} Sludge density, kg·m^{-3}

ρ_{m} Mixture density, kg·m^{-3}

σ'_{e} Derivative of effective solid stress, m^2·s^{-2}

σ_{e} Effective solids stress, $\text{kg·m}^{-1}\text{·s}^{-2}$

$\mathcal{T}$ Viscous stress tensor, $\text{kg·m}^{-1}\text{·s}^{-2}$

$\mathcal{T}^{t}$ Turbulent stress tensor, $\text{kg·m}^{-1}\text{·s}^{-2}$

$\mathcal{T}_{\text{Dm}}$ Diffusion stress tensor, $\text{kg·m}^{-1}\text{·s}^{-2}$

τ_{y} Yield stress, $\text{kg·m}^{-1}\text{·s}^{-2}$

Introduction

Conventional Activated Sludge (CAS) technology for wastewater treatment is the most used technique to eliminate pollutants of domestic water. In this process, bacteria and wastewater are in contact (mixture) in a reactor in order to reduce the amount of organic material and other nutrients such as nitrogen and phosphorus. This biomass (activated sludge) grows and forms biological flocs that must be separated from treated water. This is usually performed by means of gravity in a clarifier also called a Secondary Settling Tanks (SST). Settling tanks are the bottle neck of wastewater treatment (Ekama and Marais, 2004) as they must complete three main functions: effluent clarification, sludge storage during peak flows and sludge recycling back to the biological.

As a consequence, activated sludge sedimentation within the SST governs effluent quality directly in terms of Total Suspended Solids (TSS) and indirectly as it will affect the biomass retention within the system (through recycling), thus affecting the biokinetic processes occurring in the biological reactor (Torfs et al., 2015a).

Activated sludge particles can undergo different settling behaviours, depending on their properties (density, particle size, concentration...). One can classify the settling behaviours in a SST into four main mechanisms: *discrete settling, flocculation, hindered settling, compression regime*.

1D models are used in most commercial simulation platforms for wastewater treatment plant-wide simulation. They enable for instance the assessment of SST operational strategies and response to inflow variability. In order to fully understand the mechanisms of activated sludge settling in combination with the hydrodynamics occurring in the SST, Computational Fluid Dynamics (CFD) has also become a well-accepted tool. The simulation of activated sludge SST is probably the most well-developed area of application for CFD in wastewater treatment (Samstag et al., 2016). Larsen (1977) and Ueberl (1995) carried out experiments in SST and found a density current (similar to a waterfall) created by the concentration of the dispersed phase. This was also first modelled in 3D by Kahane, Schwarz, and Johnston (1997) and Kahane, Nguyen, and Schwarz (2002) using industrial thickeners. Hence, in the SST inlet the flow tends to be three-dimensional (Brennan, 2001). To optimize SST geometry and operation, CFD modelling is of great interest as it allows to capture the complex hydrodynamics within the clarifier. Even if it is considered that particles settling and the arriving flow is constant and uniform, regions with high circulation

exist and the flow field deviates from ideal uniform distribution (Tamayol, Firooz-abadi, and Ashjari, 2010).

In the last decade, considerable effort has been (and still is) undertaken concerning one-dimensional models improvement. This work has already led to the addition of compression as a second order term in the underlying partial differential equation (Bürger, Diehl, and Nopens, 2011; Plósz et al., 2007) as well as a critical analysis of hindered settling function that also considers power-law functions instead of exponential ones (Torfs et al., 2017). Torfs et al. (2016) proposed a unified 1D framework for all these settling regimes. Surprisingly, to date, most of these improvements have not been included in CFD models.

Indeed, most authors modelling SST with CFD still rely on a closed-form function of solids concentration to describe settling velocity in both hindered and compression regimes (usually exponential functions) (Lakehal et al., 1999; Griborio, 2004; Flamant et al., 2004; Weiss et al., 2007; Patziger, 2016). Discrete settling and flocculation are usually modeled separately within different kinds of settlers. *e.g.* primary settling tanks.

Some Wastewater Resource Recovery Facilitys (WRRFs) often operate with an intermittent flow, *i.e.* the inlet flow is discontinuous, and it depends on the period of the day. It is often the case for small WRRFs where the inlet flow is controlled by a pumping station operating with on/off control according to the water level in the sump. Furthermore, the recirculation pump often also works discontinuously: the Return Activated Sludge (RAS) flow-rate is constant but the pump operates only several minutes (5 to 30 minutes) per hour according to the inlet and RAS ratio. This phenomenon is likely to impact both sludge blanket height and sludge inventory in the settling tank.

In the near future the number of small water treatment facilities will increase and it will be accompanied by a high demand for information on technologies and optimization procedures. In small WRRFs, different boundary conditions are present e.g. load fluctuations, operations and maintenance problems... (Boller, 1997). In France, 95% of the CAS WRRFs have a capacity of less than 9000 P.E., which indicates that a huge number of such facilities operates with those different boundary conditions.

The objective of this thesis is to implement the Bürger-Diehl framework, (Bürger, Diehl, and Nopens, 2011), which has been assessed in terms of well-posedness and numerical convergence (Bürger et al., 2012), within a CFD numerical code based on the mixture approach. Model parameters identification is performed using DAKOTA. DAKOTA is a Multilevel Parallel Object-Oriented Framework for Design Optimization, Parameter Estimation, Uncertainty Quantification, and Sensitivity Analysis. In this work, it has been coupled with the CFD platform OpenFOAM. Field experimental data monitored on a full-scale clarifier is then used to validate the model.

Thus, this work is divided in 5 chapters :

Chapter 1 makes an introduction of the sludge settling behavior process and the different reported CFD models that simulates this phenomenon. It will highlight the most significant mechanisms and their mathematical description.

Chapter 2 is focused on the development of the new CFD code based on an open-source software called OpenFOAM®. This model includes the mechanism of compression within the sludge settling velocity model. A validation of the model is first performed through the simulation of a batch settling column. Hypothetical CFD case studies simulations are then performed in order to compare the results of the improved model against the model without this extra-term.

In chapter 3, we describe the measurements of sludge blanket height and settling velocities campaigns carried out in a laboratory batch settling column. This information is required to calibrate and validate the code developed in chapter 2. Model parameters are calibrated in OpenFOAM® thanks to an additional toolkit called DAKOTA®. The activated sludge employed for the batch tests was sampled from the Achenheim WRRF located at 13Km from Strasbourg (France), which is the location that was selected for the field measurement campaigns and full-scale SST simulations.

Thus, in chapter 4, a quasi-3D model is tested. By representing, the real geometry of the clarifier, sludge properties and hydraulic loads of the Achenheim WRRF, the validation of the model is done performed on the field using punctual and continuous monitoring of Sludge Blanket Height (SBH) and particles velocities. The calibrated parameters from chapter 3, are used in the quasi-3d model in order to validate the accuracy of model calibration.

Finally, chapter 5 deals with hypothetical CFD case studies (not validation) to assess the impact of different sub-models and parameters involved in the model. Compression and rheological functions/parameters have been investigated be comparing the results of the reference case (from chapter 4) to simulations results with different sets of parameters.

Chapter 1

State of the art

1.1 Description of Conventional Activated Sludge process

Wastewater Resource Recovery Facilities (WRRF) consists of different unit operations in order to recover different matter contained in wastewater: branches, leaves, sand, garbage, clay, suspended solids, alkalinity, oils, organic matter, salts, nutrients, microorganisms, metals, etc.

To eliminate most of these pollutants, one can employ different processes which are divided in three main categories (Tebbutt, 2001):

- *Physical processes.* Those are based in the physical properties of the water and of the targeted substances, i.e. particle size, specific weight, viscosity. . . such as: screening, sedimentation, filtration, membranes, grit removal, oil skimming, dissolved air flotation, activated carbon absorption.

- *Chemical processes.* Related to the chemical properties of added reactants, i.e. flocculation, coagulation, ionic exchange, chemical oxidation, electrochemical oxidation, neutralization, precipitation, etc.

- *Biological processes.* Biochemical reactions to recover soluble or colloid nitrogen and phosphorus, and to stabilize organic matter divided as well in suspended growth processes *e.g.* conventional activated sludge, sequential batch reactors glssbr, high rate activated sludge High Rate Activated Sludge (HRAS), ponds; and fixed growth processes *e.g.* moving bed bioreactors, wetlands, submerged aerobic fixed film (SAFF), percolated biological films; or it can be an hybrid like IFAS (Immersed Fixed Activated Sludge).

WRRF configurations are different. Most of the time, WRRF starts by a pretreatment (screening, grit removal...) to remove big suspended solids, oils and greases that may damage the forthcoming processes. Then, the primary treatment consists most of the times in sedimentation to recover suspended solids and organic carbon e.g. for anaerobic digestion.
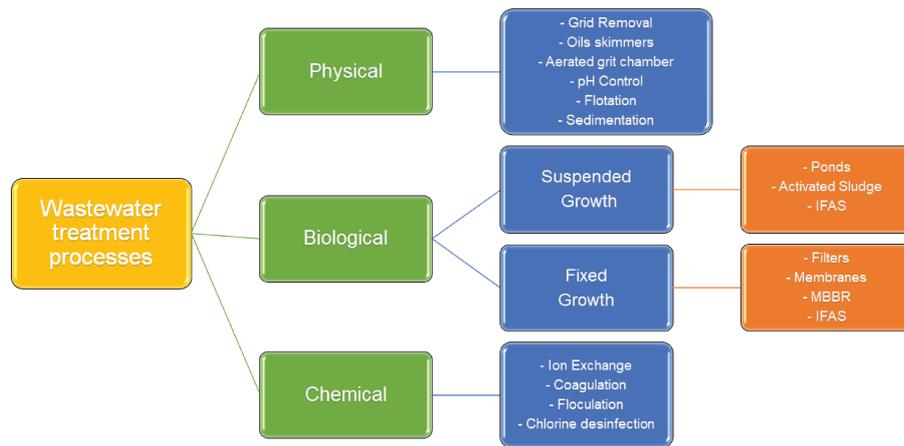
FIGURE 1.1: Different unit operations for wastewater treatment

The secondary treatment is biological. Some WRRF finishes the water treatment at this step, but other includes a tertiary treatment which can be disinfection, micropollutants oxidation or filtration with activated carbon, sand or membranes. A sludge treatment train is included in a WRRF for sludge dewatering before disposal. Optionally, energy recovery through anaerobic digestion is included. A schematic view of this configuration can be seen in figure 1.2.
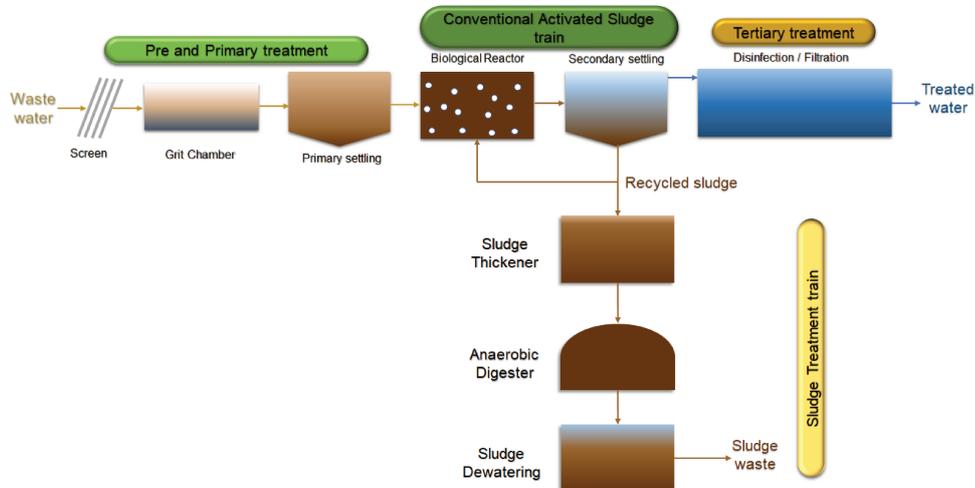
FIGURE 1.2: Configuration of a Wastewater Resource Recovery Facility. Tertiary Treatment is optional in some cases.

Some technologies such as Membrane Bio-Reactor (MBR) offer more advantages in mixture separation, less sludge production, higher solids concentration operation and/or no clarifier tank, (Sari Erkan, Bakaraki Turan, and Engin, 2018); however they are expensive and present fouling problems (Judd and Judd, 2011). Therefore, CAS (Biological Reactor and Secondary settling in figure 1.2) still remains the most widespread technology for biological wastewater treatment.

CAS employees a mixture of polluted water and bacteria, exo-polymeric substances

(EPS) and other microorganisms known as Mixed Liquor Suspended Solids (MLSS). Usually, the biological reactor is aerated to foster biological oxidation to transform organic matter and nitrogen. In the case of biological nutrients removal and enhanced biological phosphorus removal, additional anoxic or anaerobic tanks are also included. While growing, activated sludge microorganisms are colliding and forming flocs. This allows a better separation of MLSS and treated effluent.

After biological reactions are completed, MLSS must be separated from the treated water. Due to the higher density of the MLSS the easiest way to separate them, is by means of gravity. Thus, the mixture is conducted into a SST in quiescent conditions to allow the separation. Even if this technology fails when operated at high Sludge Retention Time (SRT) (> 20 days) and high MLSS concentration (> 12 g/l) (Sari Erkan, Bakaraki Turan, and Engin, 2018); CAS can still offer some advantages e.g. good effluent quality, self-sustaining system, less cost operation and capital, and no fouling issues when compared to a Membrane Bio Reactor (MBR).

Other technologies, based on suspended growth such as HRAS relies on bioflocculation, adsorption and bioaccumulation of organics, its main purpose is to capture the organic matter and to reduce biological oxidation (Jimenez et al., 2015). Thus, this type of processes depends on sludge setteability.

According to (Ekama et al., 1997) secondary clarifiers must fulfill three main functions:

- *Thickener.* Sludge is compressed to increase its concentration and then can be returned to the biological reactor. In the same manner, thickening depends on sludge concentration in the biological reactor. The thickening function limits the capacity of the plant to have a good performance, i.e., if the thickening capacity depends on decreasing the sludge age, then the efficiency of the biological reactor can be reduced. For high sludge concentrations a larger surface area of the clarifier is needed for thickening. Thickening capacity is determined by SST geometry, flow rates, settleability of the sludge and the solids concentration in the biological reactor (De Clercq, 2003).

- *Separation.* The separation efficiency depends on keeping the sludge inside the tank. Generally, 98% of the mass is stored, thickened and returned to the biological reactor (Ekama et al., 1997). Treated water quality not only depend on COD, FSA, $TKN - N$, NO_3^-, NO_2^-, or PO_4^- concentrations but also in TSS concentration in the effluent. Failure to achieve a poor clarification can result in a non-compliance of the regulatory TSS standards, and thus sometimes to total phosphorus and nitrogen standards as these can be included in suspended particles.

- *Storage.* During wet weather conditions (high hydraulic peaks), SST must store sludge without compromising the effluent quality. Sludge within the biological reactor is washed out due to the high flow rates. The mass transfer from

the aeration tank to the clarifier can occur due to an overload of the thickening function and an increase on the recirculation concentration, which requires a longer thickening time, thus long sludge residence time at the clarifier.

If SST failure in one of these functions the effluent can be charged in *BOD*, *COD*, *TSS*, *TN* or *TP* as well it can affect the biological treatment by uncontrolled MLSS and not proper sludge ages.

1.2 Sludge settling theory

1.2.1 Activated Sludge Morphology

Activated sludge or MLSS is a complex heterogeneous mixture of different elements: bacteria, virus, fungi, protozoa, metazoa, ions, minerals, dead cells, Exo Polymeric Substances (EPS), in some cases heavy metals (Tao et al., 2012) with different particle size and pore spaces. The activated sludge biodiversity depends on water temperature (Xu et al., 2018), oxygenation, type and quantity of substrate. The diversity of the activated sludge community also depends on every WRRF, it can be affected by the influent characteristics (domestic or industrial wastewater), as well as the biological treatment units. However, diversity does not compromise water quality, they only exhibit minor metabolic differences (Zhang et al., 2006). Depending on the process conditions bacteria will initiate bioflocculation which leads to the formation of bigger particles called flocs.

Sludge flocs morphology is irregular (not spherical). The adhesion is due to several mechanisms (EPS secretion, cation bridging...). Filamentous bacteria also play significant role as they can strengthen floc structure, acting like a skeleton. However, there shall be a good balance of filamentous bacteria because a proliferation of them can generate an open floc structure (Eikelboom, 2000) and thus hampers the floc settling (bulking).
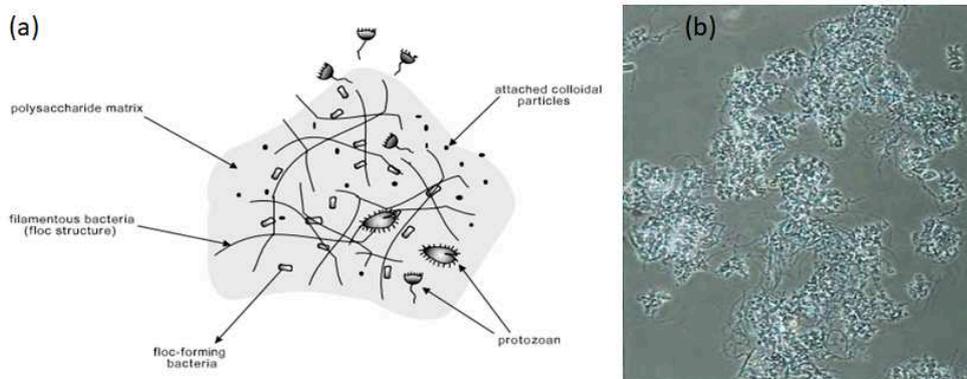
FIGURE 1.3: Illustration of an a) activated sludge floc (Von Sperling, 2007), b) photo of an open floc (150x) (Eikelboom, 2000)

Sludge flocs can be classified in different sizes: small (diameter < 25μm), medium (diameter 25-250μm) and large (diameter > 250 μm). Small flocs with low settling velocities are easily discharged into the effluent, leading to low effluent quality. Aeration can affect floc's size, with diffused air aeration flocs are larger (often > 500μm). Maintaining strong flocs is important to have a good settleability. Strong flocs can be maintained if a lower sludge load is applied. Floc forming decreases if more food is available (Eikelboom, 2000).

1.2.2   Sludge Settling Behavior

The removal of suspended and colloidal solids by gravity is one of the most used processes in Wastewater treatment. Gravity is the driving force to perform sludge-water separation. Thus, accelerated settling is the removal of suspended particles by gravity in accelerated flow field (Tchobanoglous, Burton, and Stensel, 2003).

Due to the complex morphology of activated sludge, particles can undergo different settling behaviors. One can classify such settling behavior into four main mechanisms (Takács, Patry, and Nolasco, 1991; Carlsson, 1998) (figure 1.4):

- **Discrete settling regime (Class I).** This settling regime is normally associated to sand particles, as they settle with individual velocities and with no interactions among them. Once the particles start to collide, they will form bigger flocs. The collision efficiency (two particles sticking together) will determine the floc size and they can be characterized by a Threshold of Flocculation (TOF) value. The TOF is the transition between discrete and flocculant zones (Mancell-Egala et al., 2017).

- **Flocculent settling regime (Class II)**. This regime is characterized by the flocculation of floc particles. Flocs are settling with individual velocities. The velocity of the particles is increasing as they are growing bigger. The transition from flocculent to hindered settling is called the Limit of Stockesian Settling (LOSS), this limit characterizes the floc settling velocity (Mancell-Egala et al., 2017; Mancell-Egala et al., 2016). This limit between the flocculent and the hindered settling can be also known as the transition concentration (Torfs et al., 2016), however within this nomenclature the discrete regime embraces both discrete and flocculent settling.

- **Hindered settling regime (Class III).** Particles are in permanent contact which hinders the settling velocity. Thus, sludge particles are considered to settle all at the same velocity depending on the local concentration (Torfs et al., 2016). In a batch settling column, hindered zone is observed at the interface between water and sludge; this interface is known as sludge blanket height SBH. This regime is limited by the critical concentration (X_{crit}).

- **Compression settling zone (Class IV).** The weight of the particles results in sludge compression. After the critical concentration is reached, the flocs are subjected to a force resulting from the interparticle solids stress. As the solids concentration and compressive force increases, the hydrodynamic force of the flocs decreases (De Clercq, 2006) and thus the settling velocity slows down.

Suspended particles can settle following these regimes which are governed by local concentration and flocculation state (Ekama et al., 1997). This relation can be outlined in figure 1.4.
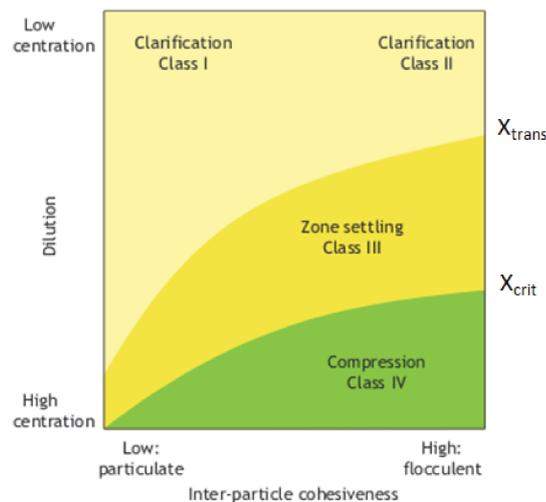
FIGURE 1.4: The relation between concentration and flocculation in the four settling regimes, taken from Ekama et al. (1997)

One of the most common methods to characterize sludge settling properties is performing batch column settling tests: they allow to measure the velocity of discrete particles (Griborio, 2004), the hindered settling velocity (Locatelli, 2015) and/or measuring the concentration profiles (De Clercq, 2006). Those experiments can represent the ideal behavior of sludge settling step by step. However, the different sludge settling regimes in a secondary clarifier occur simultaneously at different locations of the tank.

From the batch settling test, the settling curves (time vs height) are obtained to determine the velocity of the hindered settling. Figure 1.5 shows a settling curve where one can distinguish four phases of the settling behavior: *1) lag phase*, the time in which the turbulent fluid created by filling the column is over; *2) settling zone*, the solids settle with the same velocity and concentration is constant; *3) transition phase*, the concentration increases with the increasing depth and; *4) compression stage*, the sludge at the bottom increases as the transition stage ends, velocity is governed by the compression behavior.

The different settling regimes can also be identified through the concentration and/or velocity profiles, however they are time dependent. In the first moments of sludge
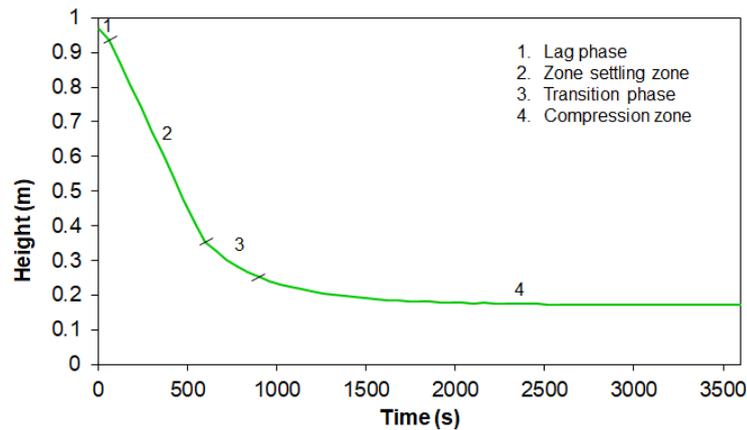
FIGURE 1.5: Settling curve of activated sludge and the phases/zones
presented through time

settling, five zones or layers can be appreciated through the concentration profile
(figure 1.6a) (Locatelli, 2015):

- *Layer 1.* Zone of clear water. No sludge remains or just a few suspended discrete particles are present within this zone.

- *Layer 2.* Flocculation zone. At the top the sludge concentration remains low but this will increase up to the initial concentration at the level of the beginning of the layer 3. The settling velocity is close to the a maximum settling velocity ($\vec{v}_0$).

- *Layer 3.* Hindered zone. The sludge settles with the initial concentration and there is no velocity/concentration gradient.

- *Layer 4.* Within this zone the concentration increases from the initial concentration to the critical concentration. Flocs are not still in permanent contact which allows a sharp concentration gradient. This zone is rarely described within the sludge settling models.

- *Layer 5.* At the top of this layer the sludge reaches the critical concentration. Thus, flocs are in permanent contact and form a matrix that withstand a certain effective solids stress.

After a certain time (it depends on the sludge properties and/or concentration), only two layers can be distinguished: the clear interface and the compressed sludge (Figure 1.6b)

Even if authors still rely only on the hindered settling modelling to describe the complete settling behavior of activated sludge, from the research of Torfs et al., 2013 it is seen that individual properties of the particle also affect settling velocity and thus modelling the four settling regimes is closer to the real behavior.
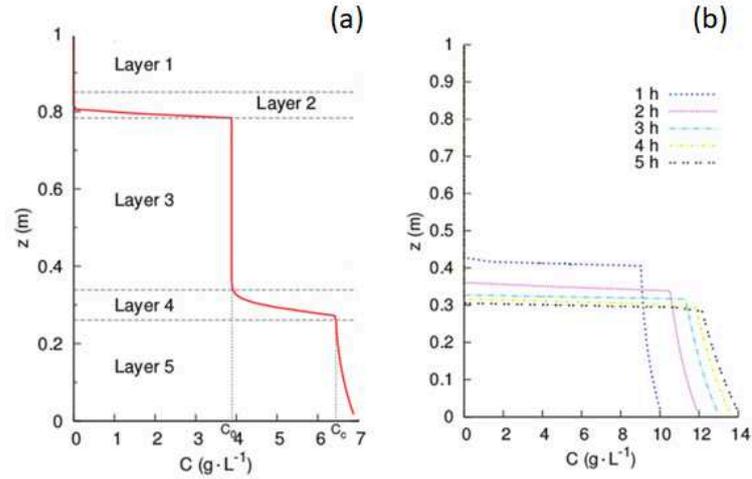
FIGURE 1.6: Simulated profiles in batch column a) at 15 min and b)
after one hour of sedimentation (Locatelli, 2015)

1.3 Mathematical representation of sludge settling

1.3.1 Discrete settling models

The Stokes law is the most used equation to describe the settling for regular particles. It states that the settling velocity of the particle is determined by 3 main forces (figure 1.7):

- gravity;

- lifting force from the liquid;

- friction force between the particle and the liquid and gravity.

This law considers a spherical particle and thus, the settling velocity ($\vec{v}_P$) is determined (in laminar conditions) by equation:

$$\vec{v}_P = \frac{g}{18\mu_l}(\rho_P - \rho_l) \cdot d^2 \tag{1.1}$$

However this law is applicable only for regular particles, within activated sludge irregular particle shapes can be found. Hence, this model approach must consider all particles: size distribution, density, shape... which make it impossible to measure in practice. Some authors have developed techniques such a VICAS (G. Chebbo, 2009) in which the mass and particle distribution can be determined. However, this technique is limited to raw water with low suspended solids.

Furthermore, in activated sludge, sludge particles formation evolves in time due to the flocculation/deflocculation phenomenon, making even more inconvenient the modeling by stokes law.
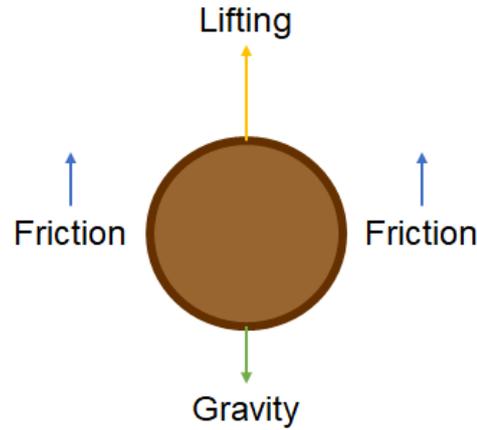
FIGURE 1.7: The different forces acting during the particle settling
Bürger, Diehl, and Nopens, 2011

Clarifiers design is based on the settling velocity. Hazen (1904) introduced the overflow rate concept, which is still useful for settling tanks design. The theory of Hazen states that the Hydraulic Retention Time (HRT) should be equal to the time needed for a particle to settle, *i.e.*, all particles with a higher velocity than the design velocity shall settle. However, this assumption considers that fluid is not turbulent and the settling velocity of the particles is constant, making this approach inadequate for SST modeling.

1.3.2 Sludge Flocculation modeling

Sludge flocculation is inherent to the settling process it takes place prior arriving to the clarifier. In recently research, has been found that flocculation state caused by the make-up of sludge flocs impacts on the dynamics of compression (Torfs et al., 2015b).

Different models exist to describe the flocculation state of sludge particles. The most simple model is proposed by Parker (Parker, Kaufman, and Jenkins, 1972) which stands only for two classes of particles: primary particles and flocs.

The **Parker model** considers that the break-up and aggregation kinetics occurs at the same time. The net rate of change of the number of primary particles (n_p) and flocs (n_f) with respect to time are described by the following equations:

$$\frac{dn_\text{p}}{dt} = K_\text{a} \cdot X \cdot G^\text{m} - K_\text{a} \cdot X \cdot G \tag{1.2}$$

$$\frac{dn_\text{f}}{dt} = -K_\text{b} \cdot X \cdot G^\text{m} - K_\text{b} \cdot X \cdot G \tag{1.3}$$

Where: X is the concentration of suspended particles, G the mixing intensity and m a parameter. The coefficients K_a and K_b represents the aggregation and break-up rate respectively.

Due that such model only considers two classes of particles, a very coarse approximation of the real flocculation behavior is obtained.

Another approach which is more complex and accurate is the **Population Balance Model (PBM)**. It describes the whole dynamic distribution of floc sizes influenced by the aggregation and break-up mechanisms, using different parameters such as: distributed property, number density function, continuous growth and reaction terms. The model has been used extensively in chemical engineering (Ramkrishna, 2000; Marchisio, 2013).

The governing equation in the general form is (Nopens et al., 2015):

$$\frac{\partial f_1(x,t)}{\partial t} + \frac{\partial}{\partial x}\left[\dot{X}(x,t)f_1(x,t)\right] = h(x,t) \tag{1.4}$$

Where x is the distributed property, f1(x,t) is the distribution of the distributed property, $\dot{X}(x,t)$ is the continuous growth term of x and h(x,t) is the PBM reaction term (through discrete events).

Biggs, Lant, and Hounslow (2003) made a new Population Balance Model (PBM) approach to describe the dynamics of the number density (N_i) in different size particles (i); considering that the continuous growth is equal to 0 within a SST. Thus, aggregation and break-up processes give birth and death to flocs of certain size.

$$\frac{dN_i}{dt} = Birth_{aggregation} - Death_{aggregation} + Birth_{breakage} - Death_{breakage} \tag{1.5}$$

Within this approach, the mathematical functions used to describe these parameters, particle collision, efficiency of collisions, breakage rate... are difficult to determine for activated sludge flocculation (Nopens, 2005; Ding, Hounslow, and Biggs, 2006).

A research made by Guo et al. (2009) using a Particle Image Velocity technique, found that the particle diameter led to a higher settling velocity. They used a modified Vesilind equation to correlate the velocity of individual flocs and their size, under turbulent conditions. The turbulence intensity impacts the floc diameter and consequently the settling velocity. However, a study held by Vahedi and Gorczyca (2012) and Vahedi and Gorczyca (2014) determined that flocs with same size may have different mass distribution and therefore different settling velocities.

Anyhow, the flocculation impact on the performance of SST was largely studied by Griborio (2004) and Griborio and McCorquodale (2006). They concluded that a center well feed, supports the hydrodynamics performance rather than the flocculation of sludge. Thus, the CFD models could give a first approach into the floc settling

velocity by representing the flocculation process in a determined location at a given time.

1.3.3 Hindered settling functions

The most studied and still used relations for activated sludge settling are those describing only the hindered settling because they simply link the sludge concentration with the settling velocity. Experimentally, this velocity can be calculated as the slope of the batch sludge settling curve (figure 1.4). An increase in the sludge concentration will cause a slow-down of the settling velocity.

The Vesilind (1968) equation is one of the most common used expressions to relate the sludge concentration (X) and its settling velocity ($\vec{v}_{hs}$):

$$\vec{v}_{hs} = \vec{v}_0 e^{-r_v X} \tag{1.6}$$

Parameter $\vec{v}_0$ represents the theoretical maximum settling velocity for the sludge.

In a more operational way, expressions such as the ones proposed by Härtel and Pöpel (1992) and Koopman and Cadee (1983) relate the Sludge Index Volume (SVI) or Diluted Sludge Index Volume (DSVI) with the parameters of Vesilind equation (2.2). However, SVI and DVSI are not accurate enough to represent the hindered velocity.

An inconvenient of Vesilind equation is the prediction of unrealistic high velocities for low concentration zone, when X tends to 0 then $\vec{v}_{hs}$ tends to $\vec{v}_0$.

To overcome this problem, Takács, Patry, and Nolasco (1991) developed a double exponential function which can capture the velocity in the low concentration zone by limiting the maximum settling velocity to a given value $\vec{v}_{0,max}$. The parameter r_p represents the settling characteristic at low sludge concentrations. However, the value is difficult to identify.

$$\vec{v}_{hs} = max\left(0, min\left(\vec{v}_{0,max}, \vec{v}_0\left(e^{(-r_h \cdot (X-X_{min}))} - e^{(-r_p \cdot (X-X_{min}))}\right)\right)\right) \tag{1.7}$$

When using the Bürger-Diehl framework (section 2.1.1), care must be taken if an exponential function is chosen to describe only the hindered settling. It has been shown that such exponential functions underestimate the thickening behavior resulting in an increasing of the sludge blanket with low sludge concentration at the bottom when they are coupled to a compression function (Torfs et al., 2015b).

Thus, to mitigate this effect and allow a smooth transition between the hindered and compression zones, one can choose a power-law function such as Diehl (2015) (equation 1.8) or Cole (1968) (equation 1.9) relations to couple to a compression term.

$$\vec{v}_{\text{hs}}(X) = \frac{\vec{v}_0}{1 + (X/\bar{X})^q} \tag{1.8}$$

$$\vec{v}_{\text{hs}} = kX^{-n} \tag{1.9}$$

With $\bar{X}$, q, k and n parameters to be calibrated

Equation 1.9 has been evaluated by Cho et al. (1993) and Grijspeerdt, Vanrolleghem, and Verstraete (1995) and found that it yields to higher settling velocities for higher sludge concentrations at the bottom, which is contradictory to batch settling tests. The relation of Cole predicts an infinite settling velocity when sludge concentration is zero. A maximum settling velocity should be imposed to overcome this infinity problem.

Both functions showed to predict lower settling velocities and higher sludge concentrations within the sludge blanket when compared to the exponential equations results.

1.3.4 Compression

In batch settling experimentation, it has been demonstrated that sludge compression is time-dependant (De Clercq et al., 2008; Locatelli, 2015). The compression of the sludge is located just below the discontinuity of the SBH, where the concentration is stabilized again (see figure 1.8). In De Clercq et al. (2008) experimentation, the compression solids concentration was defined to be equal to the concentration where the concentration gradient reaches values below $200\,\text{Kg}\cdot\text{m}^{-3}\cdot\text{m}^{-1}$.

Compression regime begins at the called critical concentration X_{crit} where particles are in a constant contact and form a network which slows down the settling velocity. Accounting for this regime within the settling model is important as compression has a large impact on the prediction of the sludge blanket height and the concentration at the bottom of the tank. Hence its prediction becomes crucial during rainy events in the WRRF.

Härtel and Pöpel (1992), Otterpohl and Freund (1992), and Cacossa and Vaccari (1994) used the Vesilind equation to describe not only the hindered velocity but also the compression regime. They calibrated such models with experimental data obtained in a settling column to simulate a steady-state pilot-scale concentration profiles. None of the models gave good predictions of the behaviour in the clarifier.
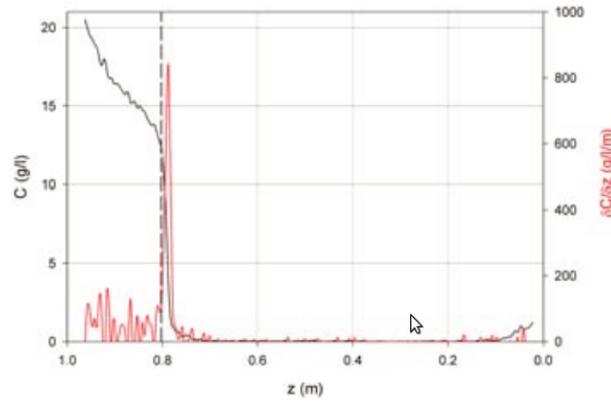
FIGURE 1.8: Concentration profile and its concentration gradient profile, dashed line corresponds to the compression solids concentration location. Source: De Clercq et al. (2008)

Bürger, Wendland, and Concha (2000) developed a phenomenological theory of sedimentation consolidation processes of flocculated suspensions. In such approach the total sludge velocity (v_s) is defined as:

$$\vec{v}_s = \begin{cases} \vec{v}_{hs}(X) & \text{for } 0 \leq X < X_{crit} \\ \vec{v}_{hs}(X) - \frac{d_{comp}}{X}\frac{\partial X}{\partial z} & \text{for } X \geq X_{crit} \end{cases} \qquad (1.10)$$

Where d_{comp} is the compressive term and it can be describe as:

$$d_{comp} = \frac{\rho_s}{(\rho_s - \rho_w)}\vec{v}_{hs}(X)\sigma_e'(X) \qquad (1.11)$$

Where ρ_s is the sludge density, ρ_w is the water density, X the sludge concentration and g the gravity acceleration. The compression regime can be defined as the hindered settling slowed down by d_{comp} above a certain critical concentration X_{crit}

During the compression phase the particles form a network that can carry a certain stress called the *effective solids stress* (σ_e). This stress is an increasing function of the solids concentration higher than X_{crit} (De Clercq et al., 2008; Bürger, Diehl, and Nopens, 2011).

De Clercq et al. (2008) described the effective solids stress (σ_e) with a logarithmic relation that correlates the sludge concentration and the critical concentration:

$$\sigma_e(X) = \begin{cases} 0 & \text{for } 0 \leq X < X_{crit} \\ \lambda ln(\frac{X - X_{crit} + \beta}{\beta}) & \text{for } X \geq X_{crit} \end{cases} \qquad (1.12)$$

A simplified form of this equation is used by Torfs et al. (2015a) to reduce the number of compression parameters to calibrate. Either way, an identification problem was found for both parameters (λ and X_{crit})

$$\sigma_{\mathrm{e}}(X) = \begin{cases} 0 & \text{for } 0 \leq X < X_{\mathrm{crit}} \\ \lambda(X - X_{\mathrm{crit}}) & \text{for } X \geq X_{\mathrm{crit}} \end{cases} \tag{1.13}$$

Ramin et al. (2014a) proposed a new approach to describe settling behavior including the compression regime, the model is known as Hindered, Transient and Compression settling (HTC) model. The derivative of the effective solids stress is described with two parameters (equation 1.14). This formulation avoids the discontinuity in the mathematical formulation and optimize the numerical resolution.

$$\sigma_{\mathrm{e}}'(X) = \begin{cases} 0 & \text{for } X < X_{\mathrm{crit}} \\ \left(\frac{X - X_{\mathrm{c}}}{C_1}\right)^{C_2} & \text{for } X \geq X_{\mathrm{crit}} \end{cases} \tag{1.14}$$

The complete formulation for the HTC model is:

$$\vec{v}_s = \begin{cases} \vec{v}_0 e^{-r_{\mathrm{h}} \cdot X} - \vec{v}_0 e^{-r_{\mathrm{p}} \cdot X} & \text{for } X \leq X_0 \\ \vec{v}_{0,\mathrm{t}} e^{-r_{\mathrm{t}} X} & \text{for } X_0 < X < X_{\mathrm{crit}} \\ \vec{v}_{0,\mathrm{t}} e^{-r_{\mathrm{t}} X} \left(1 - \frac{\rho_{\mathrm{s}}}{(\rho_{\mathrm{s}} - \rho_{\mathrm{w}})gX} \sigma_{\mathrm{e}}'(X)\right) & \text{for } X \geq X_{\mathrm{crit}} \end{cases} \tag{1.15}$$

In the HTC model only three parameters needs to be calibrated (r_{t}, C_1, C_2). X_{crit} has been defined equal to $1.1 * X_0$. However, in a SST setting X_{crit} equal to X_0 is not always accurate since the initial concentration (X_0) is tricky to define. r_{t} is a transient settling parameter. The expression, $\vec{v}_{0,\mathrm{t}} e^{-r_{\mathrm{t}}}$, is added to avoid the discontinuity in the transition from hindered to transient regime.

Flocculation within compression zone   Particle size distribution influences also the formation of the compressive network at the bottom of the SST. Experimental evidence proved that the sludge flocculation state affects the dynamics of the compression zone (Torfs et al., 2016). Flocculation is affected by sludge microbiology, shear stress exposition before settling and local variation within the tank's depth (Torfs et al., 2015b).

It is suggested by the experimentation of Locatelli et al., 2015 that segregation of particles is occurring within the hindered zone resulting in a variation in floc size distribution, so this could explain the variation in the critical concentration at the top of the compression zone

Several authors consider that more experimental research within the compression zone is needed to understand the sludge compressibility phenomena (Li and Stenstrom, 2014; Torfs et al., 2013).

1.4 Description of sedimentation process and flow behavior of a Secondary Settling Tank

1.4.1 Secondary Settling Tanks configuration and performance

The SST or secondary clarifier is always placed after to the biological reactor. The separation is usually performed by gravity in quiescent conditions, however other methods, such as flotation, can be used (Bratby and Marais, 1976). Due to the more stringent effluent requirements the function of the SST shall ensure a good effluent quality and thus, design becomes more restrictive.

The performance of a SST can be affected by 4 factors: 1) hydraulic features (flow pattern and rates), 2) physical features (geometry of the clarifier), 3) weather conditions and, 4) sludge characteristics (rheology, settling behavior, flocculation state).

Flow pattern

Contrary to what is supposed to occur in a batch sludge settling test, the particles settling inside a SST tends to be highly three dimensional, *e.g.* Anderson and Gould (1945) found that sludge flow is not uniform because of the density stratification.

The high sludge density at the inlet creates a density waterfall and consequently the flow runs along the bottom of the tank as a *density current*, which is induced by the sludge settling. The density current is present at high velocities at the vicinity of the SBH (Kinnear and Deines, 2001). Hence, it generates a recirculation flow in the upper part of the tank. Since the sludge concentration is relatively low in this region, the flow at the surface tends to go towards the inlet, see figure 1.10. If the flow field is uniform, the settled sludge will be uniform all over the width of the tank.

In figure 1.9 the density current created inside the settling tank is represented. Near the bottom of the tank the velocity changes from a jetting to a stream shape. This is due to the energy dissipation of the current created by the viscous forces and turbulent mixing.

Van Marle and Kranenburg (1994) pinpointed that density currents maybe beneficial for the sludge settling because they can prevent short circuiting. However, strong density currents can produce no quiescent conditions and the slude particles are re-suspended again.

Larsen (1977) found that the accumulated solids at the bottom of the tank, can form a layer or blanket up to 0.5m with sludge concentrations from 10 to 15 g.L-1. Hence, the non-Newtonian character of the sludge blanket can resist to deformation. In a well-designed tank, the flow field is 2D in character downstream the inlet.
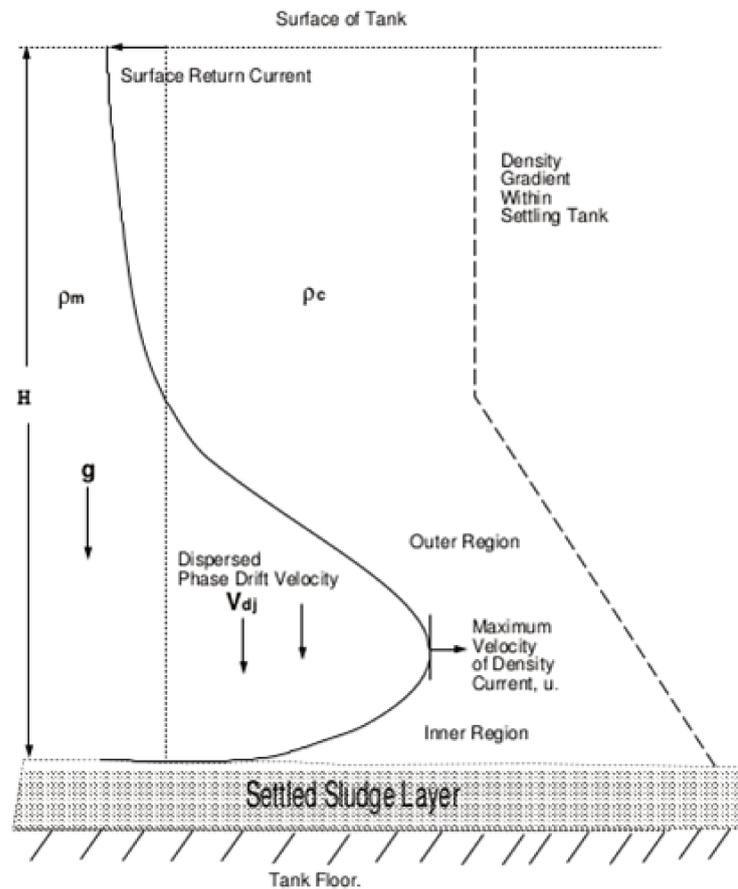
FIGURE 1.9: Density current within a Settling Tank extracted from Brennan, 2001

Physical features

Different SST configurations can be found on the field: circular, rectangular, lamellar or vertical flow known as "Dortmund tanks" (Dahl, 1993).

Vertical tanks are found when the horizontal dimension is smaller than the vertical dimension, thus, the flow is to be assumed predominantly vertical (Ekama et al., 1997). Within this configuration very fine particles can be retained due to SBH acting as a floc filter (Fuchs and Staudinger, 1999).

Lamellar clarifiers are usually used for primary settling. They are horizontal rectangular clarifiers but with added parallel inclined plates or *lamellas* to establish a laminar flow. The plates increase the capacity and velocity of the settling, nevertheless this configuration tends to clog because of the biofouling mechanism.

Circular and rectangular clarifiers are the most wide-spread employed and show the same removal efficiency when they are well designed (Parker, Kinnear, and Wahlberg, 2001). The rectangular clarifier have a length to width ratio that varies from 3:1 to 5:1. The minimum length is set to 3m and the depth varies from 2 to 6 meters (Voutchkov, 2005). Circular clarifiers can be classified into central or peripherical feed. The most common are the central feed (Tchobanoglous, Burton, and Stensel, 2003; De Clercq, 2003). Voutchkov (2005) makes a comparison of the advantages and disadvantages between circular and rectangular clarifiers.

In a circular central feed clarifier, the MLSS coming from the biological reactor, enters through a feed pipe at the center of the tank into a feedwell. The function of the feedwell is to slow-down the fluid's velocity and to create a uniform radial distribution of the flow. Through the clarifier length (diameters varying from 3 to 100 meters (Voutchkov, 2005) water is flowing towards the outlet (located at the opposite end of the inlet) ensuring that the treated water is free from suspended solids. At the surface of the clarifier a scrapper is placed in order to remove the floating sludge particles that are conducted to a spillway or hopper. Then, settled sludge is thickened at the bottom of the tank and a skimmer, in circular motion, is pushing the sludge towards the withdrawal. The sludge can then be pumped back to the biological reactor or to a sludge thickener when it is in excess. In both configurations, the scrapper affects tank hydrodynamics and disturbs sediment layer (Smethurst, 1992).

No matter the geometry of the SST is, the sedimentation shall be carried in quiescent conditions.

Sludge characteristics

Properties and processes such as: concentration, flocculation state, settling and compression phenomena, rheological behaviour and denitrification accelerates/decelerates the settling velocity of the activated sludge and Efluent Suspended Solids (ESS) quality.

According to the Kynch Theory Kynch, 1952 hindered settling velocity depends on the local concentration. Such concentration is measured as MLSS. As the MLSS concentration increases the settling velocity decreases in an exponential manner. However, Locatelli (2015) found that the quantity of Non-Volatile Suspended Solids (NVSS) also govern the settling velocity. The higher the amount of NVSS, higher the settling velocity is.

Activated sludge is considered as a non-newtonian fluid due to the particle-particle interactions. The viscosity of activated sludge is not directly proportional to the applied shear rate but also depends on the MLSS. Indeed the mixture can present
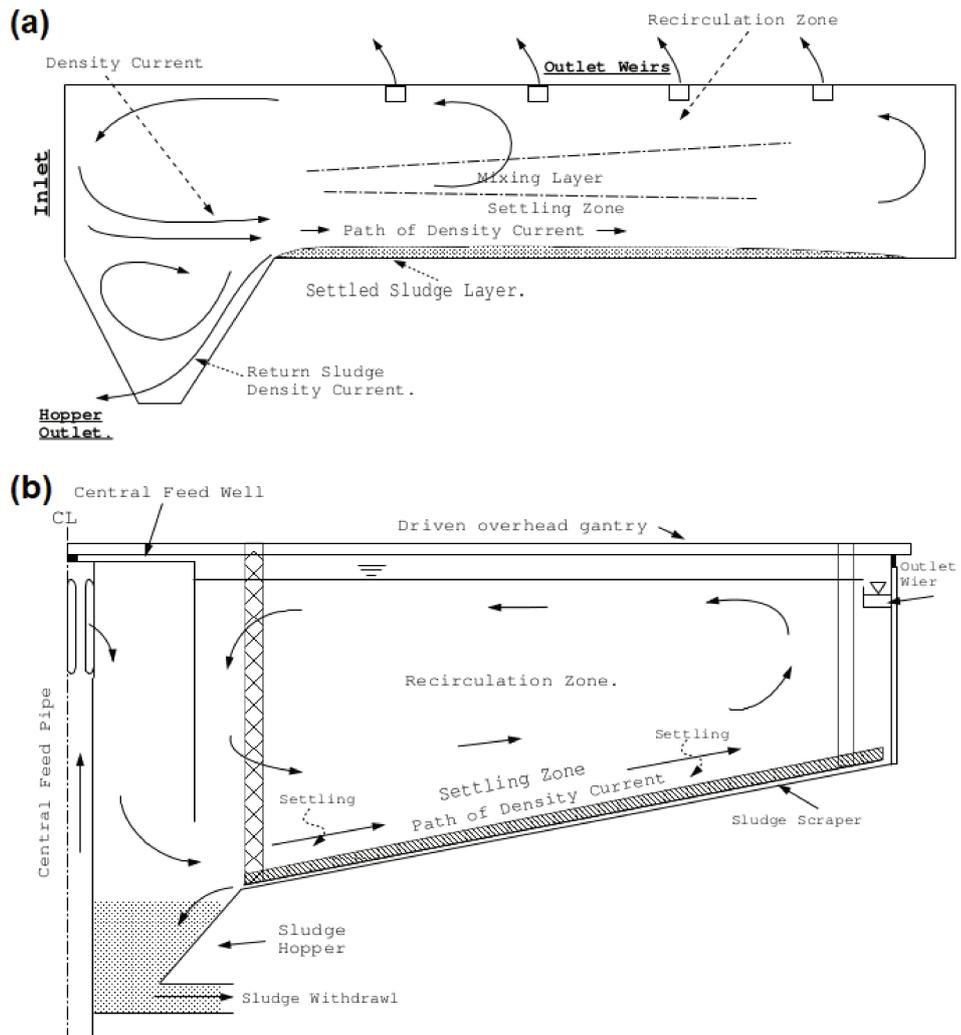
FIGURE 1.10: a) Rectangular and b) Central feed circular, horizontal
flow settling tanks (Brennan, 2001)

different viscosity behaviors: plastic, bingham-plastic, depending on the concentration. According to Ratkovich et al. (2013) every author finds a different approach due to the lack of good modelling practices in rheology measurements.

Sludge rheology properties are inherent to the flow pattern behavior and thus, essential to the mass transfer for WRRF design (*e.g* calculation of pressure losses or recycling pump selection and operation). Activated sludge rheology is used to study particles characteristics: size, shape, degree of hydratation, state of aggregation, rigidity of particles, etc (Dick and Ewing, 1967).

Hence, the high solids concentration within the SBH can lead to different viscosity behaviours at different blanket positions. The higher MLSS concentration the more significant rheological properties and energy consumption (pumping) Ratkovich et al. (2013). Nevertheless, it is generally assumed, that viscoelasticity has little influence on the flow field in the main body of a settling tank (Brennan, 2001).

More details about the sludge rheology modeling can be found in section 1.6.3.

Weather conditions

From a design and operational point of view, water flow pattern (including geometry) and sludge characteristics are the most important factors that impact sludge settling. Thus, most research and models are done in understanding sludge settling behavior or by optimizing and improving SST configurations.

However, weather conditions such as wind and/or temperature gradients also affect the sludge settling. Wells and LaLiberte (1998) indicated that settling velocity is slower when temperature decreases and according to Stokes Law the settling velocity of a particle increases with temperature.

Zhou, McCorquodale, and Godo (1994) observed, through a numerical model, that the flow pattern in a primary clarifier is affected by the warm inflow when discharged to the ambient flow. This is also confirmed by McCorquodale (1976) indicating that short circuiting can occur due to temperature gradients caused by the diurnal variations of wastewater loadings. Short circuiting is presented when the incoming suspended solids stay at the water surface.

An experimental study developed by Taebi-Harandy and Schroeder (2000), stated that the primary cause of density currents (surface and bottom) in SST will depend on the gradient of temperature inside the SST. They also found, that density currents are originated due to the temperature gradient of the inflow to the rest of the tank. Such density currents can be created even when the gradient of temperature is about only 0.2°C

Goula et al. (2008) made a CFD study to analyse the impact of temperature in primary settling tanks when it varies 1°C from the inflow to the tank content. They realized that this difference is enough to produce a temperature-driven density current which causes a non-uniform distribution of solids and therefore, a short-circuiting through the tank. Only with a model representation (not validated), it is observed that a relation exists between influent temperature and sedimentation efficiency.

Few research has been conducted to study the impact of the wind on the sludge settling. Wind shear affects only the water surface producing turbulence near the surface of the SST (Matko et al., 1996) and thus maybe affecting the discrete settling. Most of the times the effect of wind shear is neglected in the settling models, since the minimum required wind velocity capable of rising waves is ranging from 0.4 to $12\,\mathrm{m\cdot s^{-1}}$ (Phillips, 1957).

1.5 1D modeling frameworks

Different models have been developed in order to describe the operation of SSTs. From the simplest ones that only described hindered settling in an empirical way (Vesilind, 1968), to the more complex where all the settling regimes are described (Torfs et al., 2016).

Activated sludge settling can be considered as one-dimensional phenomenon occurring in the vertical direction (z), thus sludge concentration depends on space and time (figure 1.11).
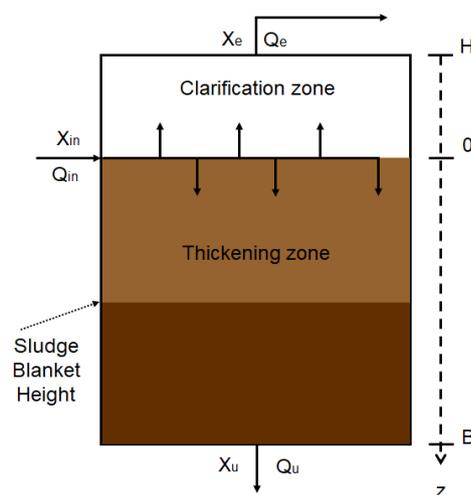
FIGURE 1.11: Overview of an ideal 1D SST. Source: Bürger, Diehl, and Nopens (2011)

The simplest mechanistic model to describe sludge settling behavior is often described in a batch approach, *i.e.*, the flow rate (Q_{in}) and recirculation rate (Q_r) are neglected. The batch modeling approach is based on the conservation of mass and

momentum of the continuous phase (liquid) and dispersed phase (particles). Five different forces interfere for the batch settling motion: gravity (g), buoyancy, liquid pressure, friction and effective solids stress (De Clercq, 2006.)

Considering the Kynch theory for sedimentation (Kynch, 1952), which assumes that the velocity of the dispersed particles is determined only by it is local concentration, equation 1.16 can be expressed in terms of concentration (X), and effective slid stress (σ_e):

$$\frac{\partial X}{\partial t} = -\frac{\partial f_{bk}(X)}{\partial z} + \frac{\partial}{\partial z}\left(\frac{\rho_d}{(\rho_d - \rho_c)Xg}f_{bk}(X)\frac{\partial \sigma_e(X)}{\partial X}\frac{\partial X}{\partial z}\right) \tag{1.16}$$

The Kynch function (f_{bk}) is described as:

$$f_{bk}(X) = \frac{(\rho_d - \rho_c)gX^2(\rho_d^2 - X^2)}{\rho_d^2 r\alpha_d} \tag{1.17}$$

Where ρ_d and ρ_c are the densities of the sludge and the water respectively, r is a resistance coefficient $kg \cdot m^{-3} \cdot s^{-1}$, and α_d is the solids volume fraction

The equation 1.17 is difficult to determine analytically. Thus, it is usually expressed in function of a hindered settling expression or phenomenological function:

$$f_{bk}(X) = X\vec{v}_{hs}(X) \tag{1.18}$$

This model is presented as an unified kinematic process for ideal suspensions (homogeneous small particles and no mass transfer between components) in ideal batch settlers. The model does not describe accurately the flocculation process (Concha and Bustos, 1991), and does not consider the horizontal velocities neither the particles dispersion and the cross-sectional area is established constant (De Clercq, 2003).

To obtain a more robust model for sludge settling behavior, Bürger, Diehl, and Nopens (2011) developed a mechanistic model consisting of a non-linear Partial Differential Equation (PDE). This is a one dimensional, convection-diffusion second order equation in which the solids concentration varies in depth and height (equation 2.1). Chapter 2 also deals with this framework.

One advantage of this model is that one can choose among different phenomenological functions for hindered and compression settling description (*e.g.*, those mentioned in sections 1.3.3 and 1.3.4)

$$\begin{aligned}
\frac{\partial X}{\partial t} = &- \frac{\partial}{\partial z}\left(X\vec{v}_{\mathrm{hs}}(X)\right) \\
&- \frac{\partial}{\partial z}\left(X\vec{v}_{\mathrm{conv}}(z,t)\right) \\
&+ \frac{\partial}{\partial z}\left(d_{\mathrm{comp}}(X)\frac{\partial X}{\partial z}\right) \\
&+ \frac{\partial}{\partial z}\left(d_{\mathrm{disp}}(z,Q_{\mathrm{in}}(t))\frac{\partial X}{\partial z}\right) \\
&+ \frac{Q_{\mathrm{in}}(t)X_{\mathrm{in}}(t)}{A}\delta(z)
\end{aligned} \tag{1.19}$$

The first term stands for the hindered settling velocity. The second term describes the convective velocity of the activated sludge. d_{comp} and d_{disp} are terms modeling the compression settling and the particles dispersion respectively and the last term corresponds to the feed mechanism given by the inflow rate (Q_{in}).

This model has showed to be reliable and that the numerical solution is accurate even when the compression and/or dispersion terms are switched off.

As already discussed in section 1.3, the distribution of different particle classes and their properties (size, porosity, density, shape,...) affects individual particle velocities during discrete settling. It has been proved that the initial particle velocitiy distribution and flocculation affect also the hindered and compression regimes (Torfs et al., 2015b). This behavior is hypothesized to explain the time variable critical concentration that was observed by several authors e.g. Locatelli, 2015.

Within this statement, Torfs et al. (2016) unified all the sludge settling regimes and extended the Bürger, Diehl, and Nopens (2011) framework in an improved particle-distribution framework. Considering different classes of particles, a PDE is defined for each different type of particle.

The distribution of the different particles is considered within the framework. Each class of particle has its own discrete settling velocity ($\vec{v}_0$) and after crossing the transition concentration (X_{trans}) the hindered settling takes part into the settling behavior velocity. Equation 1.20 represents these considerations:

$$\vec{v}_{\mathrm{dhs,i}} = \begin{cases} \vec{v}_{0,\mathrm{i}} & \text{if } \vec{v}_{0,\mathrm{i}} < X_{\mathrm{trans}} \\ \vec{v}_{0,\mathrm{i}}\vec{v}_{\mathrm{hs}}(X - X_{trans}) & \text{if } X \geq X_{\mathrm{trans}} \end{cases} \tag{1.20}$$

The velocity $\vec{v}_{\mathrm{hs}}$ represents any equation to model the hindered settling velocity.

Thus, the solids total flux function (F) for a given class of particle (i) is:

$$F_i\left(X, \frac{\partial X}{\partial z}, X_i, z, t\right) = \left(\vec{v}_{\mathrm{conv}}(z,t) + \vec{v}_{\mathrm{dhs,i}}(X) - \frac{d_{\mathrm{comp,i}}(X)}{X}\frac{\partial X}{\partial z}\right) X_i \tag{1.21}$$

Following this statement, for each class of particle there is one critical concentration. However, the particles converge in a unique critical concentration. Thus, the total critical concentration can be calculated as the weighted sum of all the individual critical concentrations ($X_{\text{crit,i}}$):

$$X_{\text{crit,i}}(X_1....X_n) = \sum_{i=1}^{N} \frac{X_i}{X} X_{\text{crit,i}} \tag{1.22}$$

Even if 1D modeling has shown great improvements to describe the complete sludge settling behavior, those models consider obviously only a one dimensional approach. Recent works on 1D modeling include the simulation of settling in vessels with varying cross-sectional area (cones). This approach can consider different geometries without going into heavy 2D simulation models (Bürger, Careaga, and Diehl, 2017).

Nevertheless, sludge settling is also affected by horizontal flow's patterns, flow field turbulence, solids transportation, solids removal mechanism among others. (Krebs et al., 1996; Ekama et al., 1997).

1.6 Computational Fluid Dynamics modeling

Computational fluid dynamics (CFD) is the numerical analysis of systems involving fluid flow, heat transfer or even chemical reactions. It has become a widely used and successful tool for process analysis in different domains: aerospace, aeronautics, automotive, ocean, chemical and mechanical engineering, power plants, turbomachinery, biomedical engineering, etc. CFD models have become increasingly available with commercial and opensource packages providing graphical user interfaces to assist with model development, operation, and post processing (Wicklein et al., 2015).

Larsen, 1977 was the pioneer in introducing the CFD tool into the wastewater treatment field, by modeling activated sludge sedimentation by solids transport. The use of CFD as transport modeling within wastewater treatment tanks was visualized over 25 years ago (Samstag et al., 2012). CFD being mainly a tool to understand the fluid transportation, it can be associated to biokinetic models too. However, this is currently challenging due to computing and numerical issues (Laurent et al., 2014). Nevertheless, CFD is becoming increasingly popular as design, troubleshooting and optimization tool.

1.6.1 Fluid modelling of multi-phase approach

The strategy of CFD is to replace the continuous domain into a discrete domain by using a mesh/grid. The grid contains smaller sub-volumes called cells or control

volumes. The solution of the fluid problem (temperature, velocity, pressure, mass) is defined in each control volume. Then the governing equations (conservation laws of physics for mass, momentum and heat) are integrated all over the control volumes. Applying numerical methods, the governing equations (equations 1.23, 1.25, 1.26, 1.27) are discretised, *i.e.,* the integral equations are converted into algebraic equations. The resolution of the algebraic equations is made iteratively for each cell.

In continuity (mass conservation) equation 1.23, the first term in the left side ($\frac{\partial \rho}{\partial t}$) is the rate of change in time of the density. The second term represents the flow of mass out of the element across its boundaries, *i.e.,* a convective term.

$$\frac{\partial \rho}{\partial t} + \nabla \cdot (\rho \vec{v}) = 0 \tag{1.23}$$

In the case of an incompressible fluid, density is constant and $\frac{\partial \rho}{\partial t}$ becomes 0. Thus, equation 1.23 is expressed:

$$\nabla \cdot (\vec{v}) = 0 \tag{1.24}$$

The momentum equations (equations 1.25 1.26 and 1.27) are a derivation of Newton's second law. The rate of increase of momentum of fluid particle is equal to the sum of surface (viscous, pressure and gravity) and body (centrifugal, Coriolis, electromagnetic) forces on a fluid particle. The stress of a fluid is defined in terms of pressure (p) and nine viscous stress (τ_{ij}), where i and j indicate that the stress components acting in the j-direction on a surface normal to the i-direction. The terms S_{Mx}, S_{My} and S_{Mz} represents the body forces, *e.g.,* S_{My} is equal to $-\rho g$ when the gravity is considered.

$$\rho \frac{\partial u}{\partial t} = -\frac{\partial p}{\partial x} + \frac{\partial \tau_{xx}}{\partial x} + \frac{\partial \tau_{yx}}{\partial y} + \frac{\partial \tau_{zx}}{\partial z} + S_{Mx} \tag{1.25}$$

$$\rho \frac{\partial v}{\partial t} = -\frac{\partial p}{\partial y} + \frac{\partial \tau_{xy}}{\partial x} + \frac{\partial \tau_{yy}}{\partial y} + \frac{\partial \tau_{zy}}{\partial z} + S_{My} \tag{1.26}$$

$$\rho \frac{\partial w}{\partial t} = -\frac{\partial p}{\partial z} + \frac{\partial \tau_{xz}}{\partial x} + \frac{\partial \tau_{yz}}{\partial y} + \frac{\partial \tau_{zz}}{\partial z} + S_{Mz} \tag{1.27}$$

The heat conservation equation is not included here, since heat transfer is not considered within the scope of this study.

The continuity and momentum equations can be combined with other equations that describe different phenomena such as flocculation, turbulence, particle settling etc. (De Clercq, 2003).

The activated sludge is considered as a multiphase flow, where water is the continuous phase and activated sludge or solids are the dispersed phase. To model sludge flow motion different approaches can be applied, they are listed in the following sections.

Euler-Lagrange model

This approach is mainly used when the dispersed phase has no significant impact on the bulk fluid, *e.g.,* within grit removal processes. Each one of the particles within the fluid is tracked through a flow domain. Thus, the momentum equation for the particle describes the motion of the particle in the continuous medium: it relates the rate of change of the particle's velocity to the sum of forces acting on it.

$$\rho_{\mathrm{d}} \frac{d\vec{v}_{\mathrm{d}}}{dt} = \Sigma F \tag{1.28}$$

where: $\vec{v}_{\mathrm{d}}$ is the particle velocity, ρ_{d} is the particle density and F, the individual forces acting on the particle.

One fundamental consideration in this model is that dispersed phase must have a low volume fraction (maximum 10-12 %) (De Clercq et al., 2005). This approach has been successfully employed to estimate the trapping efficiency of settlers by Isenmann (2016).

Euler + transport model

Considering the sludge concentration as a scalar term, is probably the most common approach for activated sludge settling modeling (Zhou and McCorquodale, 1992; Lakehal et al., 1999; De Clercq, 2003; Griborio, 2004; Xanthos et al., 2011; Samstag et al., 2016).

For this approach the fluid mechanics governing equations are only solved for the continuous phase (*i.e.* water). The sludge mass motion is described by a scalar transport equation (equation 1.29) that uses the computed flow field for the advective term:

$$\frac{\partial X}{\partial t} + \nabla \cdot [(\vec{v} + \vec{v}_{\mathrm{hs}})X] = \nabla \cdot \left(D_{\mathrm{m}} + \frac{\nu_{\mathrm{t}}}{Sc_{\mathrm{t}}} \nabla X \right) \tag{1.29}$$

Where X is the solids concentration, ν_t / Sc_t is the turbulent diffusion (*i.e.* the parameter Sc_t is the turbulent Schmidt number). The settling velocity ($\vec{v}_{hs}$) can be defined with any expression stated on section 1.3.3.

The Schmidt number describes the ratio of momentum transport relative to the transport of molecules (Anderson and Gould, 1945). Its typical value is 0.7 but it

can vary according to the situation (Hreiz et al., 2019). Zhou, McCorquodale, and Vitasovic (1992) proposed a model to represent both the velocity and turbulent viscosity field and the suspended solids transportation to determine the particle concentration field. This model was chosen to define the mass transport according to the Schmidt number. Matko et al. (1996) found that using this model the turbulent mass diffusion is dependent on the localized turbulence or the background fluid.

This approach requires to couple solids transport to momentum and continuity equations. This is performed using specific relations for viscosity (discussed in section 1.6.3) and density coupled between the phases through the following relation (Wicklein and Samstag, 2009; Samstag et al., 2012):

$$\rho = \rho_c + X \left(1 - \frac{\rho_c}{\rho_d}\right) \tag{1.30}$$

If one wants to model the fate of multiple particle properties classes and flocculation, a scalar transport equation should be defined for each particle class.

Euler-Euler model

In this approach, the sludge is considered as a second continuous medium, having similar conservation equations to the continuous phase. Therefore, two sets of Navier-Stokes equation will be solved (equations 1.31 and 1.32) (Brennan, 2001): one set for the sludge particles and the other set for the water. They are solved by introducing the volume fraction and the mechanisms for the exchange of momentum and mass between the phases which make it more complex and computationally demanding.

$$\frac{\partial \alpha_k \rho_k}{\partial t} + \nabla \cdot (\alpha_k \rho_k \vec{v}_k) = 0 \tag{1.31}$$

$$\frac{\partial \alpha_k \rho_k \vec{v}_k}{\partial t} + \nabla \cdot (\alpha_k \rho_k \vec{v}_k \vec{v}_k) = \nabla \cdot (\alpha_k \tau - k) + \alpha_k \rho_k g + (-1)_k F \tag{1.32}$$

Where: α_k is the volume fraction of phase k, $\vec{v}_k$ is the velocity of the phase, τ_k is the stress tensor which includes the pressure and viscous stresses for each phase, g is the gravity acceleration and F is the two-way coupling force per unit volume.

However, this approach requires the input of a particular particle's size or characteristic to solve the drag force, which may be an issue as a wide range of particle diameters are presented within the activated sludge (Wicklein and Samstag, 2009) (Flamant et al., 2004)

Mixture model

Within this approach the activated sludge motion is treated as a whole mixture, instead as two different phases. This approach was first developed by Ishii and Hibiki (1975) and results in the derivation of a single mixture continuity equation and a single mixture momentum equation based on the mixture centre of mass. The distribution of the dispersed phase is modeled by a convection-diffusion equation derived from the continuity equation of the dispersed phase. This approach is extensively described in chapter 2.

1.6.2 Turbulence model

Turbulence is the fluid motion characterized by random three-dimensional vorticity. It usually dominates all phenomena and makes energy dissipation, mixing, heat transfer, and drag go higher. In a SST the turbulence is created at the flow's inlet, along the walls as well as the effect of wind in the water surface (Matko et al., 1996))

Whether the Reynolds number is higher than 10000 the flow is considered turbulent. Between 10000-2100 the flow is in transition and under 2100 flow is considered laminar. Brennan (2001) states that in a SST the flow field is turbulent as the Reynolds number is in the range of 8000-45000.

According to Versteeg and Malalasekera (2007), the turbulence models can be classified in 3 categories: Reynolds Average Navier-Stokes (RANS)-based models, Large Eddy Simulation (LES) models and Direct Numerical Simulation (DNS).

RANS models

These models deal with the mean flow and turbulence effects on mean flow properties. The governing equations are time averaged or Reynolds averaged. Extra terms are included to describe the interactions between various turbulent fluctuations. Those terms are modelled with two-parameters equations (e.g. k-ϵ model) or the Reynolds Stress Model (RSM).

The RANS models predicts the Reynolds stresses and the scalar transport terms. They are classified on the number of additional transport equations to be solved:

- **Zero:** Mixing length model

- **One:** Spalart-Allmaras model

- **Two:** $(k - \epsilon)$; $(k - \omega)$ and Algebraic stress models

- **Seven:** RSM

The RSM models can describe more accurately the Reynolds stresses than the models with two-equations. However, they are computationally demanding due they solve one PDE per each one of the six independent Reynolds stresses.

Here, only the $(k - \epsilon)$ model is described since it is the approach used in the CFD simulations. However, information about the other RANS models can be found in general CFD literature or in Versteeg and Malalasekera (2007) book.

The $k - \epsilon$ model. This model is proper for fluids where convection and diffusion cause significant differences between production/destruction of turbulence (*e.g.* re-circulation flows). The model is focused on the mechanisms that affects the turbulent kinetic energy (k).

The $k - \epsilon$ model employs the following transport equations:

$$\frac{\partial(\rho k)}{\partial t} + \nabla \cdot (\rho k \vec{v}_= \nabla \cdot \left[\frac{\nu_t}{\sigma_k} \nabla k \right] + 2\nu_t S_{ij}.S_{ij} - \rho \epsilon \tag{1.33}$$

$$\frac{\partial(\rho \epsilon)}{\partial t} + \nabla \cdot (\rho \epsilon \vec{v}) = \nabla \cdot \left[\frac{\nu_c t}{\sigma_\epsilon} \nabla \epsilon \right] + C_{1\epsilon} \frac{\epsilon}{k} 2\nu_t S_{ij}.S_{ij} - C_{2\epsilon} \rho \frac{\epsilon^2}{k} \tag{1.34}$$

Where: ν_t is the eddy viscosity, S_{ij} the rate of deformation. The eddy viscosity can be defined as follows:

$$\nu_t = \rho C \text{-} \frac{k^2}{\epsilon} \tag{1.35}$$

The dimensionless values for the constants in the model are:

$C\text{-} = 0.09$; $\sigma_k = 1.00$; $\sigma_\epsilon = 1.30$; $C_{1\epsilon} = 1.44$; $C_{2\epsilon} = 1.92$.

Within this formulation, ϵ increases rapidly as k increases rapidly, and it decreases quickly to avoid negative values of k. One assumption within this model is that the eddy viscosity (ν_t) is isotropic, *i.e.*, the same viscosity for all Reynolds Stress.

The CFD model of Das et al. (2016) used a realizable $k - \epsilon$ to simulate a 3D industrial clarifier. Such model, considers a different transport equation for the dissipation rate based on the mean-square vorticity fluctuation. They found that the realizable $k - \epsilon$ model gives a much more accurate prediction of turbulence for rotating flows than the standard $k - \epsilon$ model.

Buoyancy $k - \epsilon$ model. In multiphase flows, the $k - \epsilon$ model can be extended to take into account buoyancy effects. Buoyancy is an exchange between the potential energy of the flow and the turbulent kinetic energy. The presence of a dispersed phase produce modifications in the structure of turbulence. This term can be added

to a $k - \epsilon$ model to represent its effects. A study made by Brennan (2001) showed that adding the buoyancy modification term produced changes in the generation and distribution of the turbulent viscosity, modifying the flow field and improving the accuracy of the simulations.

The buoyancy effect is represented by G_k and has the following form:

$$G_k = g \frac{\nu_t}{\rho \sigma_k} \frac{\partial \rho}{\partial x_i}$$ (1.36)

Thus, the modified $k - \epsilon$ equations including the buoyancy term, are equation 1.37 for turbulent kinetic energy and equation 1.38 for dissipation rate

$$\frac{\partial (\rho k)}{\partial t} + \nabla \cdot (\rho k \vec{v}) = \nabla \cdot \left[\frac{\nu_t}{\sigma_k} \nabla k \right] + 2 \nu_t S_{ij}.S_{ij} + G_k - \rho \epsilon$$ (1.37)

$$\frac{\partial (\rho \epsilon)}{\partial t} + \nabla \cdot (\rho \epsilon \vec{v}) = \nabla \cdot \left[\frac{\nu_t}{\sigma_\epsilon} \nabla \epsilon \right] + C_{1\epsilon} \frac{\epsilon}{k} \left(2 \nu_t S_{ij}.S_{ij} + G_k - C_{3\epsilon} G_k \right) - C_{2\epsilon} \rho \frac{\epsilon^2}{k}$$ (1.38)

Lakehal et al. (1999) stated that the density current dissipates more rapidly and turbulent diffusivity increases when $C_{3\epsilon} = 0$. The values of the constants are the same of those presented in the previous section.

Large Eddy Simulation and Direct Numerical Simulation models

The LES uses a spatial filer to separate the large and small eddies. LES is designed to model eddy motion or strong shear which is prominent in the situation. Unlike RANS turbulence models, the large eddy motion (containing turbulent energy) is computed directly and in small scale. LES is the most viable numerical tool for simulating realistic turbulent/transitional flows (Zhiyin, 2015). Nevertheless, LES approach has not yet reach a good level of maturity (Zhiyin, 2015) so users with no experience could not take advantage of it and could not interpret properly results of the model. Al-Sammarraee and Chan (2009) used a LES turbulence model for a rectangular SST that accurately solved the small-scale flow patterns around the particles.

The DNS models calculates the mean flow and all the turbulent fluctuations. The governing equations are solved in very fine grids to solve the Kolmogorov length scales, with very small time steps to solve the periods of fast fluctuations. Thus, they are not used for industrial flow applications.

However, most CFD users are satisfied with information about the time-averaged properties of the flow (*e.g.*, mean velocity) (Versteeg and Malalasekera, 2007). Hence,

SST modelers (Lakehal et al., 1999; Brennan, 2001; Matko et al., 1996; Flamant et al., 2004; Kim et al., 2005; Goula et al., 2008...) still rely on the use of $k - \epsilon$ model for clarifiers simulations. One of the advantages of the well established $(k - \epsilon)$ is that only the initial boundary conditions are needed.

Since a deep analysis of the turbulence modeling in activated sludge is not in the scope of this work, the approach suggested by Brennan, 2001 considering the buoyancy term, will be used for our simulations.

1.6.3 Sludge rheology modeling

The viscosity of the activated sludge affects the interaction with the continuous phase (water) and the flow behaviour. Thus, it is important to consider a term of viscosity in the governing equations. This viscosity (μ) is defined as the ratio between the shear stress (τ) and the shear rate ($\dot{\gamma}$). Equation 1.39 describes the viscosity of a Newtonian fluid.

$$\mu = \frac{\tau}{\dot{\gamma}} \tag{1.39}$$

Sludge viscosity can be measured with a rheometer and thus, obtain the shear rate and shear stress of the fluid. Such relation can be represented in a rheogram (figure 1.12) and different behaviors can be observed. For example, a Newtonian fluid, like water, has a constant viscosity no matter the amount of shear rate is applied. In a non-Newtonian fluid (*e.g.* viscoplastic), the apparent viscosity depends on the shear rate.

However, activated sludge rarely exhibit a Newtonian Fluid behaviour. According to Dick and Ewing (1967), the laboratory sludge presents more a newtonian behaviour. This is not the case with the activated sludge from WRRF which are found to be more plastic, and show a yield strength that varies exponentially with the concentration.

Relations for shear rate vs. shear stress relationship

There exist different models describing the sludge rheological behaviour. All of them predict the viscosity with different degrees of complexity (number of parameters) and they are purely empirical. Table 1.1 shows the different Non-Newtonian relationships, where: τ_0 is the yield stress (Pa), n the flow behaviour index (-), k the flow consistency index (Pa s), μ_∞ the infinite rate apparent viscosity (Pa s), μ_0 the zero shear apparent viscosity (Pa s), λ a time constant (s), and m a rate constant (dimensionless)
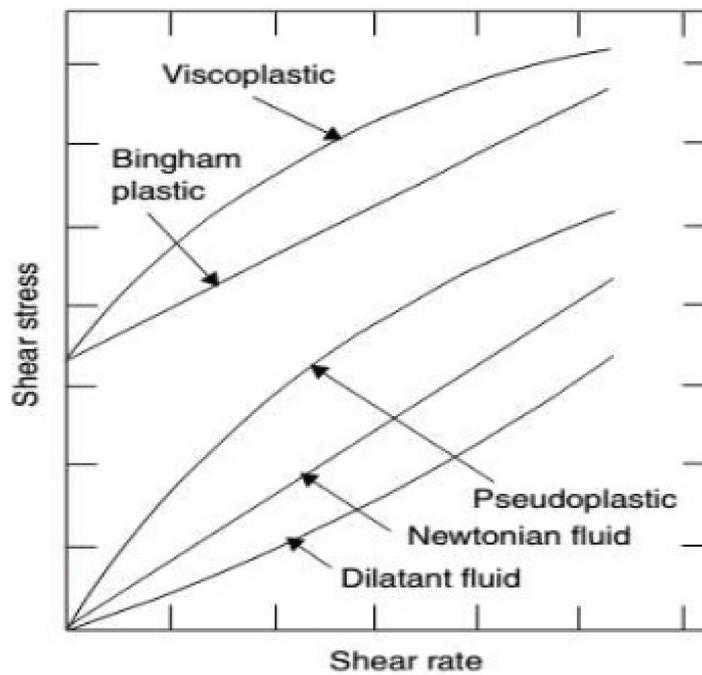
FIGURE 1.12: Flow curves for different fluids

TABLE 1.1: Rheology models for non-Newtonians fluids

Model Name	Equation
Reiner (1926)	$\tau = k\,\dot{\gamma}$
Bingham (1992)	$\tau = \tau_0 + \mu_0\,\dot{\gamma}$
Herschel-Bulkley (1926)	$\tau = \tau_0 + k\,\dot{\gamma}$
Casson (1956)	$\tau - \tau_0 = \mu_\infty^{\frac{1}{2}}\,\dot{\gamma}^{\frac{1}{2}}$
Sisko (1958)	$\mu = \mu_\infty + k\,\dot{\gamma}^{(n-1)}$
Carreau (1968)	$\frac{\mu-\mu_\infty}{\mu_0-\mu_\infty} = \left(1 + (\lambda\dot{\gamma})^2\right)^{\frac{n-1}{2}}$
Cross (1965)	$\frac{\mu-\mu_\infty}{\mu_0-\mu_\infty} = \frac{1}{(1+\lambda\dot{\gamma})^m}$

Relations linking rheological behavior and sludge concentration

The parameters of the rheological models (*i.e.* apparent viscosity, yield stress...) depend on MLSS concentration and temperature. The viscosity increases exponentially with MLSS concentration. Empirical models have been developed to correlate the zero shear apparent viscosity (μ_0) and the solids concentration (X) (Equation 1.40, Bokil and Bewtra, 1972); the yield stress (τ_0) and the solids concentration (Equation 1.41, Dick and Ewing, 1967) or the apparent viscosity and the MLSS concentration and temperature in the same equation (Equation 1.42, Yang et al., 2009)

$$\mu_0 = 0.00327.10^{0.132X} \tag{1.40}$$

$$\tau_0 = \beta_1 exp^{(\beta_2 X)} \tag{1.41}$$

$$\mu = a[MLSS]^b T^c \tag{1.42}$$

where: $[MLSS]$ is the sludge concentration, T is temperature and a b c are calibrated parameters.

Impact of rheological model on simulation results

In a batch settling simulation, the choice of a certain viscosity model has no effect on the prediction of the settling velocities (Locatelli et al., 2013), as the fluid is considered laminar. This is not the case when modelling a 3D fluid. Lakehal et al. (1999) argued that the relation of Bokil and Bewtra (1972) is over-predicting the SBH when applied to a continuous flow simulation. De Clercq (2003) stated that a low shear rate value may cause an excessive rise of the SBH.

Many researchers have used different rheology models for sludge viscosity prediction.

Dick and Ewing (1967) found that the yield stress depends on the biological condition of the sludge. A "bulking" sludge is found to have the same yield stress at a lower concentration ($1.5\,\text{Kg}\cdot\text{m}^{-3}$) than a normal sludge with higher concentration ($4.8\,\text{Kg}\cdot\text{m}^{-3}$). The difference is also due to the type of rheometer used.

The behavior of a Bingham plastic fluid is that at least a minimum yield stress needs to be exerted in order to start deformation (see figure 1.12). In activated sludge, the stress needed to deform the fluid is due to the network formed by the microorganisms and other particles dwelling in the sludge.

Griborio (2004) chose to use the correlation of Bokil and Bewtra (1972) due to its simplicity (just 2 parameters to calibrate) and because De Clercq (2003) stated that

a true yield stress in activated sludge is nonexistent. Locatelli (2015) found that the model that better describes activated sludge rheology is a Cross type (which is used for polymers in solution, Rao, 2014). He suggested that a rheology model should consider the EPS concentration and temperature.

Khalili-Garakani et al. (2011) made a comparisson among 7 different rheology models to better understand the activated sludge and flow characteristics. According to their findings, a Carreau model provides the best viscosity prediction in a wide range of MLSS concentrations ($2.41 - 30 g.L^{-1}$). However, at low MLSS concentration (less than $10 g.L^{-1}$) Bingham equation can give also an accurate description of the sludge viscosity.

In conclusion, even if activated sludge rheology is an important property for wastewater treatment process performance and modeling, most of the authors describing an activated sludge rheology model, found different values and viscosity models that can fit to the experimental data of sludge rheology. These differences are impacted by the type or rheometer used, lack of detailed experimental data collection protocol, lack of a protocol in how the rheology measurements were done, or lack of Good Modeling Practices for parameter estimation. (Ratkovich et al., 2013).

Hence, further research should demonstrate if the activated sludge presents a thixotrophic behaviour, however within this thesis activated sludge viscosity is considered time independent.

1.6.4 Brief review on the use of CFD models for SST modeling

As mentioned before, Larsen (1977) was the pioneer in introducing the CFD tools in the wastewater treatment field. Since then, different approaches have been performed in order to understand and optimize the hydrodynamics of SST. The approaches include: improvement on settling models, changes in geometry or position of baffles, scenarios with high hydraulics loads, etc.

Many studies can be found in literature that focus on *e.g.* the settling behavior of the sludge (Griborio, 2004, Ramin et al., 2014a), tank's geometry (Larsen, 1977; Lakehal et al., 1999; Griborio, 2004; Flamant et al., 2004; Patziger et al., 2012; Ramalingam et al., 2009; Ramin et al., 2014b; Xanthos et al., 2013, etc.)

Matko et al. (1996) identified the main parameters that a CFD model has to include to better represent the flow pattern and effluent quality:

- Velocity distribution of the fluid (Hydrodynamics),

- Tank's geometry (solids removal mechanisms, inlet design, weir placement, baffle designs, slope of the tank),

- Settling velocity distribution (dispersed, hindered and compression regimes),

- Particles density and size,

- Turbulent mass diffusion especially at the inlet.

Tank geometry is one of the most important aspects that may influence the settling behavior and of course the effluent quality.

Baffle modeling

Authors modeling secondary settling tanks (Zhou, McCorquodale, and Vitasovic, 1992; Krebs et al., 1996; Matko et al., 1996; Goula et al., 2008) agree that including the baffle at the inlet improves the settling behavior and the effluent quality by diminishing the turbulent energy associated to the flow velocity and the potential energy of the high sludge concentration. Krebs et al. (1996) modeled different inlet arrangements to evaluate the effect of it in kinetic dissipation to improve the flocculation behavior and increasing the solids removal. Griborio and McCorquodale (2006) and Gong et al. (2011) used flocculation models into their CFD approaches in order to understand the flocculation process by changing the geometry of the tank *i.e.* the effects of the central baffle. Brouckaert and Buckley (1999) made a CFD study of two different circular clarifiers were a baffle was installed and both showed a higher underflow solids concentration under high-load conditions. Nevertheless, the concentration of the incoming sludge, the settling behavior, the underflow withdrawal affects the underflow sludge concentration even if the baffle is used. A study made by Ghawi and Kriš (2012) states that an energy dissipation inlet (EDI) baffle have proved a better performance (suspended soids removal with respect to the HRT and SRT) of the SST even in overloading episodes than an SST without EDI baffle. By adding this mechanism into the settler, the solids removal efficiency can be higher, around 90.4 to 98.6% (Goula et al., 2008).

Sludge withdrawal mechanism

The purpose of this mechanism it to move the settled sludge from the tank's bottom to one or more pipes connected to the biological reactors. The ideal sludge draw-off mechanism must be quick enough to keep sludge freshness and concentrate sludge to reduce pumping efforts at the same time (Anderson and Gould, 1945). A study by Weiss et al. (2007) showed that whether the sludge removal mechanism is not taken into account in the model, an overestimation of the SBH will be observed, besides within the sludge blanket; the flow and the sedimentation of sludge is dominated by the viscous forces. There are authors who tried to represent this mechanism by adding an additional term, *i.e.* Lakehal et al. (1999) employed a negative source term on the governing equations that represent the sludge removal by a suction-lift mechanism. Das et al. (2016) obtained the first model which could represent the

sludge removal mechanism by adding a rotating rake term ($\dot{\omega}$) in the solids transport equation.

Other aspects within the settling tank modeling

Almost all research in CFD for SST analyses the effects of the baffle at the inlet, but there are other aspects to be considered; *e.g.* Stamou and Gkesouli (2015) worked in a CFD model to investigate the negative effect of the wind on the hydraulic and settling performance and they realized that it has a strong influence on the flow field and the hydraulics, however removal efficiency is not highly influenced.

Xanthos et al. (2013) also compared rectangular SST 2D simulations with 3D approaches and concluded that a 2D model underpredicts the ESS because it does not consider the length and the inlet baffle arrangements as well as the corner effects of the clarifier. They also realized that whether the effluent weir length is much longer and located far from the ending walls the effluent quality is better than in other configurations.

1.7 Experimental techniques for model calibration/validation

To validate a numerical model it is necessary to compare the results of such model with experimental data. As we have seen, the activated sludge behaves in a different manner according the settling zone, this is why different experimental techniques have been developed.

1.7.1 Methods for sludge settling properties determination

The most common and used one is the Sludge Volume Index (SVI) because it is easy implemented and gives a general idea of the quality of the sludge settling. Hindered settling velocity can be calculated from values of SVI. Equations of Pitman (1984), Härtel and Pöpel (1992), and Wilson (1996) relate the SVI values for a certain sludge with the parameters of the Vesilind model (V0 and rv). Nevertheless, this method is not accurate since only describes the hindered settling. Other techniques like sludge stirred specific volume index (SSVI) or diluted sludge volume index (DSVI) are also used to determine the hindered settling parameters by relations such as Ekama, 1986 and Koopman and Cadee, 1983 respectively for example.

Methods for measuring discrete settling velocity have been developed such as those of Griborio, 2004 and Ramalingam et al., 2009 where the settling velocity has been measured accurately using batch settling columns to follow the path of discrete particles in a certain time. The shortcommings of this technique are that it only takes

into account the discrete settling, the measurements must be repeated several times and settling distances are taken from naked eye.

However, the former technique can be improved by means of Particle Image Velocimetry (PIV), where a video-camera tracks the particle settling. Mancell-Egala et al. (2016), using PIV, determined the TOF and the LOSS for particles in discrete zone. Hence different particles properties, velocity, size, porosity, particle surface and roundness, can be obtained using PIV. The main shortcomings are, that is it only useful for transparent basins (such as batch settling columns) and it has not been explored for compression settling. Mancell-Egala et al. (2017) has developed a technique using a video-camera and image analysis software to obtain different data about the sludge characteristics such as: size, porosity and form of the particles, settling velocity of particles, particles filaments, etc. Image analysis can also be used to track the SBH within a settling column as presented by Derlon et al. (2017).

Obtaining such data we can consider the flocculation state needed to represent the complete settling behavior.

There is also laboratory size equipment to measure settling behavior, i.e. the Automated Settlometer developed by Vanderhasselt et al. (1999), to obtain the settling curve of sludge in a 10 litter pyrex decanter with a light scanner that detects the sludge blanket height. Even if the technique showed good results in settling prediction, it is only functional for hindered settling. Another lab-scale technique for settling behavior was implemented by G. Chebbo (2009). It is called VICAS ("Vitesse de chute en Assainissement", in French), this technique uses a batch settling column to obtain the velocity and mass of discrete particles. The objective is to obtain total particles cumulative percentage vs. settling velocity. Nevertheless, this technique is more accurate for raw sewage with low concentration of particles (discrete settling mainly).

1.7.2 Methods for in-situ validation

Most methods for field validation of CFD models rely either on more or less manual sampling (for sludge concentration profiles mainly) and measurements using ultrasonic techniques. Depending on the type of equipment and signal processing, these techniques allows to track the SBH, particles velocities and even concentrations (Locatelli et al., 2015; François et al., 2016; Pallares et al., 2017).

Ultrasonic transducer is a device that measures the Doppler shift frequency at different depths within the sludge suspension. One can obtain the settling velocity and the sludge blanket height. A batch settling test was conducted by Locatelli et al. (2015) in order to obtain the concentration profile and settling curves at different initial concentrations of sludge. One advantage of this technique is that the device can

be placed in a full size clarifier, concentration and velocity profiles are obtained by statistic treatment of data and it is non-invasive.

Different authors have also used those techniques to calibrate and validate their models, *i.e.* Patziger (2016) developed a CFD model for SST. They used video-motion analysis to obtain the settling velocity profile in a settling column, an optical turbidimeter for TSS concentration and a Nortek-Vector Acoustic Doppler Velocimeter to measure 3D velocities directly in the clarifier.

Most of the CFD models are calibrated using batch settling columns to obtain the settling velocity profile (Griborio, 2004; Flamant et al., 2004; Xanthos et al., 2013). Other developers made measurements in a full-size clarifiers but only to obtain the hydrodynamics of the system (Patziger, 2016)) or for low concentration of particles (Tarpagkou and Pantokratoras, 2013; Xie et al., 2014).

1.8   Conclusion about the literature review

The settling behavior of the activated sludge is a complex process involving several mechanisms and different physical laws (discrete, hindered, compression...). The sludge settling is also greatly impacted by the hydrodynamics of the clarifier. The classical settling models only describe the settling velocity as function on the local concentration.

CFD models have proven to be an excellent tool for understanding the clarifier performance. The most part of them are focused on geometry optimization and impact on the effluent conditions. These models indeed, include a high level of physical representation regarding hydrodynamics itself, sludge rheological behavior, turbulence, etc. Some of them also include complex relations or equations describing flocculation of sludge particles in relation with hydrodynamics and turbulence. However, regarding settling velocity models themselves, most of the models published in literature still rely only empirical relationships developed decades ago. These relationships only describe hindered settling as a function of the local sludge concentration. In our opinion, the complexity of the sludge settling mechanisms has to be taken into account with the same level of complexity than other components of a CFD model.

Since about 10 years, 1D models have experienced a dramatic improvement with the development of consistent modeling frameworks describing complex additional mechanisms like compression, multi-class particles models and impact of flocculation state on the whole settling behavior, etc.

The objective of the present work is then, to develop a CFD code based on the Bürger-Diehl (Bürger, Diehl, and Nopens, 2011) framework and integrating the compression function of DeClercq (De Clercq, 2006). To reduce the computational time

an axisymmetric approach of a circular clarifier will be used. Since the base code is based on the mixture approach for fluid transport modeling, we remain into this approach. As suggested by Brennan, 2001, the k-epsilon model including the buoyancy term is employed.

Finally, the results of the simulations will be compared to experimental data obtained directly in field and used for studying some scenarios including changes in model parameters and operational conditions.

Chapter 2

Incorporation of a compression term in a CFD model based on the mixture approach to simulate activated sludge sedimentation

The conventional activated sludge process is the most widespread technology used in wastewater treatment plants. In this process, bacteria and wastewater are in contact (mixture) in a reactor in order to reduce the amount of organic material and other nutrients such as nitrogen and phosphorus. This biomass (activated sludge) grows and forms biological flocs that must be separated from treated water. This is usually performed by means of gravity in a clarifier also called a Secondary Settling Tank (SST).

SSTs are the bottleneck of the activated sludge process. They must achieve three main functions: sludge-water separation (clarification), activated sludge recycling and storage in the case of hydraulic overloading. As a consequence, activated sludge sedimentation within the SST governs effluent quality directly in terms of total suspended solids (TSS) and indirectly as it will affect the biomass retention within the system (through recycling), thus affecting the biokinetic processes occurring in the biological reactor (Torfs et al., 2015b).

Activated sludge particles can undergo different settling behaviours, depending on their properties (density, particle size, concentration...). One can classify the settling behaviours in a SST into four main mechanisms:

1. Discrete settling: particles settle with individual velocities and with no interactions among them; this regime is limited by the threshold of flocculation (Mancell-Egala et al., 2016; Mancell-Egala et al., 2017);

2. Flocculating zone: particles collide forming flocs that settle with individual velocities;

3. Hindered settling: above a certain concentration (Mancell-Egala et al., 2016; Mancell-Egala et al., 2017; Torfs et al., 2016), particles are considered to settle all at the same velocity depending on the local concentration (Kynch, 1952). This regime is limited by the critical concentration (X_{crit}).

4. Compression: after the critical concentration is reached, particles form a network and sludge starts to thicken due to the high interaction between particles. This network exerts a solid stress that slows down settling velocity. Nevertheless, recent evidence suggests that even for higher concentrations, the individual properties of the particle also affect settling velocity (Torfs et al., 2015b).

SST modeling is helpful to understand the sludge settling behavior but also for tank design, troubleshooting, process optimisation and control. Modeling approaches range from point-settler models (0D) and 1D models (Bürger, Diehl, and Nopens, 2011) to 2D/3D CFD models (Griborio, 2004; Samstag et al., 2016). 1D models are used in most commercial simulation platforms for wastewater treatment plant-wide simulation. They enable for instance the assessment of SST operational strategies and respond to inflow variability. In order to fully understand the mechanisms of activated sludge settling in combination with the hydrodynamics occurring in the SST, CFD has also become a well-accepted tool. The simulation of activated sludge SST is probably the most well-developed area of application for CFD in wastewater treatment (Samstag et al., 2016).

Larsen (1977) and Ueberl (1995) carried out experiments in SST and found a density current (similar to a waterfall) created by the concentration of the dispersed phase. This was also first modelled in 3D by Kahane, Schwarz, and Johnston (1997); using industrial thickeners. Hence, in the SST inlet the flow tends to be three-dimensional (Brennan, 2001).

SST must be simulated considering the two phases (solid and liquid). This can be achieved using a two-fluid Euler–Euler technique as performed by Kahane, Nguyen, and Schwarz (2002). In this approach, one set of continuity and momentum equations is solved for each phase. This is computationally intensive as many parameters are involved to describe interphase momentum exchange terms (*e.g.* drag between the liquid and particles...). In the wastewater field, CFD modeling of SST is thus usually performed via a single-fluid Eulerian approach with an active scalar transport model to describe the dispersed phase (sludge) (Lakehal et al., 1999; Griborio, 2004; Kim et al., 2005; Patziger, 2016). The governing equations for fluid motion of the continuous phase are solved; the dispersed phase follows the advective flow and is

then modelled as a scalar. Diffusion, mainly related to turbulence, is also considered in the resulting transport equation. This approach necessitates density and viscosity coupling as a function of scalar concentration (Ungarish, 1995).

A less common approach to model sedimentation is using a mixture model in which the phases are treated as a single continuous phase that is a blend of the discrete phases (Wicklein et al., 2015). A single set of continuity and momentum equations is solved for the mixture. The introduction of the drift velocity concept allows for the description of the relative motion of the dispersed phase. This approach is currently the only one implemented in the set of default solvers within the open-source CFD platform OpenFOAM®. This solver called *driftFluxFoam* originates from the work of Brennan, 2001.

Whatever the approach used, most authors modelling SST with CFD still rely on a closed-form function of solids concentration to describe settling velocity in both hindered and compression regimes (usually exponential functions) (Lakehal et al., 1999; Griborio, 2004; Flamant et al., 2004; Weiss et al., 2007; Patziger, 2016).

Discrete settling and floculation are usually modeled separately within different kinds of settlers. *e.g.* primary settling tanks. Ramin et al. (2014a) modelled hindered, transient and compression settling with a combination of two exponential expressions and a compression factor. Bürger, Ruiz-Baier, and Torres (2012) implemented a compression term in their 2D axi-symmetric code.

Nevertheless, most of the settling models used in CFD do not consider compression as a separate constitutive function, even the most recent ones (*i.e.* Gao and Stenstrom, 2018). This requires changing the structure of the model by including effective solid stress involving dependence on the gradient of concentration.

In this respect, effort is being undertaken concerning one-dimensional model improvement, and this work has already led to the addition of compression as a second order term in the underlying partial differential equation (Plósz et al., 2007) as well as a critical analysis of hindered settling function that also considers power-law functions instead of exponential ones(Torfs et al., 2017). Torfs et al. (2016) proposed a unified 1D framework for all these settling regimes, which surprisingly, has not been the case to date concerning CFD models.

The objective of this paper is to implement the Bürger-Diehl framework, (Bürger, Diehl, and Nopens, 2011), which has been assessed in terms of well-posedness and numerical convergence (Bürger et al., 2012), within a CFD numerical code based on the mixture approach.

The simulation of an activated sludge batch settling column was performed to validate the results against the SBH (height of the sludge/clarified water interface) experimental data. Then, simulations of a full-scale clarifier were carried out to compare results obtained with the original solver considering only hindered settling and

the improved one with both hindered settling and compression. The improvements of SBH and sludge concentration in the RAS (settled sludge which is pumped back to the biological reactor) predictions are analyzed.

2.1 Materials and Methods

2.1.1 State-of-the-art one dimensional settling model

The one-dimensional (1D) partial differential equation of Bürger-Diehl (Equation 2.1) is employed to model the activated sludge settling behavior. This equation has the advantage to enable switching among different constitutive relations for the hindered settling, compression and dispersion terms (Bürger et al., 2013), without affecting the solvability of the model.

$$
\begin{aligned}
\frac{\partial X}{\partial t} = & -\frac{\partial}{\partial z}\left(X\vec{v}_{\mathrm{hs}}(X)\right) \\
& -\frac{\partial}{\partial z}\left(X\vec{v}_{\mathrm{conv}}(z,t)\right) \\
& +\frac{\partial}{\partial z}\left(d_{\mathrm{comp}}(X)\frac{\partial X}{\partial z}\right) \\
& +\frac{\partial}{\partial z}\left(d_{\mathrm{disp}}(z,Q_{\mathrm{in}}(t))\frac{\partial X}{\partial z}\right) \\
& +\frac{Q_{\mathrm{in}}(t)X_{\mathrm{in}}(t)}{A}\delta(z)
\end{aligned}
\tag{2.1}
$$

The first and second terms in the right side of the equation stand for particle displacement by hindered settling and advection (through the bulk velocity) respectively. The third term models the sludge compression. The fourth term describes the dispersion of the mixture at the inlet (turbulence effect). The last term models the feed mechanism at a given height of the system.

Hindered settling velocity modeling

According to Kynch theory (Kynch, 1952), hindered settling velocity ($\vec{v}_{hs}$)is supposed to depend only on solids concentration (X). Several empirical laws are available in the literature to link these two variables. The most common are exponential relationships such as Vesilind's function (Vesilind, 1968):

$$
\vec{v}_{\mathrm{hs}}(X) = \vec{v}_0 e^{-r_{\mathrm{h}}X}
\tag{2.2}
$$

Recently, the use of power law functions has been suggested to be more accurate when coupled with compression settling (Torfs et al., 2017). One of these relations is the one proposed by Diehl (Diehl, 2015):

$$\vec{v}_{hs}(X) = \frac{\vec{v}_0}{1 + (X/\bar{X})^q} \tag{2.3}$$

where $\vec{v}0$, $\bar{X}$ and q are parameters to be calibrated.

Sludge compression behavior modeling

The compression function d_{comp} in Equation 2.1 represents the decrease of settling velocity occurring when sludge reaches compression regime, *i.e.* sludge compressibility. This function is given by Bürger, Karlsen, and Towers (2005):

$$d_{comp} = \begin{cases} 0 & \text{for } 0 \leq X < X_{crit} \\ \frac{\rho_d}{g(\rho_d - \rho_c)} \vec{v}_{hs}(X)\sigma'_e(X) & \text{for } X \geq X_{crit} \end{cases} \tag{2.4}$$

where ρ_d and ρ_c are respectively the sludge and water density, g is gravity, and σ'_e the derivative of effective solids stress.

The effective solids stress σ_e is the stress supported by the solid skeleton De Clercq, 2006, *i.e.* the sludge particles form a network that exerts a force in the vertical direction (pushing up). This is only valid when the sludge concentration is higher than the critical concentration (X_{crit}). Authors use different expressions with two parameters to calculate the value of effective solids stress (Ramin et al., 2014a; De Clercq et al., 2008). Here, the De Clercq's function (Equation 2.5) (De Clercq et al., 2008) is employed to describe σ_e depending on sludge concentration and three parameters (λ, β and X_{crit}) to be calibrated.

$$\sigma_e(X) = \begin{cases} 0 & \text{for } 0 \leq X < X_{crit} \\ \lambda ln\left(\frac{X - X_{crit} + \beta}{\beta}\right) & \text{for } X \geq X_{crit} \end{cases} \tag{2.5}$$

2.1.2 Continuity, momentum and dispersed phase modelling in the original CFD code

Activated sludge can be considered as a two-phase mixture, where water is the continuous phase and the sludge (particles) is the dispersed phase. Based on Brennan's work (Brennan, 2001), the original *driftFluxFoam* solver is built on the mixture model approximation, which states that only one continuity and one momentum equation is solved for the mixture. The distribution of the dispersed phase is modelled with a

advection-dispersion equation that introduces the concept of drift velocity. It is assumed that in the horizontal direction, both phases act as just one. To employ such a model, one must consider that both phases are isothermal, non-reactive, incompressible and non-phase changing.

The solver uses the volume fraction of the dispersed phase and not the dispersed phase concentration as in the 1D model. Therefore, the sludge concentration variable X as well as model empirical functions for hindered and compression regimes are replaced by the following variable:

$$\alpha_d = \frac{X}{\rho_d} \tag{2.6}$$

The mixture density ρ_m is defined as the sum of the individual densities of the continuous phase ρ_c and the dispersed phase ρ_d multiplied by their volume fractions α_c and α_d respectively (Equation 2.7).

$$\rho_m = \alpha_c \rho_c + \alpha_d \rho_d \tag{2.7}$$

The mixture velocity ($\vec{v}_m$) is defined by equation 2.8:

$$\vec{v}_m = \frac{\alpha_c \rho_c \vec{v}_c + \alpha_d \rho_d \vec{v}_d}{\rho_m} \tag{2.8}$$

Considering the mixture density and velocity, one can obtain the continuity (Equation 2.9) and momentum (Equation 2.10) equations:

$$\frac{\partial \rho_m}{\partial t} = -\nabla \cdot (\rho_m \vec{v}_m) \tag{2.9}$$

$$\frac{\partial \rho_m \vec{v}_m}{\partial t} + \nabla \cdot (\rho_m \vec{v}_m \vec{v}_m) = -\nabla P_m + \nabla \cdot (\mathcal{T} + \mathcal{T}^t + \mathcal{T}_{Dm}) + \rho_m \vec{g} + \vec{M}_m \tag{2.10}$$

In this equation, $\vec{v}_m$ is the mixture velocity. The second term in the right side is the stress tensor, composed of viscous stress $\mathcal{T}$, turbulent stress $\mathcal{T}^t$ and diffusion stress $\mathcal{T}_{Dm}$. P_m is the pressure of the mixture (equal to the sum of phases pressure); $\vec{g}$ is gravity; and $\vec{M}_m$ is the surface tension force on the mixture.

The diffusion stress term $\nabla \cdot \mathcal{T}_{Dm}$ represents the momentum diffusion due to the relative motions of the phases. According to Verloop (1995) if $\nabla \cdot \mathcal{T}_{Dm}$ is missing then the mixture model is inaccurate. Refer to Manninen, Taivassalo, and Kallio (1996) for more details on the development of Equations 2.9 and 2.10 and the stress tensors.

The solids transport equation or drift equation Brennan (2001) is then given by:

$$\frac{\partial \alpha_d}{\partial t} + \nabla \cdot (\alpha_d \vec{v}_d) = \nabla \cdot (\Gamma \nabla \alpha_d) \tag{2.11}$$

The diffusion coefficient Γ, equal to the eddy diffusivity (Stamou and Gkesouli, 2015), considers the effects of the turbulent diffusion on the dispersed phase.

The dispersed phase velocity $\vec{v}_d$ has to be related to the velocity of the mixture $\vec{v}_m$, *i.e.*, the diffusion velocity $\vec{v}_{dm}$ (Equation 2.12)

$$\vec{v}_{dm} = \vec{v}_d - \vec{v}_m \tag{2.12}$$

Thus, Equation 2.11 becomes:

$$\frac{\partial \alpha_d}{\partial t} + \nabla \cdot (\alpha_d \vec{v}_m) = -\nabla \cdot (\alpha_d \vec{v}_{dm}) + \nabla \cdot (\Gamma \nabla \alpha_d) \tag{2.13}$$

The diffusion velocity of the dispersed phase is due to the phase density differences, resulting in forces on the particles different from those on the fluid. Those forces are balanced by the drag force (Manninen, Taivassalo, and Kallio, 1996). According to Ishii and Mishima (1984) the drag correlation should be expressed in terms of the drift velocity $\vec{v}_{dj}$. Equation 2.14 relates the drift velocity to the diffusion velocity:

$$\vec{v}_{dm} = \frac{\rho_c}{\rho_m} \vec{v}_{dj} \tag{2.14}$$

The drift velocity $\vec{v}_{dj}$ is considered as the hindered settling velocity. Hindered settling affected by gravity is only acting downwards therefore:

$$\vec{v}_{dj} = v_{dj} \vec{k} \tag{2.15}$$

The vector $\vec{k}$ is the unit vector pointing in the direction of gravity. The value of v_{dj} can be calculated from empirical functions of the concentration, or here volume fraction. The original solvers includes Vesilind (Vesilind, 1968) (Equation 2.2) and Takacs (Takács, Patry, and Nolasco, 1991) exponential functions. They are here expressed in power 10 basis, as a function of the dispersed phase volume fraction.

Finally the drift equation in the existing code of OpenFOAM® is:

$$\frac{\partial \alpha_d}{\partial t} = - \nabla \cdot (\alpha_d \vec{v}_m)$$
$$- \nabla \cdot \left(\frac{\alpha_d \rho_c}{\rho_m} \vec{v}_{dj}\right) \tag{2.16}$$
$$+ \nabla \cdot (\Gamma \nabla \alpha_d)$$

2.1.3 Development of the modified solver

In the modified code the mixture approach is still used, *i.e.*, continuity and momentum equations remain the same. The improvements made in the code include:

- the addition of the compression term of the 1D equation 2.1 into the drift equation 2.16, which gives Equation 2.17 ;

- the addition of the modified Diehl's Equation for hindered settling (Equation 2.20).

Thus, the equation for solids transport in the CFD code becomes:

$$\frac{\partial \alpha_d}{\partial t} = - \nabla \cdot (\alpha_d \vec{v}_m)$$
$$- \nabla \cdot \left(\frac{\alpha_d \rho_c}{\rho_m} \vec{v}_{dj}\right) \tag{2.17}$$
$$+ \nabla \cdot (d_{comp} \nabla \alpha_d)$$
$$+ \nabla \cdot (\Gamma \nabla \alpha_d)$$

Compression term

The third term of equation 2.17 describing the compression settling was included in the drift equation. The compression function d_{comp} is coded as follows:

$$d_{comp} = \frac{\rho_d}{g(\rho_d - \rho_c)} \frac{\rho_c}{\rho_m} \vec{v}_{dj}(\alpha_d) \sigma'_e(\alpha_d) \tag{2.18}$$

The derivative of the effective solid stress σ'_e is computed as the derivative of Equation 2.5. However, X and X_{crit} must be expressed in terms of volume fraction (Equation 2.6), which gives:

$$\sigma_{e'}(\alpha_d) = \begin{cases} 0 & \text{for } 0 \leq \alpha_d < X_{crit}/\rho_d \\ \frac{\lambda}{\beta + (\alpha_d - X_{crit}/\rho_d) * \rho_d} & \text{for } \alpha_d \geq X_{crit}/\rho_d \end{cases} \tag{2.19}$$

Therefore, similarly to the 1D model, the compression function is only active when the volume fraction (α_d) is higher than the critical volume fraction *i.e.* X_{crit}/ρ_d. This relation has three parameters to be calibrated: λ, β and X_{crit}.

Hindered settling term

OpenFOAM® allows the user to select among several hindered settling functions. The original solver includes Vesilind (1968) and Takács, Patry, and Nolasco (1991) expressions. Diehl's function (Equation 2.3) (Diehl, 2015) was added because it has been suggested to give more accurate predictions than exponential expressions when coupled to compression function (Torfs et al., 2017). The combination of this relation with equation 2.6 now results in:

$$\vec{v}_{dj}(\alpha_d) = \frac{\vec{v}_0}{1 + (\alpha_d/\bar{X}/\rho_d)^q} \tag{2.20}$$

2.1.4 Numerical procedure

OpenFOAM® uses the finite volume method to discretize the partial differential equations, by integrating them over each element/cell (different schemes are available). This method is conservative, the flux entering the cell is the same leaving to the adjacent cell. The finite volume method can be applied to unstructured meshes (providing that there are no overlapping elements) since the variables are evaluated in the center of the cells and not at the cells faces (Moukalled, Mangani, and Darwish, 2016).

In OpenFOAM® the integration of the algebraic equations is based on the sum of the values on the cell faces being interpolated to the center of the cell. The discretization schemes used are: Euler for the time derivative and Gauss Linear for the space derivatives (gradient, divergent, Laplacian). To ensure the stability and convergence of the simulation, the solver includes an automatic time step adjustment according to stability criteria (Courant number < 0.9).

2.1.5 Test case: batch settling column

To demonstrate the reliability of the solver, a 2D mesh was built to represent the sludge settling behavior in a batch settling column. The dimensions of the column are 1m in height and 0.40m in diameter: only rigid walls and free surface boundary conditions are considered (see section 2.1.6). Mesh independence of the column was reached for 500 cells in the vertical direction.

2.1.6 Test case: axisymmetric clarifier

Geometry and meshing

The dimensions of the circular clarifier are based on the data of Lakehal et al. (1999). The clarifier is 20m in radius and 4m height. Assuming that flow is axisymmetric, a 2D geometry can be chosen to simulate the hydrodynamics of the system (Griborio, 2004) which will reduce the number of cells of the geometry and therefore lower the computational cost. Patziger (2016) also uses this approach to study the effects of the inlet design on SST performance.

Thus, the same five patches as used by Lakehal et al. (1999) are appliedd: inlet, outlet, sludge removal, walls, symmetry and wedge as explained in Section 2.1.6 (Figure 2.1).
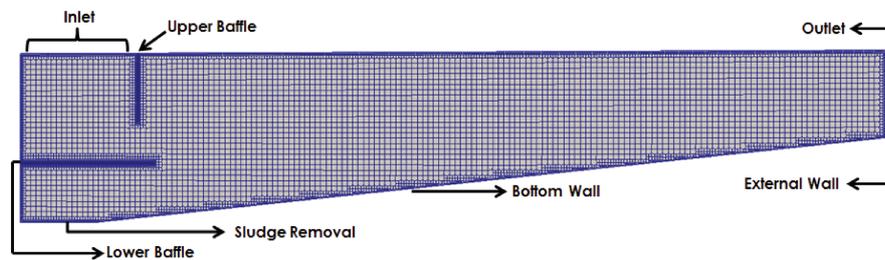
FIGURE 2.1: Mesh of the axisymmetric clarifier

The *snappyHexMesh* tool for meshing in OpenFOAM® generates 3D meshes containing unstructured hexahedral cells. The original geometry is enclosed in a rectangular coarse mesh (called *blockMesh*). Then, *snappyHexMesh* iteratively refines the mesh over the defined geometry (given as *stl* files input) according to the surface refinement and to the number of cells between layers one has assigned (Greenshields, 2017).

Surface refinement is an important feature to get a flat boundary. To obtain a 90° intersection between the boundaries (surfaces), *i.e.* avoid incomplete corners, one should extract the lines of the boundary and define a level of refinement. The bigger the level is, the more complete the corner will be; but the number of cells will increase. This mesh has a Level 5 refinement for back, front, walls and baffles boundaries. As OpenFOAM® works natively in 3D, the generated mesh has to be converted into a 2D axisymmetric mesh. An extrusion tool *extrudeMesh* allows such conversion. To perform mesh sensitivity analysis, three different meshes were generated (6900, 13307 and 21647 cells).

Turbulence Model

The implemented turbulence model is the buoyant $k - \epsilon$, which includes a buoyancy term (Brennan, 2001; Lakehal et al., 1999). It is based on the density gradient generated by the variation of the composition in the mixture. The model is described in section 1.6.2, on paragraph *buoyancy $k - \epsilon$ model*.

Boundary conditions

Inlet   This is a patch with fixed values for inlet volume fraction α_d, kinetic energy k, dissipation rate ϵ, turbulent viscosity ν_t, velocity of the mixture $\vec{v}_m$, and pressure p. The inlet mixture velocity is calculated by dividing the inflow Q_{in} by the inlet section A_{in}. The initial values of k and ϵ are calculated from Equations 2.21 and 2.22 respectively assuming values of $T_u^2 = 0.05$, $C_- = 0.09$ and turbulence length scale (l_u) of 0.5 times the inflow radius to the inlet baffle (Lakehal et al., 1999). Turbulent viscosity v_t is computed automatically by OpenFOAM®.

$$k = 1.5(T_u \vec{v}_m)^2 \tag{2.21}$$

$$\varepsilon = \frac{C_\mu k^{\frac{3}{2}}}{l_u} \tag{2.22}$$

Effluent outlet   Since the outlet is located far from any geometry disturbances that impact the flow direction, all the variables outlet boundary conditions are set to *zeroGradient* (Versteeg and Malalasekera, 2007) except for the pressure which is set to a fixed value of 0 Pa (relative pressure). The *zeroGradient* boundary condition extrapolates a quantity to the patch from the nearest cell value: the quantity is developed in space and its gradient is equal to zero in the normal direction of the boundary.

Sludge removal   Mixture velocity at the recirculation boundary $\vec{v}_{mrec}$ is imposed and calculated with Equation 2.23, where R is the recirculation ratio and A_{rec} the section of the withdrawal. R is the ratio of the RAS flow-rate returning to the biological reactor over the through-flow of the wastewater treatment plant. The rest of the variable boundary conditions are set-up to *zeroGradient*.

$$\vec{v}_{mrec} = \frac{Q_{in}R}{(1 + R)A_{rec}} \tag{2.23}$$

Walls No-slip boundary condition is applied for velocity. The volume fraction and pressure boundary conditions are set up to *zeroGradient* and *fixedFluxPressure* respectively. The latter is used for pressure in situations where *zeroGradient* is generally used, but where body forces such as gravity and surface tension are present in the solution equations. The gradient is adjusted accordingly to Greenshields (2017). Concerning turbulence variables, standard OpenFOAM® wall functions are used (Greenshields, 2017).

Free surface Symmetry boundary is applied here. Similar to *zeroGradient* for scalars, the normal component is set to zero for vectors.

Wedge boundaries The wedge boundary makes sure that one cell thick is running along the centre line, straddling one of the coordinates planes Greenshields, 2017. It is only imposed to front and back boundaries of the 2D axisymmetric clarifier, ensuring that OpenFOAM® will use the cylindrical coordinates.

Sludge properties

Sludge properties used in this study originate from experimental work carried out in previous studies by Locatelli (Locatelli et al., 2015) The sludge inlet concentration and density are $3.9\,\mathrm{kg \cdot m^{-3}}$ and $1050\,\mathrm{kg \cdot m^{-3}}$ respectively.

A Bingham rheological model Bingham, 1916 is used. The Dick and Ewing (Dick and Ewing, 1967) exponential function (Equation 2.24) correlates the sludge concentration and the yield stress. Parameters a_1 and b_1 can be obtained by fitting the modeled yield stress to the experimental data for different sludge concentrations. Here, the solver correlates the yield stress to the volume fraction. The corresponding values for a_1 and b_1 are $5*10^{-3}$ Pa and 141.363 respectively. Then, the obtained viscosity is used in the stress tensor in the momentum equation 2.10.

$$\tau_\mathrm{y} = a_1 * 10^{b_1 \alpha_\mathrm{d}} \tag{2.24}$$

2.2 Results and discussion

2.2.1 Code verification in batch settling column

To validate the simulation results of the improved solver, the batch settling curves (SBH vs time) obtained from the simulations and experimentally during one hour of sedimentation are compared. The sludge properties and initial conditions are those mentioned in Section 2.1.6.

Two different model configurations are assessed:

1. Scenario considering only hindered settling (no compression): Diehl's function (equation 2.20) is used to describe settling velocity;

2. Scenario considering both hindered and compression settling regimes: Diehl's function describes hindered settling velocity and the constitutive function d_{comp} (relation 2.18) describes compression.

Such configurations are based on the research carried out by Torfs et al. (2017) which pinpointed that power-law functions for hindered settling coupled to the compression function describe more accurate SBH dynamics in 1D models than exponential ones.

The parameters for the settling model are calibrated with the experimental data of Locatelli (2015). The corresponding values are summarized in Table 2.1.

Elaborating an independent calibration process only for Vesilind or Diehl equations would result in similar values to those shown in Table 2.1 coupling the compression parameters. The parameters of Vesilind and Diehl equations are only valid for the hindered zone.

TABLE 2.1: Settling model parameters. Diehl's function and the compression function

Parameters	Value
V_0	$6.1143.10^{-3}$ m·s^{-1}
q	1.7003
$\bar{X}$	8.4958 kg·m^{-3}
λ	$8.4228.10^{-1}$ kg·m^{-1}·s^{-2}
β	2.4603 kg·m^{-3}
X_{crit}	4.8815 kg·m^{-3}

Comparison to the batch settling curves obtained experimentally and with both model configurations is provided in Figure 2.2. Physically, one can observe a clear interface between the water and the sludge, this is the SBH. Initially, the SBH linearly decreases for the first 860 s. This is characteristic of the hindered settling regime. The determined slope is the hindered settling velocity which is a function of sludge concentration (or volume fraction in the solver). Here, this function is the power-law established by Diehl (Diehl, 2015) (Equations 2.3 and 2.20). As expected, this regime is equally predicted by both model configurations that use the same parameters for the Diehl function. The original 1D model (Bürger et al., 2013) shows similar predicted heights to those of the CFD code in one dimension (figure 2.2 blue line).

After 860 s, the compression regime starts to be predominant and the settling velocity decreases. The model without compression fails to predict this accurately: the settling velocity remains constant much later and the SBH is highly underestimated. In comparison, the model including compression constitutive function fits very well

with the experimental data: above the critical sludge concentration, the sludge starts to exert a solid stress acting up in the vertical direction, this slows down the observed settling velocity.

These results clearly illustrate the validity of the equations and constitutive functions implementation in the new solver. They are equivalent to what can be obtained using the 1D framework presented in Section 2.1.1. However, the added value of a CFD code is to simulate the processes occurring within the actual geometry. The following section therefore presents the benefits of the improved solver within a full-scale clarifier geometry.
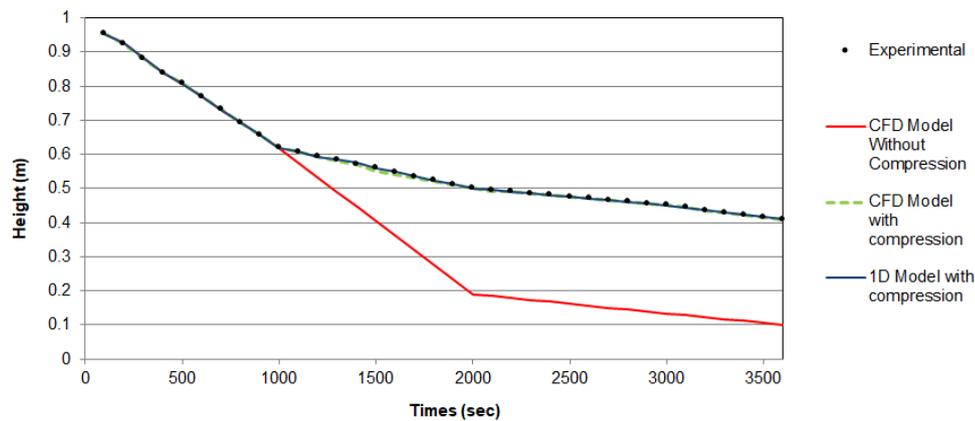
FIGURE 2.2: Settling curves for: experimental data (black points), model using the compression function (blue continuous line) and model without the compression function (red continuous line)

2.2.2 Simulation of full-scale clarifier

Results obtained in a batch settling column showed that the compression term now included in the drift-flux solver successfully fits the experimental data. The impact of this modification on results obtained within a realistic clarifier geometry was investigated by conducting simulations with the design and operating conditions suggested by Lakehal et al. (1999).

Results of the scenarios with and without compression constitutive function are compared in terms of SBH and sludge concentration.

First, constant inlet ($1685 \, \mathrm{m^3 \cdot h^{-1}}$) and RAS flow-rates ($779 \, \mathrm{m^3 \cdot h^{-1}}$) were applied until reaching steady-state of the system. Then, hourly inlet flow-rate fluctuations were applied using previous values as average and the pattern defined by Copp (2001). The RAS flow-rate also varied proportionally according to boundary conditions exposed in Section 2.1.6 (Equation 2.23).

Steady-state simulation

Convergence to steady-state was reached when SBH and RAS concentrations were constant and the overall mass conservation of suspended solids was satisfied.

The CFD simulation results allow for the description of the clarifier hydrodynamics and sludge behavior in the vertical and horizontal directions. Figure 2.3 shows the sludge blanket height and sludge concentration inside the clarifier for the two model configurations.

Using the model with the compression function, a higher SBH is expected as this was previously shown using 1D models including compression as a constitutive function (Torfs et al., 2015a). This was confirmed as the predicted SBH was 1.95m and 1.55m at 5m radial distance for the models with and without compression function respectively.

As expected, the compression slows down the settling velocity. Indeed, compression can be understood as a force exerted by the sludge that does not allow itself to accumulate quickly at the bottom. Thus, lower concentrations along the bottom of the clarifier are observed (Figure 2.3, upper). This is particularly relevant at the right side of the SBH. Without compression, concentrations up to $40\,\mathrm{g\cdot L^{-1}}$ are observed locally. This high predicted concentration is probably the consequence of two phenomena:

- overestimated settling velocity in these conditions: one main reason for this is that the hindered-settling function is not zero at a finite concentration. The function of Diehl (Diehl, 2015) is meant to be used together with a compression term. The often used Vesilind (1968) function, or double-exponential function Takács, Patry, and Nolasco (1991), are neither zero at a finite concentration. However, they consist of exponential functions that tend to zero very fast, which means they are effectively zero for high concentrations when used by any numerical method; hence, the problem is not visible. An alternative would be to slightly redefine the function so that it is zero at a large concentration when using it without compression.

- rheological behavior: as the concentration is very high in this zone, the yield stress increases to a high extent (equation 2.24). As this is a zone with low velocity and low shear stress, sludge phase is not going down along the slope of the clarifier.

Hence, it can be observed that, without compression, the model predicts some sludge accumulation in the lower baffle of the inlet device. The model without compression is giving more realistic predictions in this respect.

Different conclusion can be drawn regarding the RAS concentration. It should be noticed that it was computed as the average of solid phase concentration over the

removal patch. The predicted concentration is similar with the two model configurations (7.59 kg·m^{-3} and 7.37 kg·m^{-3} with and without compression respectively). This may be due to the particular geometry of the clarifier simulated here (large sludge removal zone, horizontal baffle).

All of these results illustrate the added value of using a compression term and its constitutive function within a CFD model. This could allow to better evaluate the impact of geometrical features and operation modes on predicted SBH and RAS concentration.
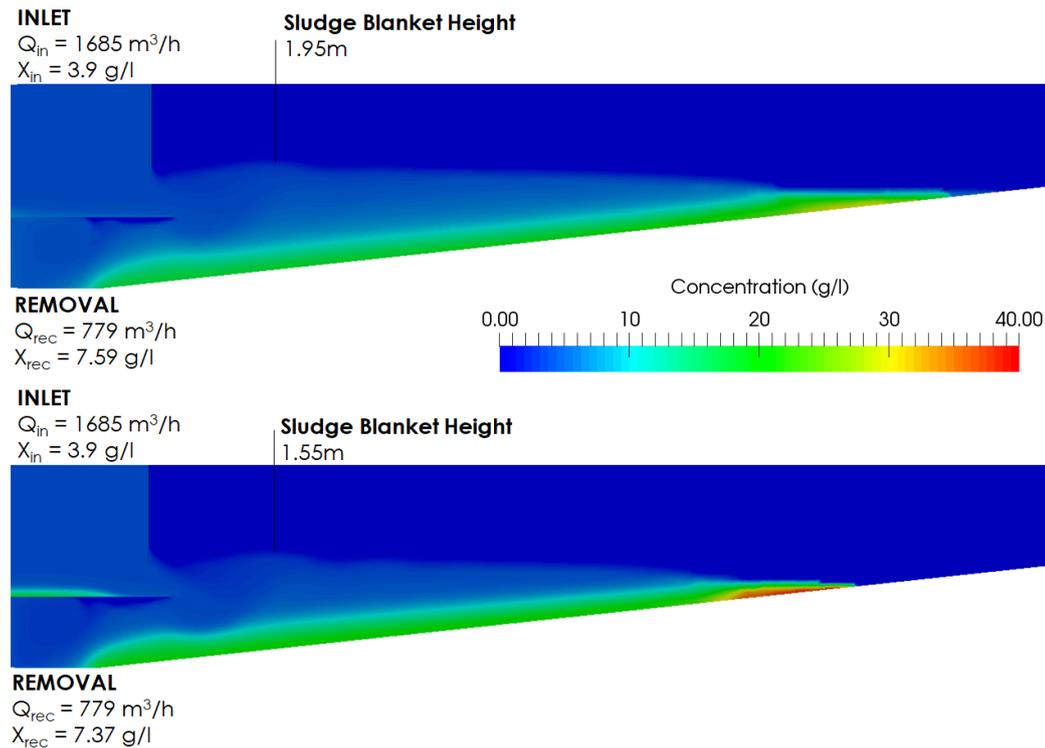
FIGURE 2.3: Sludge concentration and SBH at steady state, upper: Diehl and compression function, lower: Diehl with no compression function

Transient simulation

In order to simulate transient state conditions, flow-rate variations were simulated by changing hydraulic loads at the inlet and the RAS variation according to equation 2.23 for 2 days. Inlet sludge concentration (3.9 kg·m^{-3}) is kept constant. The SBH at radial distances of 5m and 15m and the average RAS concentration are monitored (Figures 2.4 and 2.5 respectively).

The simulation starts with the initial conditions from the steady state obtained for each case. For both models, there is a decrease of SBH when the inflow decreases (Figure 2.4). This is a normal behavior: less mass coming into the system results in
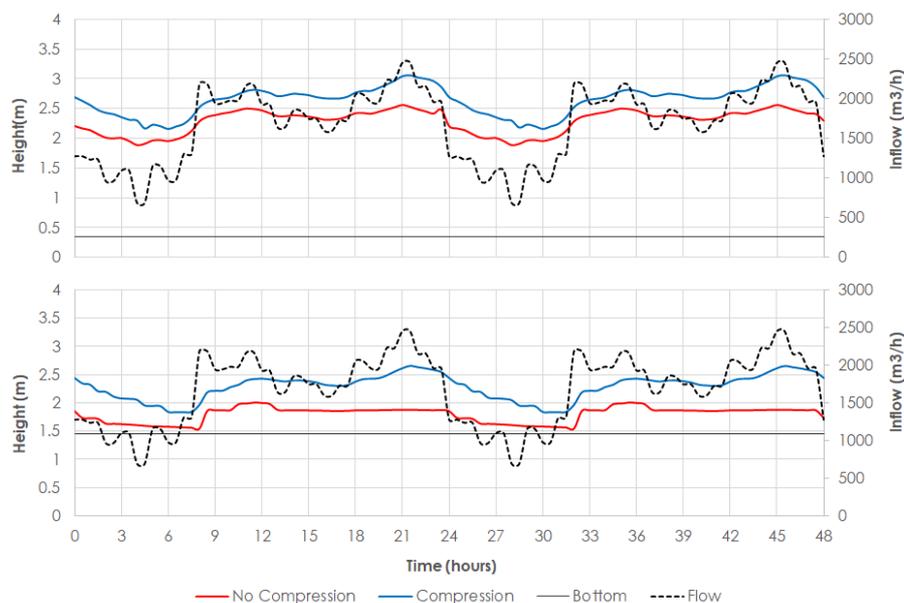
FIGURE 2.4: SBH measured at a radial distance from the inlet of 5m (Upper) and 15m (Lower) with model using and not using the compression function respectively during 2 days transient simulation

less mass settling. Whatever the radial distance, the predicted SBH with the compression model is still higher than the predicted SBH with no compression model *e.g.* maximum 3.05m and 2.56m respectively at 5m radial distance (Figure 2.4 - upper). This is in agreement with the results of steady-state simulation.

One interesting observation is that the model with compression function seems to be more sensitive to flow-rate variations. The relative SBH elevation is indeed higher during peak flows with this model configuration. Afterwards, when the hydraulic load drops, SBH diminution is slower with the model considering compression.

Regarding the RAS concentration, both simulations predict a lower value with higher flow-rate (Figure 2.5), which was expected. There is a dilution of this concentration. Comparing the results obtained with the Takacs 1D model (Takács, Patry, and Nolasco, 1991) not considering compression and the Bürger-Diehl model (Bürger, Diehl, and Nopens, 2011), Torfs et al. (2015a) observed that this dilution effect as well as the relative RAS concentration variations were significantly less pronounced with the latter model. However, Takacs and Bürger-Diehl 1D models differ not only by the absence or presence of the compression term but also by considering or not a separate underflow zone. Here, the 2D CFD model considers this underflow zone in a similar way for the two approaches. Thus, in this study, the observed effect in RAS trend is due only to the consideration of compression. The difference between two modeling frameworks is less important but still significant. It should be also noticed that model parameters used here were calibrated on a real activated sludge and results in a lower solid stress than parameters used by Torfs et al. (2015a).
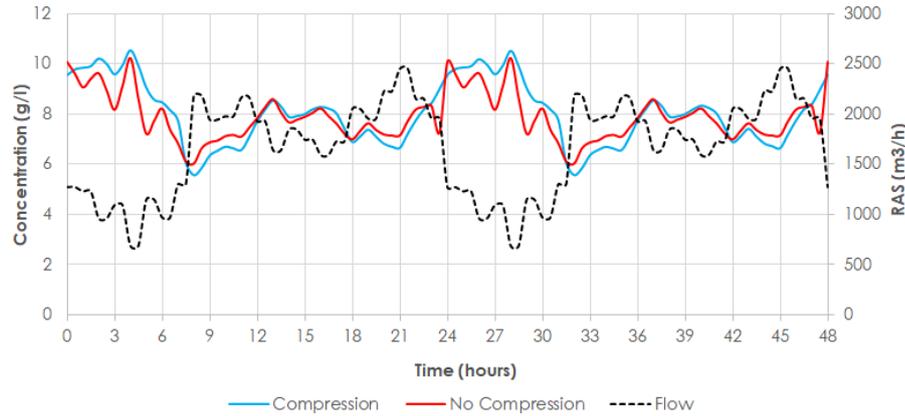
FIGURE 2.5: Average sludge concentration measured at the sludge withdrawal using and not using the compression function respectively during 2 days transient simulation

2.3 Conclusions

This study presents the development of a modified drift-flux solver for the Open-FOAM® open-source platform. The solids transport equation includes an extra second-order term that accounts for compression. Here, the constitutive function of De Clercq (De Clercq et al., 2008) is used but one can select another expression in a modular way. In addition to Takacs (Takács, Patry, and Nolasco, 1991) and Vesilind (Vesilind, 1968) hindered-settling velocity functions, the power-law expression of Diehl (Diehl, 2015) was also implemented. These developments integrate the most up-to-date knowledge of activated sludge sedimentation mechanisms that were surprisingly never implemented in the present form in a CFD code.

To validate this approach, a batch settling column was simulated. By comparing experimental settling curves and the simulations, it has been concluded that the sludge blanket height prediction is improved by using the compression function.

Simulations of a 2D axisymmetric clarifier geometry were also performed in order to evaluate the advantages of considering compression in a continuous system. Through such simulations, it was found that the settling velocity is slowed down above a critical concentration when adding the compression function, thus leading to a higher sludge blanket prediction.

Transient simulation with high hydraulic loads showed that sludge blanket height varied to a higher extent with compression. Return activated sludge concentration was also more impacted despite the fact that these variations were less important in comparison with 1D models. However, these 1D models obviously do not consider the clarifier geometry (baffles, removal, slope...).

Further research will focus on model validation with experimental data measured

within a full-scale clarifier (refer to chapters 3 and 4. Future development also includes the incorporation of discrete settling behavior which requires the inclusion of several particles classes or even the use of Population Balance Models.

Chapter 3

Parameter estimation and validation in Batch settling column by coupling DAKOTA toolkit and OpenFOAM

3.1 Introduction

In order to build a robust SST model, it is necessary to estimate the values of the parameters of the hindered and compression settling functions. Batch settling test are the most widespread method to evaluate settling velocities (Ramin et al., 2014a, Griborio, 2004).

For this purpose, a mathematical algorithm is performed to evaluate an objective function. The objective function qualifies the output/results of a certain variable of the model and compare it to the physical measurements of the same variable.

In the well-posed 1D Bürger-Diehl framework (Bürger, Diehl, and Nopens, 2011), used for activated sludge settling modeling, one can choose among different constitutive functions for hindered and compression settling description. This is where calibration becomes complex, due one can have different numbers of parameters according to the chosen functions.

Different optimization processes can be carried out to find the correct set of parameters. Most of them are a global optimization algorithms.

Torfs et al. (2013) performed a Global Sensitivity Analysis (GSA) using a Brute Force Monte Carlo method to calibrate 2 hindered settling models, and 1 compression model. They found that parameters of the Vesilind (equation 1.6, Vesilind, 1968) function are identifiable while one of the parameters of the Takacs equation (equation 1.7 Takács, Patry, and Nolasco, 1991) is unable to be identifiable. The compression parameters of the simplified function of DeClercq (equation 1.13, De Clercq et

al., 2008) are not able to describe different batch settling curves with a unique set of parameters (Torfs et al., 2013). In summary, no unique set of parameters can be found for the combined equations for hindered and compression settling.

Locatelli (2015) used an automatic differentiation tool to model sludge settling. He chose a Vesilind-DeClercq (equations 1.6 and 2.5) coupling for hindered and compression settling respectively in the Bürger-Diehl (Bürger, Diehl, and Nopens, 2011) approach. Those four parameters have an important effect on the prediction of the simulated sludge blanket height. The model with the calibrated parameters can be accurate only within the three first hours of settling, beyond this time the SBH is overestimated. Seven different parameter sets were tested and the quality of the estimation was measured by visually comparing the simulated and observed sludge blanket height.

The HTC model (equation 1.15) calculates the solids flux in a domain of 60 horizontal layers to represent the settling behavior in a batch column. Ramin et al. (2014a) used only 3 parameters to estimate. The global calibration optimization method selected was Markov Chain Monte Carlo (MCMC), in which a large number of iterations (sometimes more than 100000) are made in order to find the best parameters set to fit the experimental data. They reported no identification issues for the three calibrated parameters. Even if MCMC is an accurate method, the main disadvantage of the method is that it requires a large number of simulations making it computationally intensive.

These calibration methodologies are usually performed using 1D models and the associated numerical methods. The identified parameters could then be used within a CFD simulation, usually performed by another software package with different numerical methods.

One of the advantages of the OpenFOAM platform is that the same solver can be used to perform 3D, 2D-axisymmetric, 2D or even 1D simulations. In practice, the user has always to provide a 3D mesh but by defining specific "empty" or "wedge" boundary conditions into the mesh, the solver adapts the numerical procedure to the dimensions of the system. Therefore, the same solver and numerical methods can be used for parameter estimation and validation in a batch settling column as well as for simulation of a full-size clarifier. This makes the process easier and more reliable.

DAKOTA® (`https://dakota.sandia.gov/`) is an open-source (GNU LGPL license) toolkit that provides an interface between simulation codes and a variety of iterative systems analysis methods, including optimization, uncertainty quantification... It has applications spanning defense programs for climate modeling, computational materials, nuclear power, renewable energy, and many others. DAKOTA® can therefore be coupled to OpenFOAM in order to perform the identification of the best set of parameters for the settling model developped in chapter 2.

The objective of this chapter is to show a local process of calibration and validation of the settling model developed in OpenFOAM (2) using the sludge blanket height (SBH) experimental information obtained in a batch column and the simulated SBH. Calibration is made by using a 1D mesh created in OpenFOAM.

This study is using a local optimization method: this allows to lower the computational cost (as a CFD code is used). In addition, not enough experimental points were available to perform a global analysis.

In order to illustrate this calibration and validation procedure, two sets of experimental data were chosen, due to the extremely varying characteristics of the sludge in the studied treatment plant. According to the number of experimental data points available, a different settling model (hindered and compression functions) is chosen for calibration. Indeed, the settling functions assessed in this study involve a different number of parameters. The choice of different functions therefore allowed to adjust the degrees of freedom of the calibration process.

A non-linear squares method is performed in order to minimize an objective function. In such method, the model equation is fitted to the experimental data rather than transforming it into a linear form (Sagnella, 1985). Estimation consist in finding the optimal values for the parameters that can minimize a cost function or Quantity of Interest (QoI). The cost function, often described as the sum of the squared errors between the observed data and the simulated data, is minimized with respect to the parameters.

In this approach, we will evaluate the quality/accuracy of the model outputs by introducing a statistic called Nash Sutcliffe Efficiency (NSE). Hence, the NSE statistic can be decomposed in three components: correlation, the bias and the relative variability in the simulated and observed values to show the inherent systematic problems due to calibration (Gupta et al., 2009).

Finally, validation of the model is carried out by using another set of batch sludge settling experimental data and the settling velocities, and evaluating it through the NSE statistic. With the found values of the settling parameters, the CFD model will be validated in a full-scale clarifier.

3.2   Materials and Methods

3.2.1   Sludge settling Model

Equation 2.17 is the model of interest. Such model can be used for 1, 2 or 3 dimensions. As stated before, this model consists of 1 general PDE, where one can choose

among different hindered settling velocities ($\vec{v}_{hs}$) and effective solids stress (σ_e) functions to describe the settling behavior. Two different sets of experimental data are used to calibrate the model, thus the model 2.17 is used in two configurations:

- Vesilind equation (Vesilind, 1968), and the simplified function of DeClercq for effective solids stress (equation 3.1).

- Diehl equation (equation 2.20) and simplified function of DeClercq for effective solids stress (equation 3.1).

$$\sigma_e(\alpha_d) = \begin{cases} 0 & \text{for } 0 \leq \alpha_d < X_{crit}/\rho_d \\ \lambda(\alpha_d - \frac{X_{crit}}{\rho_d}) & \text{for } \alpha_d \geq X_{crit}/\rho_d \end{cases} \tag{3.1}$$

In the OpenFOAM code, equation 2.2 is expressed as the volume fraction of the dispersed phase (α_d) and not the sludge concentration (X) (see chapter 2).

Parameter λ indicates the magnitude in which the settling velocity is slowed down. The compression function is calculated with equation 2.18, but is only active when the sludge volume fraction crosses the critical volume fraction defined as X_{crit}/ρ_d.

3.2.2 Experimental Test on Batch settling column

For the calibration analysis different sludge samples were grabbed at different seasons (January to October 2018) from the aerated tank of the WRRF of Achenheim (WRRF details in chapter 4). Batch settling tests were performed in order to obtain the settling velocities and the sludge blanket heights using an Ultrasonic Transducer device developed by ICube laboratory (Abda et al., 2009; François et al., 2016; Pallares et al., 2017).

The batch settling column consisted of a cylindrical transparent PEXIGLAS column of 1m height and 0.4m diameter with a total volume of 126 liters (figure 3.1 right). Prior to sedimentation test, the sludge mixture was homogenized by a reversible pump system working in closed-loop. Air bubbles must be removed from the entire column, since they can disturb the velocity measurements. Wall effects can be neglected due to the large diameter of the cylinder.

Determination of the sludge properties

Prior to data acquisition, the homogeneous activated sludge was sampled to determine the TSS, Volatile Suspended Solids (VSS) and sludge densities. The TSS and the VSS were determined following the procedure AFNOR NFT 90-105, 1997 (*Qualité de l'eau - Dosage des matières en suspension*). The sludge floc density was measured by pycnometer, centrifuging the bulk sludge following the procedure described in Locatelli (2015). The properties were measured three times for each dilution.
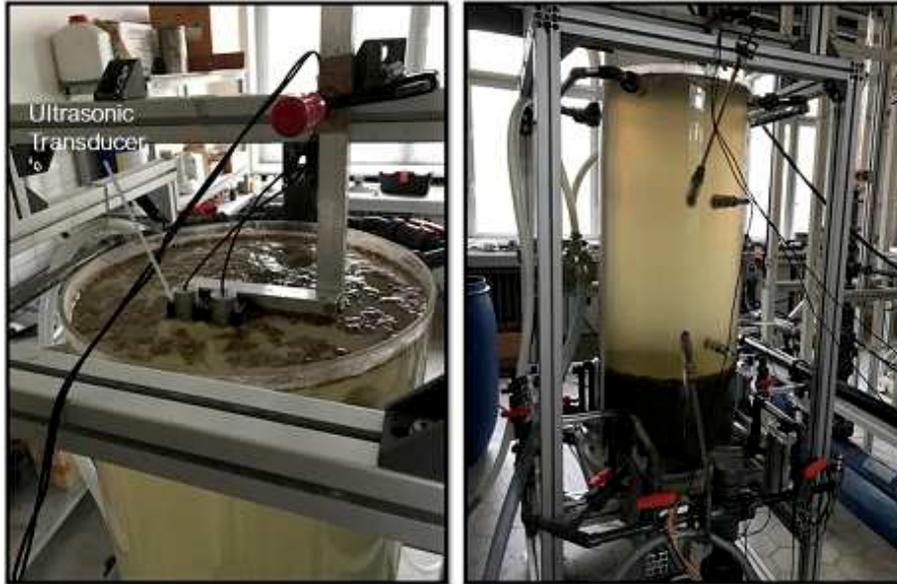
FIGURE 3.1: Ultrasonic transducer device position (left) and Experimental batch column with settled sludge from January 16th 2018 (right)

Table 3.1 presents a summary of the sludge properties for all the batch tests from January to October (without dilution). The sludge floc density is an intrinsic property that is not affected by the dilution.

TABLE 3.1: Sludge properties of the Achenheim WRRF

Date	TSS $(kg.m^{-3})$	VSS $(kg.m^{-3})$	NVSS $(\%)$	Density $(kg.m^{-3})$
January	4.16 ± 0.06	2.63 ± 0.03	36.68 ± 1.52	1018.2 ± 5.9
February	5.39 ± 0.03	3.32 ± 0.03	38.44 ± 0.48	1000.2 ± 2.0
April †	5.54 ± 0.020	3.41 ± 0.007	38.49 ± 0.10	1010.4 ± 4.2
August ‡	2.84 ± 0.003	1.18 ± 0.003	58.57 ± 0.49	1012.7 ± 0.8
October †	4.55 ± 0.03	2.05 ± 0.07	54.88 ± 1.39	1001.1 ± 1.6

† Dilutions were made during these tests
‡ Not a representative value, maintenance at the WRRF was done during the measurements.

Ultrasonic transducer description

The data obtained from the Ultrasonic transducer device is based on the Doppler effect. The transducer sends an acoustic signal to the activated sludge suspension and it receives back an echo called *backscattered* signal. From this signal, the position and velocity of a particle (scatterer) can be known. This is a non-invansive technique for sludge settling velocity recording. The device is placed over the surface of settling column (see figure 3.1 left) to perform vertical measurements.

The transducer emits a Pulse Repetition Frequency (PRF) at an emission frequency (f_0), then the acoustic beam will be propagated in a conical shape measurement

TABLE 3.2: Properties and parameters of the ultrasonic transducer, can be fixed to the desired measures.

Sensor diameter	1 cm
Maximum Pulse Repetition Frequency +	300 Hz
Maximum Pulse Repetition Frequency$_{eff}$*	15 Hz
Maximum measurable velocity	0.001 m/s
Central frequency	1.565 MHz
Carrier frequency	1.5-1.25 MHz
Spatial Resolution	2 mm
Time Resolution	0.66 s
+ Number of ultrasonic bursts emitted per second	
* Number of emitted ultrasonic bursts recorded per second	

cell (spatial resolution). After emitting the ultrasonic pulse, the electronic system switches to "receiving" mode. The acoustic wave propagates along the beam axis and each scatter that crosses the beam will diffuse an echo towards the transducer. The backscattered signal (*echo*) is composed, at a given time, by the sum of the echoes of all scatterers located in the measurement cell. The scatters/particles will induce a frequency shift in the backscattered signal, *i.e.*, the Doppler shift f_D. In each cell, the information obtained from several pulses is processed by the instrument to estimate the projection of the velocity vector over the beam axis. The features of the Ultrasonic device are summarized in table 3.2.

To get the information for the sludge blanket height, the values of amplitude are needed. The strength of the backscattered signal increases sharply giving a higher value in the amplitude signal. Thus, the amplitude will show a high value when the ultrasound burst reach the top of the sludge blanket (François et al., 2016). Higher the backscattered intensity is, higher the particle concentration (Thorne and Hanes, 2002). Therefore, the interface of the clear water and the sludge or SBH, can be estimated by relating the height where the sharp intensity jump of the amplitude sign was found.

To obtain the settling velocity of the particles $\vec{v}_s$ within the sludge blanket, the Doppler shift frequency (f_D) is needed, equation 3.2 correlates both variables:

$$\vec{v}_s = \frac{C f_D}{2 f_c} \tag{3.2}$$

Where C is the sound speed and f_c the carrier frequency (Hz). The settling velocity can be obtained by measuring f_D at different depths. A variation of 1°C in water temperature will produce a variation of 0.1 and 0.3 % in the particle velocity and cell position. Thus, a correction by the speed of sound at 20°C has to be done.

The average time for velocities and amplitude data acquisition was 1 hour. Separate tests were also carried out for more than 5 hours. Particles settling velocity and the amplitude (backscattered intensity) of the signal were recorded every 0.15 sec.

3.2.3   1D simulation in OpenFOAM®

OpenFOAM® natively performs 3D simulations. However, calibration and validation of the settling behavior is studied here in batch. It is therefore necessary to set specific boundary conditions to convert the 3D mesh into a 1D mesh.

The initial mesh reproduces the PLEXYGLASS column structure (figure 3.1). A 1m height, 40cm long and 1mm thick mesh is built. To create the 1D mesh, one cell thickness in the horizontal and depth directions are set up.

At the beginning of the simulation the column is considered to have an homogeneous sludge concentration, therefore the initial concentration is set to the same value in each one of the cells/layers. The rectangular system is limited by walls located at the bottom, left and right side. The atmosphere is located in the upper part of the column, this is a free surface indicating that no walls/inlets/outlets are present (figure 3.2).

The one cell thickness is required in the x direction. By setting the "empty" condition to the front and back patches, will make OpenFOAM® to understand that no calculation is required in the z direction. The vertical axis (y direction) is divided into 500 layers, indicating a cell size of 2mm.
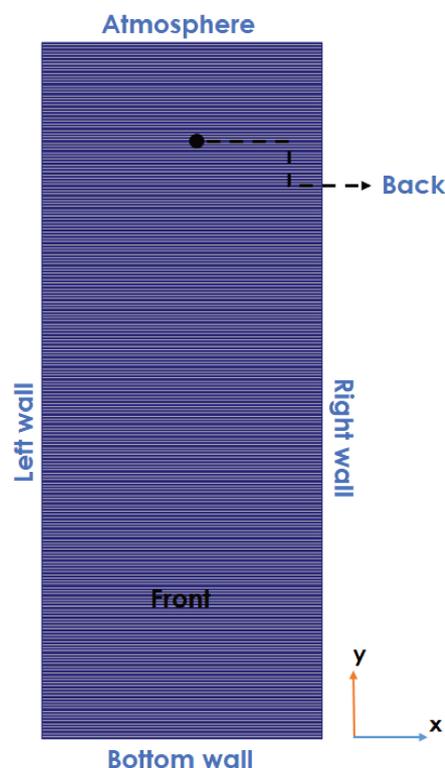
FIGURE 3.2: OpenFOAM 1D mesh and boundary conditions

The code used for the simulations is *compressionFluxFoam* described in section 2.1.3 and Valle Medina and Laurent (2020).

The Courant-Friedrichs-Lewy condition (CFL) condition (equation 3.3) is fixed to 0.9, to ensure the convergence of the simulation. This condition assures the information of a cell traveling directly to its neighbor and do not skip it.

$$CFL = d\frac{\Delta t}{\Delta z} \tag{3.3}$$

Where: d is the velocity magnitude, ΔT is the time step and Δz is the length between mesh elements.

3.2.4   DAKOTA® optimization process

DAKOTA® is a software developed by U.S. Sandia National Labs and stands for Design and Analysis toolkit for Optimization and Terascale Application. This software allows for model optimization, uncertainty quantification, parameter study and design of experiments. It can be used with its own syntax or it can be coupled to an external software (acting like a black box tool) to perform the optimization process.

Optimization process with DAKOTA®

DAKOTA® can perform an optimization process just by setting-up an input file, with the experimental and model output information, and choosing the optimization model/code.

Dakota has different optimization methods (gradient-based, efficient global optimization, nonlinear least squares, etc.) to find the response for the objective function. The model to be optimized can be set directly into DAKOTA® environment or it can be linked to another software (see next section). One can set the initial guess and domain of the values of the parameters where the optimization method should seek. Finally, a series of calculations are performed to obtain the objective function and make a new iteration (if necessary) with a new set of parameters automatically calculated by DAKOTA®.

Figure 3.3 illustrates the closed-loop of an optimization process using DAKOTA environment. DAKOTA already contains algorithms to perform an estimation process, such as the *Rosenbrock function*, which is a test problem used to evaluate the characteristics of an optimization process (convergence, precision).

Optimization process coupling DAKOTA® and OpenFOAM®

Coupling DAKOTA and OpenFOAM® mainly consists in running an OpenFOAM solver in order to get a response or output, in which later, DAKOTA will read to analyze the response. If the response has not a desirable value then DAKOTA will
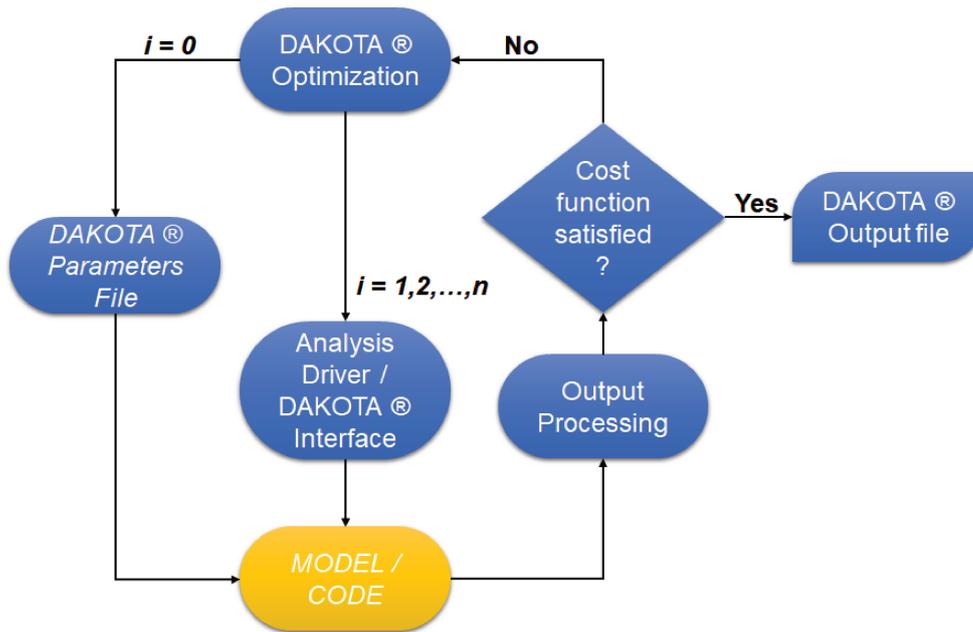
FIGURE 3.3: Optimization process used by DAKOTA. In italics the
information that the user needs to provide to start the process.

set new conditions for a new simulation in OpenFOAM until a convergence criterion
is reached.

When coupling DAKOTA to an another software, an external analysis driver (it can
be a shell code) will link both. DAKOTA calls OpenFOAM through it and acts like a
black box simulator to calculate the objective function and estimate the parameters.

OpenFOAM and some other shell codes included in the case base, perform the re-
quired calculations for DAKOTA to obtain the cost function and then to estimate the
new values of the parameters to complete the identification process.

The basic OpenFOAM case must contain: the initial and boundary conditions, mesh
information, constant values, time controls and tools to extract the information of
interest (simulated data). After setting the optimization method and the initial guess
of the parameters, DAKOTA® will call OpenFOAM® to run a simulation with the
initial guess of the parameters. Then, OpenFOAM will sample the points of interest
in the mesh. With the additional shell codes, the simulated settling curve is extracted
and the values are compared to the experimental data. The latter values are then
used by DAKOTA to obtain the cost function and estimates the new parameter set if
needed. Figure 3.4 illustrates the coupling process for both softwares.

In general, DAKOTA is linked to OpenFOAM to perform parametric study, e.g. to
find the optimal velocity or for geometry/shape optimization ("Coupling of Dakota
and OpenFOAM for automatic parameterized optimization") and geometry parametriza-
tion like the Ahmed body, a geometrical body used for aerodynamic studies (Ahmed,
Ramm, and Faltin, 1984). This is logical if we consider that OpenFOAM® is a CFD
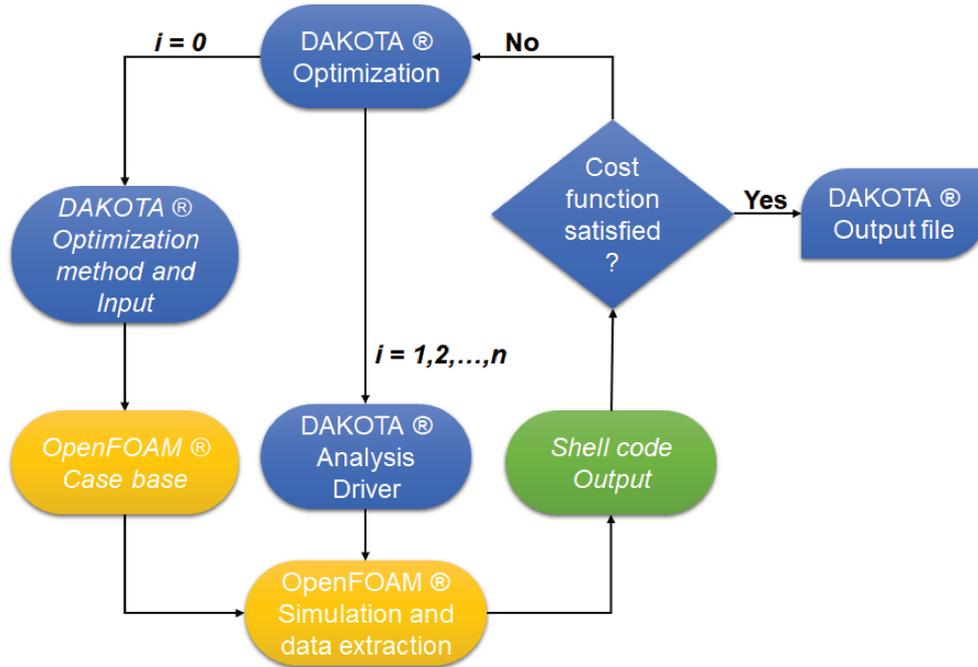
FIGURE 3.4: Dakota environment (continuous blue line) coupled to an OpenFOAM

software applied mainly for aerospace, aeronautics, automotive industries. Some of these optimization processes consist in changing the position of the inlet in order to see how this movement change the output field.

In our study, the novelty comes when DAKOTA® is coupled to OpenFOAM to make a parameter estimation in a 1D model, to further use these parameters in a 2D approach for sludge settling modeling (refer to chapter 4).

3.2.5 Parameter Estimation using the Non-Linear Squares (NLS) method of DAKOTA®

The least squares method is the most widely used procedure to estimate the model parameters (Sweeney, Williams, and Anderson, 2019). This is a deterministic calibration where parameters are adjusted in order that simulation data points are the closest to the experimental data points.

When using, Non-Linear Squares (NLS) method in DAKOTA, the case is considered as unconstrained problem. The Gauss-Newton based algorithms neglect terms in which residuals multiply Hessians (second partial derivatives) when assuming that residuals tends to 0 at the solution. Thus, the first order information is enough to define the objective function.

Optimization problems through the NLS, involve the minimization of an objective function f(x) such as:

$$f(x) = \sum_{i=1}^{n} [H_{\text{sim,i}}(\theta) - H_{\text{obs,i}}]^2 \tag{3.4}$$

This objective function $f(x)$, called sum Sum of Squared Errors (SSE), is defined as the difference between experimental data (H_{obs}) and the model predictions (H_{sim}) in a particular location or time step.

Here, θ would be the set of the model parameters that are being calibrated.

The NL2SOL gradient based method

The NL2SOL method looks for a local minimum, the gradient acts as a compass and always points downhill. The method starts with an initial guess of the parameters values and then moves to a set of parameters that can minimize the cost function. An iteration process is created to improve the performance of such initial guess to reach the best fit.

To illustrate this problem, only the compression parameters: λ and X_{crit} are considered, but the calibration process include also the hindered settling parameters (equations 2.2 and 2.20). With the initial guess, the model function is expressed as a Taylor series expansion near the initial values (λ_0 and X_{crit0}), the expansion can be represented in a linear parameter equation:

$$Y_i - f(\lambda, X_{\text{crit}} \cdot t) = f(\lambda_0, X_{\text{crit0}}, \cdot t_i) + \frac{df}{d\lambda}(\lambda - \lambda_0) + \frac{df}{dX_{\text{crit}}}(X_{\text{crit}} - X_{\text{crit0}}) \tag{3.5}$$

Where T_{sim} is the independent experimental variable assumed to be free of error for n pairs of data points and Y_i the experimental value. Values can be obtained for $(\lambda - \lambda_0)$ and $(X_{\text{crit}} - X_{\text{crit0}})$ by solving the difference between the experimental and predicted values with the initial parameter guess.

The new obtained values are used for the next initial guess and repeated several times. In each iteration the SSE (equation 3.4) is calculated and evaluated until a converging criterion is achieved. Convergence is reached when the change in the value of the SSE from one iteration to another is below a tolerance value (here a value of 10^{-5} is used).

Thus, the *NL2Sol* algorithm in Dakota®, uses the Gauss-Newton gradient method to minimize the cost function. Assuming that the first derivative of $[H_{\text{sim}}(\theta) - H_{\text{obs}}]^2$ tends to zero and thus the Hessian matrix of the second derivative of $f(x)$ can be

approximated by using only the first derivative of $[H_{\text{sim}}(\theta) - H_{\text{obs}}]^2$. This approximation is corrected by a secant update method.

Confidence intervals on estimation

The 95 % confidence intervals are computed as the optimal value of the estimated parameters $\pm$ a t-test statistic times the standard error of the estimated parameter vector. The standard error is a linearization involving the matrix of the derivatives of the model with respect to the derivatives of the estimated parameters (Adams et al., 2014).

3.2.6 Evaluating the estimated parameters

The Nash-Sutcliff Efficiency (NSE) normalized statistic evaluates the quality of the estimation by determining the relative magnitude of the residual variance compared to the measured data variance, thus it is expressed as:

$$NSE = 1 - \frac{\sum\limits_{i=1}^{n} \left(H_i^{obs} - H_i^{sim}\right)^2}{\sum\limits_{i=1}^{n} \left(H_i^{obs} - \widehat{H}^{obs}\right)^2} \tag{3.6}$$

Where $\widehat{H}_{\text{i,obs}}$ is the mean of the measured data for the constituent being evaluated.

NSE can range from ∞ to 1. Moriasi D. N. et al. (2015) developed this evaluation criteria based on measures for watershed hydrological modeling (nutriments, flow and sediments). To determine the quality of the calibrated parameters one can take such criteria for the NSE, as it is shown in table 3.3

TABLE 3.3: Evaluation criteria for estimated parameters

Criteria	NSE Value
Very Good	> 0.8
Good	$0.6 \leq NSE \leq 0.8$
Satisfactory	$0.5 < NSE < 0.6$
Not Satisfactory	≤ 0.5

3.3 Results

3.3.1 Experimental study

The results for the hindered settling velocities measured in the batch column are shown in graphic 3.5. One can observe that the correlation between the settling velocities and the MLSS concentrations is more or less acceptable. However, gathering all the points to do just one calibration process may be inaccurate. For example, the sludge of October and January have similar concentrations, but the sludge of October settles almost four times faster than the sludge of January. This behavior may be due to the high content in mineral matter of the October sludge (see table 3.1). Visually, the sludge of October had more a gray color, instead of having a brown sludge normal color.
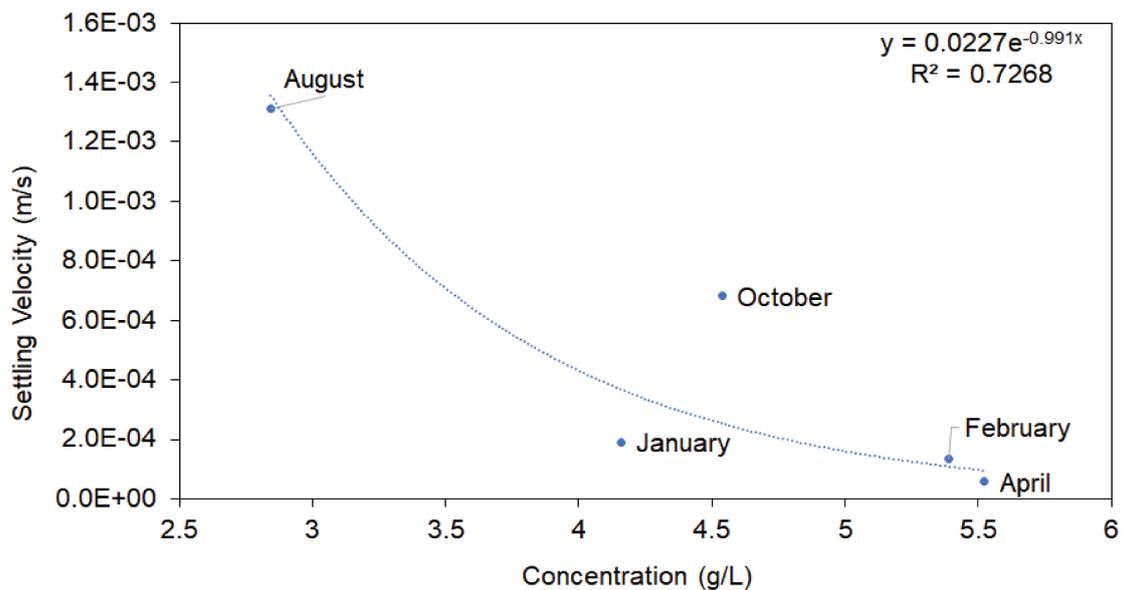
FIGURE 3.5: Relation between the sludge concentration and settling velocities from the batch experimental tests

Therefore, two different calibration process are carried on. One calibration process for the experiments held in April and other using the experimental data of October. Those experiences, where chosen because of two reasons:

1. For both sampling campaigns, batch tests with several dilutions of the same sludge using treated water from the same WRRF were performed;

2. The experimental data obtained in the full-scale clarifier is representative (chapter 4).

Measured data in April

The sludge blanket height information was extracted for the three different initial concentrations durint the first hour. Figure 3.6 shows the experimental settling curves for the three different initial concentrations (X_0). Only the test with initial concentration of X_0=3.95 Kg·m^{-3} was performed during 11 hours (see figure 3.8b)
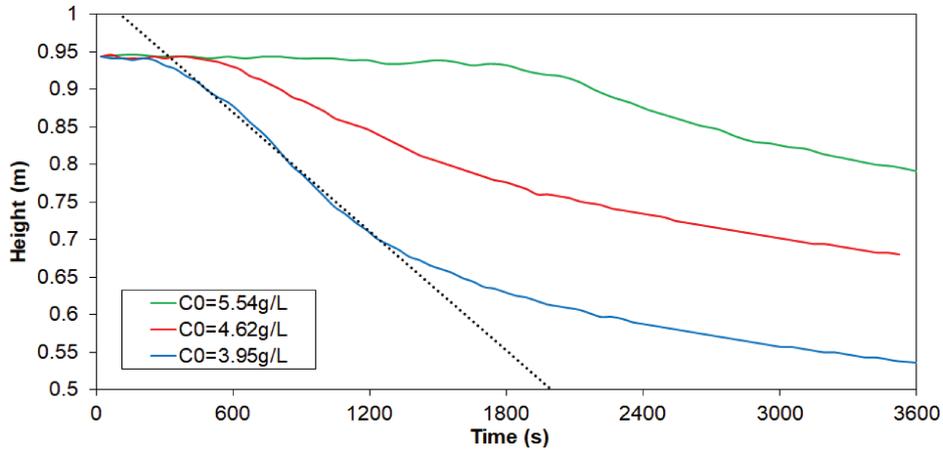
FIGURE 3.6: Experimental settling curves from the batch tests held in April

The experimental hindered settling velocity ($\vec{v}_{hse}$) can be obtained by calculating the slope in the linear part of the curve (dotted black line in figure 3.6). The slope can be defined by visually setting the limits, i.e., for the settling curve at $X_0 = 3.95$ Kg·m^{-3} it is located between 300 and 1200 seconds.

However, this visual technique may not be accurate enough due to human subjectivity on setting up the limits of the slope. This can be the case for the settling curve at $X_0 = 4.62$ Kg·m^{-3}, which do not show a clear hindered zone and by consequence there is hardly a steep slope. The settling curve at $X_0 = 5.54$ Kg·m^{-3} shows a large lag-phase, suggesting that the sludge is already in compression and thus it is hard to determine a true settling velocity within the hindered zone.

To avoid the bias, the method of Stricker (Stricker, Takács, and Marquot, 2007) is used. To calculate the slope of the curve, such method makes a correction by considering the lag phase in the settling curve and the compression zone. Table 3.4 shows the values of the experimental hindered settling velocities (V_{hse}) using the Stricker method.

TABLE 3.4: Measured settling velocities at different sludge concentrations with the samples taken in April

Concentration (Kg·m^{-3})	V_{hse}(m·s^{-1})
3.95	$1.83.10^{-4}$
4.62	$8.25.10^{-5}$
5.54	$5.98.10^{-5}$

To calibrate this experimental data, configuration one is used (section 3.2.1) *i.e.,* the coupling of equation 2.2 and equation 3.1. Therefore 4 parameters need to be calibrated.

The measured settling velocities are needed to determine the initial guess of the parameters of the Vesilind equation for further calibration. This was made by minimizing the cost function (equation 3.4) using the values of the hindered settling velocities. The GRG Non-Linear algorithm of Excel for the estimation process was used. The found values for the initial guess of the parameters of Vesilind equation are in table 3.5.

The initial values for the compression parameters (λ and X_{crit}) are based on literature values (table 3.5). Another guide to set-up the initial value of X_{crit} is that it shall be higher than the initial concentration.

TABLE 3.5: Initial guess of the parameters and their limits

Parameter	Initial Guess	Upper bound	Lower bound
$\vec{v}_0(\mathrm{m\cdot s^{-1}})$	0.0024	0.1	0.001
$r_h(\mathrm{m^3\cdot Kg^{-1}})$	0.682	0.912	0.456
$\lambda(\mathrm{m^2\cdot s^{-2}})$	0.05	0.1	0.001
$X_{crit}(\mathrm{Kg\cdot m^{-3}})$	5.5	6	5

Measured data in October

The 3 settling curves of the sludge sample taken in October 2018 are shown in figure 3.7. For each sludge dilution the sludge blanket height was tracked during one hour.
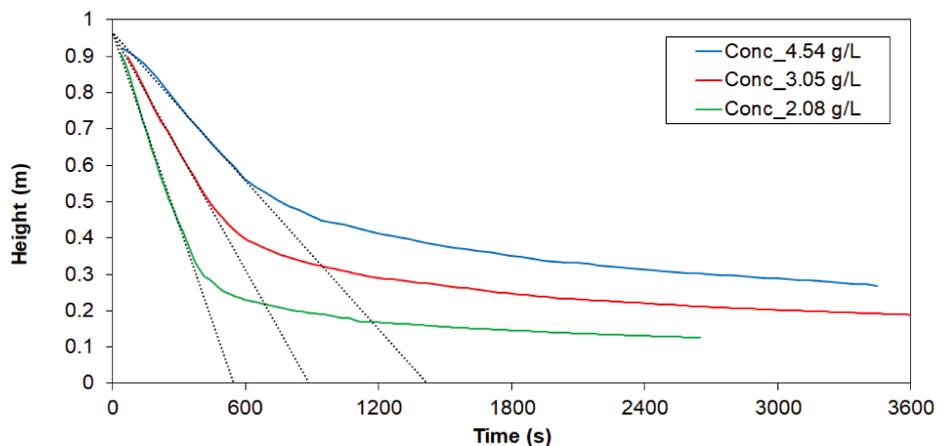
FIGURE 3.7: Experimental settling curves from the batch tests held in April

For the three sludge dilutions, a clear delimitation between the hindered and compression zones is distinguished. Steeper slopes are present for this sludge, indicating a higher hindered settling velocity. Hence, at the lowest sludge concentration, the sludge blanket is low ($\simeq$ 14cm) by the end of the experiment. Only a visual method

is used to determine the limits of the hindered zone. With a linear regression, the values of the slopes of the settling curves are obtained. The hindered velocity values are shown in table 3.6.

TABLE 3.6: Measured settling velocities at different sludge concentrations with the samples taken in October

Concentration (Kg·m^{-3})	$\vec{v}_{\text{hse}}(\text{m·s}^{-1})$
2.08	$1.765.10^{-3}$
3.05	$1.089.10^{-4}$
4.54	$6.817.10^{-4}$

Comparing the velocity values at similar concentrations, (for the same WRRF sludge but in different season), it results that velocity for $X_0 = 4.54\,\text{Kg·m}^{-3}$ is 20 times higher than the velocity for the sludge at $X_0 = 4.62\,\text{Kg·m}^{-3}$. This increase in the velocity can be due to the fact that the sludge of October has a higher percentage of NVSS.

For this experimental data, the calibration/validation process is made with configuration two (section 3.2.1), *i.e.,* the coupling of equation 2.20 and equation 3.1. Thus, 5 parameters are calibrated. The initial guess for the values are listed in table 3.7.

TABLE 3.7: Initial guess of the parameters and their limits

Parameter	Initial Guess	Upper bound	Lower bound
$\vec{v}_0(\text{m·s}^{-1})$	0.009	0.1	0.001
q	1.5	2	0.5
$\bar{X}(\text{Kg·m}^{-3})$	0.7	1	0.1
$\lambda(\text{m}^2\text{·s}^{-2})$	0.02	0.01	0.001
$X_{\text{crit}}(\text{Kg·m}^{-3})$	5	6	4.6

3.3.2 Calibration and Validation on sludge blanket height

April data

Calibration process for the complete settling curve, (estimation of the 4 settling parameters at the same time) was done taking the results of the measured sludge blanket at the initial concentration of $X_0 = 3.95\,\text{Kg·m}^{-3}$ for one hour of settling. The simulated SBH is where a high volume fraction gradient is observed. In the simulation results, the value of such height was obtained at the layer where the sludge concentration is $X = 0.9\,\text{Kg·m}^{-3}$. The values of the estimated settling parameters and their confidence intervals are shown in table 3.8.

Calculating the NSE for the complete settling curve yields a value of 0.995 which indicates a good quality of the estimated parameters according to Moriasi D. N. et al. (2015) criteria. If the same statistic is applied separately for both zones, hindered and compression, values of 0.987 and 0.945 are obtained respectively. Thus, even if

TABLE 3.8: Values for the estimated settling parameters and their confidence intervals for April data

Parameter	Estimated Value	Confidence intervals
$v_0(\text{m·s}^{-1})$	0.0046	$\pm 1.28.10^{-4}$
$r_h(\text{m}^3\text{·Kg}^{-1})$	0.7573	$\pm 5.19.10^{-3}$
$\lambda(\text{m}^2\text{·s}^{-2})$	0.05	$\pm 8.76.10^{-4}$
$X_{\text{crit}}(\text{Kg·m}^{-3})$	5.51	± 0.045
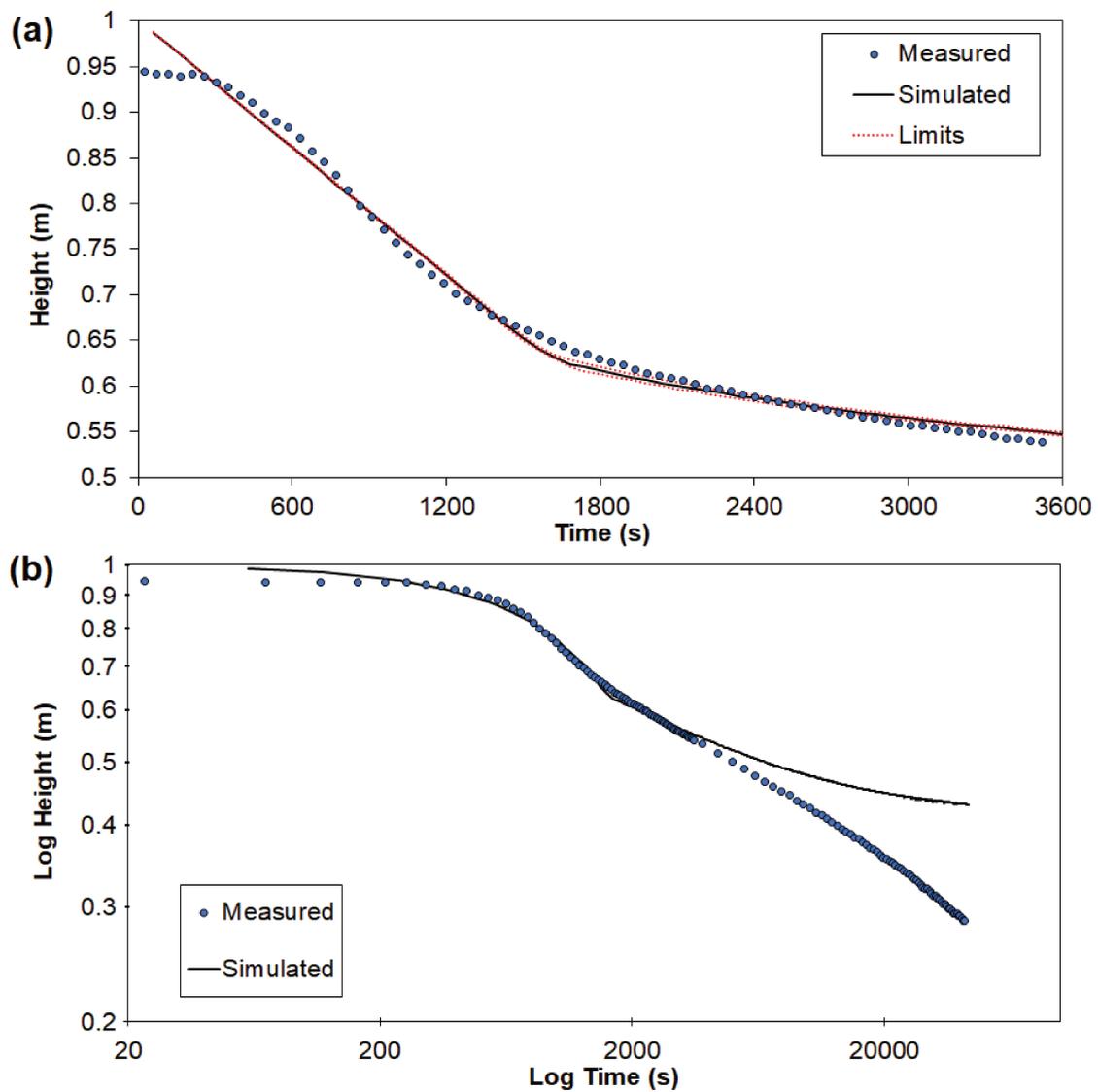
FIGURE 3.8: a) Measured and simulated settling curve at 1hour. b) Log-Log settling curve for measured and simulated data during 11 hours of settling for $X_0 = 3.95\,\text{Kg·m}^{-3}$

a local minimum of the cost function is found, the estimated values perform a good simulation of the batch settling behavior within the first hour of settling. Hence, the low uncertainty (red dotted lines in figure 3.8a) of the parameters ensures the good definition of the estimation process.

The log-log plot of the experimental data (figure 3.8b) shows a linear trend which indicates that the SBH moves according to a power law. The simulated SBH shows a marked breakdown around 1800 s caused by the constant sludge critical concentration. Hence, after 4200 s, the simulated SBH does not follow a linear trend, suggesting that compression parameters should vary with time.

To validate the 1D model the estimated parameters are used to model batch settling behavior at two different initial concentrations. The estimated parameters seem to reproduce the same behavior as the experimental data within the hindered zone at $X_0 = 4.62\,\text{Kg·m}^{-3}$ (figure 3.9a). Within the first hour the model can predicts accurately the settling behavior. After this time, the models over predicts the sludge height, indicating again that compression parameters should vary with time (figure 3.9b).

Validation at the initial concentration of $X_0 = 5.54\,\text{Kg·m}^{-3}$ is not included due to the large lag-phase during the settling experiment where it is complex to determine a true hindered settling velocity. Within this experiment, the compression parameters are not truly validated in batch column due to the lack of measurement points. But for hindered settling zone the model makes a good agreement with experimental data when using the estimated parameters.

October data

Calibration process was done in the same manner as in the previous campaign but using a Diehl's function (equation 2.20) for hindered settling modeling. Thus, the estimation is made simultaneously for 5 parameters. The values of the estimated settling parameters and their confidence intervals are reported in table 3.9. The initial concentration was set to $X_0 = 4.54\,\text{Kg·m}^{-3}$

TABLE 3.9: Values for the estimated settling parameters and their confidence intervals for October data

Parameter	Estimated Value	Confidence intervals
$v_0(\text{m·s}^{-1})$	0.00926	$\pm 1.57.10^{-4}$
q	1.36	± 0.01
$\bar{X}(\text{Kg·m}^{-3})$	0.7146	± 0.0105
$\lambda(\text{m}^2\text{·s}^{-2})$	0.01671	$\pm 2.00.10^{-4}$
$X_{\text{crit}}(\text{Kg·m}^{-3})$	4.6	± 0.0992

Calculating the NSE for the complete settling curve yields to a value of 0.982 which indicates a good quality of the estimated parameters. The NSE for the hindered and
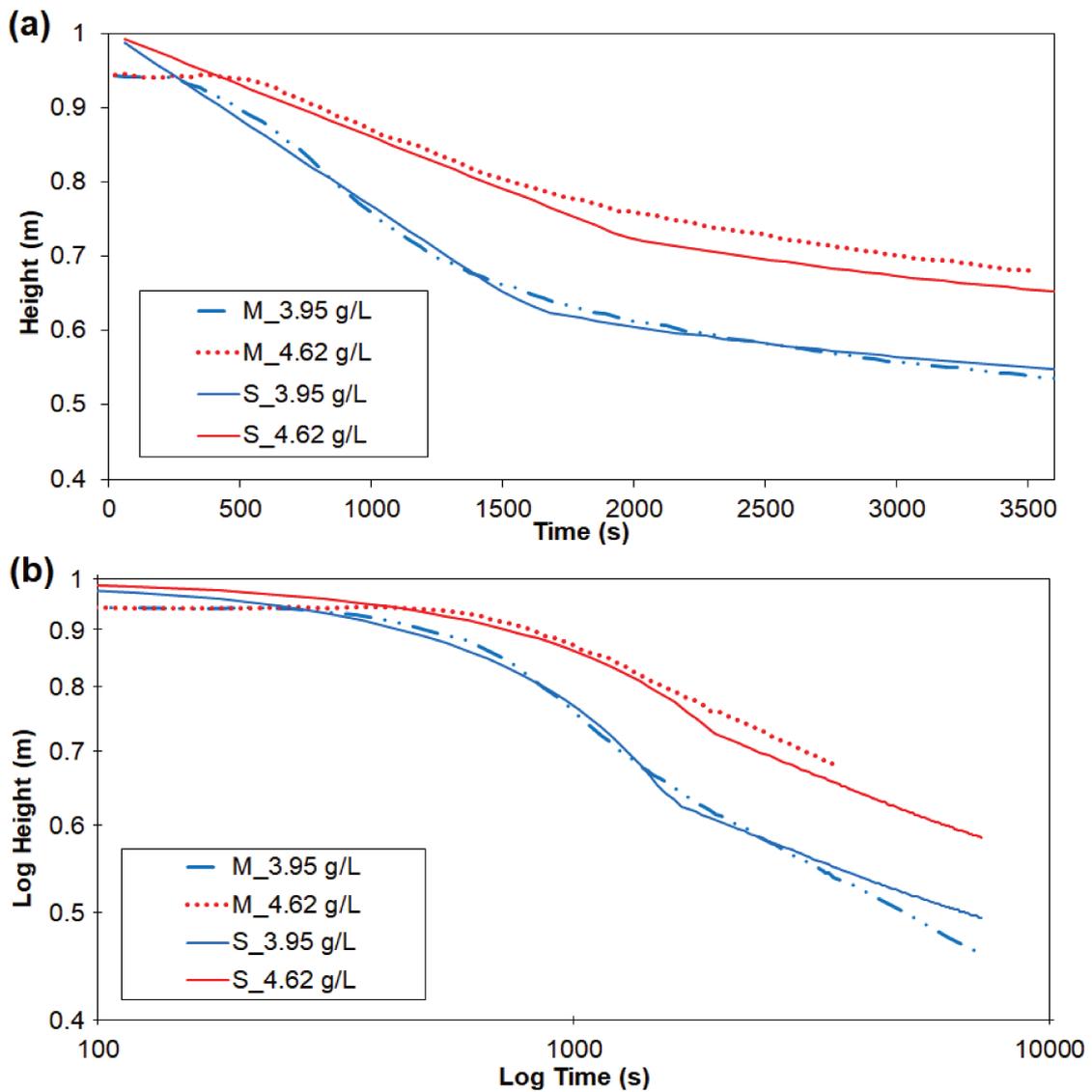
FIGURE 3.9: Simulated (continuous lines) and measured (symbols) settling curves at different initial concentrations in April. a)normal settling curve b) log-log settling curve.

(a)

(b)
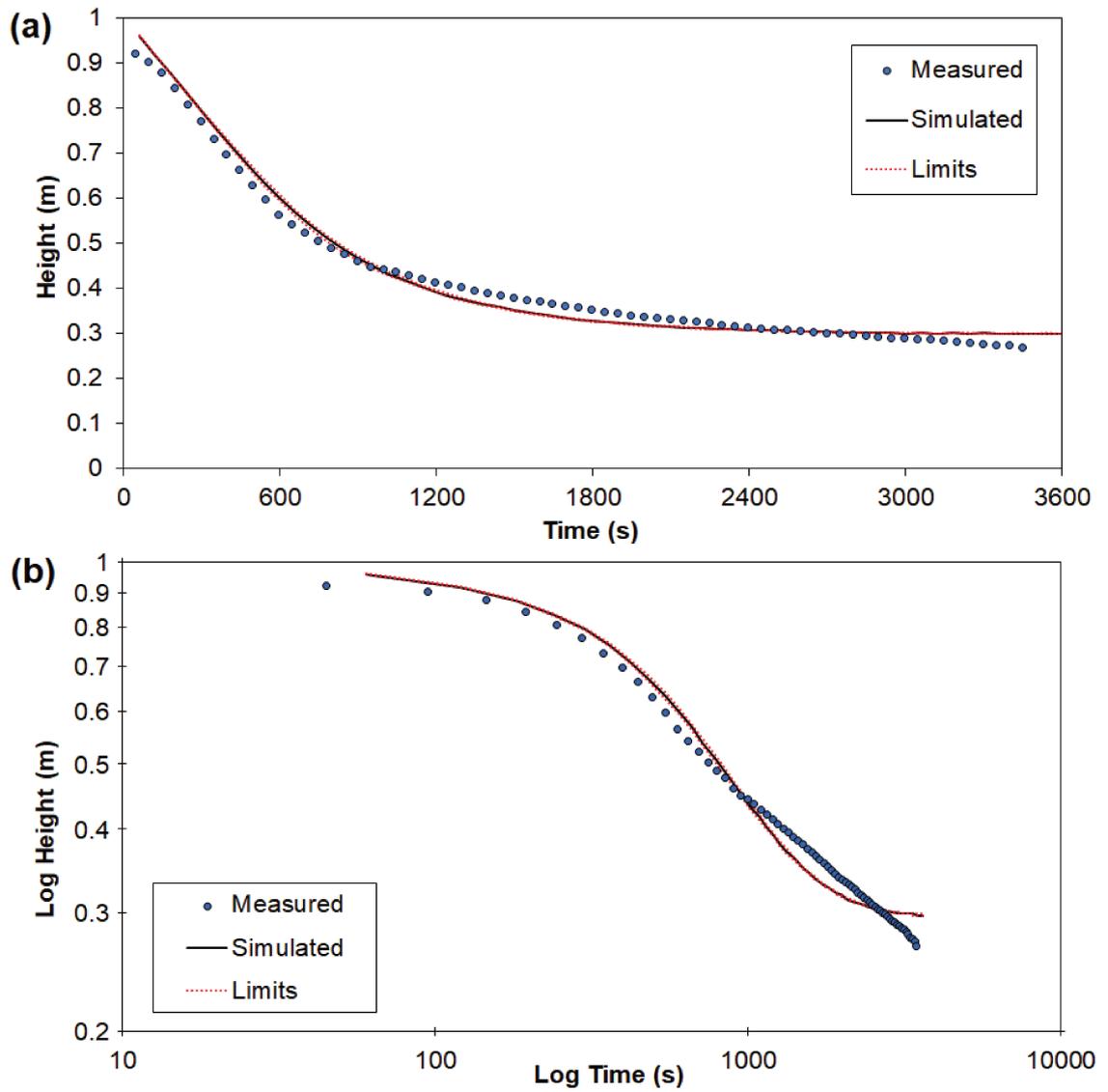
FIGURE 3.10: Measured and simulated settling curve at 1hour (October campaign). b) Log-Log settling curve for measured and simulated data during 11 hours of settling for X0 = 4.54 $Kg.m^{-3}$

compression zones are 0.933 and 0.916 respectively. As in the previous case, the estimated values perform a good simulation of the batch settling behavior within the first hour of settling. The low uncertainty of the estimated parameters ensures the good estimation of the parameters (dotted red lines figure 3.10).

The normal settling curve (figure 3.10a) shows the good fit of the predicted SBH, however after 1 hour it seems that the simulated height will be overestimated by the model. This can be confirmed with the log-log plot (figure 3.10b) in which the linear trend of the simulated curve is finished after 1800 seconds and not following the same trend as the experimental curve.
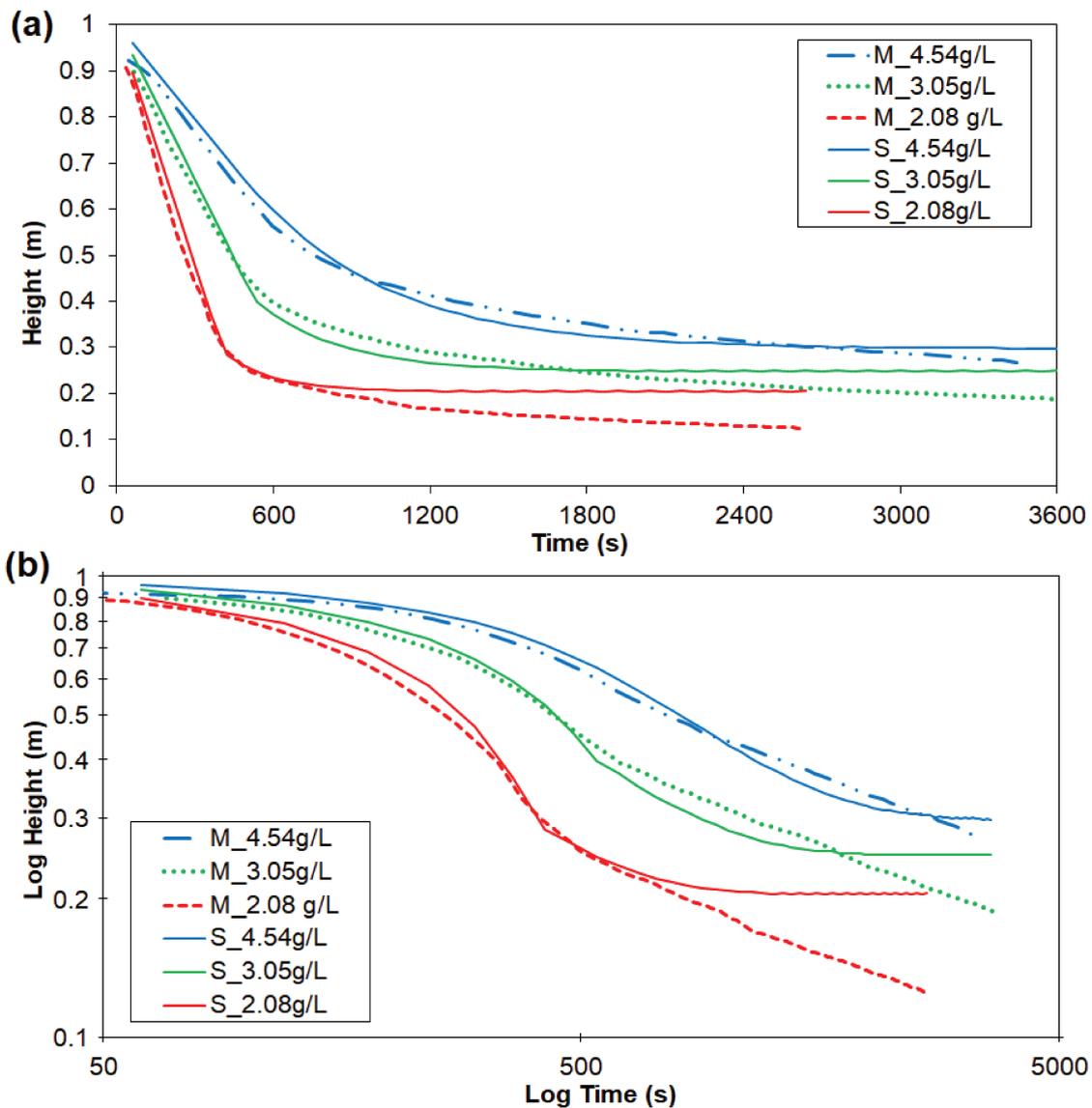
FIGURE 3.11: Simulated (continuous lines) and experimental (symbols) settling curves at different initial concentrations in October. a)normal settling curve b) log-log settling curve. The red lines indicate the 95% of confidence interval

Validation of the model is done with the two supplementary set of experimental data. Figure 3.11a shows the normal settling curves of the measured and predicted

sludge blanket for these additional initial concentrations. The parameters of the hindered settling can accurately describe the settling zone.

The log-log plot (figure 3.11b) illustrates again the power law behavior of the settling curves, and that the estimated parameters can accurately describe the hindered zone marked by the curvy trend of the line. The model can also reproduce accurately the compression curve within the first hour. However, the trend of the curve is to remain constant with time once in the compression regime.

For this sludge, it is observed that a unique set of compression parameters can accurately describe the sludge blanket height during the first settling hour for all sludge concentrations. However those parameters fails to predict an accurate SBH after one hour. This unsuccessful prediction is expected as the compression parameters do not change in time.

Ramin et al. (2014a) introduced a model with a varying critical concentration which is estimated in function of the initial concentration. Even if their model seems to overcome this problem, the approximation of X_{crit} being dependant of the initial concentration is not feasible in a full-size clarifier where the initial concentration is not know and a sludge blanket height is physically hard to track. (Refer to chapter 4 to see the problems when measuring the sludge blanket height in a full SST).

Locatelli (2015) implemented a time varying critical concentration model. The time dependant critical concentration was described with an empirical equation. The sludge blanket model predictions were successful for different parameters sets, but only within the first 3 hours of batch settling.

3.3.3   Validation on settling velocities for October data

The validation on the settling velocity in column presented here, only concerns the initial concentration at $X_0 = 4.54\,\text{Kg·m}^{-3}$ at two different times. The experimental velocity profiles are compared to the calibrated model, using the found values, and a model that do not use the compression function. The model without compression function employs the same calibrated parameters for the Diehl function used to simulate the hindered settling.

Both models do not follow the distribution of the settling velocities within the discrete and hindered zone, hence the ending of the hindered zone (represented by the vertical continuous line on figure 3.12-right) is overestimated. This is expected, the models do not calculate the individual particles velocities and thus the distribution is impossible to predict including the distribution in the hindered zone (Locatelli, 2015, Torfs et al., 2017). Only in the bottom of the column the model with the compression function predicts accurately the settling velocities, where such velocities mostly depend on the local sludge concentration.

However, after 44 minutes of settling (figure 3.12 right). The model do not predict a linear behavior of the velocities within the compression zone, and a discontinuity between the clear zone and the compression zone is created. This is due to the constant critical concentration through time.

Despite the fact that the prediction of the individual settling velocities are not included in both models, the model including the compression function, estimates better settling velocities when compared to a model that do not use the compression function (figure 3.12 black dotted line).

To evaluate the accuracy of the model, the Mean Absolute Error (MAE) is obtained, lower is the value closer the predicted values are to the measured ones. Such statistic measures how close the predicted values are to the measured ones by summing the absolute differences of the values, *i.e.*

$$MAE = \frac{\sum\limits_{i=1}^{n} |\vec{v}^{sim} - \vec{v}^{obs}|}{n} \tag{3.7}$$

where: $\vec{v}^{sim}$ and $\vec{v}^{obs}$ are the simulated and measured settling velocities respectively. At 5 minutes, the model within the compression function, shows a MAE of $3.68x10^{-4}$ within the compression part. Compared to the MAE ($8.75x10^{-3}$) of the model without compression function, the latter is clearly less accurate when predicting the particles settling velocities within a batch column.

The same evaluation made with the velocity profiles at 44 minutes is performed. The MAE are $3.15x10^{-4}$ and $8.58x10^{-3}$ for the model with compression and without compression function respectively. The model including the compression function is still more accurate for the predictions of the settling velocities even at longer times.

3.4   Conclusions

DAKOTA software was successfully coupled to a 1D model performed in Open-FOAM®. A local minimum gradient based method for parameter optimization was used. This allows to have a less computationally intensive process and obtain accurate values for the estimated parameters. DAKOTA constitutes a powerful tool that can be used also to perform a global optimization process opening a new opportunity for developers to study deeply the compression parameters in the OpenFOAM model.

The two calibration processes were made with different couples of settling functions (hindered + compression): this was because there was a lack of experimental points for some datasets. Calibration performed with equations of Vesilind (1968) and simplified form for σ_e of Declercq was chosen because only two sets of experimental
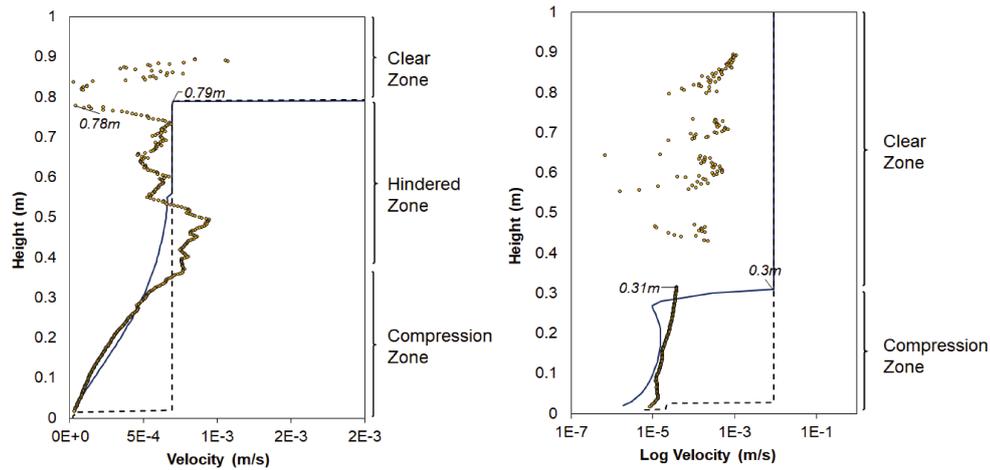
FIGURE 3.12: Settling velocity profiles at 5 (left) and 44 minutes (right). The Continuous blue line represent the model using a compression function. The black dotted line indicates the model without using the compression function and the symbols indicate the measured velocities. The height values indicates the beginning of the sludge blanket

data were available and this reduces the number degrees of freedom for the hindered settling model. Such settling model showed a good fit of the SBH within the first hour of batch settling. Validation in batch settling was hard to evaluate since only one set of experimental data was available. Using the calibrated parameters into a new experimental data set resulted in an underestimation of the SBH in the compression zone.

Calibration made with equations of Diehl (2015) and simplified form for σ_e of Declercq was chosen in order to follow the suggestions made by Torfs et al. (2017) when using the Bürger-Diehl framework (Bürger et al., 2013). As in the former calibration process, such model approach gave accurate results during the first hour of settling. The estimated parameters can predict accurately the SBH within the hindered zone when they are used in other experimental data set. However, they tend to overestimate the SBH in the compression zone.

One of the reasons why the model (in both approaches) is over predicting the SBH is because the critical concentration is modeled as a constant value in time. The research made by De Clercq (2006), Ramin et al. (2014a) and Locatelli et al. (2015) indicates that compression parameters should vary with time to obtain a more robust model. However, no physical evidence proves this statement. In Ramin et al. (2014a) approach the critical concentration is in function of the initial concentration, such suggestion is difficult to consider in a full-size clarifier due that a true initial concentration is impossible to identify.

Hence, the different nature of the sludge taken from the WRRF in different seasons made difficult to obtain a general relation between the concentration and the settling

velocity (higher is the concentration, lower is the settling velocity). The settling velocity is highly affected by the content in NVSS. Faster velocities were found when the content of NVSS was higher at similar MLSS concentrations. This behavior lead us to realize two calibration/validation processes with the sludge of Achenheim WRRF.

Identification problems can occur within the model, due to the fact that values for the optimized parameters depend on the initial guess. This is because a gradient based method tries to find a local minimum quantity of interest or cost function. However, the estimated parameters showed a good accuracy, the quality has been measured through the NSE statistic for the different settling zones and the complete settling curve, the values showed a very good evaluation (NSE > 0.75). Using a global sensitivity analysis was not within the scope of this study.

The flocculation state is a possible phenomenon that can explain the time-dependant compression parameters, this was included in a multiclass 1D settling model by Torfs et al. (2016). However, the same methodology would be hardly compatible with a drift-flux approach in CFD since to this stage there is no code to model the velocity of the different class of particles.

Nevertheless, it was decided to use the estimated parameters from the batch settling tests and 1D simulations presented here to simulate the intermittent operation of the full-scale WRRF (clarifier feeding and recirculation every 20 minutes). They can predict an accurate sludge blanket height within the first hour of settling which is in the order of magnitude of the sludge residence time within the clarifier.

Chapter 4

Hydrodynamic study of the full-scale Clarifier

4.1 Introduction

Within suspended growth biological processes, Secondary Settling Tanks (SST) must achieve sludge-water separation, biomass recycling and storage in case of hydraulic overloading. Hence, SST govern effluent quality in terms of suspended solids and indirectly in terms of biokinetic processes (Torfs et al., 2015a). Modelling this unit process is therefore essential to achieve an optimal operation of WRRF.

When using 1D models based on the Bürger-Diehl framework (Locatelli, 2015) (Torfs et al., 2017) to describe sludge settling behaviour, adding a compression function resulted in improved predictions of sludge blanket height in a settling column. In Torfs et al. (2015a), a 1D continuous flow simulation of a conventional activated sludge process is performed. It reveals that adding compression as constitutive function, greatly improves the sludge blanket height prediction when high loads are present into the clarifier, hence predicting a more realistic sludge concentration in the biological reactor.

Since the 70's, CFD has been used increasingly for analysis and design of water and wastewater treatment. Its use for mass transport modelling was visualized 20 years ago (Samstag et al., 2012). The advantage of such approach is that one can have an insight of the internal behavior of the tank. Secondary sedimentation was one of the first unit processes to be modelled using Computational Fluid Dynamics (CFD) (Samstag et al., 2016). However, to date, few CFDstudies incorporate a mechanistic compression equation to describe settling tanks and no validation of such a model exists at full-scale.

To optimize SST geometry and operation, CFD modelling is of great interest as it allows to capture the complex hydrodynamics within the clarifier. Even if it is considered that particles settling and the arriving flow is constant and uniform, regions

with high circulation exist and the flow field deviates from ideal uniform distribution (Tamayol, Firoozabadi, and Ashjari, 2010).

Some WRRF often operate with an intermittent flow, *i.e.* the inlet and recirculation flows are discontinuous, and depend on the period of the day. This is the case for small WRRFs, *e.g.*, in France, the 95% of the WRRF based on CAS technology have a capacity less than 9000 People Equivalent.

In small WRRF the inlet flow is controlled by a pumping station operating with on/off control according to the water level in the sump. Hence, the recirculation pump often also works discontinuously: the return activated sludge RAS flow-rate is constant but the pump operates only several minutes (5 to 30 minutes) per hour according to the inlet and RAS ratio. Thus, the discontinuous feeding and extraction is likely to impact both sludge blanket height and sludge inventory in the settling tank.

The objective of this chapter is to employ the CFD solver described in chapter 2 (Valle Medina and Laurent, 2020) including: hindered settling and mechanistic compression equations to simulate a full-scale SST operating discontinuously.

The small Achenheim WRRF, has a sequential flow, *i.e.*, depending on the upstream flow coming from the combined sewer network, level sensors will trigger one or two pumps to feed the tanks. Water is fed when the level on the pump station rises 1.3m and it stop when level is up to 0.8m.

Therefore, this intermittent behavior may affect the prediction of the sludge blanket height as well as the RAS concentration and the quality of the ESS. However, the quality of the ESS is not included in this approach since the model (described before in chapter 2) does not include the discrete settling modeling.

For this hydrodynamic simulation, the conditions of April and October 2018 experimental campaigns are presented. These experimental campaigns were held in order to gather data about the sludge blanket height and particles settling velocity.

The simulations with different sludge concentrations and boundary conditions were made to validate the data obtained in April and October. Thus, the cases were set as follows:

- **April**. First, a simulation with constant inflow (Q_{in}) and RAS flow (Q_r) was performed until the simulation reached the convergence. Departing from this state, another simulation with dynamic inflow and RAS flow during 24 hours was performed. Validation is made at different radial positions, only during the time were the experimental data was done, *i.e.* from 9:00-11:00 am.

- **October**. Also, a first simulation was performed to set the basis of the dynamic scenario, such simulation is finished when a constant SBH and RAS are

observed. Thus, the dynamic scenario deals with the intermittent inflow and RAS flow of the Achenheim WRRF during 51 continuous hours.

According to the mass balance, the incoming flow to the clarifier (Q_{in}) is calculated as follows:

$$Q_{in} = Q + Q_r \tag{4.1}$$

Where Q is the incoming flow to the wastewater treatment plant, Q_{in} is the incoming flow to the clarifier, Q_r is the recirculation flow of the activated sludge (RAS). Thus, Q is equal to Q_e, which is the effluent flow.

The MLSS concentration coming into the clarifier will be noted by X_{in}. The sludge concentration at the removal/recirculation is represented by X_r and the sludge concentration at the effluent will be X_e. However, the model does not include the prediction on the X_e, thus this parameter may be not mentioned later. A representation of the dynamics of the CAS process in given in figure 4.1.
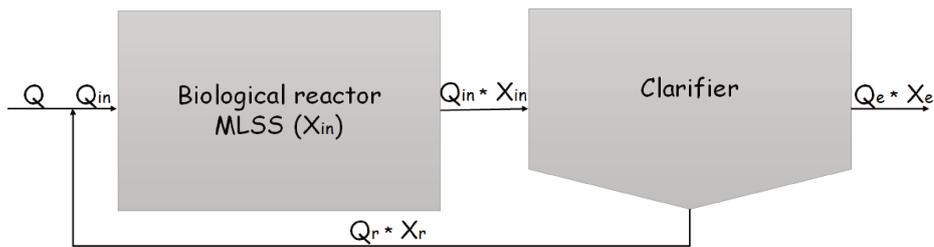
FIGURE 4.1: Representation of the flow configuration in the CAS process

The turbulence and viscosity models are kept the same for the three different cases. The settling model parameters (hindered, compression) are those calibrated using the batch settling test as presented in chapter 3. The numerical solution and algorithms are also kept the same, however because of the changing inflow the CFL conditions may be modified.

4.2 Materials and methods

4.2.1 Achenheim WRRF and Clarifier description

The Achenheim WRRF is located 13 Km far from the city of Strasbourg in France. Its capacity is of 9930 people-equivalent and it has a design average flow of $2735 \, m^{-3} \cdot d^{-1}$ ($114 \, m^{-3} \cdot h^{-1}$) and a design peak flow of $200 \, m^{-3} \cdot h^{-1}$.

The wastewater treatment is based on a conventional activated sludge process performing biological nitrogen removal through nitrification/denitrification process and

chemical phosphorus removal with iron chloride (*FeCl₃*). Wastewater comes from a combined sewage network of domestic places and some wineries.

The process of wastewater treatment is as follows:

- Wastewater arrives first to a pumping station where level sensors control pumps operation based on on/off control.

- Then, water passes to an automatic screening to retain solids larger than 1cm.

- Water is conducted to a dissolved air flotation tank for grit and greases removal.

- Wastewater arrives to a cylindrical biological reactor composed of two zones: one external aerobic zone for carbon and nitrogen removal (alternate aeration for nitrification/denitrification), and an internal anaerobic zone for enhanced biological phosphorus removal . Iron chloride is added to the mixture for PO_4^{3-} precipitation.

- The mixed liquor suspension passes through a degasser before entering the secondary clarifier

- Treated water is finally released in the receiving aquatic medium which is the Bruche canal.

Effluent quality limits should fulfill the *Arreté du 21 juillet 2015*, which is the French national regulation, and should also fulfill the local regulation for discharging the treated wastewater into the water sources (see table 4.1).

The dimensions and design parameters of Achenheim WRRF are listed on table 4.2. Image 4.2 shows an aerial view of the Achenheim WRFF. The red circle encloses the secondary settling tank. The yellow circle confines the biological treatment.

TABLE 4.1: French national and local effluent quality limits concentrations. All limits are in mg·L^{-1}

Biological Oxygen Demand BOD5	25
Chemical Oxygen Demand COD	100
Total Suspended Solids TSS	30
Ammonium $N - NH_4$	10
Total Phosphorus	2

Achenheim Clarifier

The cylindro-conical clarifier is 21.4m of diameter, the height at the center and near the external walls is 3.8m and 3m respectively (Figure 4.3). The inflow (Q_{in}), enters through a center feed well at design average velocity of 0.0109m·s^{-1}. The inlet is limited by an internal baffle in order to reduce the velocity and turbulence of the mixture to allow quiescent conditions. An external baffle is placed near the outlet to

TABLE 4.2: Achenheim WRRF design parameters and biological reactor dimensions

Maximum Peak flow in dry weather	165	$m^3 \cdot h^{-1}$
Maximum Peak flow in wet weather	220	$m^3 \cdot h^{-1}$
Average flow in dry weather	114	$m^3 \cdot h^{-1}$
COD maximum load capacity	1022	$kg \cdot d^{-1}$
Volume of the aerobic tank	3085	m^3
Volume of the anaerobic and contact tank	375	m^3
Hydraulic retention time in the biological tanks	53.2	h
Sludge concentration in biological treatment	$4 - 6$	$Kg \cdot m^{-3}$

FIGURE 4.2: Aerial view of the Achenheim WRRF

avoid floating particles to escape into the treated stream. The sludge at the bottom of the clarifier is conducted to the center by a scrapper (which velocity is 3 revolutions per hour). The RAS flow (Q_r) is designed to be 1.15 times Q_{in}. The design variables of the clarifier are listed in table 4.3

<div align="center">TABLE 4.3: Clarifier dimensions and design parameters</div>

Clarifier volume	1200	m^3
Maximum peak RAS flow rate in dry weather	190	$m^3 \cdot h^{-1}$
Average RAS flow rate in dry weather	130	$m^3 \cdot h^{-1}$
Diameter	21.4	m
Surface area	330	m^2
Design Hydraulic retention time	3.87	h
Maximum peak surface overflow rate	0.61	$m \cdot h^{-1}$
Average peak surface overflow rate	0.31	$m \cdot h^{-1}$

4.2.2 Experimental campaigns carried on SST

Several experimental campaigns were carried out from January to October 2018 in order to study the behavior of the sludge blanket and the settling velocities inside the clarifier. The measurement campaigns can be divided in two arrangements:

1. Punctual measurements

2. Continuous measurements.

Punctual measurements

Four experimental campaigns: one in January, one in February, one in April and one in August were done using the following methodology:

For each campaign the same ultrasonic transducer used for batch experiments (chapter 3), was employed to track the vertical velocity and amplitude of the particles in the clarifier. The ultrasonic transducer device was placed, vertically, over the surface of the water at three radial distances: 3.5m, 7.4m and 8.6m from the inlet.

To perform the measurements at 7.4m and 8.6m, the ultrasonic device was held on a vertical aluminum tube which is fixed to 4m long horizontal tube, we will call this ensemble "big T". The horizontal tube was fixed as well, to a heavy base standing outside of the clarifier (figure 4.4). The length of the horizontal tube was adjustable. The "big T" was pushed manually into the clarifier just right after the skimmer of the clarifier has passed by. Once the "big T" stopped shaking from the former movement, the data acquisition began. The acquisition time lasted around 20 minutes which is the time for the skimmer to perform a complete tour of the clarifier. In this manner, the settling process is not perturbed by a sudden stop of the skimmer.
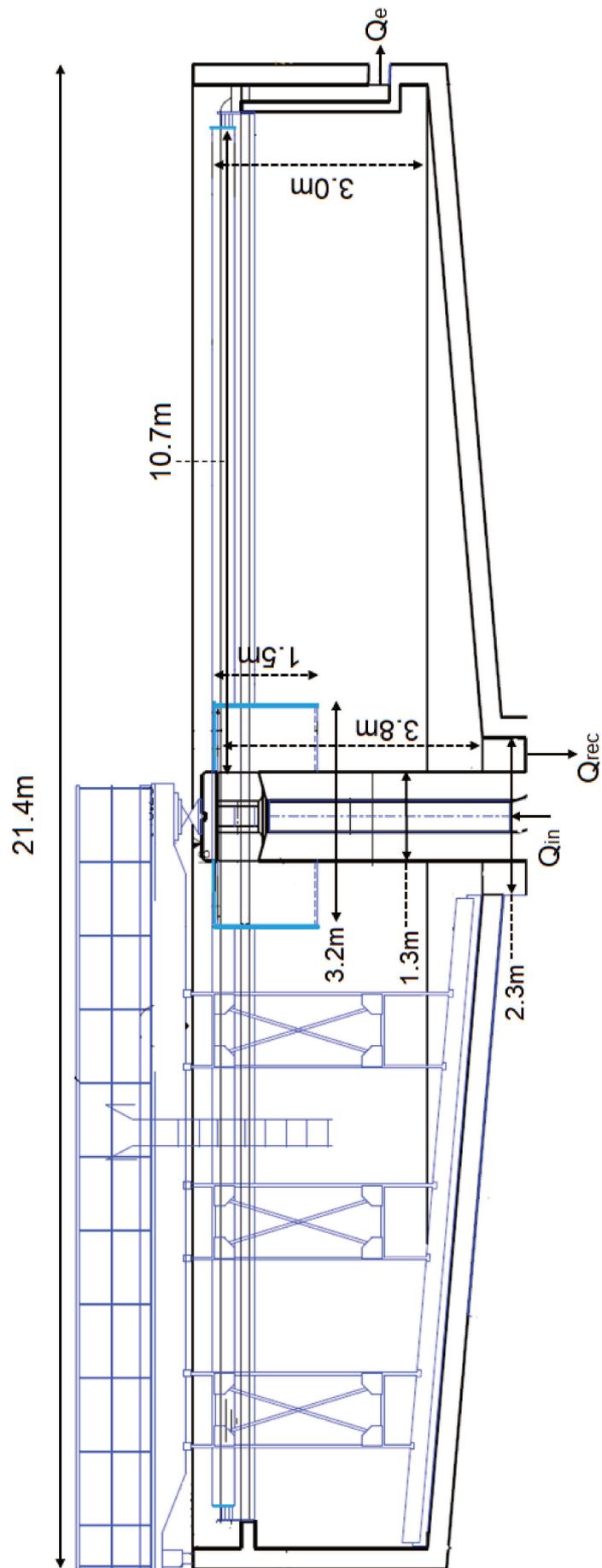
FIGURE 4.3: Main dimensions of Achenheim SST

FIGURE 4.4: Layout for the data acquisition system

The measuring process at a radial distance of 3.5 m was different because the length of the horizontal tube was not enough to reach this distance. Therefore, we asked the operators of the WRRF to stop for a moment the movement of the scraper. Then we placed only the "big L" over the scraper and after it stopped shaking, the data acquisition began. The acquisition process at this position finished after 30 minutes.

Unfortunately, the data acquired in January, February and August is not representative: it was hard to obtain a real value of the sludge blanket height and no particles velocities were recorded. Therefore, the experimental results presented here concern only the campaign carried on during the morning of April 6th 2018 from 8h00 to 13h00.

The water temperature at the surface of the clarifier was 10.8°C during the test carried out in April and the water temperature in October was 16°C. Settling velocity is temperature dependent, therefore the obtained velocity values from the transducer shall be corrected, *i.e.*, the measured velocity is adjusted by the sound velocity at 25°C.

On-site data acquisition

The features of the ultrasonic device used for this experimental campaign appear on table 4.4. The procedure to obtain the data for the amplitude and particles settling velocity is the same described in section 3.2.2

Figure 4.5, illustrates an example of how the recorded values can be interpreted. The amplitude profile obtained during the data acquisition process at a radial position of 8.6m is shown at a given time. The high amplitude value found at 1.70m depth corresponds to the beginning of the sludge blanket. Another amplitude peak is observed at 3.5m indicating the bottom of the clarifier. If the amplitude profile is

TABLE 4.4: Configuration of the ultrasonic transducer used in the clarifier.

Sensor diameter	1 cm
Maximum Pulse Repetition Frequency +	300 Hz
Maximum Pulse Repetition Frequency$_{eff}$*	15 Hz
Maximum measurable velocity	0.001 m/s
Central frequency	1.565 MHz
Carrier frequency	1.25MHz
Spatial Resolution	1 cm
Time Resolution	1 s
+ Number of ultrasonic bursts emitted per second	
* Number of emitted ultrasonic bursts recorded per second	

decreasing from the upper part of the SBH to the bottom, it is due to the diffusion of the ultrasounds induced by the particles.
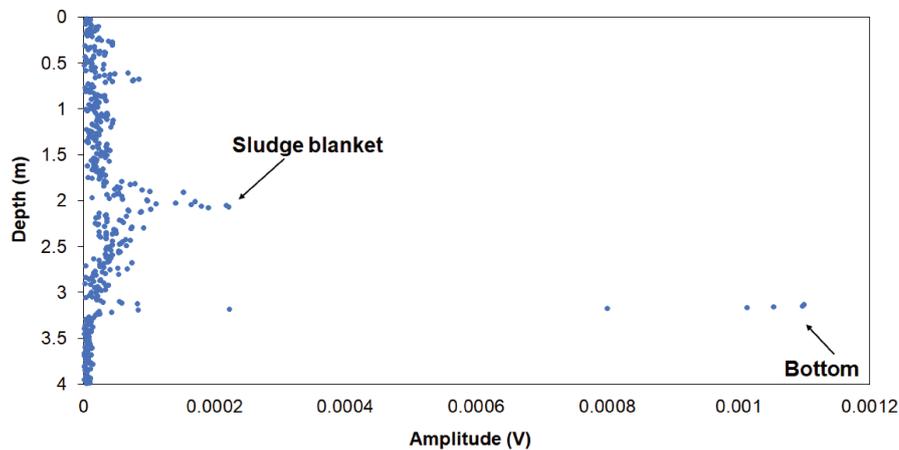
FIGURE 4.5: Amplitude profile measured at the clarifier at a given time

Continuous measurements

Continuous particle velocities and amplitude measurements began at 11h00 on October 17th and ended at 14h00 on October 19th. To get the continuous measurements, a different system (Peacok UVP device developed by Ubertone, France® www.ubertone.com) was installed in the clarifier.

The Peacok UVP system consists of an electronic system, two ultrasonic transducers (centered at 1.5MHz and 500kHz) and a battery powered logger (figure 4.7). This device, is based on coded pulsed coherent Doppler system (Burckbuchler and Fischer, 2017) and gives access to the acoustic turbidity through the backscattered ultrasonic energy from the suspended particles. The procedure in how the ultrasonic

device obtains the amplitude and velocity information is the same described in section 3.2.2. One of the advantages of this system is that data can be recorded online and no power connection is needed.

The Peacok UVP device was placed at 3.5m away from the centre of the clarifier on the skimmer. A vertical support containing the ultrasonic transducers was held on the skimmer and placed over the water surface in a vertical position. Due to the skimmer motion, the device tracked the sludge blanket height and particles settling velocity in a radial way (figure 4.6).

FIGURE 4.6: Overview of the support and Peacock UVP system placed in the clarifier

Measurements were performed at three different carrier frequencies (f_0), 1.64MHz, 1.29MHz and 0.5MHz. According to Pallares et al., 2017 the radius of a particle can be correlated to the frequency of the acoustic signal but this has been made only with regular particles. The results presented here concerns just to one frequency emission, 1.64 MHz. No significant differences in the values of the velocities or blanket height were found at the other carrier frequencies (f_0). The characteristics of the transducer using the carrier frequency of 1.64MHz are in table 4.5

TABLE 4.5: Characteristics of the ultrasonic transducer used at a carrier frequency of 1.64MHz

Setting	Value
Sensor Diameter	2 cm
Central frequency	0.5 MHz
Maximum PRF	50 Hz
Interval of measured velocities	$-2.0.10^{-2}$ to $2.53.10^{-3}$ m.s^{-1}
Time Resolution	45 s
Spacial Resolution	2 cm

The vertical orientation of the device means that only the vertical velocity is recorded. Positive velocities indicates a direction towards the transducer.
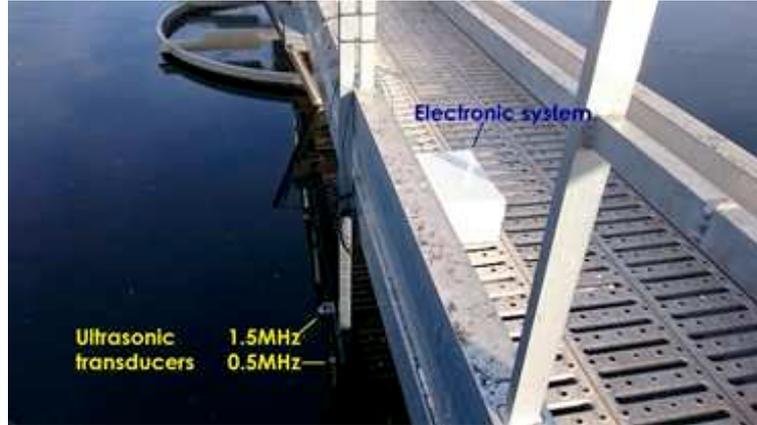
FIGURE 4.7: Layout of the Peacok UVP system placed in the skimmer of the clarifier

4.2.3 Sludge rheology measurements

Sludge rheology is an important characteristic impacting the description of the fluid domain (the viscous tensors intervene in the momentum equations). The sludge viscosity was determined experimentally by using an AR2000 (TA Instruments) rheometer. Such rheometer uses a double plate geometry with a gap of 2.0mm which rotates progressively until a maximum shear rate (Locatelli, 2015).

The rheology test was only made with the sludge samples from April. Thus, the viscosity of same samples used for the batch experiment (section 3.3.1) was measured. The samples were sieved at 2mm prior to testing. The initial operating conditions for the rheometer are in table 4.6.

TABLE 4.6: Rheometer Characteristics

Setting	Parameter
Plate diameter	2cm
Gap	2mm
Temperature	20°C
Pre-shear duration	1 min
Accelaration mode	Linear
Maximum shear rate	$500s^{-1}$
Duration of the ramp	5 min

The evolution of the shear stress with respect to the shear rate for one of the sludge samples can be observed in figure 4.8. The point corresponding to the intercept of the curve is considered as the yield stress (τ) and the slope of the curve is the apparent viscosity (μ_0). The sludge presents a viscoelastic behavior at the beginning of the test. After crossing the shear stress of $100\,s^{-1}$ the behavior is plastic, thus the sludge can be considered as a plastic fluid.

The apparent viscosity and the yield stress can be both related to the sludge concentration in an exponential equation (figure 4.9). Table 4.7 shows the values of the
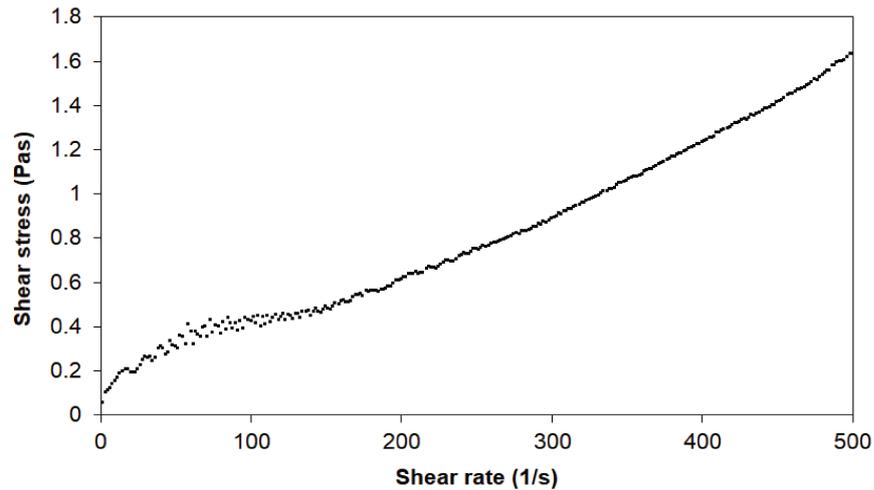
FIGURE 4.8: Rheogram for the sludge sample at initial concentration of $5.54 Kg.m^{-3}$

parameters of the models. For the simulations, an equation type Bokil and Bewtra (1972) is used to model the sludge rheology:

$$\mu_0 = C_1.10^{C_2 X} \qquad (4.2)$$

The values used for parameters C_1 and C_2 are in table 4.7.
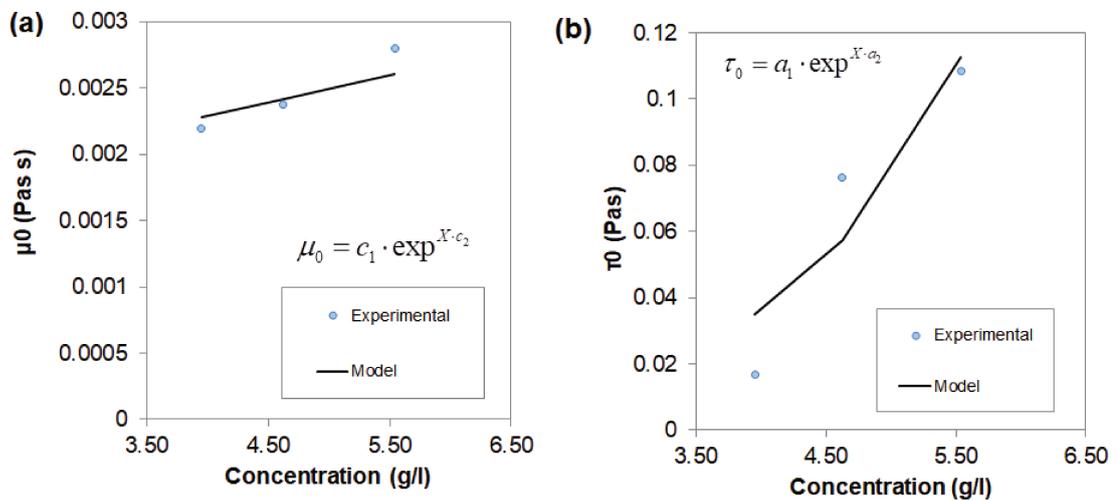
FIGURE 4.9: Relation a) Concentration and apparent viscosity and b) Concentration and yield stress for the sludge samples taken in April 2018

The found values for the yield stress and apparent viscosity of the activated sludge are sightly slower to those reported in Khalili-Garakani et al. (2011).

TABLE 4.7: Parameters for the viscosity models

Parameter	Value
C_1	0.0017Pass
C_2	0.0852L·g^{-1}
A_1	0.0019Pas
A_2	0.432L·g^{-1}

4.2.4 CFD Simulation Description

Sludge Settling Model

The settling model used for the simulations is the one described in section 2.1.3. The objective is to validate the model, with the calibrated parameters found in the batch settling column, with the measurements taken in the full-size clarifier. April and October experimental campaigns conditions are simulated using the same model functions and parameters described in section 3.3.1.

Sludge Rheology Model

Sludge viscosity is modeled by a plastic model, *i.e.* the yield stress of the sludge is not considered. The Bokil and Bewtra (1972) equation 4.2, is used to describe the relation between the apparent viscosity (μ_0) and the MLSS concentration. μ_0 increases exponentially with the MLSS concentration. One advantage of the equation is that it has only two parameters and is valid for sludge concentrations above 0.7 kg·m^{-3}.

The values of the parameters C_1 and C_2 used for the simulations are presented in table 4.7. However, in the OpenFOAM code, equation 4.2 is computed in function of the volume fraction of the mixture (α) and is based 10.

The sludge density used for the simulations was 1010 Kg·m^{-3} (based on the values obtained experimentally). The considered water density is 998 Kg·m$-$3.

Geometry meshing

To reduce the computational cost of the simulation, an axisymmetric representation (known as 2D or quasi3D model) was chosen. The same dimensions illustrated in figure (4.3) are used to build the geometry and mesh. The scrapper is not included in the mesh.

To construct the mesh, again the snappyHexMesh tool from OpenFOAM was used. First a rectangular 3D block of the half part of the clarifier (from the middle to the external wall) was built. Perfect squared corners are needed in the intersection of three limits therefore refinement is done in the external and internal baffles (figure

102
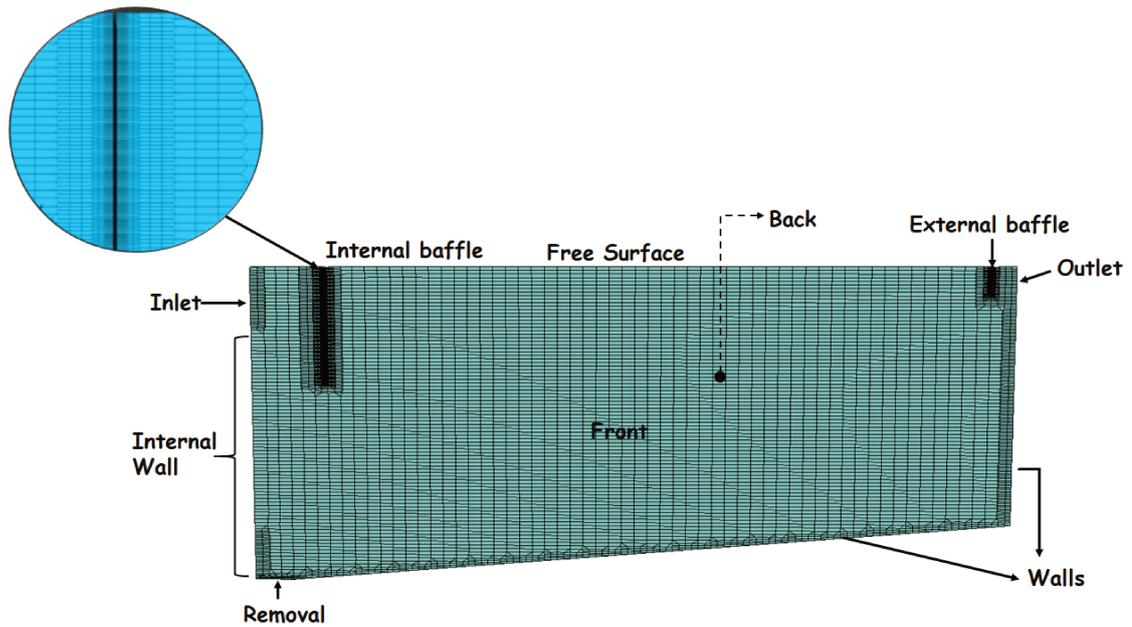
FIGURE 4.10: Mesh of the Achenheim clarifier. Refinement is required near the walls of the geometry. A zoom is made into the internal baffles.

4.10). This is important, because failure in this step may produce a bad quality axisymmetric mesh.

Three main aspects can be evaluated numerically within the mesh (www.openfoamwiki.net):

- *Aspect Ratio.* It is a qualitative measure indicating the ratio between the longest and the shortest length. Or in a 2D approach, it is the ratio between the biggest and the smallest area of the cell. A value of 1 is considered the best.

- *Non-Orthogonality.* Measures the angle between the line connecting two cell centres and the normal of their common face by following this criteria :

  – Non-Orthogonality < 70, indicates safe values

  – 70 < Non-Orthogonality < 90, need numerical correction controlled in the files fvSolution and fvSchemes.

  – Non-Orthogonality > 90, bad mesh not useful for simulation

- *Skewness.* Measures the distance between the intersection of the line connecting two cell centres with their common face and the centre of that face. High values (> 20) of this parameter affect the accuracy of the results.

Thus, the quality of the rectangular mesh is:

- Aspect Ratio = 9.15

- Non-Orthogonality = 14.63

- Skewness = 18.09

The mesh can be evaluated with good quality and therefore it can be used for the next step.

The mesh was extruded in a radial manner with an angle of 5° in the z direction to account just for one cell thickness to create the axisymmetric configuration (figure 4.11b).
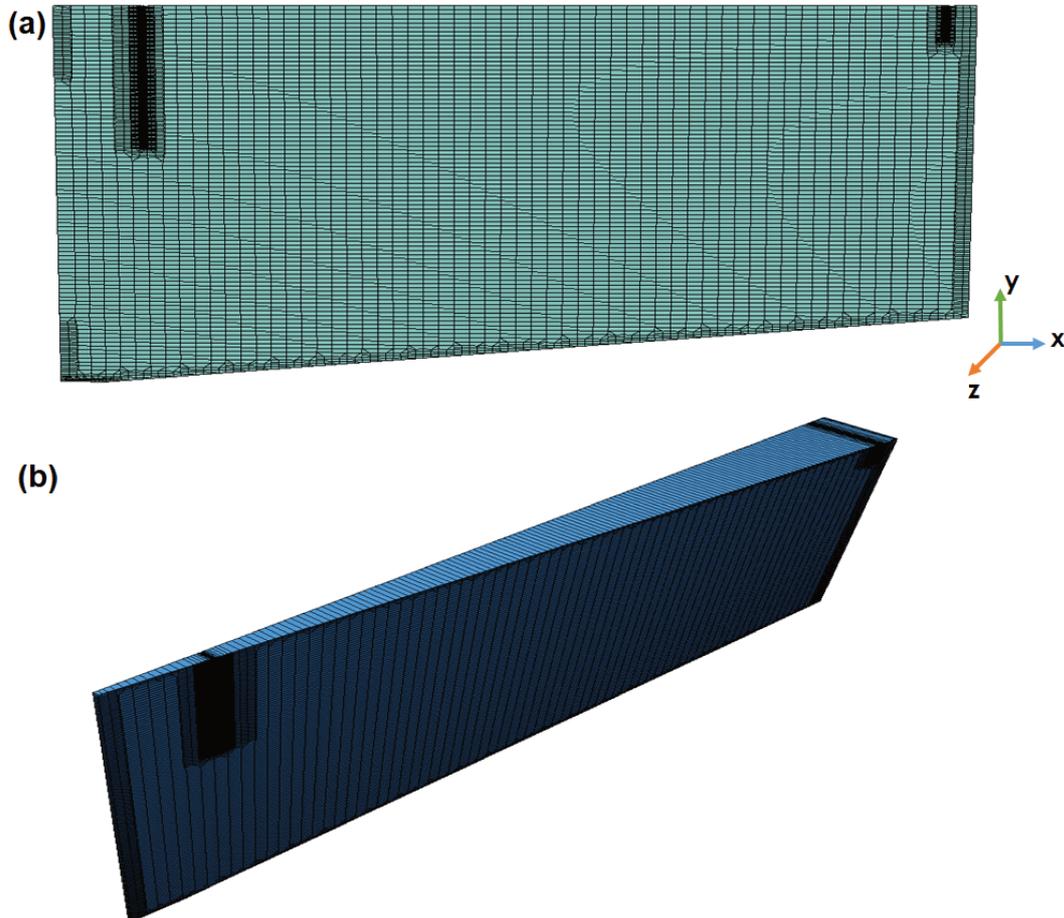
FIGURE 4.11: a) Frontal view of the mesh b) Mesh extrusion into 1 cell thick in the z-direction.

The quality of the axisymmetric mesh is:

- Aspect Ratio = 13.06

- Non-Orthogonality = 14.51

- Skewness = 2.72

Then, different meshes of 7970, 8897 and 12816 cells were used to assess the mesh independence of the simulations. A t-test is used to determine if there is no significant differences among the predicted results of the meshes. Comparison is made on:

- The vertical volume fraction profile at 5400s in a radial distance of 5m;

- The RAS volume fraction.

The p-value is calculated to determine if the differences between the variances are likely or unlikely. For this test, if the p-value is > 0.05 then the variances are not different and we consider that the meshes do not produce different results.

Table 4.8, shows the p-value when comparing the variances of the different couples of the three different meshes for both concentration profile and RAS concentration. The found p-values are higher than 0.05, thus no significant differences are found when changing the mesh. Therefore, the coarsest mesh can be used in order to reduce the computational time.

TABLE 4.8: P-values for the t-student test to compare the variances of the calculated RAS volume fraction and the volume fraction profile.

Couple of meshes	RAS Volume fraction	Volume fraction profile
7970-8897	0.9264	0.9787
7970-12816	0.7796	0.9692
8897-12816	0.7130	0.9479

Thus, the axisymmetric mesh of 7970 cells, which average cell dimensions are 16.34cm in the horizontal direction and 4.48cm in the vertical direction is used. The smallest cells (refinements near the baffles) dimensions are: 1.51 and 0.56cm in the horizontal and vertical axes respectively.

Turbulence Model

The same buoyancy k-epsilon model described in section 1.6.2 is used for all the simulation cases. Buoyancy effect can occur due to the sediment-induced density differences (Lakehal et al., 1999). Indeed, under the influence of the gravity, a particle having a density higher than the surroundings will settle faster, until the buoyancy force equals the drag force. Therefore, an important force shaping the flow field is the buoyancy, this is produced when the density ratio between the phases is low and the drag between them is high (Brennan, 2001).

General boundary conditions for the simulation cases

Boundary conditions have to be set to each one of the patches constituting the geometry of the 2D axisymmetric clarifier (figure 4.10). Table 4.11 summarizes the input set to the base case. The description of those boundary conditions appear below the table.

The initial sludge concentrations are $5.54 \, \mathrm{Kg \cdot m^{-3}}$ for April simulations and $4.54 \, \mathrm{Kg \cdot m^{-3}}$ for October simulations.

The boundary condition for the velocity of the incoming flow ($\vec{v}_{\mathrm{in}}$) depends on the configuration and is calculated as the ratio of Q_{in} and the sectional area of the inlet A_{in}

A base case for both campaigns was simulated. For this, a constant velocity is imposed at the inlet and the removal patches. The velocity of the fluid is calculated using the average measured flows for Q and Q_r taken from the WRRF during the days where the experimental tests were carried on. The simulation was over when the convergence was reached (a constant SBH and RAS through time was observed)

The selected values appear on table 4.9

TABLE 4.9: Average measured flows during the campaigns carried on in April and October

	April	October
$Q\,\mathrm{m^3 \cdot h^{-1}}$	58	52
$Q_r\,\mathrm{m^3 \cdot h^{-1}}$	62	63

A brief summary of the different cases discussed within this chapter is on table 4.10:

TABLE 4.10: Summary of the simulated cases for validation

Case	Type of experimental data acquisiton for validation	Settling model Coupling	Type of Hydrodynamic simulation
Section 4.3.1	No applicable	Vesilind and Simplified form of DeClercq	Constant flow
Section 4.3.1	Punctual Measurements	Vesilind and Simplified form of DeClercq	Dyanmic flow
Section 4.3.2	No applicable	Diehl and Simplified form of DeClercq	Constant flow
Section 4.3.2	Continuous Measurements	Diehl and Simplified form of DeClercq	Dyanmic flow

TABLE 4.11: Boundary conditions for the base case (continuous inflow). In brackets () the name of the variable in OpenFOAM

Patch	Volume Fraction (alpha.sludge)	Velocity (U)	Pressure (p_rgh)	Kinetic turbulent energy (k)	Dissipation rate of k (epsilon)	Kinematic Viscosity (nut)
Inlet	Fixed value	Fixed value	zeroGradient	Fixed value	Fixed value	Calculated
Outlet	zeroGradient	zeroGradient	Fixed Value to 0	zeroGradient	zeroGradient	zeroGradient
Removal	zeroGradient	Fixed Value	zeroGradient	zeroGradient	zeroGradient	zeroGradient
Baffles and Walls	zeroGradient	Non-slip condition	zeroGradient	kqRWallFunction	epsilonWallFunction	nutkWallFunction
Free surface	Symmetry					
Front and Back	Wedge					

Fixed Value. It is a specified value of the variable. It must be always expressed in international system units.

ZeroGradient. This boundary condition extrapolates a quantity to the patch from the nearest cell value: the quantity is developed in space and its gradient is equal to zero in the normal direction of the boundary.

No-Slip. It is an alternative to the zero fixedValue boundary condition for velocity. There is no difference between them. It is applied only in the wall patch.

WallFunctions. When wall turbulence modeling, the distance from the wall to the cell centers next to the wall is stored as part of the patch. *kqRWallFunction*, acts as a zero-gradient condition at the wall. *epsilonWallFunction*, calculates epsilon and such values are added into the matrix to act as a constraint, and *nutkWallFunction* is a condition for kinematic viscosity

Calculated. It is a condition in which OpenFOAM is calculating automatically the estimated value derived from other fields.

Symmetry. This is a symmetry plane.

Wedge. Used for axisymmetric cases, the geometry is specified as a wedge of small angle (e.g. $< 5°$) and 1 cell thick running along the plane of symmetry, straddling one of the coordinate planes (OpenFOAM Manual). OpenFOAM understand that radial coordinates should be employed.

To simulate the dynamic flow behaviour, within the simulation the values of Q and Q_r changed in time. Flow values where chosen according to the real behavior of the WRRF flows during the experimentation days for both April (figure 4.12a) and October (figure 4.12b) campaigns.
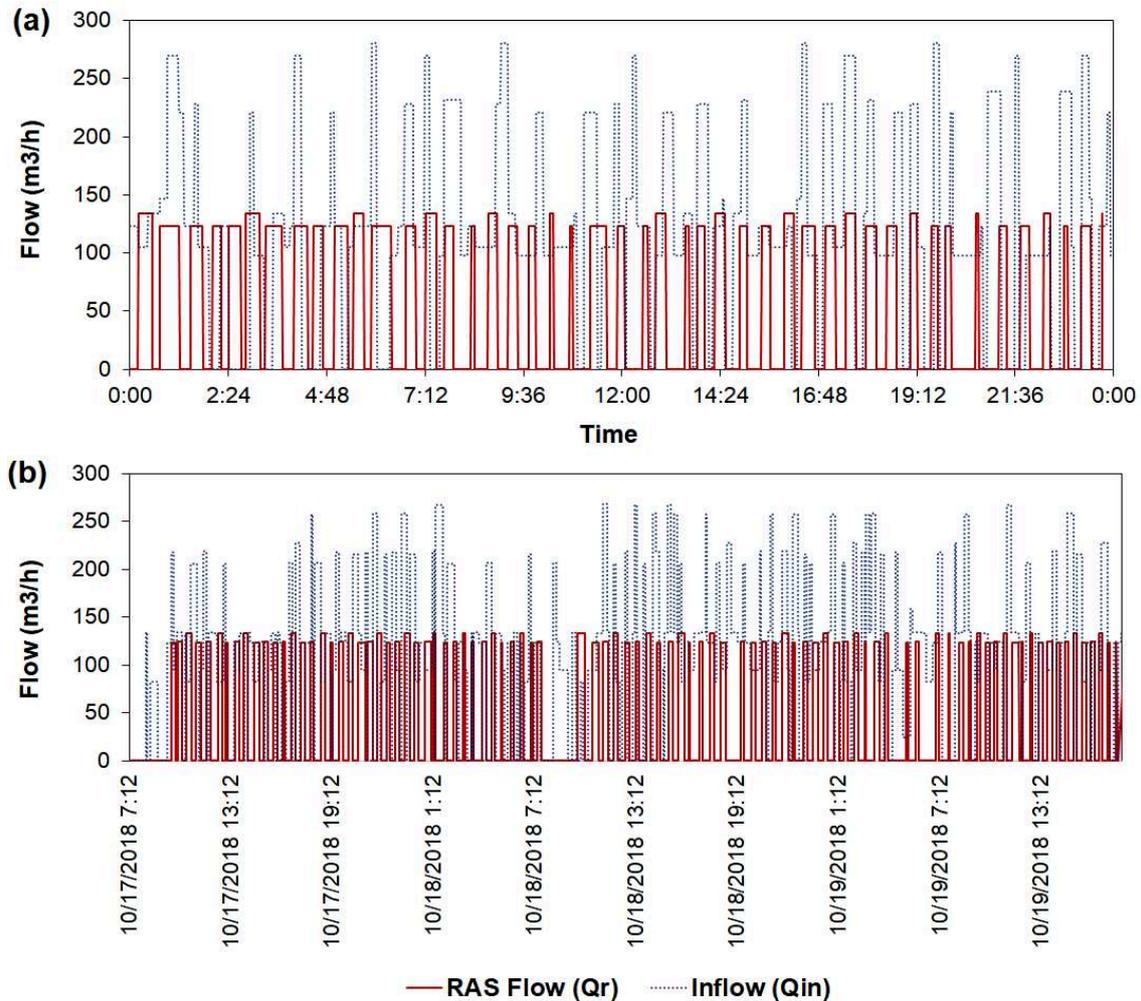
FIGURE 4.12: Clarifier and Recirculation flow during a) April 6th 2018 and b) 17th to 19th October 2018

In OpenFOAM a fixed value for velocity (U) has to be set for each time when the inflow/RAS flow is changing, therefore for the simulations held in April and October, the velocity values are set according to figure 4.12a and figure 4.12b respectively. The rest of the boundary conditions are set according to table 4.11.

4.3 Results

4.3.1 Punctual measurements results (April 2018)

Experimental Data results

Figure 4.13 shows the evolution of the amplitude during the test in the clarifier when the ultrasonic transducer was placed at 8.6 m away from the inlet. There is a clear line in the graphic with high values of amplitude (0.0011V) that indicates the bottom of the clarifier position at 3.1 m. Another constant line is observed at 1.8 m, with smaller values of amplitude ($\simeq 0.0002V$) indicating the sludge blanket height.

The maximum particle settling velocities values found were around $0.001\,12\,\text{m·s}^{-1}$ whatever the transducer position and the measurement depth.

The blue "*curtain*" all over the depth of the clarifier observed after 15 minutes is maybe due to particle dispersion cause by the inertia when the extraction pump is off. This coincides exactly when the pump is inactive.

Figure 4.14 shows the evolution of the settling velocities measured at 8.6m from the clarifier inlet. During the first 15 minutes, the sludge particles show high velocities towards the bottom of the tank. Those velocities are increased probably because of the recirculation pump, which is active during this period. After 15 minutes, the particles seem to settle slower and particles velocities seem to be more disperse within the blanket and the clear zone. This moment coincides with the stopping of the extraction pump.

During all the test, a periodic behavior with negative-positive velocities is observed more less every 30 seconds. Positive velocities indicates a direction towards the bottom of the clarifier. Thus, particles are settling and rising within the sludge blanket. The behaviour might be produced by the density currents (differences in densities of the water-sludge) created in the surface of the SBH.

The mean settling velocities found within the sludge blanket measured at 8.6m are around $0.0005\,\text{m·s}^{-1}$ which are a hundred times higher than those found in batch column. This indicates that not only the particles settling velocity takes action within the sedimentation process, but also the incoming velocity of the mixture, density currents and/or the advective transport due to recirculation flow.

Figures 4.15 and 4.16 show the amplitude and settling velocities of the sludge particles respectively, measured at 3.5m away from the inlet. The sludge blanket surface is at 1.7m. The bottom of the tank was not observed during this measurement.

During the first 7 minutes, particle velocities are observed at the bottom of the tank. The recirculation pump was active during this time. After 7 minutes, the velocities at the bottom of the tank seem to be more dispersed in the vertical direction, and the
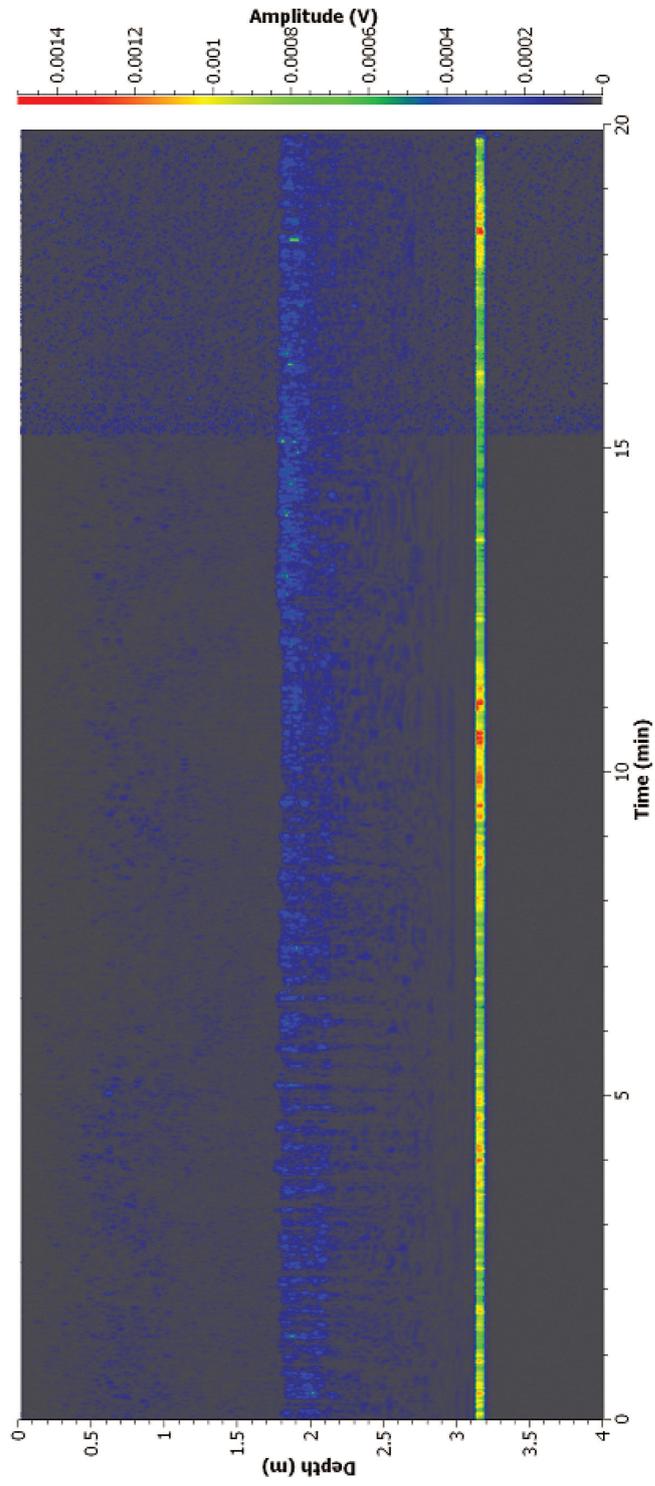
FIGURE 4.13: Evolution of the amplitude measured at 8.6m from the clarifier inlet
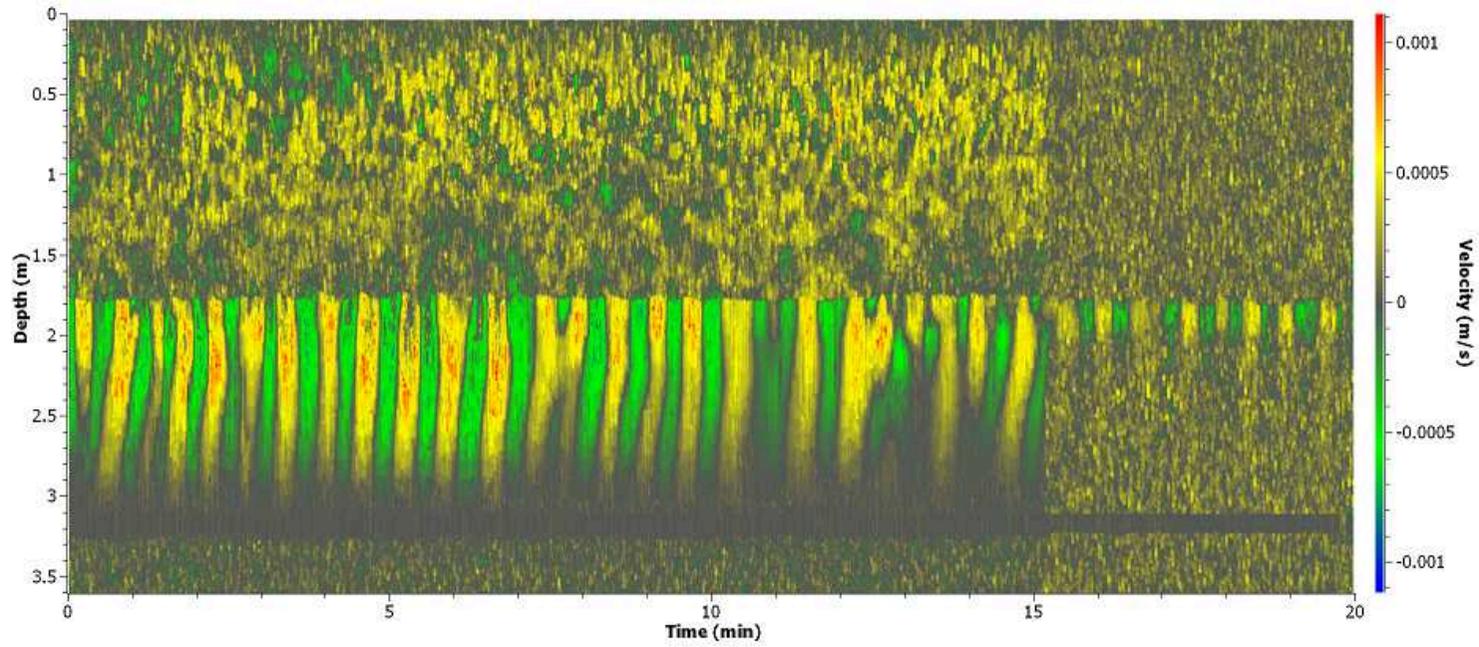
FIGURE 4.14: Evolution of the settling velocities measured at 8.6m from the clarifier inlet

velocities within the blanket seem to be lower. This, also coincides with the inactive recycling pump period.

The same trend is observed as the measurements taken at 8.6m. Periodic positive and negative velocities every 30 seconds are observed. The skimmer was stopped during the measurement, this behavior cannot be attributed to the motion of it. Thus, the rising and settling of the particles maybe attributed also to the density currents created by the incoming flow.

Within this zone settling velocities seem to be higher than those measured near the wall. Maximum values are about $0.001\,\text{m}\cdot\text{s}^{-1}$, maybe due to the incoming sludge and the extraction zone that disturbs the blanket.

Constant inflow simulations results

In order to initiate dynamic simulations, uniform and constant boundary conditions at the inlet and recirculation were first imposed in order to reach the convergence of the simulations of the settling tank.

The convergence was reached when the variations of the RAS and the SBH from one time step to other were less than 5%. The clarifier at the beginning of the simulation is supposed to be empty. The simulation converged after 10 hours of continuous flow. The average estimated RAS concentration was $8.66\,\text{Kg}\cdot\text{m}^{-3}$ and the final sludge blanket height was 1.37m. Checking the mass balance the difference between the inlet flux and the removal flux is near 17% which is acceptable.

The sludge blanket height is uniform along the horizontal axis and some waves appear in the zone near the inlet. In the inlet zone the sludge goes down and comes into contact with the thickened sludge. This, produces the fluid to decelerate and shift upward producing the waves in the upper part of the sludge blanket. The sludge particles start to settle causing an accumulation at the bottom of the clarifier (figure 4.17).

As the fluid is coming inside the tank, it goes directly towards the bottom (figure 4.18a). However, a velocity gradient is found between the inlet and the removal patches, just next to the internal wall. This velocity gradient is generated by the flow extraction made at the recirculation. Once the flow reaches the bottom it starts to spread in the horizontal direction.

The buoyant effect term (represented by Cg in the turbulence model) makes a rise up of the SBH while it is thickening. (figure 4.18a). Energy is dissipating along the clarifier producing a slow down in the velocity of the fluid towards the external part. (figure 4.18b).

The sludge concentration profile has a smoother gradient in the vertical axis near the inlet, and a higher concentration is reached at the bottom of the tank (figure 4.19a).
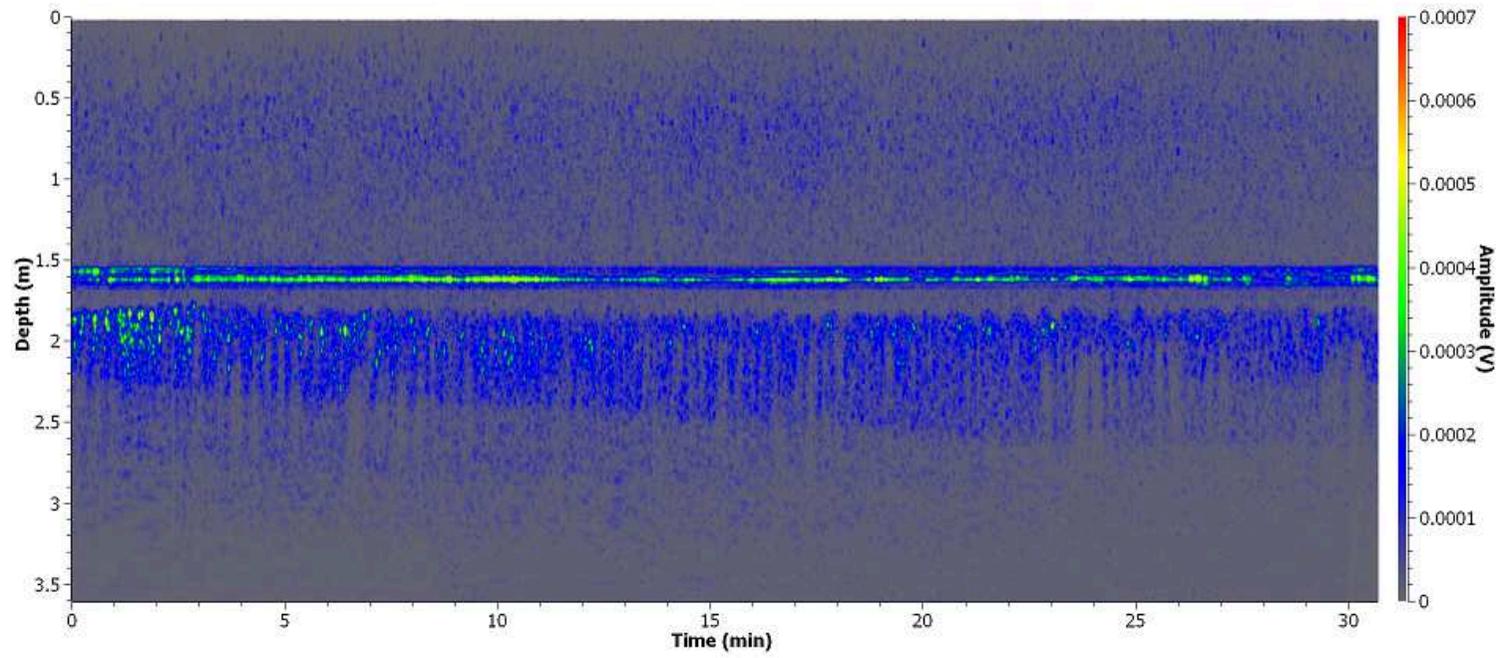
FIGURE 4.15: Evolution of the amplitude measured at 3.5m from the clarifier inlet
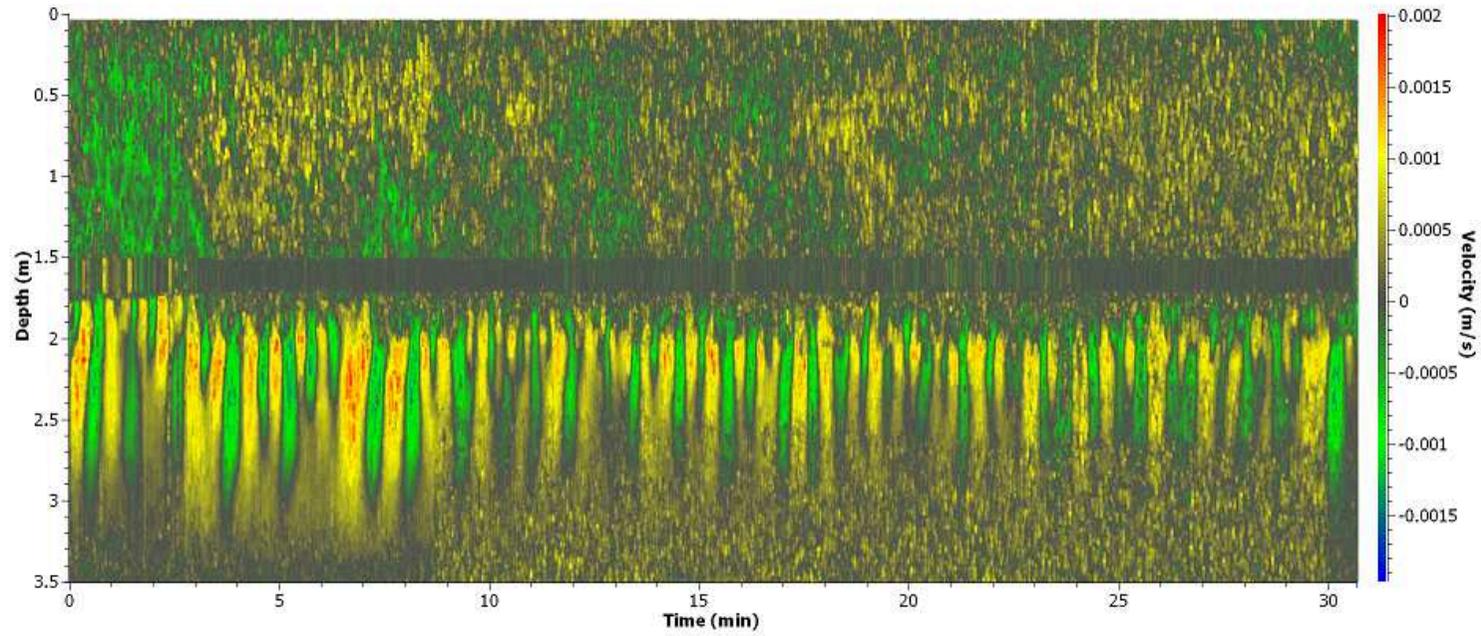
FIGURE 4.16: Evolution of the settling velocities measured at 3.5m from the clarifier inlet
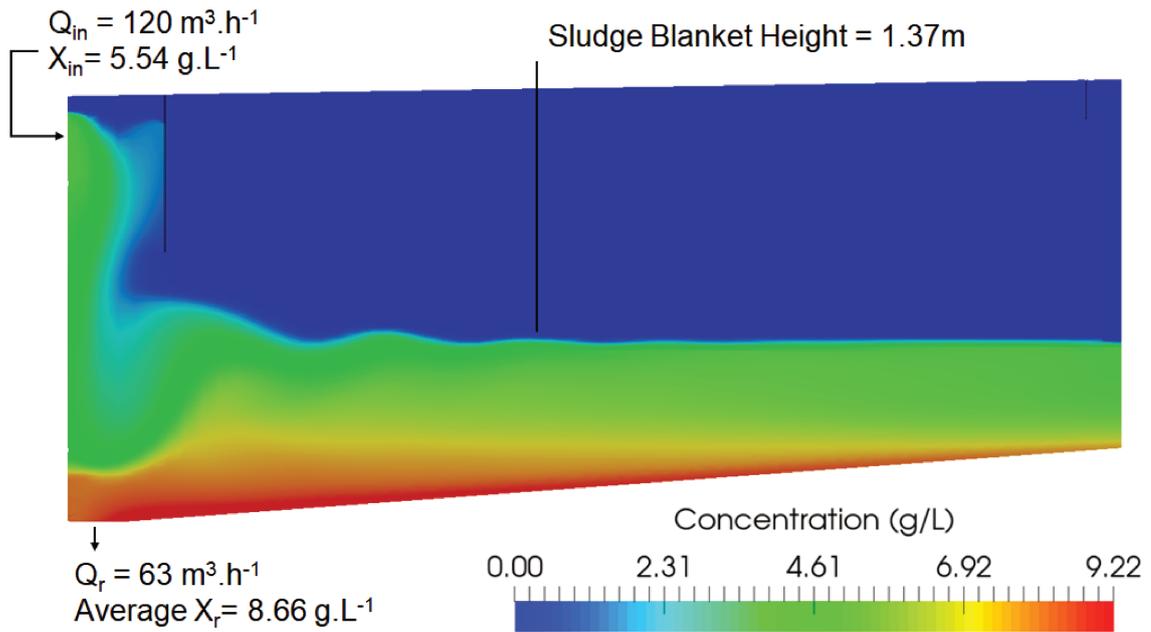
FIGURE 4.17: Concentration field after 11h of simulation

Near the external zone of the clarifier, the sludge is less thickened because there is less incoming sludge to settle and the slope of the clarifier makes the sludge slips towards the center of the clarifier.

Slightly lower values in the compression function are found at 3.5m (figure 4.19b) compared to the values captured at the external part of the clarifier. Even if the compression function, depends on the local concentration, in this case it depends on the settling velocity of the particles. The velocity profiles (figure 4.19c) show lower average values near the inlet zone. Indeed, at this zone the incoming sludge and the recirculation flow disturbs the settling process of the particles.

The profiles captured at a radial distance of 8.6m indicate that in this zone of the clarifier, quiescent conditions are established, the concentration, velocity and compression function show similar trends to those obtained in batch column. Indeed, the vertical trend in the concentration profile observed between 1 and 0.5m (when Rd = 8.6m) indicates that probably sludge is still in hindered regime at this point.

This analysis pinpointed the importance of the CFD models. Even if settling behavior is considered as a one dimensional phenomenon, the concentration profiles have a different behavior depending on the location of the measurement, *i.e.,* the geometry of the clarifier. Hence, the turbulence and nature of the fluid, affect the prediction of the blanket height, in particular near the inlet and recirculation.

(a)

$v_{in} = 0.015 \text{ m.s}^{-1}$

$v_r = 0.0062 \text{ m.s}^{-1}$

Velocity Field (m/s)

0.000   0.0069   0.014   0.021   0.028

(b)
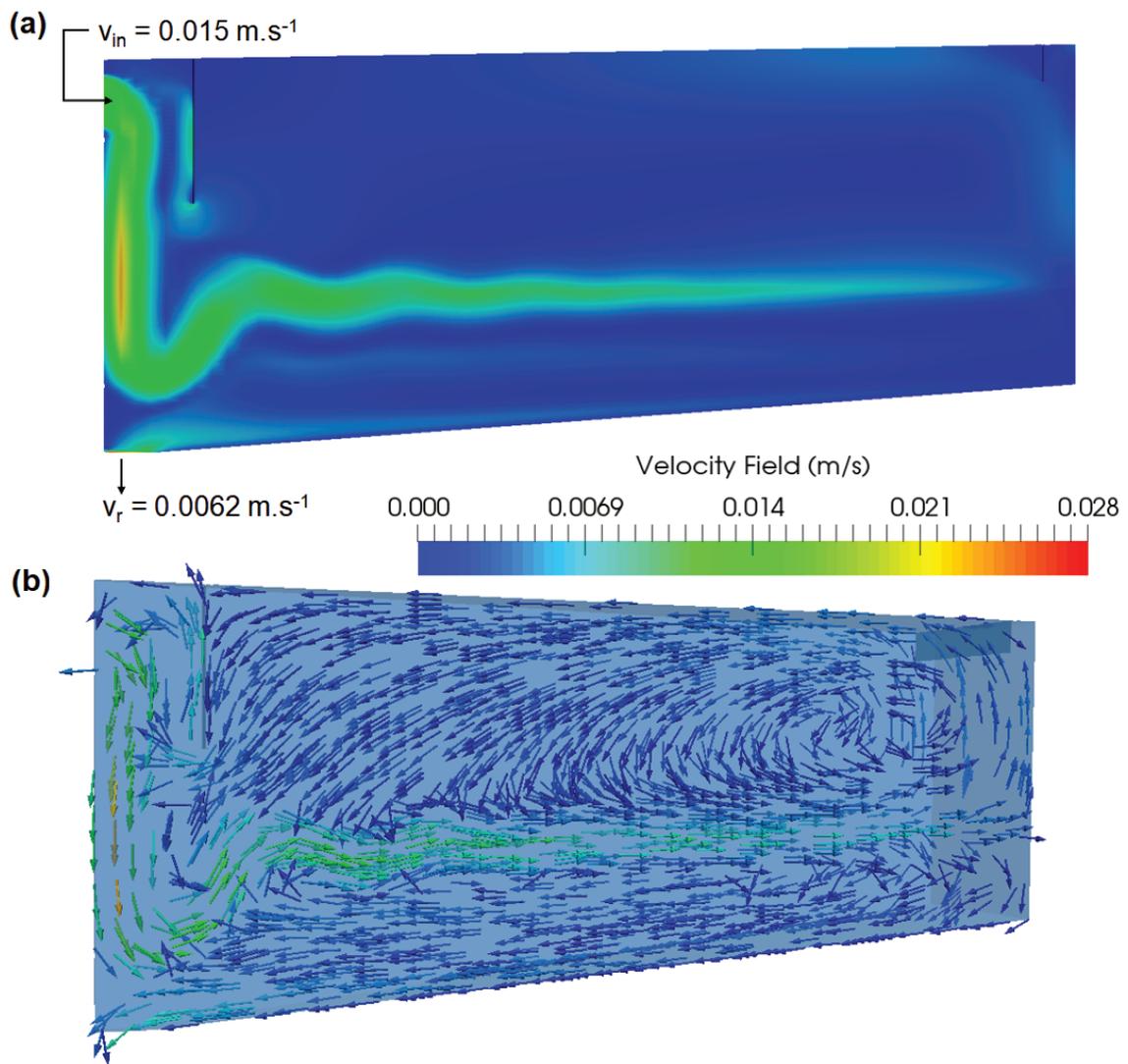
FIGURE 4.18: a) Velocity field and b) Velocity path of the fluid when
the after 11 hours of simulation
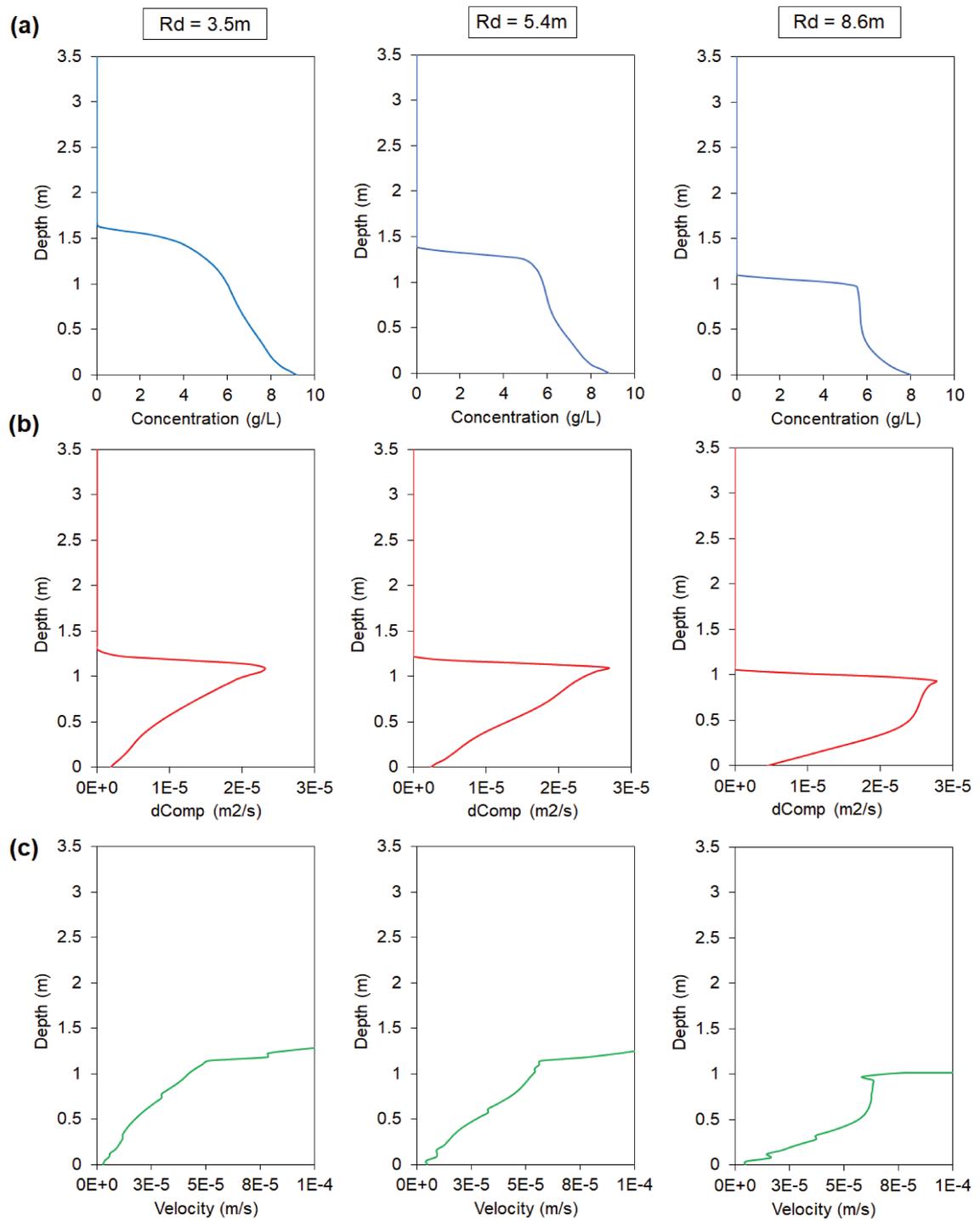
FIGURE 4.19: a) Concentration b) Compression function (dComp) and c) Settling Velocity profiles at different radial positions (Rd) after 11h of simulation

CFD modeling with dynamic Inflow and RAS flow

First, a simulation reproducing hydraulic conditions measured at the WRRF during 24h on April 6th was performed. The converged simulation obtained in the former section was used as initial condition (velocity, concentration, pressure fields, etc.).

The objective is to evaluate the ability of the CFD model to capture SBH and RAS concentration variations due to the dynamic inflow and recirculation conditions, using the estimated parameters found the batch column.

A lower incoming flow Q_{in} arrives to the clarifier in the early morning (0h00 to 8h00) compared to the longer periods during the rest of the day (8h00 to 24h) (figure 4.12a). The average Q_{in} for the early morning and the rest of the day, are $115\,m^3{\cdot}h^{-1}$ and $121\,m^3{\cdot}h^{-1}$ respectively. In contrast, the recirculation flow show longer extraction periods during the early morning compared to the shorter extraction periods during the rest of the day. Thus, the average Q_r for the early morning and the rest of the day are $70.2\,m^3{\cdot}h^{-1}$ and $53\,m^3{\cdot}h^{-1}$ respectively.

Figure 4.20 shows the variations of the predicted sludge blanket height (at two different radial distances) according to the Q_{in} and Q_r. As expected SBH decrease during the early morning due to the lower inflow and solids loading rate. During the rest of the day, the SBH increases due to a higher Q_{in}.

The recirculation flow also impacts the SBH predictions. Longer extraction periods (higher Q_r) during the early morning produce a lower SBH. The average predicted SBH rises from 1.49m in the early morning to 1.90m the rest of the day near the inlet. The same behavior is observed far away the inlet (Rd=8.6m) where the sludge blanket increases from 1m to 1.40m for the same periods during the day. The variations in the height of the predicted sludge blanket far way from the inlet are smoother due the quiescent conditions presented in this zone.
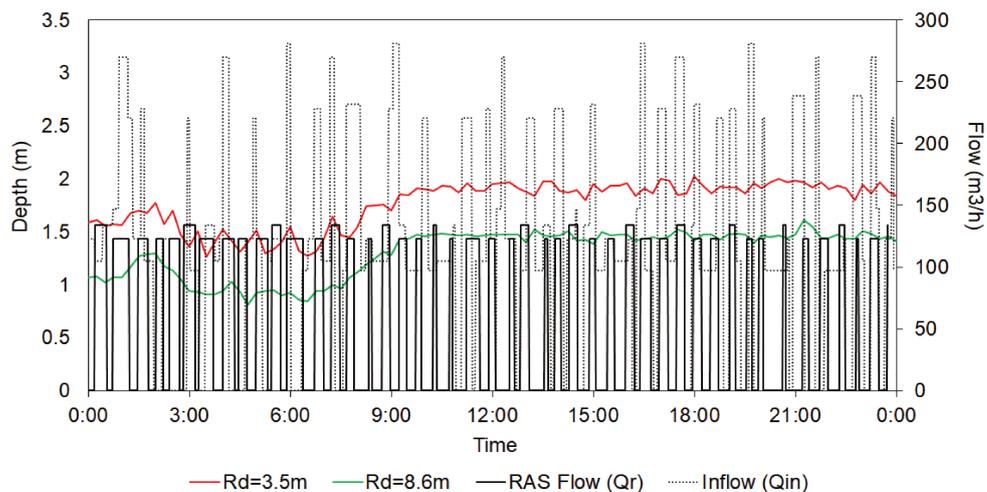
FIGURE 4.20: Simulated SBH at different radial positions (Rd) in respect to variations of Q_{in} and Q_r during the day.

The predicted RAS concentration (X_r) is also affected by the varying flows (figure 4.21). During the early morning the predicted average X_r is 8.11 Kg·m^{-3}. The average X_r for the rest of the day is 9.81 Kg·m^{-3}. Even if those values are similar, it is clear that the predicted concentration do not remain constant due to the flow rate variations during the day. During the early morning, it is observed that the relative variations in the predicted concentration are higher (the standard deviation (STD) of X_r is ±1.39 Kg·m^{-3}). As stated before the incoming flow is lower in the early morning producing a lower sludge accumulation at the bottom. Those variations are lower during the rest of the day (STD of X_r is ±0.66 Kg·m^{-3}).
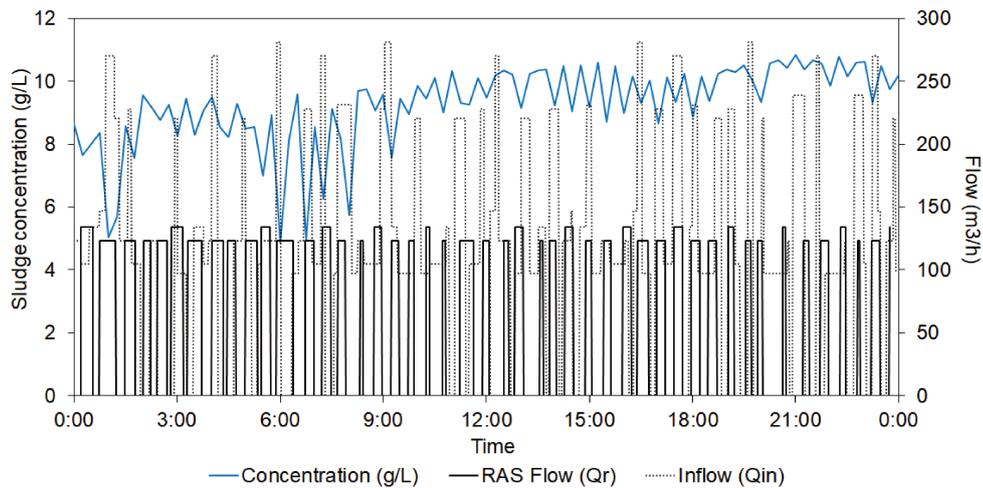
FIGURE 4.21: Predicted sludge concentration at the RAS in relation to the incoming and recirculation flows during all the day

Through the CFD model, the variability in the prediction of the SBH and the sludge concentration at the removal at different times of the day can be understood.

In figure 4.22, a low X_r = 5.04 Kg·m^{-3} is observed at 1h00. During this time a high flow (270 m^3·h^{-1}) is coming inside the clarifier and at the same time the extraction pump is active. This makes a short circuiting in the clarifier (figure 4.22b) and the incoming sludge is not accumulating.

Figure 4.23a illustrates the sludge concentration distribution within the tank when the recirculation pump is off. Previously the recirculation pump was active and because of this, the sludge blanket height is lower than the former case. However, due to the inactive recirculation pump (figure 4.23b), the sludge starts to thicken (X_r = 9.5 Kg·m^{-3}) at the bottom. After this time, the active periods of the recirculation pump become shorter, allowing the sludge to accumulate and leading to a rising in the sludge blanket.

At 23h15 when both Q_{in} and Q_r are active (figure 4.24), there is no short-circuiting in the clarifier. At this time, a high blanket (1.94m) is already present slowing down the velocity of the incoming sludge. The high elevation of the sludge blanket, slows

(a)

Q_{in} = 270 m³/h

SBH = 1.56m

X_r = 5.04 g/L
Q_r = 123 m³/h

Concentration (g/L)

0.00   2.67   5.35   8.02   10.70

(b)

Velocity Field (m/s)

0.000   0.0085   0.017   0.026   0.034
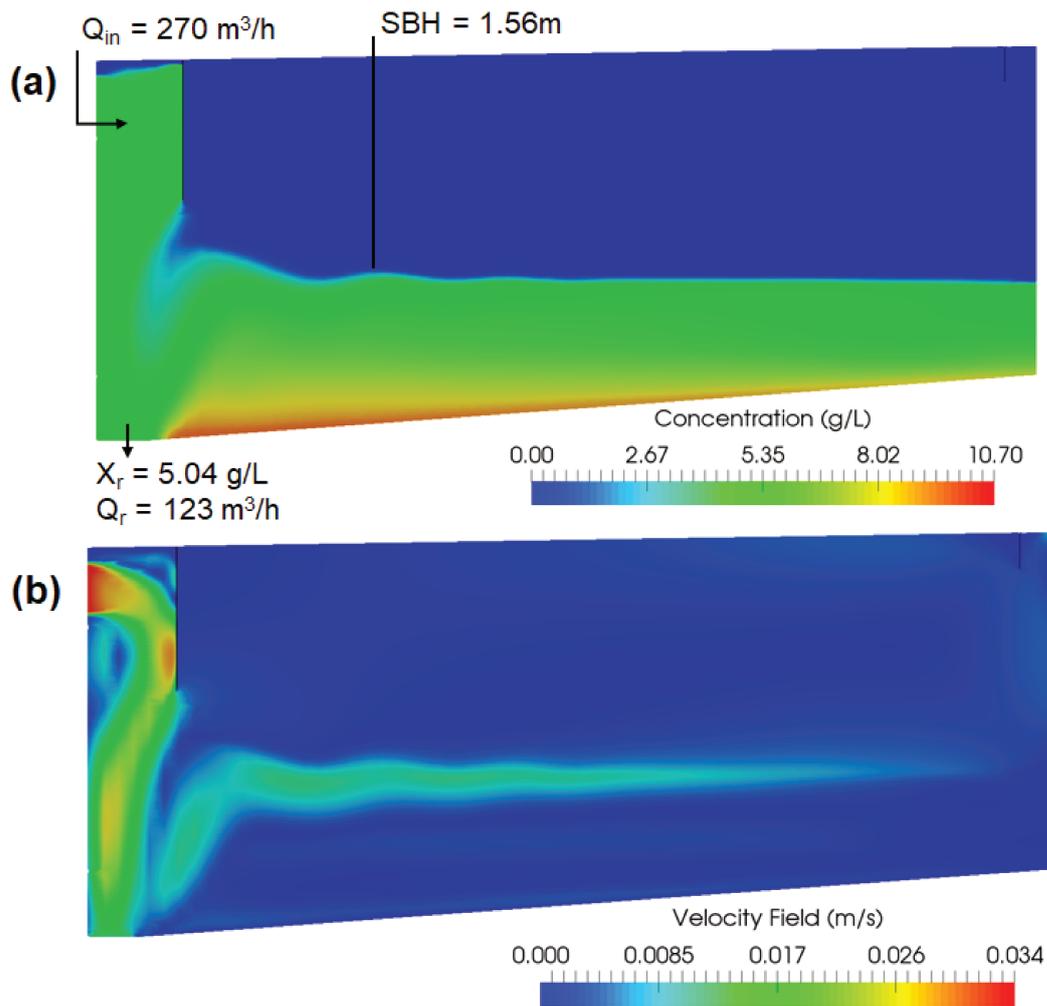
FIGURE 4.22: Simulated a) concentration and b) velocity fields when both the extraction and inlet flows are active at 1h00
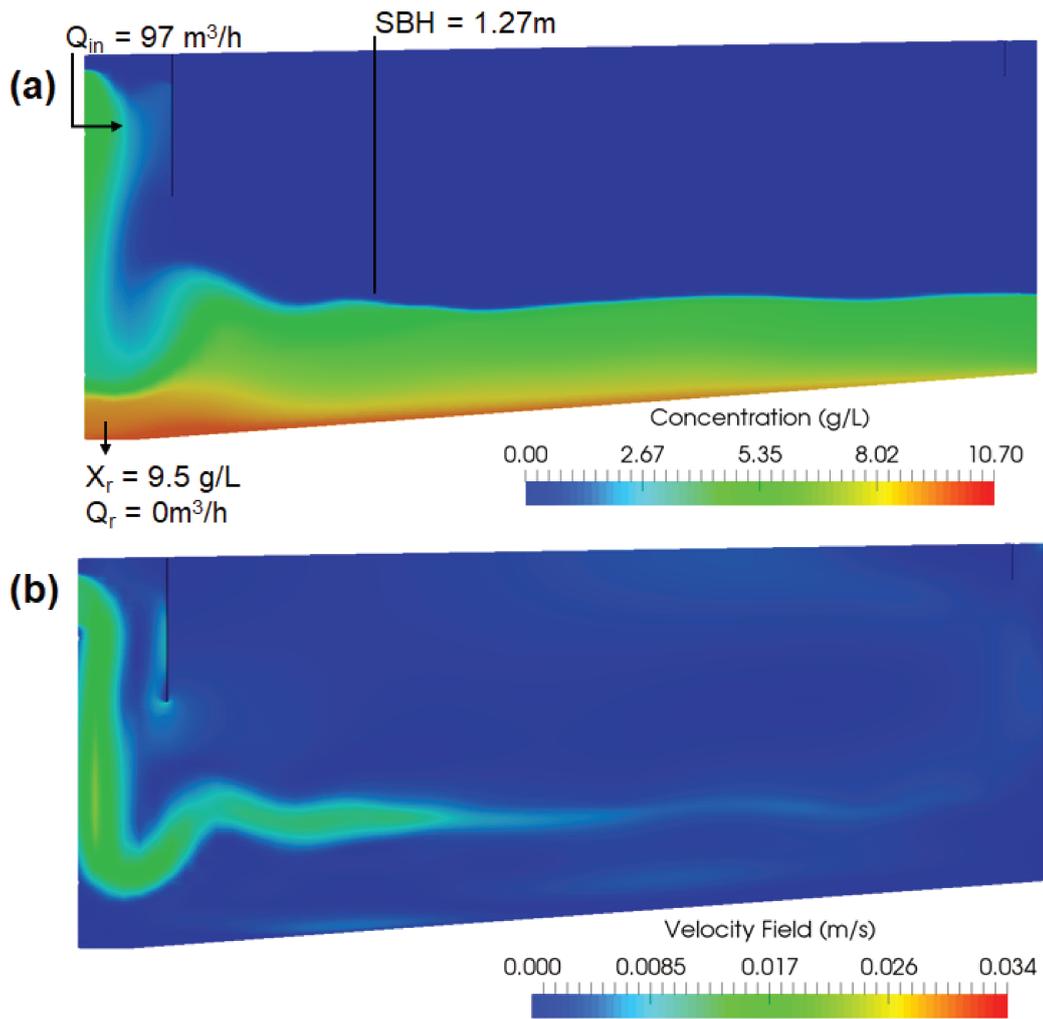
FIGURE 4.23: Simulated a) concentration and b) velocity fields when the extraction is inactive and inflow is active at 6h30

down the velocity of the incoming sludge and then to thicken at the bottom of the tank finding a higher X_r (10.7 Kg·m^{-3}).
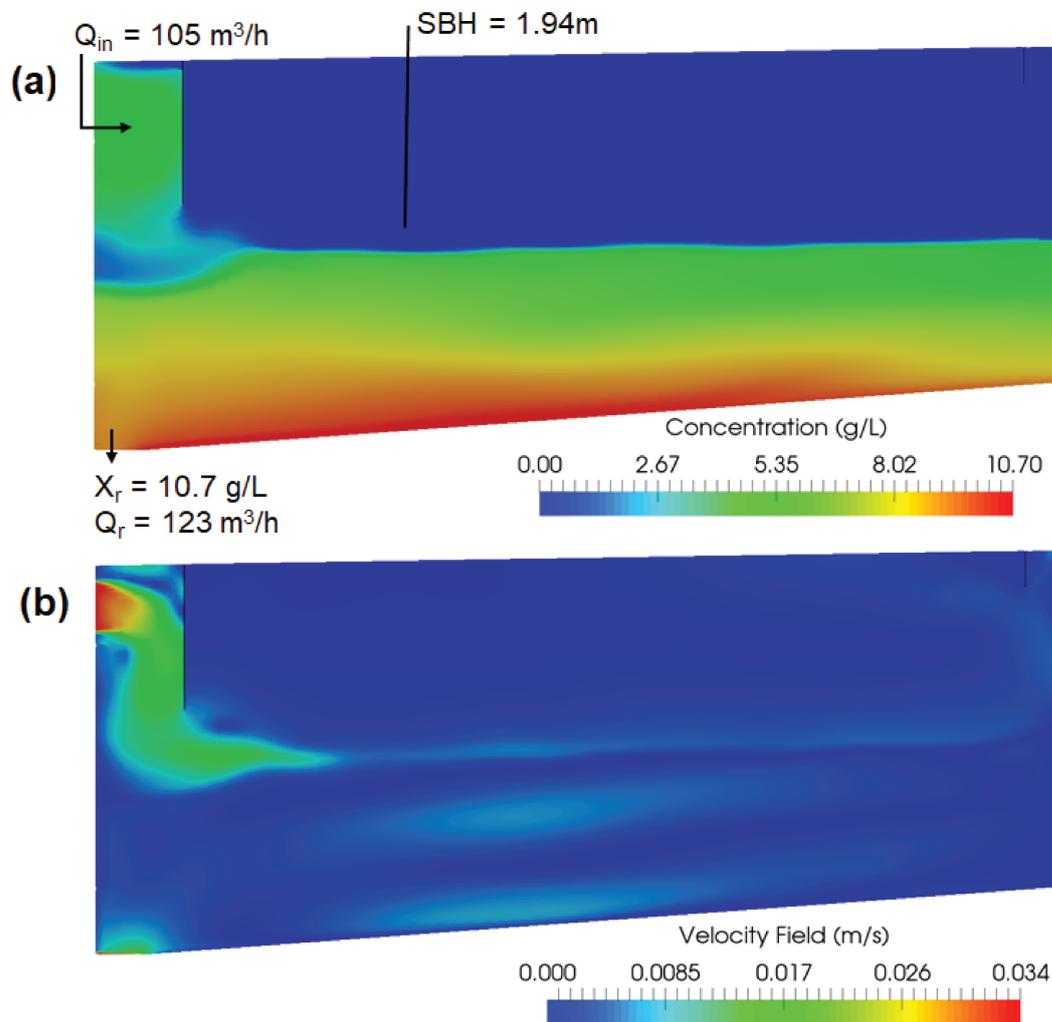
FIGURE 4.24: Simulated a) concentration and b) velocity fields when both the extraction and inlet flow are active at 23h15

As explained before, to validate the CFD model with the axisymmetric clarifier, first the measured SBH is compared to the simulated one. The mean values for the sludge blanket are calculated from the bottom of the clarifier to the surface of the blanket. For all radial distances (Rd), the CFD model makes a good prediction in the evolution of the SBH (figure 4.25) at the three different positions. The low relative errors (r_e) between the measured and simulated average blanket height also corroborates the good performance of the CFD model:

- r_e at 3.5m = 0.96 %

- r_e at 7.4m = 1.62 %

- r_e at 8.6m = 10.17 %

122
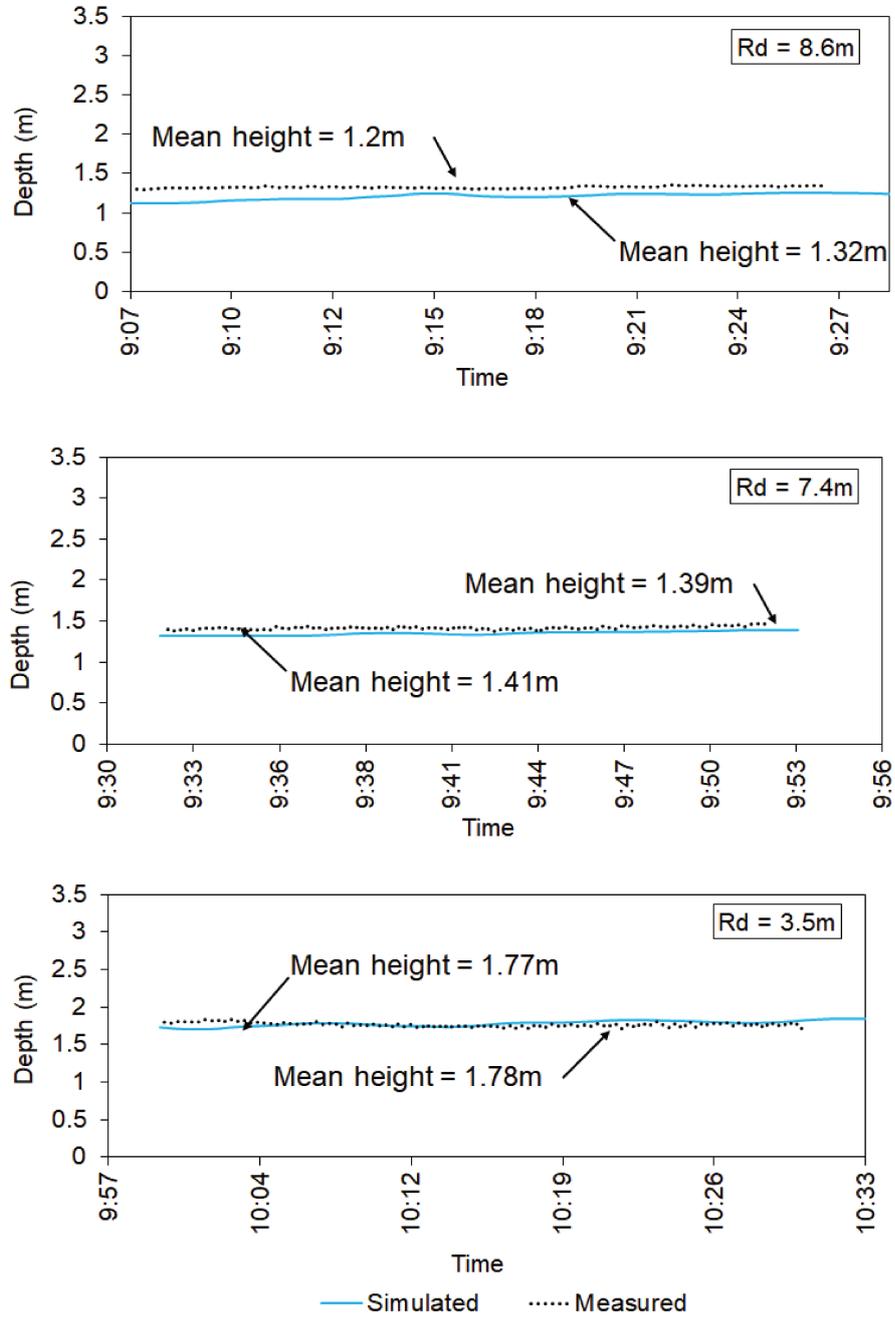
FIGURE 4.25: Simulated and measured SBH at three radial locations (Rd). The continuous blue line indicates the simulated SBH, the dotted black line corresponds to the measured SBH

The vertical velocity profiles (convective and settling) are also compared to the measured vertical particle velocity. The results presented here corresponds to the positions near and far away from the inlet, *i.e.* at 3.5 and 8.6m respectively at a given time. The results show that the mixture velocity (convective velocity) in the vertical direction is governing the velocity of the particles. Indeed, the order of magnitude of the measured velocities is around $0.001\,\text{m·s}^{-1}$ in the upper part of the sludge blanket and near the inlet (figure 4.26 left). The influence of the incoming and recycling flow is more noticeable in the zone near the inlet producing higher velocities in the vertical axis.

Hence, the trend of the simulated curve for the mixture velocity is similar to the experimental data within the sludge blanket in both positions. This indicates, that the settling velocity of the particles is eclipsed by the mixture velocity in the vertical direction: the values of the simulated settling velocities are around $1.10^{-6}\,\text{m·s}^{-1}$. Far away from the inlet, the vertical velocities are lower for both experimental and simulated velocities. Again, it is confirmed that more quiescent conditions are present in this zone.

The MAE (equation 3.7) is calculated for the particle velocity profiles all the depth of the clarifier. Near the inlet (figure 4.26 left), the MAE are $3.47x10^{-4}$ and $2.55x10^{-3}$ for the simulated mixture and settling velocities respectively. In the external part of the clarifier (figure 4.26 right) the MAE are $2.31x10^{-4}$ and $3.16x10^{-3}$ for the simulated mixture and settling velocities respectively. Indeed, the MAE indicates that the mixture vertical velocity (convective velocity) is governing the motion of the particles.
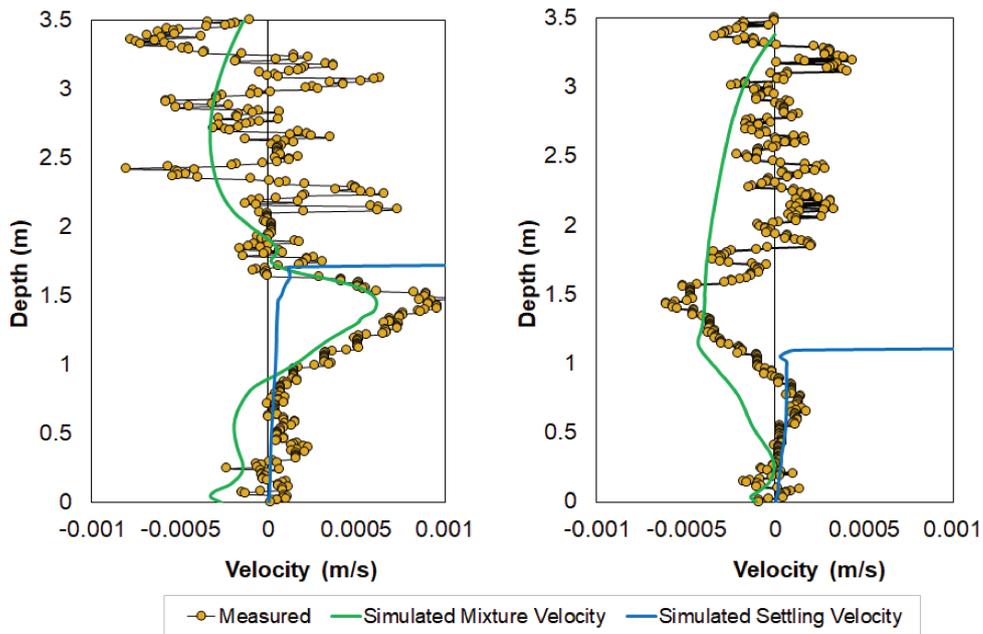
FIGURE 4.26: Velocity profiles measured *left* at 3.5m taken at 10:05am and *right* 8.6m at 9:07am

With this example, we want to point out the importance of the variability of the

flows arriving and leaving the clarifier. The prediction of the RAS concentration is different depending on the time of the day. The sludge blanket is also predicted different depending on the incoming and RAS flows.

As conclusion, the estimated parameters obtained in the batch column used for the axisymmetric simulation can describe an accurate sludge blanket height in the clarifier during the 20-30 minutes of measurements. It was observed that the settling velocity of the sludge is lumped by the convective velocity of the mixture.

This study relies on punctual experimental measurements made during 2 hours. Next section deals with this changing behavior of the sludge blanket by comparing the measured SBH during 48 continuous hours with the simulation case

4.3.2 Continuous measurements results (October 2018)

Experimental data results

Figure 4.27 shows the evolution of the SBH during all the measurement campaign (51 hours). Three zones can be distinguished: clear zone, from 0.5m to 3m: the sludge blanket (green/light blue colors between 3.0 to 3.5m) and the bottom of the tank (a red line at 3.5m). Through time, the SBH is varying from 0.6 to 0.2m suggesting that the incoming flow, recirculation flow and skimmer motion may affect the blanket height. In general, one can observe that the maximum SBH is 60 centimetres during all the test, which is not a thicken blanket. Accumulation of floating particles was also observed at the surface of the clarifier.
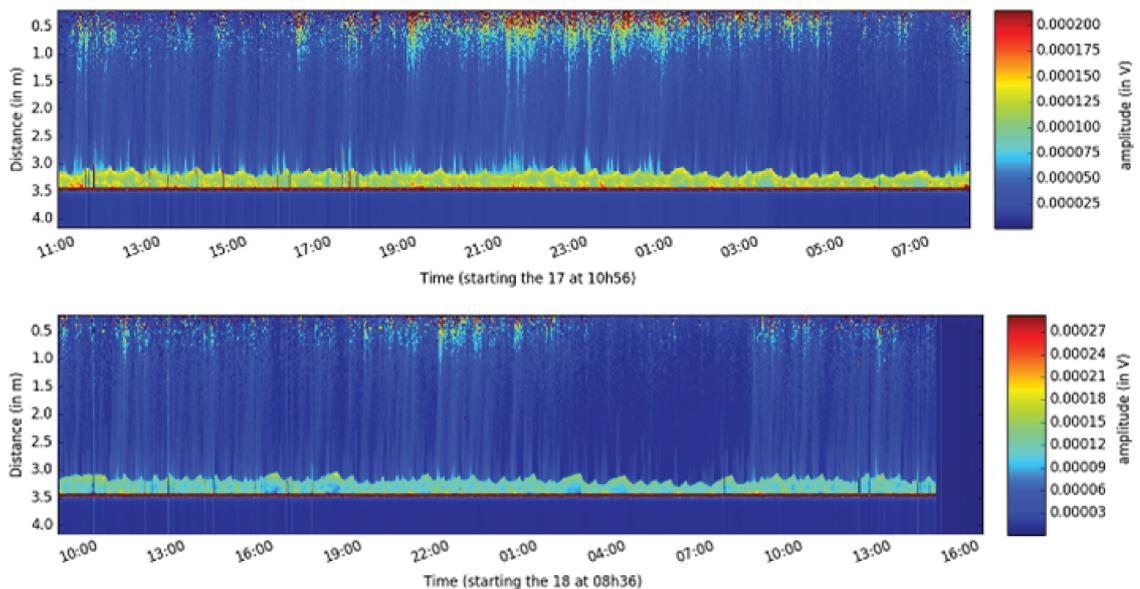
FIGURE 4.27: Evolution of the amplitude measured during 51 hours
($f_0 = 1.65 MHz$). Copyright (Ubertone)

On figure 4.28 the particle velocity evolution results show that flocs within the discrete zone achieve high velocities. This maybe due to the incoming fluid motion. The negative velocities indicates that particles are moving towards the bottom. However, during these days, the trend of positive and negative velocities every 30 seconds which was observed in April is not present in October.

And, probably the movement of the skimmer is also affecting the settling velocity of the particles, since the transducer is attached directly to the skimmer and following its path. It is tricky to establish the velocities of the particles within the blanket due to its thinness, compared to the total depth of the clarifier (3.5m).
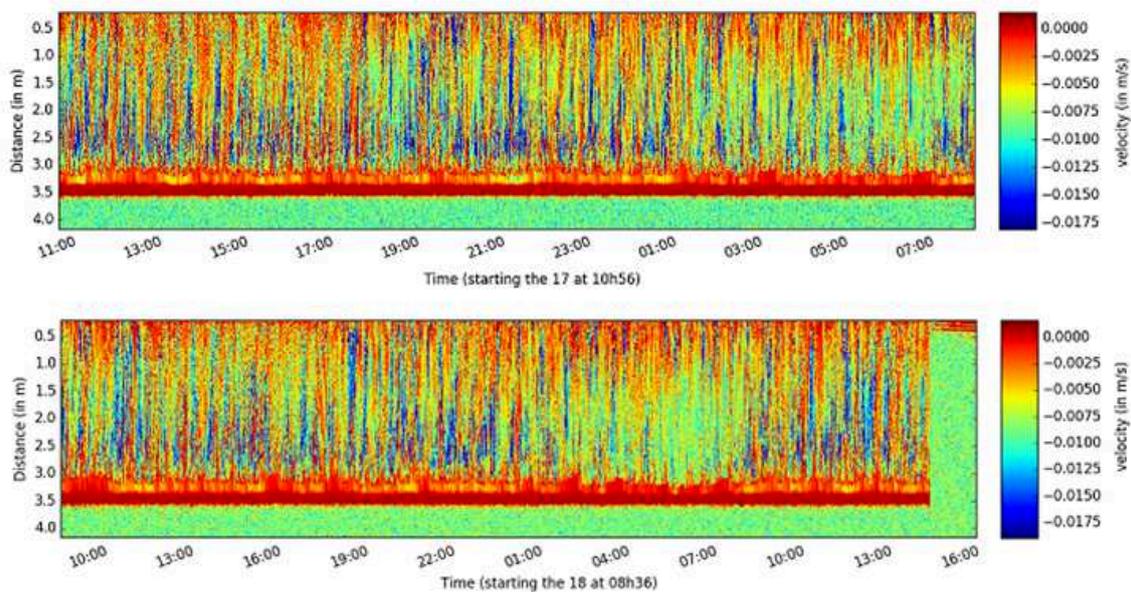
FIGURE 4.28: Evolution of the particles settling velocities measured ($f_0 = 1.65MHz$) during 51 hours. Copyright (Ubertone)

Within this experimental test, it is observed that almost all the particles velocities are negative, which indicates that they travel towards the bottom of the clarifier. The negative/positive particles velocity trend within the sludge blanket it is not observed here. One possible reason is that Peacok UVP transducer was recording the particles velocity data every 45 seconds, while the positive/negative velocity trend was observed every 30 seconds.

CFD model in continuous constant flow mode

Similarly to the previous case, before simulating the true hydrodynamic behavior of the clarifier of Achenheim, a base simulation was performed in order to reach the convergence. The inlet flow was set to $Q_{in} = 115\,\text{m}^3{\cdot}\text{h}^{-1}$ and the RAS flow was set to $Q_r = 63\,\text{m}^3{\cdot}\text{h}^{-1}$. The evolution of the predicted sludge blanket height at 3.5m away from the inlet was extracted. In section (4.3.2), the comparison of the simulated SBH to the experimental data is presented.
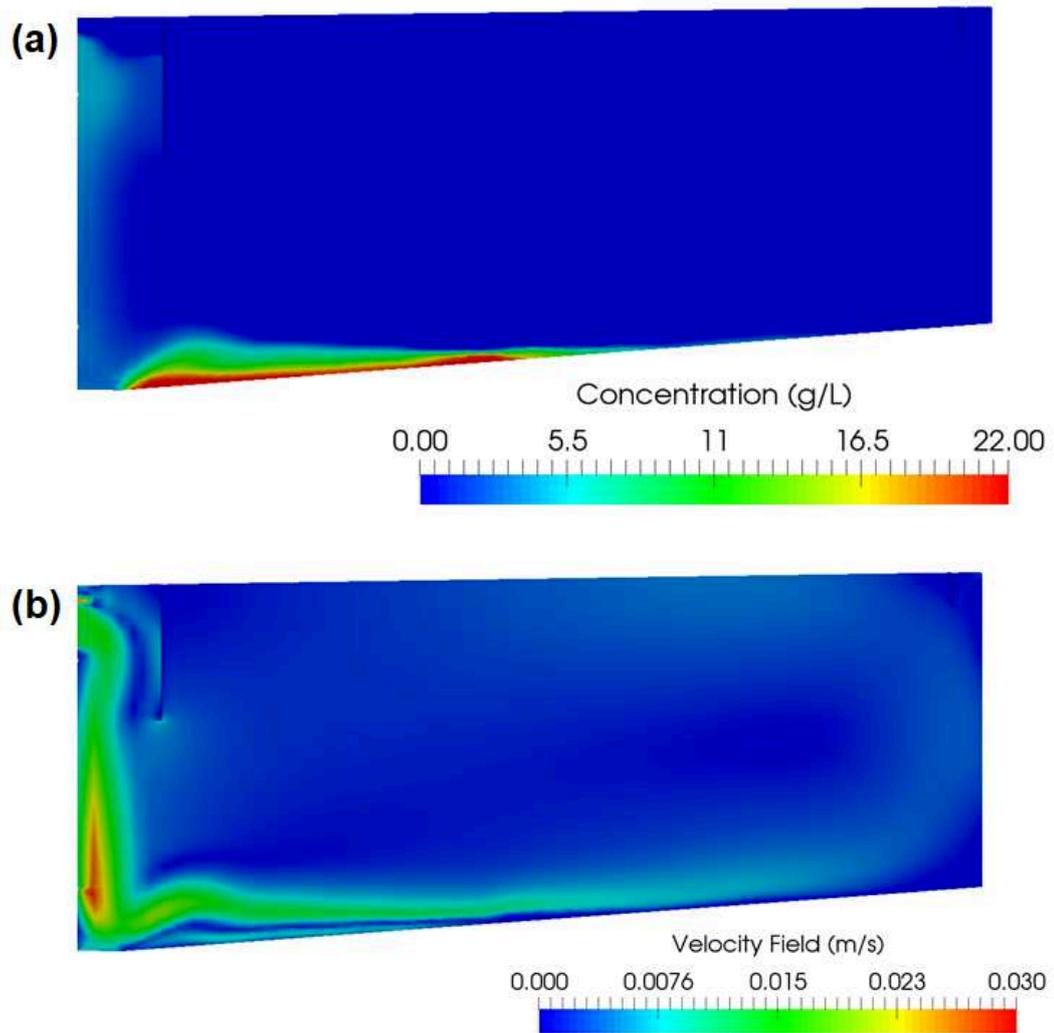
FIGURE 4.29: a) Sludge concentration and b) Velocity field after 36h
of simulation with the sludge and flow values of October

Figure 4.29a shows the sludge concentration distribution of the clarifier after 36h of simulation using the sludge characteristics of October. A thin sludge blanket is formed just near the inlet. At a radial distance of 3.5m, the blanket height is barely 20cm. The sludge concentration at the bottom slope is $22\,\mathrm{Kg\cdot m^{-3}}$ which is a high concentration. However, it was long to get the steady state; variations of concentration from $4.3\,\mathrm{kg\cdot m^{-3}}$ to $10.7\,\mathrm{kg\cdot m^{-3}}$ were observed during the 36h of simulation, indicating an average RAS concentration of $5\,\mathrm{Kg\cdot m^{-3}}$ in periods of 5 hours.

The high variations in the RAS concentration, indicates that sludge has not a constant thickening. This can be explain by the continuous recirculation extraction which is producing a short-circuiting at the inlet zone and diluting the sludge accumulated at the bottom (figure 4.29b).

CFD model validation using the dynamic boundary conditions

The objective of this campaign was to measure the SBH continuously for a longer period and compare with the simulation results.

The experimental sludge height was extracted from the amplitude profiles at a frequency of 1.64MHz. The measured SBH (red dotted line in Figure 4.30) was determined setting an amplitude limit value of 0.0001V. Then, a moving average with a period of 10 was calculated to obtain representative heights.

To simulate the intermittent flow of Achenheim clarifier the inflow and recirculation rates conditions for the CFD model, were set accordingly to figure 4.12b. The simulated SBH was measured at the same point where the ultrasonic device was placed in the full-size clarifier and compared to the measured SBH (figure 4.31). For the simulated SBH, the height was considered where the concentration in the surface of the blanket is equal to the initial concentration.

Figure 4.30 shows the simulated and measured SBH during the 51 hours of the experimental test with respect to the incoming and recirculation flows. In general, the measured sludge blanket height is low, barely 60cm from the bottom of the tank at the maximum point.

It is clear that the model is able to reproduce the SBH variations as the sludge blanket is sensitive to both flows (inlet and recirculation). However, the model tends to be overestimate these fluctuations. For instance, a high peak is observed in the simulation around 8am in October 18th (figure 4.30b). It coincides with the stop of the recycling pump and while the incoming flow is still significant. Before this event, the model under-predicts the SBH, while this is not really the case afterwards.

The model can predict at some point an accurate sludge blanket. However higher peaks and moments with no sludge blanket are predicted. The model uses an approximate real flow, *i.e.* we extracted the flow data from graphs obtained directly

128
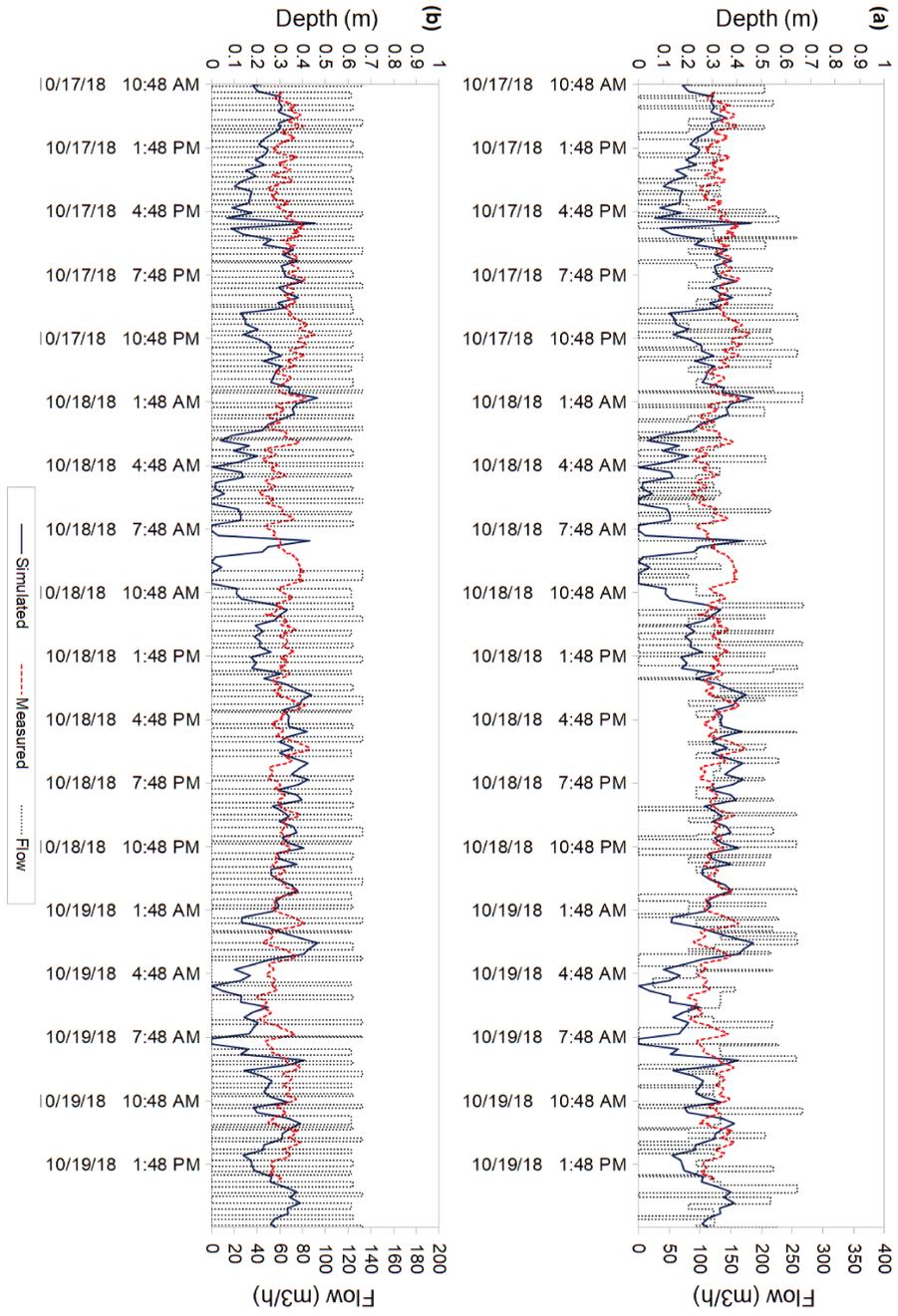
FIGURE 4.30: Simulated and measured SBH during 51 hours in respect to a) the incoming flow, b) the recycling flow.

from the WRRF. The extraction method for the flow data has done visually which may create some uncertainty in the values. This can explain why in some points the simulated sludge blanket do not agree with the measured one.

In figure 4.31, it is seen that the intermittent flow simulation seems to predict a better trend of the SBH than the constant flow simulation. The model with constant flow is under-estimating the SBH.

The intermittent flow model seems to be more sensitive to the changing loads specially when the recirculation flow is off. However, the model can represent a good height when the recirculation flow is on. The particles in the clarifier are disturbed by the scrapper motion, making possible an elevation of the blanket. This movement can be captured by the transducers, and thus lump the real settling process. One possible explanation why some elevations (peaks) do not coincide with the experimental data, is that the model does not consider the scraper motion and this may have an impact on the fate of solids and velocity field (swirl motion, increased particle flow towards the removal, De Clercq, 2003). The variations in the predicted sludge concentration are noticeable (figure 4.32). However, the average sludge concentration during the 3 days remain in $9.8\,\text{Kg·m}^{-3}$. Different sludge concentrations are expected during the day, at some moments such concentration can rise $30\,\text{Kg·m}^{-3}$, and sometimes no sludge is thickening. The intermittent behavior of the clarifier, do not allow for a constant sludge concentration at the removal. This variant sludge concentration may impact the performance of the biological reactor and the sludge processing line.

A look inside the dynamics of the SST (figure 4.33), shows that effectively, a thin sludge blanket is created inside the tank. Since no thickened sludge blanket is found, the incoming sludge goes immediately towards the removal. Different reasons can explain this behavior:

- Lower average incoming flows ($Q_{in} = 115\,\text{m}^3\text{·h}-1$) compared to those in April ($Q_{in} = 120\,\text{m}^3\text{·h}-1$) and the same RAS flow ($Q_r = 63\,\text{m}^3\text{·h}-1$) do not allow the sludge to accumulate at the bottom.

- The high mineral content in the sludge makes to settle faster and thus no thickening is carried on.

Unfortunately, the comparison of the measured settling velocities and the simulated ones are not presented here. Indeed, we analyzed the values, and it is hard to compare the measured values due to the thinness of the sludge blanket.

4.4 Conclusions

To validate the model, different experimental campaigns were carried out from January to October 2018. Only two campaigns were able to obtain satisfactory results,

FIGURE 4.31: Constant and intermittent flow simulations and measured SBH during 51 hours. The depth of 0m represents the bottom of the tank
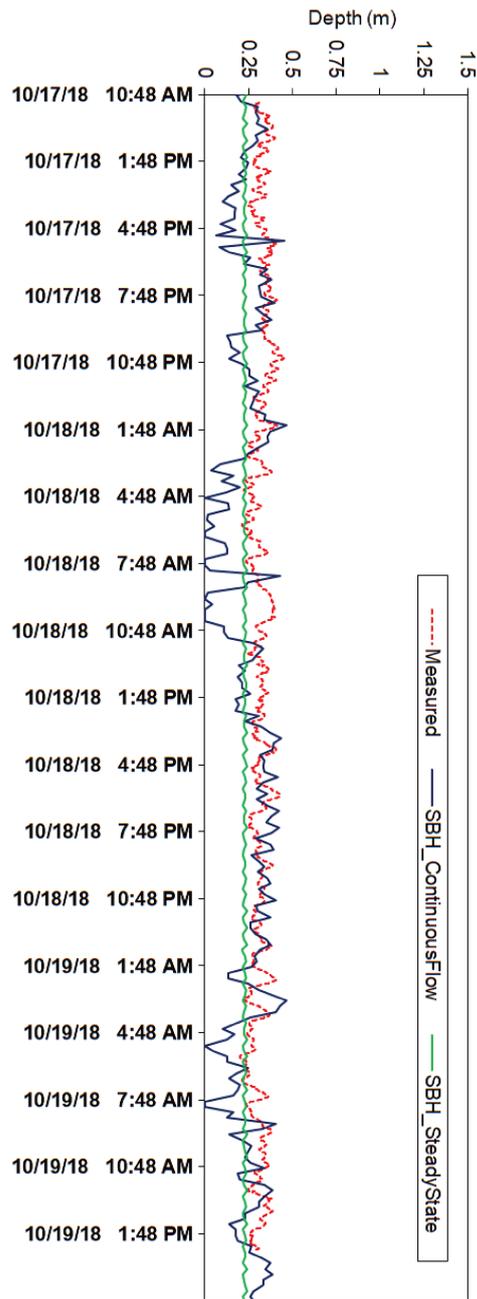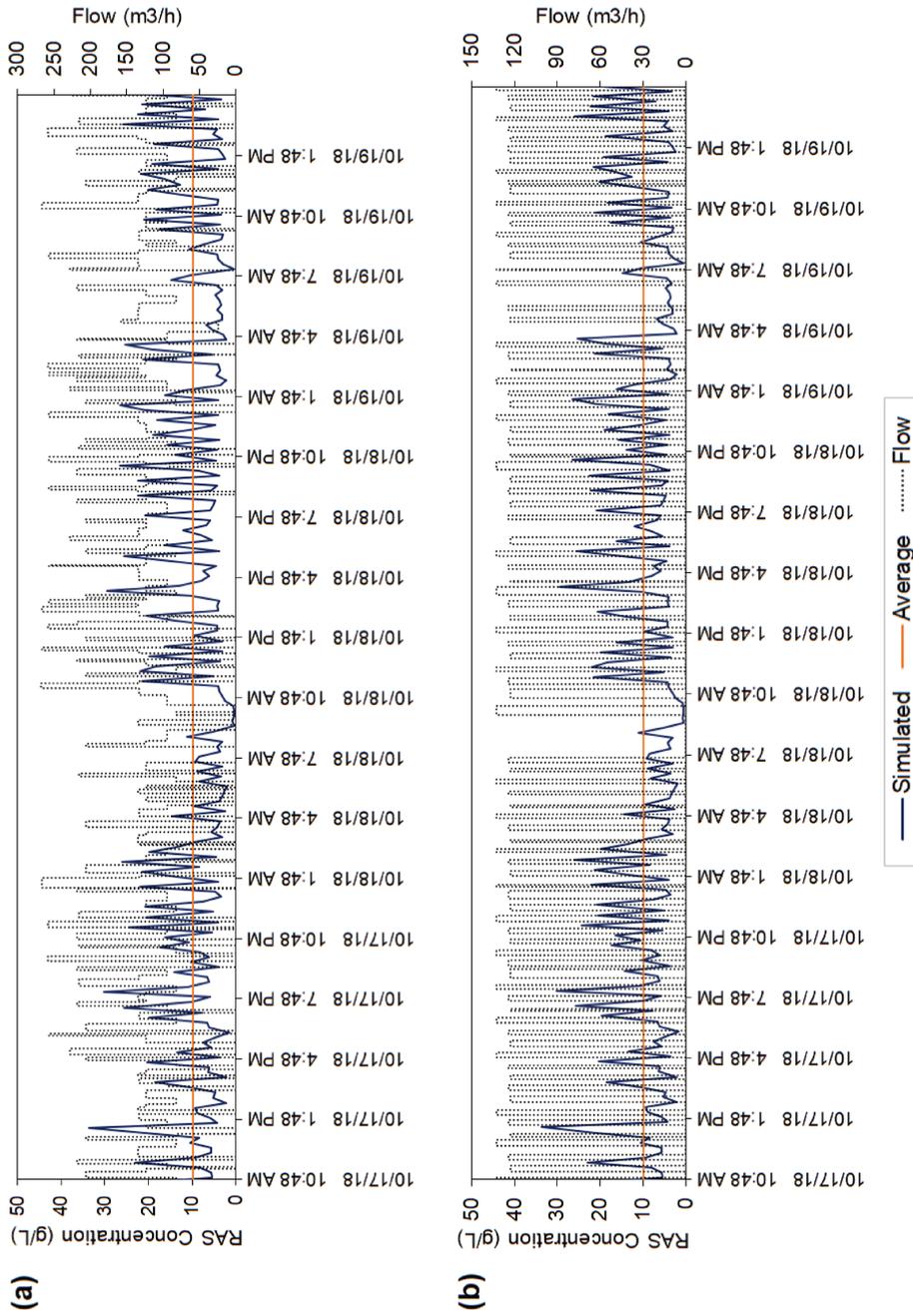
FIGURE 4.32: Simulated sludge concentration at the removal during 51 hours in respect to a) the incoming flow Q_{in}, b) the recycling flow Q_r.

(a)

(b)
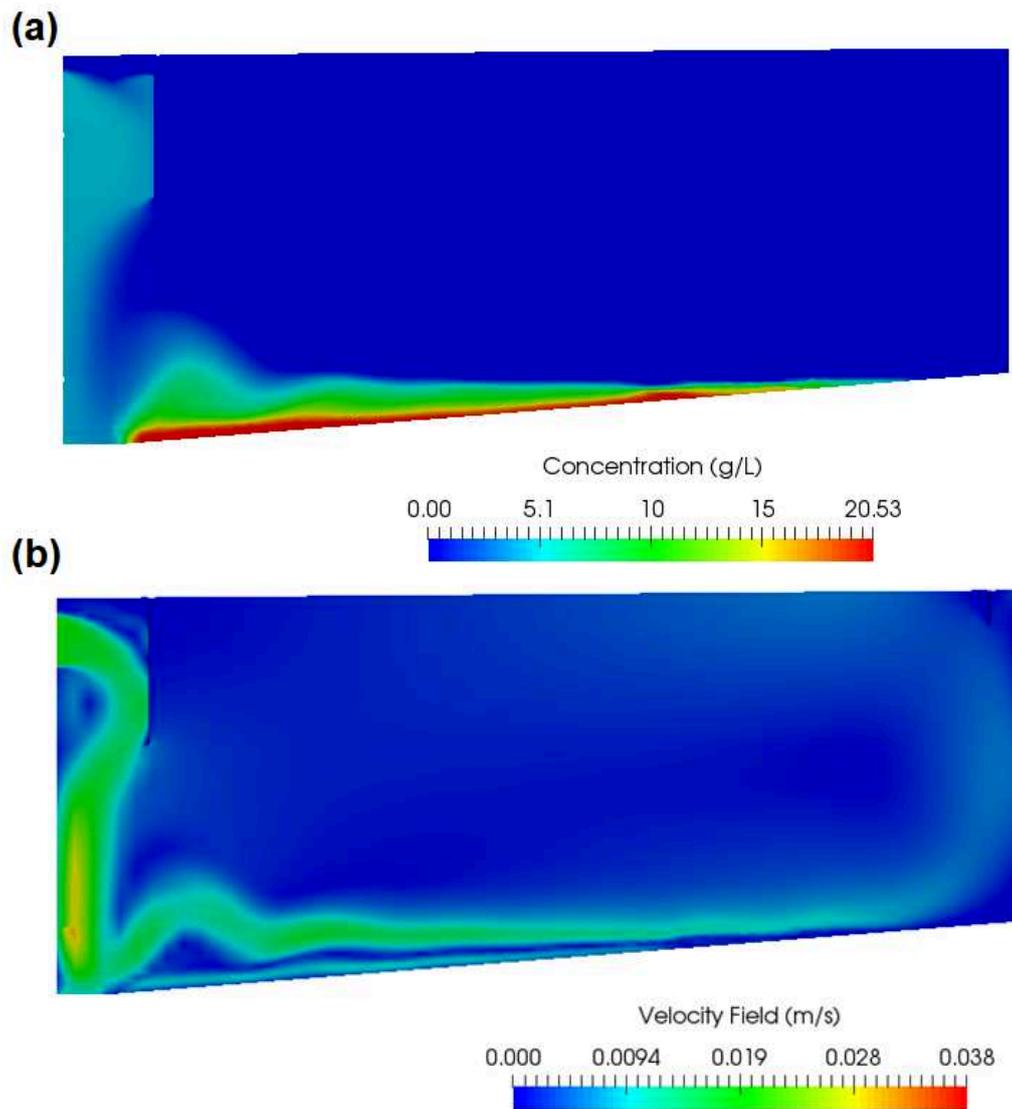
FIGURE 4.33: CFD simulation of a) sludge concentration and b) mixture velocity at 3:30pm on October 18th

in April and October.

The continuous measurements during 51 hours revealed that the sludge blanket within the clarifier has a dynamic behaviour, finding height values between 0.6 and 0.2m. The punctual measurements, carried on during 20 minutes at different radial distances, showed that particle settling is possibly disturbed by the density currents generated by the incoming flow. Indeed, the particles velocities rise and descend within the sludge blanket every 30 seconds, even at distances far away from the inlet.

From the campaigns carried on April and their respective simulations the following conclusions can be determined:

- From the continuous flow case, we observed that in the external zone of the clarifier, quiescent conditions are created. Indeed, through the velocity and concentration vertical profiles, a similar behavior to the batch settling profiles is obtained. This can be also corroborated with the lower particles velocities measured at a radial distance of 8.6m when they are compared to the particles velocities measured at 3.5m.

- The measured particle velocities in the clarifier are higher compared to those found in batch experiments (1.10^{-5} m·s^{-1}).From the comparison between the measured particles velocities and the simulated vertical convective and settling velocities, it was observed that the settling velocity of particles is lumped by the convective vertical velocity of the mixture. Thus, the convective velocity of the mixture drives the particle motion within the sludge blanket in the clarifier.

From the data extracted in October we can conclude that:

- Simulating a constant inflow and recirculation flow during 51 hours in the clarifier, the SBH will be underestimated when compared to the experimental data.

- cfd Simulations showed that SBH dynamics can be accurately represented by setting the same operating conditions of the clarifier, *i.e.,*, the inlet and recirculation flow rate were changing according to the flow values measured in the WRRF. Even if there is a later response in the prediction of higher peaks of the SBH, one can see that simulated average sludge blanket heights are similar to the measured ones.

It was observed that sludge properties, in particular the mineral content, produce different results in the measured and simulated sludge blanket and RAS concentration. Having similar initial concentrations ($5.54 Kg.m^{-3}$ in April and $4.54 Kg.m^{-3}$ in October), the thickening of the sludge blanket is different. During April campaign the SBH was in average 1.34m, while in October it was in average 0.5m.

Different couplings of settling phenomenological functions from used to describe the Achenheim sludge settling depending on the season where the data was extracted form the WRRF. For April sludge, the Vesilind-DeClercq's simplified form (equations 1.6 and 1.13 respectively) functions are used. The choice was made due to the lack of data to validate first the batch settling test data. This coupling may lead to an overestimation of the SBH within the clarifier, however such overestimation is more remarkable after two hours of settling. In Achenheim clarifier, the sludge is continuously extracted (every 20-30 minutes), thus the risk of SBH overestimation can be neglected. Anyway, results have shown that this coupling can predict an accurate sludge blanket height within the clarifier.

To validate the model using the data of Achenheim clarifier in October, a different settling model was used. The couple Diehl-DeClercq's simplified form (equations 1.8 and 1.13 respectively) is employed. The change was made because we wanted to test from the beginning this approach since Torfs et al. (2016) have found that this couple predicts a more accurate sludge blanket height in batch settling. This coupling predicts as well accurate blanket height results inside the clarifier.

One perspective of this study would be the measurement of the sludge blanket height during the rainy events on the Achenheim WRRF to see deeply the impact of the compression function used for these simulations.

Rheological parameters have also an impact but this was not investigated during this study, this will be discussed in the next chapter 5.

In brief, by using the CFD enhanced solver described in (2) (Valle Medina and Laurent, 2020) and the calibrated parameters found in chapter 3, different CFD simulations were performed and revealed satisfactory results for the prediction of the sludge blanket height and the particles velocity profile.

Chapter 5

CFD case studies

CFD has become a powerful tool for prediction, optimization and analysis of the hydrodynamics inside a WRRF. CFD allows to obtain a glassbox overview of the settling behavior, in which one can observe the behavior of the sludge mixture inside the clarifier. CFD models, being a 3D approach, are normally used to study the hydrodynamics of the clarifier when a physical part is changed (*i.e.*, shape, baffle positions and dimensions, inlet surface... (Flamant et al., 2004, Griborio, 2004, Xanthos et al., 2011, Das et al., 2016).

The aim of this chapter is to present different scenarios by changing some variables in the CFD settling model. On the one hand, the aim is to assess model responses to changes in model parameters and/or functions (compression parameters, rheology). On the other hand, simulating a wet weather condition allows to evaluate if the model is able to capture the expected SBH and RAS dynamics in these conditions.

5.1   Case studies presentation

The different case studies include the variations on:

- The parameter λ of compression function in equation 5.1.

- The critical concentration above which compression starts X_{crit} in equation 2.18.

- A change in the rheological submodel.

- A extremely high hydraulic load.

Like in the previous chapters, an axi-symmetric 2D CFD approach is used to allow faster results. The solver settings are as follows:

- Continuous simulations *i.e.* no intermittent flow is present in the inlet and recirculation;

- Convergence of the simulation is considered when the RAS concentration and the SBH are constant through time;

- The sludge settling model is the coupling of Vesilind function (equation 2.2) and constant solid stress parameter (equation 5.1) for hindered and compression settling respectively. This choice was made because we departed from the validated case of the clarifier of Achenheim using the experimental data in April. During this month a true sludge blanket was seen, therefore within this case the impact of changing the compression parameters will be more remarkable.

- The *buoyancy k-ε* turbulence model is used.

- The inlet sludge concentration is (X_0) of 5.54 Kg·m^{-3}

However, the case with extremely high hydraulic condition has a different setup: the settling velocity model is chosen to be the couple of equations 2.20 and 5.1. As in the previous case, the departing point was the validated case for Achenheim clarifier using the data in October. During this month, a low sludge blanket height was observed, and thus by a CFD approach we want to demonstrate that the clarifier has the capacity of retain solids even at high hydraulic loads. The inlet sludge concentration was set to 4.54 Kg·m^{-3}. The incoming flow was set to a value higher than the maximal flow capacity of the WRRF. For all the cases, the sludge blanket height SBH was measured at the after 36h of simulation. In the simulations the SBH was calculated as the limit between the settled sludge and the clear water, *i.e.* where the concentration in the upper part of the blanket is equal to the initial concentration (X_0).

The velocity, concentration and compression function (d_{Comp}) profiles at 5.4m away from the inlet, and the RAS concentration are measured after 36h of simulation, except for the case with a different rheology model where the profiles were measured at three different radial positions.

Table 5.1 shows a summary of the different cases discussed in the following sections

TABLE 5.1: Summary of the analyzed cases

Case	Modified Parameters Conditions	Objective
Section 5.2	λ for effective solids stress	To observe the impact of the effective solids stress parameters in the prediction of the SBH and RAS concentration
Section 5.3	Critical concentration for compression function	To review the impact of critical concentration value in the prediction of the SBH and and RAS concentration
Section 5.4	Rheology model for sludge viscosity	To understand the hydrodynamics inside the clarifier when the viscosity of the sludge is changed
Section 5.5	Flow initial condition	To analyse the impact of a high hydraulic load in the clarifier performance using a settling model including compression

5.2 Impact of compression parameter λ

In the compression function, the effective solids stress (σ_e') accounts for the property of activated sludge to thicken due to the permanent contact between the flocs and to resist to deformation (Buscall and White, 1987, Aziz et al., 2000). De Clercq (2006) determined in batch experimentation, that the effective solids stress has high values when the initial concentration is high.

To reduce the number of compression parameters within the CFD solver/code, the parameter λ is set equivalent to the derivative of the effective solid stress (σ_e'), and it is only valid when the sludge concentration crosses the critical concentration (X_{crit}). Thus, the primitive of (σ_e') becomes:

$$\sigma_e(\alpha_d) = \begin{cases} 0 & \text{for } 0 \leq \alpha_d < X_{crit}/\rho_d \\ \lambda(\alpha_d - \frac{X_{crit}}{\rho_d}) & \text{for } \alpha_d \geq X_{crit}/\rho_d \end{cases} \tag{5.1}$$

Thus, the parameter λ indicates the magnitude of the slow-down of the settling velocity when the compression is active

Through the calibration process described in chapter 3, we obtained different set of parameters that could describe the settling behavior. We set the limits of parameter λ between 0.01 and $0.1\,\mathrm{m^2 \cdot s^{-2}}$ and the estimated parameter set gave satisfactory results within the first hour of batch settling.

To highlight its influence on the CFD simulation results, a value of $1\,\mathrm{m^2 \cdot s^{-2}}$ is imposed. If the value is higher this will indicate that the settling velocities within the sludge blanket shall be lower than those found in the base case where $\lambda = 0.046\,\mathrm{m^2 \cdot s^{-2}}$ (section 3.3.1) and therefore the prediction of the SBH should be higher.

The case when λ is $1\,\mathrm{m^2 \cdot s^{-2}}$ is compared to the base case at a time step of 36h. Figure 5.1a shows the sludge concentration distribution in the clarifier at such time. It is observed that the average concentration found at the removal patch is $6.18\,\mathrm{Kg \cdot m^{-3}}$. This average predicted RAS concentration is lower compared to the predicted value for the base scenario ($8.66\,\mathrm{Kg \cdot m^{-3}}$). The predicted concentration within all the clarifier is similar (maximal concentration of $6.5\,\mathrm{Kg \cdot m^{-3}}$).

Since, the effective solids stress (σ_e) is analogous to a dispersion term (equation 2.1), its higher value in the simulation yields to a relatively homogeneous solids distribution along the horizontal and vertical axis of the blanket.

The measured SBH at the middle of the clarifier is higher (1.66m) when λ is equal to $1\,\mathrm{m^2 \cdot s^{-2}}$, than when the value of λ is $0.046\,1\,\mathrm{m^2 \cdot s^{-2}}$. A higher value in the compression function, due to a higher value in the effective solids stress, makes that settling velocity to be slower and then an elevation in the SBH is expected.
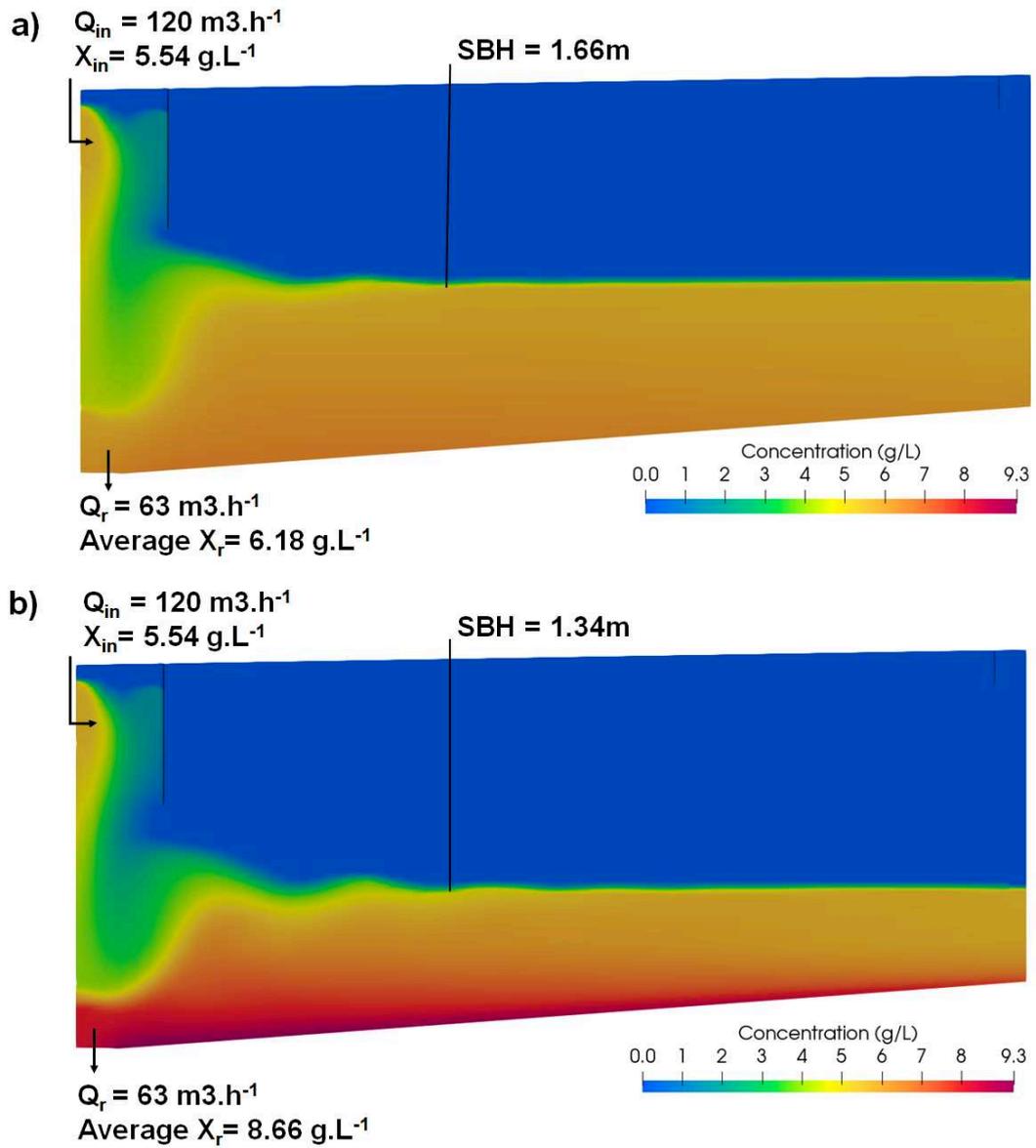
FIGURE 5.1: Concentration distribution after 36h of simulation when
a) $\lambda = 1\,\mathrm{m}^2{\cdot}\mathrm{s}^{-2}$ and b) $\lambda = 0.046\,\mathrm{m}^2{\cdot}\mathrm{s}^{-2}$

The model using λ equal to 1 1 m$^2\cdot$s^{-2} predicts a more constant sludge concentration in the vertical axis (figure 5.2a) . The high dispersion of the sludge is due to the high magnitude of the compression function (dComp) (figure 5.2b)). Hence, the high values of dComp make that settling velocities to be low (figure 5.2c). At the bottom of the clarifier, the velocities seem to rise and to slow-down, this an effect of the constant concentration along the vertical axis.

FIGURE 5.2: a) Concentration b) Compression function (dComp) and
c) Velocity profiles after 36h of simulation, measured at 5.4m away
from the inlet

In summary, a high value of parameter λ results in a very high sludge dispersion within the blanket. A sludge with such compression behavior would have bad thickening properties as the sludge concentration barely increased, from 5.54 Kg$\cdot$m^{-3} at the inlet to 6.18 Kg$\cdot$m^{-3} at the outlet. Thus, a high amount of sludge would remain inside the clarifier, producing maybe some denitrification or sludge bulking trouble.

5.3 Impact of critical concentration X_{crit}

The critical concentration (X_{crit}) dictates the limit between the hindered and the compression regimes. Thus, in batch settling, a higher value of X_{crit} yields to a lower SBH as compression will start later. In the calibration process, the limits for the X_{crit} values were initially set between 4 to 6 Kg$\cdot$m^{-3}.

In this simulation scenario, a significantly higher value of 8 Kg$\cdot$m^{-3} has been set. The simulation results do not show a constant sludge blanket height after 36 hours of continuous simulation. However, the concentration at the removal reaches an average constant value of 9.51 Kg$\cdot$m^{-3}.

From equation 3.1 the compression function is only active when the sludge concentration crosses the 8 Kg$\cdot$m^{-3} and this occurs after 1 hour of continuous flowing. The

compression function is active after 30 minutes. This delay is expected as the sludge needs more time to thicken to reach the $8\,\mathrm{Kg\cdot m^{-3}}$.

Surprisingly, the higher value of X_{crit} predicts a higher sludge blanket (figure 5.3a) (2m against 1.34m). This behevior was not expected as a higher compression limit would lead to a lower sludge blanket. One hypothesis to explain this is as follows: as compression is only active for a high concentration, the sludge thickens faster in the upper parts of the sludge blanket (hindered settling only). This solids flux coming to the bottom yields to a higher concentration that crosses the X_{crit} value. The higher MLSS concentration leads to a higher viscosity as computed by the Bokil and Bewtra (1972) relation (equation 1.40). As the shear stress at the bottom is low, this restrains the flow to reach out the removal and induces the observed SBH increase. The motion of the scrapper at the bottom of the tank may overcome this viscosity problem by breaking the shear stress of the sludge.

In figure 5.4a and 5.4b the concentration profile and compression function profile are shown respectively. In contrast to the previous case, when the value of X_{crit} is $8\,\mathrm{Kg\cdot m^{-3}}$, the difference between the beginning of the compression zone (0.95m, figure 5.4b) and the sludge blanket (2m, figure 5.4a) do not coincide. The former behavior can be explained by the fact that compression function is constant through time depending only on the local concentration. The limit of the compression zone will rise only when the concentration in each cell will be higher than $8\,\mathrm{Kg\cdot m^{-3}}$.

When $X_{\mathrm{crit}} = 8\,\mathrm{Kg\cdot m^{-3}}$:

- The concentration profile (figure 5.4a) clearly displays a concentration trend similar to the one observed in a batch column. This confirms that in this zone of the clarifier quiescent conditions are present. Due to the delay of sludge to cross the critical concentration, sludge accumulation is higher and thus the prediction of the concentration at the bottom of the clarifier is higher ($9.8\,\mathrm{Kg\cdot m^{-3}}$) than the simulated one with the reference scenario ($8.8\,\mathrm{Kg\cdot m^{-3}}$).

- As expected, the values of the compression function (figure 5.4b) are lower to those of the reference case. Within the sludge blanket, settling velocities are lower and produce the small values for *dComp*.

- The velocity profile (figure 5.4c), again show the trend of the settling velocity expected in a batch column. A constant velocity between 1.9–1.42m is observed indicating that sludge is in hindered regime.

Table 5.2 shows the differences of the values obtained for the SBH and the RAS concentration between the reference case and the study cases. In this simple approach, it is observed that λ will have a bigger impact on the prediction of the sludge concentration, while X_{crit} will impact on the prediction of the SBH.

a) Q_{in} = 120 m3.h^{-1}
X_{in}= 5.54 g.L^{-1}

SBH = 2m

Concentration (g/L)
0.0   1   2   3   4   5   6   7   8   9   10.2

Q_r = 63 m^3.h^{-1}
Average X_r= 9.51 g.L^{-1}

b) Q_{in} = 120 m3.h^{-1}
X_{in}= 5.54 g.L^{-1}

SBH = 1.34m

Concentration (g/L)
0.0   1   2   3   4   5   6   7   8   9   10.2

Q_r = 63 m3.h^{-1}
Average X_r= 8.66 g.L^{-1}
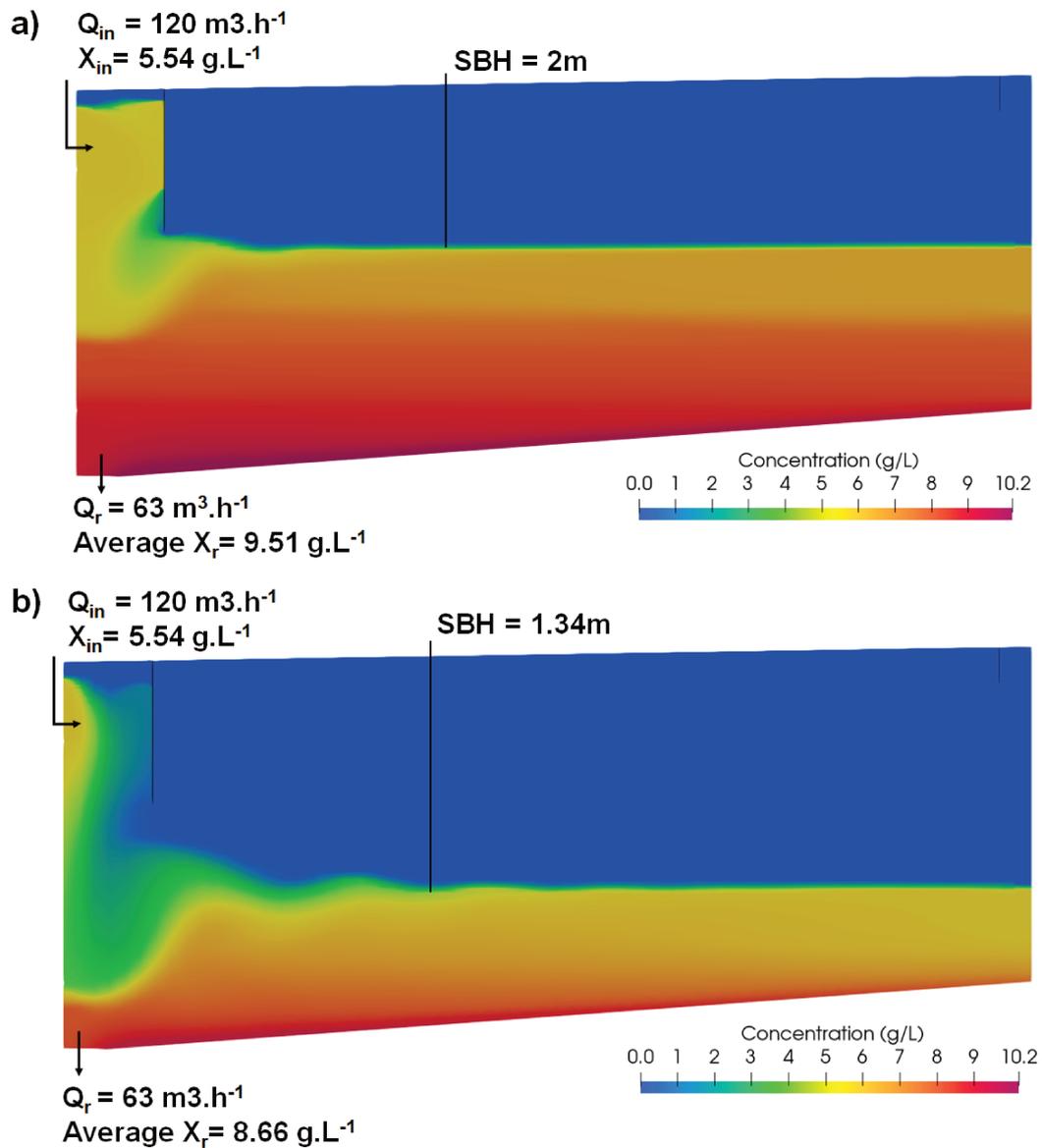
FIGURE 5.3: Concentration distribution when a) X_{crit} is equal to $8\,\mathrm{Kg\cdot m^{-3}}$ b) X_{crit} is equal to $5.5\,\mathrm{Kg\cdot m^{-3}}$

TABLE 5.2: Differences between the reference case and the predicted SBH and RAS concentration when the compression parameters are changed. Negative values indicate an underprediction in respect to the reference case.

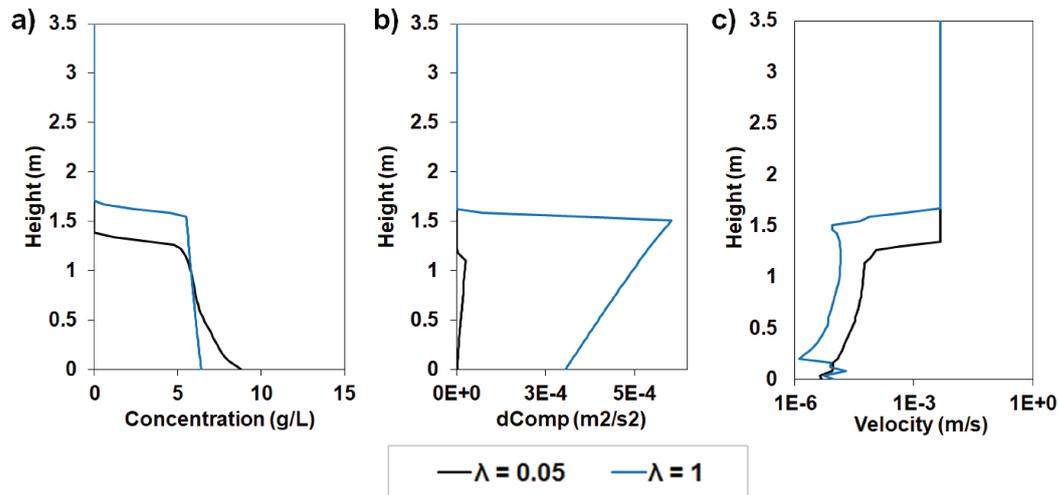|	λ	X_{crit}
SBH (m)	0.36	0.7
RAS concentration (g·L^{-3})	-2.48	0.85
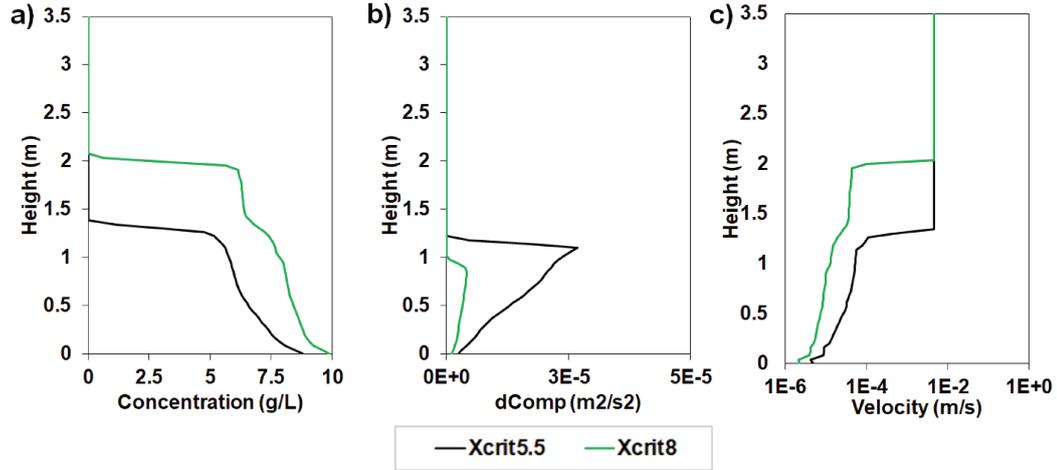
FIGURE 5.4: a) Concentration b) Compression function (dComp) and c) Velocity profiles at 36h of simulation measured at 5.4m away from the inlet when the value of X_{crit} is equal to $8\,\text{Kg·m}^{-3}$.

5.4 Modification of the rheological submodel

Rheological properties affect the mixing of the sludge and mass exchanges between solid and liquid phase. For this scenario, the effects of using the yield stress (τ_0) to describe the viscosity of the sludge are analysed.

5.4.1 Models description

Some authors concluded that a Bingham-type fluid is a proper model for sludge rheology (Lakehal et al., 1999, Dahl, 1993). Other authors prefer to use the plastic viscosity (μ_0), due it was shown that a true yield stress in the sludge do no exist (De Clercq, 2003 Griborio, 2004) or it is only valid for higher sludge concentrations ($> 10\,\text{Kg·m}^{-3}$).

Therefore, two different rheology models are applied to study:

1. Model *plastic*: the base case uses the relation of Bokil and Bewtra (1972) (equation 1.40), where the plastic viscosity dictates the fluidity of the sludge, the latter being a function of the concentration.

2. Model *Bingham plastic*: the model approach adds a yield stress which is also in relation to the sludge concentration (Dick and Ewing, 1967) (equation 1.41).

In OpenFOAM, the model to calculate the plastic viscosity of the mixture(μ_0) is exponential and independent of the shear rate. It is only dependant in the mixture volume fraction:

$$\mu_0 = PC * 10^{(PE*\alpha)} \tag{5.2}$$

Where PC and PE are parameters for the viscosity model. The parameters are set into the *transportProperties* file (see Apprendix A).

For the Bingham approach, the apparent viscosity (μ_{app}) of the mixture is calculated using the yield stress (τ_0), the plastic viscosity (μ_0) and the rate of strain (equivalent to the velocity gradient) (equation 5.3). The yield stress is calculated from the Dick and Ewing (1967) equation (equation 2.24) but noted in base 10 and in function of the volume fraction.

$$\mu_{\text{app}} = \mu_0 + \frac{\tau_0}{|\dot{\gamma}|} \tag{5.3}$$

The parameters used for the Bokil and Bewtra (1972) and Dick and Ewing (1967) equations are those in table 4.7, which describes the rheology characteristics of the sludge sample taken in April.

For this case, the sludge blanket height and the concentration and settling velocity vertical profiles, are extracted at three different radial positions. The settling velocity profiles of the Bingham plastic model are compared to the base case and the experimental ones.

5.4.2 Results: concentration profiles

The RAS concentration after 36h of simulation is $10.5\,\text{Kg·m}^{-3}$. Figure 5.5 shows the sludge concentration distribution and the calculated sludge blanket height at different radial positions.

Compared to the base case, only at the middle of the tank (Rd = 5.4m) the SBHs are estimated similar for both cases. In the base case, no yield stress is considered and thus the mixture can flow freely at the bottom of the tank and thus reach the external wall more rapidly producing an homogeneous elevation in the horizontal direction of the clarifier (figure 5.5b).

In figure 5.5a it is observed that the distribution of the sludge blanket is not uniform in the horizontal axis. The yield stress of the sludge makes that the sludge starts to thicken near the inlet zone. With the slow incoming flow, the shear stress of the sludge is hard to break producing a thickened blanket that moves hardly to the external wall. Thus, this makes a high elevation in the blanket near the inlet zone and decreasing at the external part of the clarifier. High sludge concentrations within the sludge blanket are found near the external wall. By considering a yield stress for the activated sludge, the mixture offers resistance to deformation while moving towards the outlet, and thus a more concentrated sludge can be found in a zone where no shear rates are present.
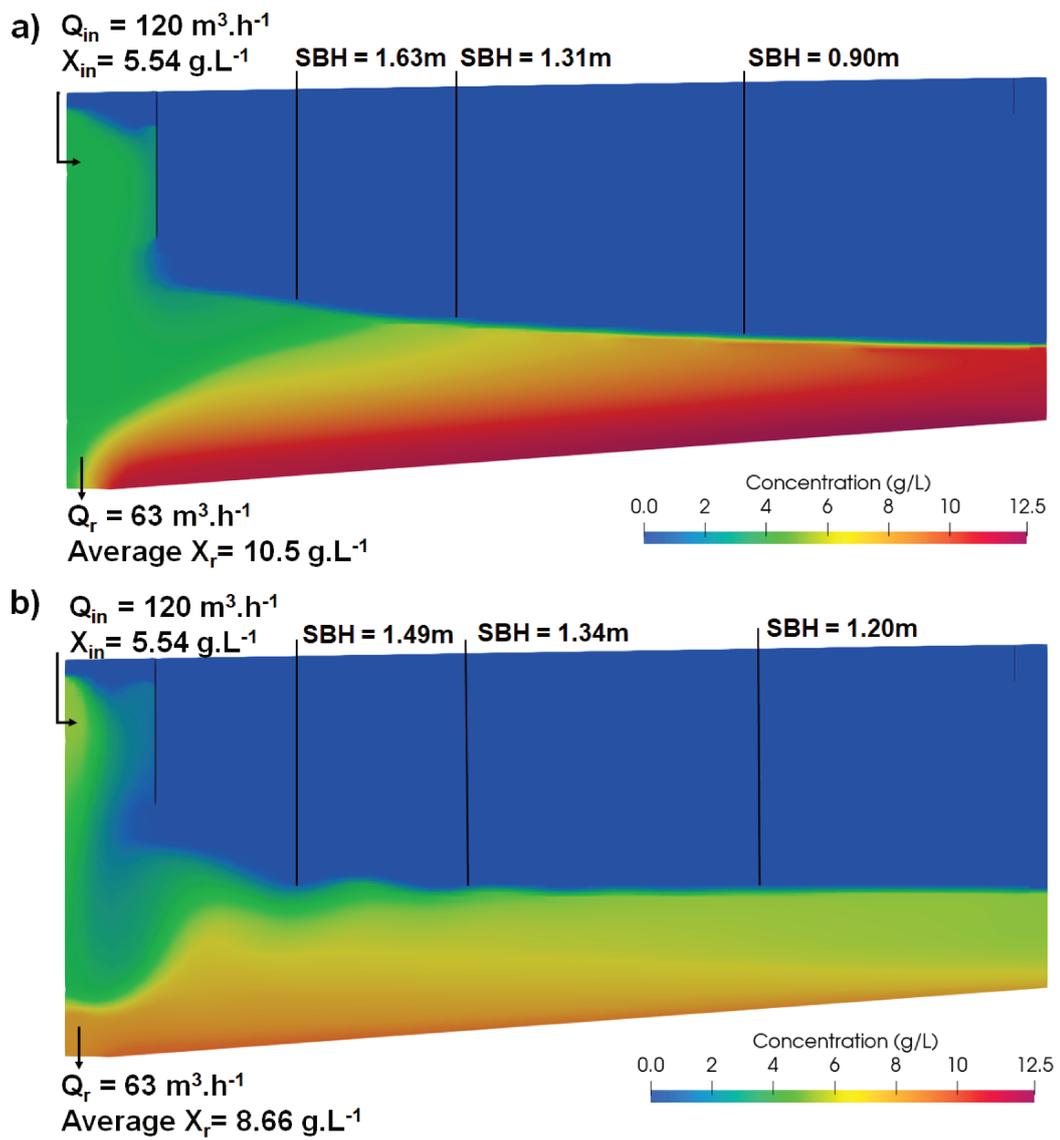
FIGURE 5.5: Sludge distribution for a) The Bingham-Plastic and b) Plastic rheology models

In the concentration profiles (figure 5.6), it is observed that the concentration at the bottom of the tank remains almost constant along the clarifier when the yield stress is computed. The high viscosity of the sludge makes it less fluid and thus, to be more concentrated and homogeneous in the horizontal axis.
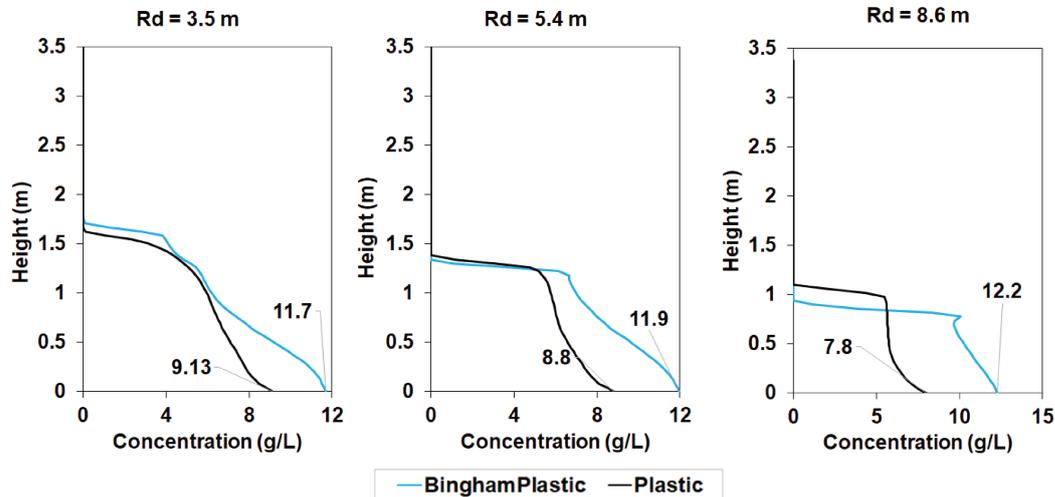
FIGURE 5.6: Concentration profiles for the model with the Bingham rheology approach and the base case at different radial distances (Rd) and the value of the concentration at the bottom of the tank

5.4.3 Results: sludge blanket height and velocities

The yield stress of the activated sludge produces a high elevation of the blanket near the inlet. Therefore, the velocity of the mixture is slowed down at the level of the sludge blanket (figure 5.7a). Indeed, the high viscosity allows the sludge to slowly disperse and thicken, restraining the direct path to the removal patch. Hence, there is a small gap between the baffle and the sludge blanket (figure 5.7a) which could block the free transit of the activated sludge along the clarifier. The yield stress of the settled sludge is difficult to overcome by the slow incoming flow.

In agreement to the Lakehal et al. (1999) findings, the settling velocities are lower when the Bingham plastic model is used, *e.g.* at a radial position of 8.6m, the domain of settling velocities within the blanket varies from $7.74.10^{-5}$ to $3.95.10^{-7}$m.s^{-1} (figure 5.8c). In comparison, the simulation using the plastic model predicts settling velocities varying from $8.11.10^{-5}$ to $4.76.10^{-6}$m.s^{-1}. Hence, at the bottom of the blanket (below 0.5m), the predicted settling velocities are in average 8 times lower when the sludge is Bingham type. With a high viscosity and no fluid motion at the bottom of the tank and near the outlet, the sludge remains in quiescent conditions to settle slowly.

According to the experimental measurements made on the full-size clarifier (section 4.3.1) the velocities within the sludge blanket can vary from 3.10^{-3}m.s^{-1} in the upper part of the blanket, to 1.10^{-6}m.s^{-1} at the bottom (figure 5.9).
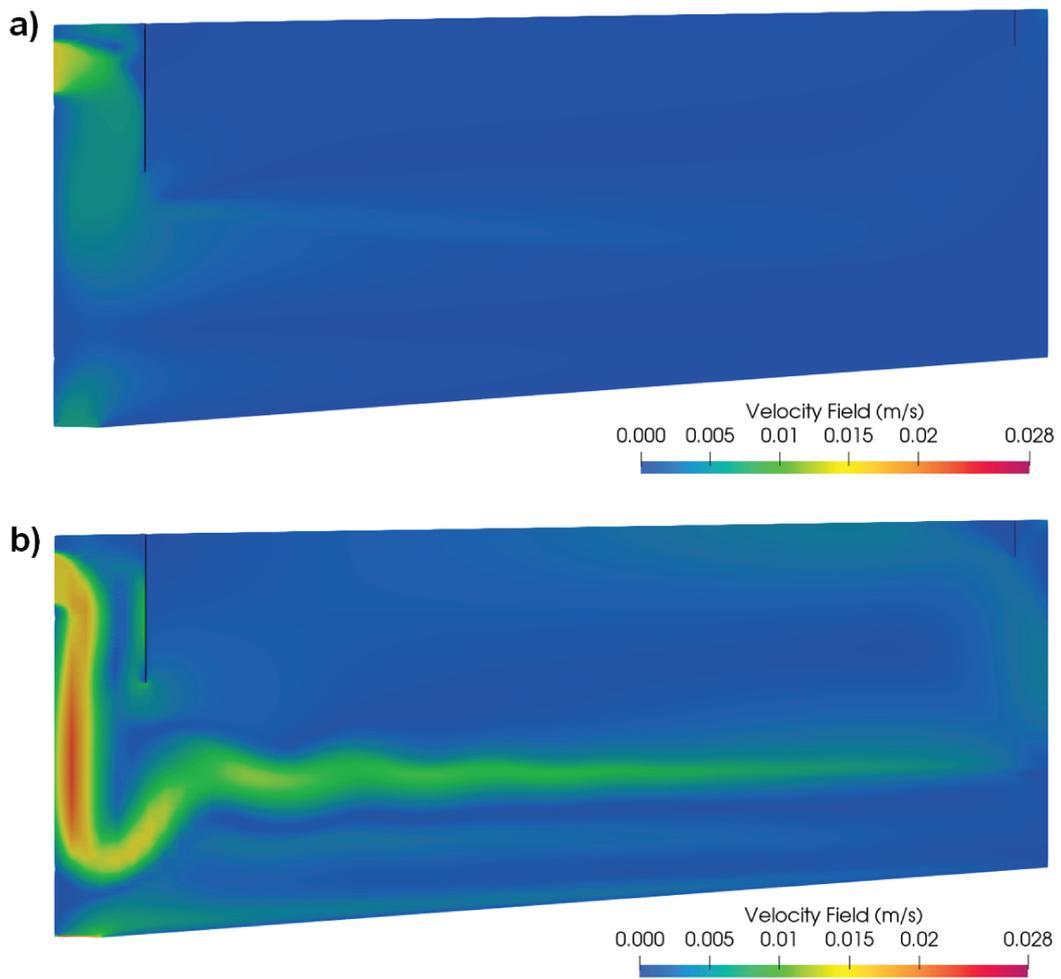
FIGURE 5.7: Mixture velocity after 36h of simulation a) Bingham-plastic and b) Plastic rheology approach in the CFD model
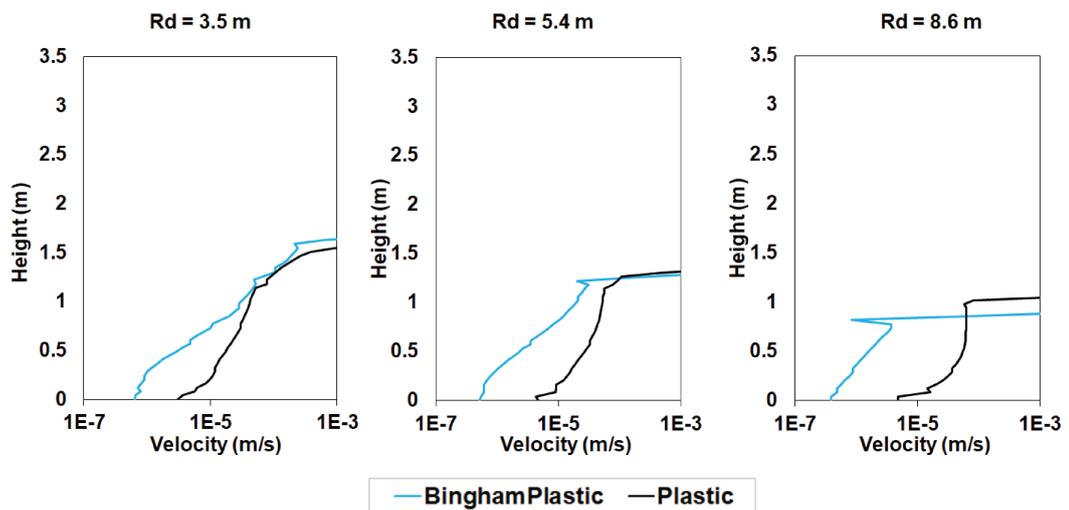
FIGURE 5.8: Velocity profiles for the Bingham and the plastic rheology approach at different radial distances (Rd)
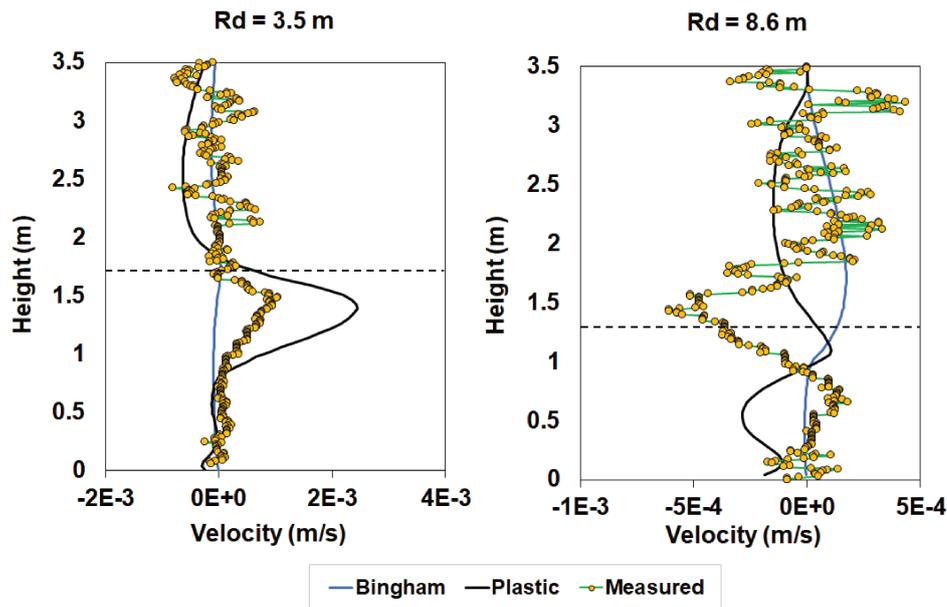
FIGURE 5.9: Vertical velocity profiles for the measured data; and simulations performed with plastic and Bingham-plastic rheology models at two different radial distances after 36h of simulation. The dotted line indicates the beginning of the sludge blanket

Figure 5.9 shows the velocity profiles of the experimental data and the plastic and Bingham-plastic models after 36h of simulation. The predicted values of the particle velocities with the Bingham-plastic model (blue continuous line) are underestimated, compared to the measured ones. Such behaviour can be observed in both radial distances. Indeed, the high yield stress of the sludge slows-down the convective velocity of the mixture in the vertical direction. The plastic model makes in average a better prediction of the settling velocities.

Again, the MAE (equation 3.7) is calculated for the particle velocity profiles all the depth of the clarifier. At a radial distance of 3.5m (figure 5.9), the MAE are $4.99x10^{-4}$ and $2.61x10^{-4}$ for the simulated bingham and plastic sub-rheological models respectively. At 8.6m the MAE are $8.77x10^{-4}$ and $2.06x10^{-4}$ for the simulated bingham and plastic sub-rheological models respectively. Indeed, the MAE confirms that a bingham plastic approach is predicting slower vertical settling velocities.

However, figure 5.9 is only illustrating, not validating, the influence of the yield stress in the vertical velocity of the particles. The CFD modeling is done in continuous flow and thus, no influence of the dynamic flow is observed in these profiles (refer to section 4.3.1 for the dynamic flow study).

Lastly, the Bingham plastic model is over predicting the SBH near the inlet and under predicting it near the external wall zone. The concentration at the bottom of the tank is predicted high and invariant along the clarifier. Hence, the estimated settling velocities within the sludge blanket are smaller compared to the measured ones.

5.4.4 Results: impact of the viscosity in the compression function

As stated in the former case, the high viscosity of the activated sludge induced lower predicted settling velocities as with less viscous sludge. Thus, if settling velocities within the hindered zone are becoming slower, the same trend can be observed with the compression function. In figure 5.10a the low values of the compression function are present esspecially near the external wall where the motion of the incoming fluid do not disturb the sludge settling. In the plastic model approach the sludge has no yield stress to beat, therefore the sludge settling is becoming faster producing in some areas a lower sludge blanket (5.10b)
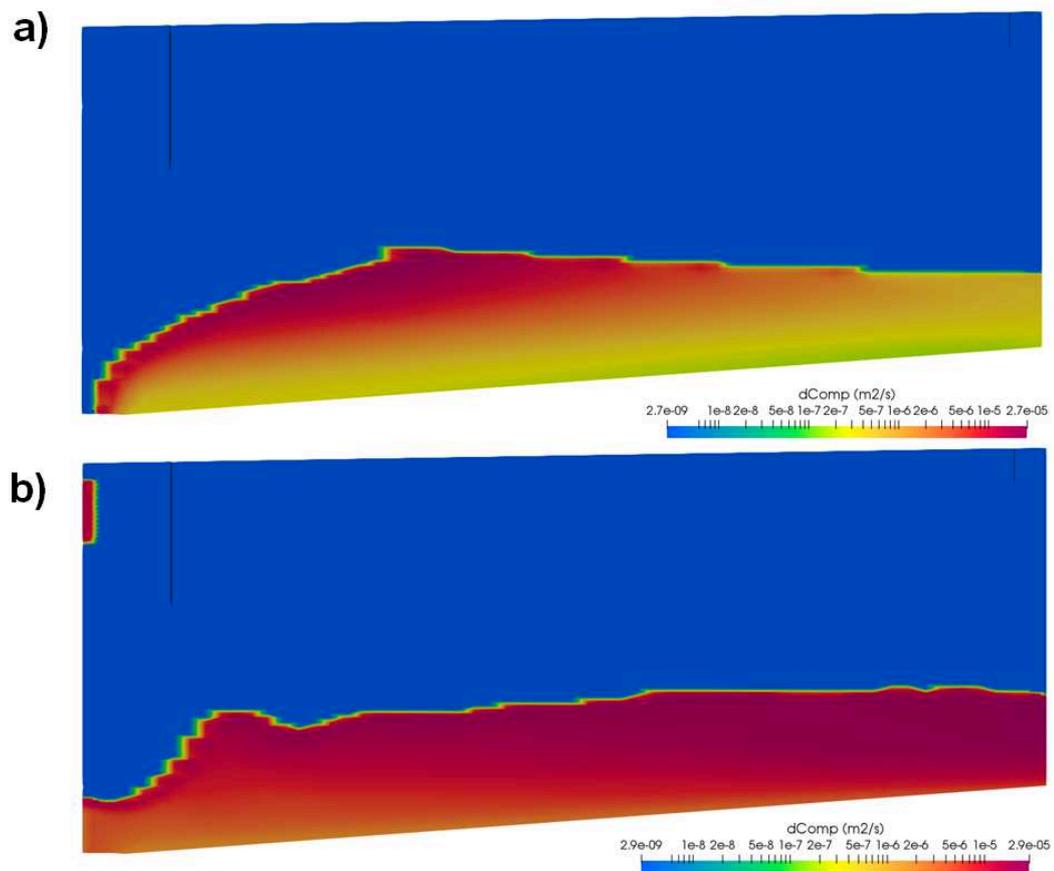
FIGURE 5.10: Compression function distribution within the clarifier
for a) Bingham plastic model and b) Plastic model

Care must be taken, if the Bingham type model is chosen to simulate the rheology of the sludge, when a slow flow is coming into the settling tank. The predictions exaggerate the elevation of the sludge blanket at the inlet, which may block the free transit of the fluid predicting a short-circuiting in the clarifier.

If a Bingham-plastic model is chosen for activated sludge modeling in a CFD approach, one should consider to include the movement of the scrapper at the bottom of the tank (Lakehal et al., 1999). This will help to overcome the yield stress of the

sludge and thus, to increase the fluidity of the settled sludge. This should allow to simulate a more realistic behavior of the sludge.

5.5   High hydraulic load scenario

In the case of a combined sewer network, rainy events that occur during the operation of a WRRF, *i.e.* high hydraulic loads can modify the normal behavior of the clarifier by washing out the sludge and worsening the effluent quality. A high hydraulic load represents a high mass of sludge and high velocities coming into the tank, producing an increase on the sludge inventory and a high content of TSS at the effluent.

In a circular clarifier, a density current is created at the bottom of the tank in the surface of the sludge blanket (figure 5.11). According to Patziger (2016), the density current vanishes before arriving to the external wall, if the surface overflow rates are lower than a surface overflow rate value of 1.1 -1.2 m·h^{-1} (Patziger et al., 2012)). Rainy episodes are characterized by exceeding the critical surface overflow rate and thus, high fluid velocities are directed towards the outlet. This could produce an increase in the effluent suspended solids (Patziger et al., 2012).
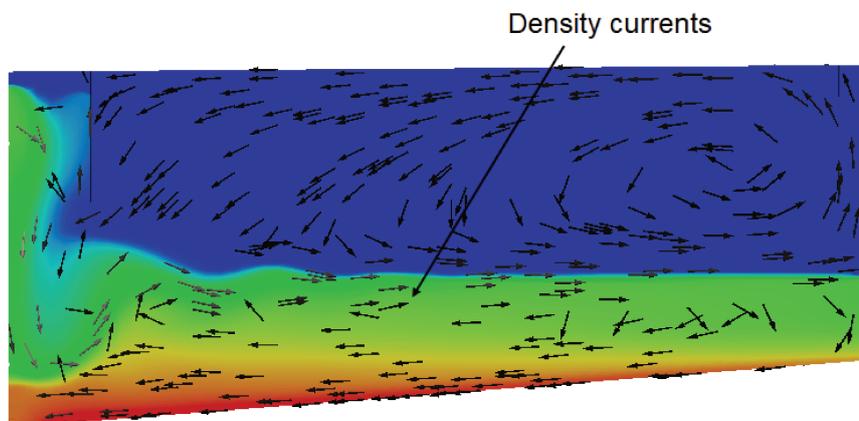
FIGURE 5.11: Density current for a dry weather scenario

For Achenheim WRRF, different hydrodynamic behaviours were observed in April and October. From the continuous sludge blanket measurements carried on in October, it was observed that a very thin sludge blanket was presented. The high mineral content in the sludge was the variable in contrast between the two seasons (see chapters 3 and 4).

This case study deals with the impact of a high hydraulic load when a highly mineral sludge is considered. A higher hydraulic load should result in an elevation of the SBH and possible failure in the settling tank by sludge leakage in the effluent.

By adding the compression function in the model, a more realistic prediction in the sludge blanket and RAS concentration is expected, than using an equation only accounting for the hindered settling during wet weather conditions (Torfs et al., 2015b).

The following case simulates a high hydraulic scenario where the surface overflow rate (SOR) is higher compared to a dry weather scenario. Thus, the values of Q_{in} and Q_r were set to $538 \, \text{m}^3 \cdot \text{h}^{-1}$ and $288 \, \text{m}^3 \cdot \text{h}^{-1}$ respectively. The sludge concentration at the inlet X_{in} is set to $4.54 \, \text{Kg} \cdot \text{m}^{-3}$. Table 5.3 makes a summary of the operation parameters for the wet weather and reference scenarios.

TABLE 5.3: Operation parameters of the clarifier in two scenarios.

	High hydraulic load	Normal flow
$Q(\text{m}^3 \cdot \text{h}^{-1})$	250	52
$Q_{in}(\text{m}^3 \cdot \text{h}^{-1})$	538	115
$X_{in}(\text{Kg} \cdot \text{m}^{-3})$	4.54	4.54
Inlet mass flux $(\text{Kg} \cdot \text{h}^{-1})$	2443	522
$Q_r(\text{m}^3 \cdot \text{h}^{-1})$	288	63
Recirculation factor	1.15	1.21

Figure 5.12b shows the distribution of the sludge within the clarifier when a higher hydraulic load comes into the clarifier. After 36 hours of simulation, the maximum reached height for the blanket is 0.8m and the RAS concentration is $7.33 \, \text{Kg} \cdot \text{m}^{-3}$, those values are higher compared to the dry scenario after (figure 5.12a). Indeed, a higher sludge inventory inside the tank is expected as more sludge is coming into the clarifier.

For both scenarios, the maximum concentrations predicted at the bottom of the tank are high. This is due to the high settling velocity of the sludge. The high mineral content of the sludge causes a very high hindered settling velocity which may lump the compression effect producing a higher sludge accumulation.

TABLE 5.4: Simulation results of the clarifier in two scenarios.

	High hydraulic load	Normal flow
$X_r(\text{Kg} \cdot \text{m}^{-3})$	7.33	4.94
Recirculation mass flux $(\text{Kg} \cdot \text{h}^{-1})$	2052	311
Mass inside the tank (Kgn)	5800	730

In the wet weather scenario, it is more noticeable that baffles acts as an energy dissipator (figure 5.13a). Hence, a higher sludge blanket is expected as more solids are entering the tank. The high elevation of the sludge blanket, makes that the fluid goes towards the external wall dissipating the energy while it is crossing the tank. Less risk of the incoming fluid moving towards the removal is presented. In contrast, in the reference case the fluid goes immediately towards the bottom of the tank causing a risk of short-circuiting (figure 5.13b).

(a)
Q_{in} = 115 $m^3.h^{-1}$
X_{in}= 4.54 $g.L^{-1}$
SBH = 0.08m

Concentration (g/L)
0.00   5.5   11   16.5   22.00

Q_r = 63 $m^3.h^{-1}$
Average X_r = 4.94 $g.L^{-1}$

(b)
Q_{in} = 538 $m^3.h^{-1}$
X_{in}= 4.54 $g.L^{-1}$
SBH =0.80m

Concentration (g/L)
0.00   7.5   15   22.5   30.00

Q_r = 288 $m^3.h^{-1}$
Average X_r = 7.33 $g.L^{-1}$
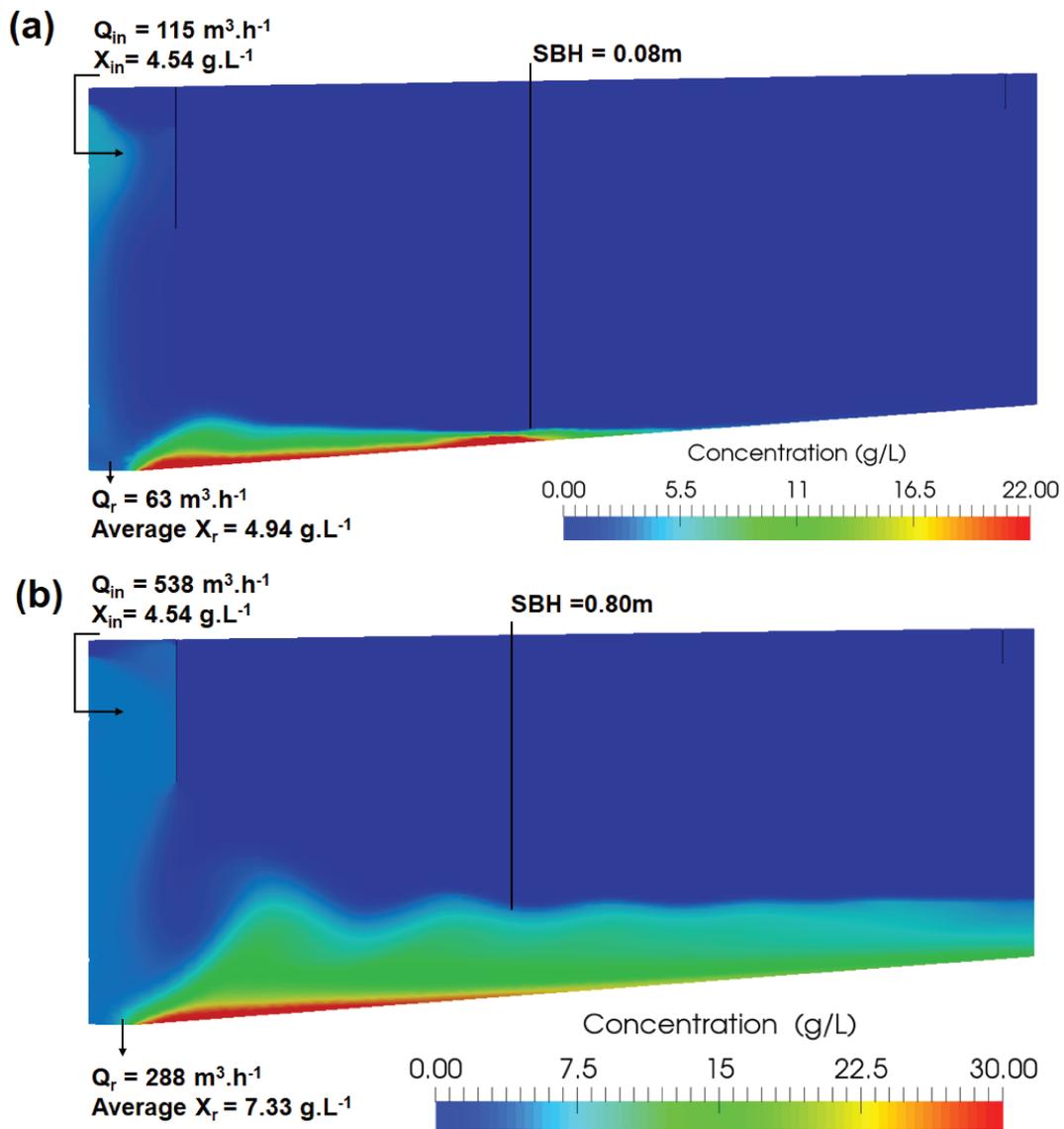
FIGURE 5.12: Concentration distribution after 36 hours of simulated
a) normal flow, and b) high hydraulic load
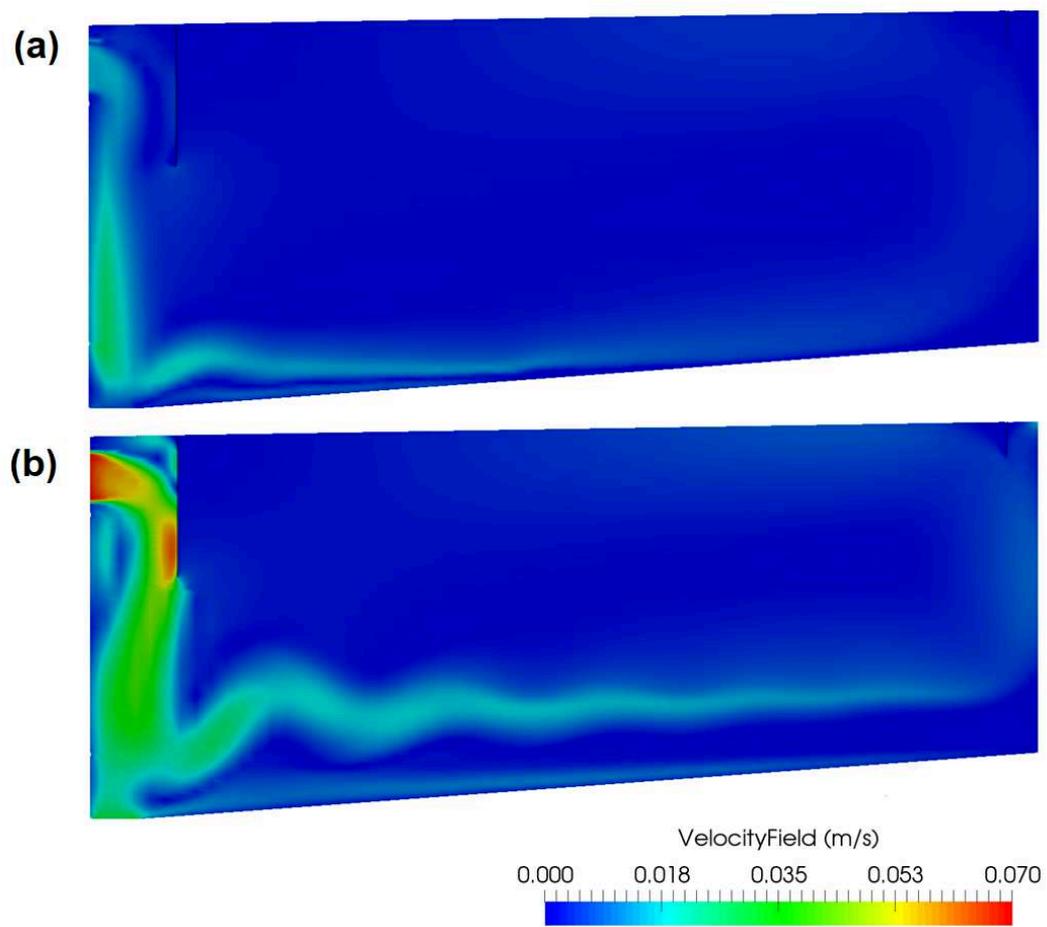
FIGURE 5.13: Fluid velocity distribution during constant a)high hydraulic load scenario, b)normal flow

It was observed, that even at a high hydraulic load, the prediction in the SBH is still low. From the statement of Patziger, 2016, the simulated SOR ($0.7\,\text{m·h}^{-1}$) in this high hydraulic load scenario, has not yet cross the critical SOR, and thus, the incoming flow can transit in quiescent conditions without risk of short-circuiting. It should be noticed that, in France, SSTs are often designed with a SOR of $0.6\,\text{m·h}^{-1}$ calculated on the peak flow.

This indicates that the WRRF can probably operate at higher hydraulic loads. The clarifier is able to retain the higher incoming sludge mass while not compromising effluent quality.

Hence, it noticeable that sludge is not really thickening near the removal zone in the normal flow scenario. The sludge tends to thicken more when a high hydraulic load is presented. This not thickening behaviour may be explained by the fast settling of the sludge produced by the high content in minerals. The sludge is then easily washed out through the continuous removal.

5.6 Conclusions

These sections showed different CFD scenarios where some parameters of the compression function in the settling model, the rheological approach or the flow at the inlet were modified. The cases revealed how important and useful CFD can be to understand the hydraulic behaviour of a settling tank.

In general, a change in the compression parameters will predict different sludge blanket heights, the distribution of the sludge inside the clarifier and the concentration at the removal of the clarifier.

The value for parameter λ was increased by 20 times the value used for the reference case. This resulted in a high sludge dispersion within the blanket zone along the clarifier. This predicts failure in the clarifier due to the no thickened sludge the removal.

The X_{crit} was increased 1.45 times the value used for the reference case. This change over-predicted the sludge blanket height. The simulation presented here, the trend of the SBH was to rise within the first 36 hours of continuous settling. The simulation seems to estimate a extremely high SBH when the steady state will be reached. Nevertheless, at this time the predicted sludge blanket height is already elevated compared to the measured sludge blanket in section (4.3.1).

In the 1D models, it was observed that exponential functions describing hindered settling may lump the effect of the compression function in the prediction of the sludge blanket height (Torfs et al., 2016). However, in the CFD model it was observed that the compression function has also a high impact in the distribution of the solids, which is not really captured by a 1D model.

Indeed, the value of λ will have a greater impact on the sludge concentration prediction along and at the removal of the clarifier. The parameter X_{crit} will have a more noticeable impact on the sludge blanket height prediction.

The WRRF of Achenheim can operate at high hydraulic loads without compromising the effluent quality. Through the CFD rainy event case it has been seen that the clarifier can store the exceeded incoming sludge and thicken it without affecting too much the sludge concentration at the removal and/or the treated water quality. The sludge properties are an important variable for the sludge settling accumulation. A high content in mineral content will lead to a fast particle settling, and thus a non-thickened sludge blanket with high sludge concentrations at the bottom. This would show that the compression function is not active.

For the sludge from Achenheim, the plastic model fits better to simulate its hydrodynamics. The experimental results showed that a uniform sludge blanket surface can be found all along the axis, and that the settling velocities are higher near the inlet and not in the external wall.

It was demonstrated that a plastic sludge flows better to the hopper due to gravity (higher bottom concentration near the removal), which is an expected behavior in a clarifier. In this case, the settling velocities are affected by the type of rheology model employed, the Bingham plastic model predicts lower settling velocities than the plastic model.

The compression function effect is almost imperceptible when a Bingham plastic model is used, particularly in zones in quiescent conditions. The estimated settling velocities are very small at the bottom of the blanket, and in zones where there is no vertical concentration gradient.

These simulations highlight the importance of calibration and validation of the CFD model applied to SST. Indeed, changing parameters of the settling/compression function and the structure of the rheological submodel have significant impact on model predictions.

Here, the choice of the turbulence model (buoyant k-ϵ) was based on Brennan (2001) suggestions. The impact of turbulence modeling was not in the scope of this research. However, other simulations performed with our solver demonstrated that the standard k-ϵ model do not predict a true limit between the clear phase and the settled sludge (data not shown), and the prediction of the SBH was excessively high. This area obviously deserves more research.

Thanks to this exercise, we can support the importance of using Computational Fluids Dynamics models as an optimization/prediction/control tool. By changing some variables, we analyzed the possible consequences in the prediction of the sludge at the removal, sludge concentration or possible short-circuiting within the tank.

Conclusions and Perspectives

Conclusions

This study presented the development of a modified drift-flux solver for the Open-FOAM® open-source platform, called now *compressionFluxFoam*. The solids transport equation includes an extra second-order term that accounts for compression. A simplified constitutive function of De Clercq et al. (2008) was used. An addtional constitutive functions to describe hindered settling was included: the power-law expression of Diehl (2015). These developments integrate the most up-to-date knowledge of activated sludge sedimentation mechanisms that were surprisingly never implemented in the present form in a CFD code.

Within this study we confirmed, in accordance to the experimental test carried on by Locatelli (2015), that the content of mineral matter in activated sludge deeply impacts the settling velocity. Indeed, the batch settling test for the same sludge showed very different settling velocities, even at similar initial concentrations. For example, the sludge with an initial concentration of $4.54\,\mathrm{Kg \cdot m^{-3}}$ settles at $6.81 \times 10^{-4}\,\mathrm{m \cdot s^{-1}}$ which is almost 4 times higher to the settling velocity when the initial sludge concentration is $4.16\,\mathrm{Kg \cdot m^{-3}}$. The high mineral content (55% of NVSS) of the sludge at $4.54\,\mathrm{Kg \cdot m^{-3}}$ makes it to settle faster.

For this reason, it was not possible to gather all the sludge batch test in just one representative model for hindered settling. Hence, it was observed that the content in mineral mineral was increasing from 37% of NVSS in January to (55% of NVSS) in October. The experimental campaigns carried on during this study had different results, not expected, but interesting as well. The campaign where a notable sludge blanket was observed and particles velocities were successfully tracked, showed an interesting behavior of the velocities within the sludge blanket. Maybe this behaviour is due to the density currents produced by the different phases, that disturbs the quiescent conditions inside the sludge blanket.

Unfortunately, we were not be able to observe this behaviour in the next campaigns. The NVSS content was increasing in the next months, reaching a value of 55% in the last campaign. This content obviously affect on the settling velocity and thus, the performance of the clarifier. The fast particles settling process observed can explain that a very thin sludge blanket was observed. Thereby, it was difficult to validate

the model with the particles settling velocities in this campaign carried out during 51 hours.

The CFD model was able to reproduce the batch settling behaviour within the first hour. The parameters describing this batch behaviour were accurate enough to use them later for the axi-symmetric clarifier simulations. Hence, the prediction on the particle settling velocities was improved by adding the compression function. Results in the axi-symmetric clarifier were satisfactory. Indeed, the sludge blanket height was reproduced accurately, for both measurements in 20 minutes and 48 hours.

It was shown that in the full-scale clarifier, the settling velocities of the particles are eclipsed by the convective vertical flux of the fluid (mixture). Experimentally, it was observed that the particles velocities are in order of magnitude between 1.10^{-3} m·s^{-1} and 1.10^{-4} m·s^{-1} while in batch the settling velocity of the particles are less than 1.10^{-5} m·s^{-1} within the sludge blanket. The CFD model could prove indeed, that in the clarifier the settling velocities of the particles are lumped by the vertical velocity of the mixture.

The rheology model in the hydrodynamic modelling of activated sludge settling plays an important role. Using a Bingham plastic approach will result in a highly viscous sludge that can damp flow fluctuations. It is recommended to use this rheology model when one is sure to break the sludge yield stress, *i.e.*, including the effect of the scrapper.

Perspectives

The CFD model still needs to improve its performance. Several studies have pointed out that the critical concentration is not constant with time. Locatelli (2015) described this behavior by an empirical exponential equation. However, from a physical point of view, the critical concentration should not be dependant of the initial/inlet sludge concentration. Thus, experimental evidence has shown that changes in the flocculation state of particles influence the compression (Torfs et al., 2015b). Including an equation for each class/size of particle like the approach described in Torfs et al. (2016), would improve the prediction of the sludge blanket height and thus, the RAS concentration will be better estimated. Hence, the prediction in the effluent quality will take part within the outputs of the CFD model and thus gives an estimation of the performance of the clarifier.

The intermittent flow of the small WRRFs, shows that they have strongly different operational conditions than the bigger ones (PE > 90 000). Indeed, the inactive/active periods of both recirculation and inlet pumps affect the performance of

the clarifier. CFD SST modellers should also look into this small WRRFs to test and improve the existing models.

In this work, we have coupled DAKOTA software to OpenFOAM for parameter estimation. This tool offers promising perspectives for:

- using global sensitivity and estimation algorithms for an improved calibration process in batch settling and full-scale SST simulation;

- improving geometrical design of the tank. DAKOTA can be used for automatic shape optimization. Within SST, several geometrical features can be modified to improve the performances: size of the internal baffles, baffles distance from the inlet, scrapper rotation and configuration, tank size, effluent dissipation inlet configuration. The possibilities are unlimited to optimize the performance of SSTs.

The CFD solver can also be improved by adding new rheological models. Currently, within the new solver, OpenFOAM only accounts for the plastic and Bingham-Plastic models to describe sludge viscosity. Other models type like Cross, Herschel-Buckley, Carreau, should be included in order to study also the effects of adding the shear-thinning (pseudo-plastic behaviour) in the hydrodynamics of the activated sludge. This open perspectives to use this solver in other unit processes that SSTs where density gradients and rheological properties can affect significantly the hydrodynamic properties like the biological reactor itself (especially in membrane bioreactors), anaerobic digesters, sludge thickening processes...

Appendix A

Setting up a base case in OpenFOAM

The mixture model approach is a model where all the participating phases are treated as a mixture, *i.e.,* in which the fluid exhibit mean properties of density and viscosity. Thus, the mixture model code in OpenFOAM is called "DriftFluxFoam" or "compressionFluxFoam". The solver is applicable for fluids with small scale interfaces (see image A.1), fluids found in settling tanks, cyclone separators, bubbles in heat exchangers, anular flow in refineries. (Márquez Damián, 2013)
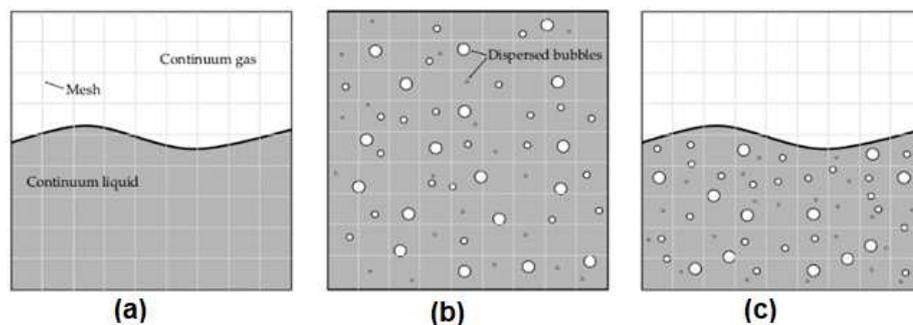
FIGURE A.1: Representation of short and long geometrical scales in a bubbly flow. a) Long scale interfaces, b) short scale interface, c) presence of both. Source from Márquez Damián, 2013.

To simulate a basic case in OpenFOAM three main directories are needed: 0, constant and system). The content of each directory depends on the code approach, *i.e.,* for the *compressionFluxFoam* code the contents are as follows:

- The *0* directory contains the variables or fields, that are used for the resolution of the fluid's motion.

- The *constant* directory contains all the parameters and constant values that affect the fluid's motion and the mesh of the employed geometry

- The *system* directory which contains the controls of the simulations and the discretization schemes (numeric methods, time step size, time interval writing, etc.)

Figure A.2 to have a complete view of all the directories and files used for a sludge settling compression case.
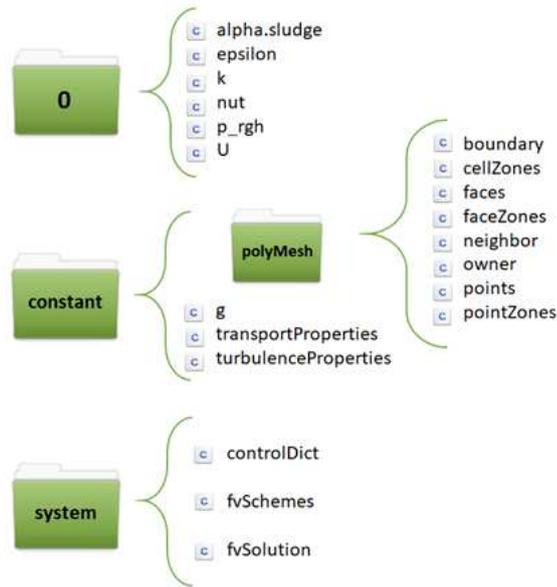
FIGURE A.2: General overview and main content of a simulation case in OpenFOAM

A.1   The zero directory

After the mesh is created in *snappyHexMesh*, which is the own OpenFOAM meshing tool, one must set the initial boundary conditions at 0 folder. However, meshes created with other tools can be used as well.

For all files the dimensions and initial values for the boundaries and internal fields shall be filled. An example of the epsilon boundary conditions file is shown in figure A.3. Dimensions in OpenFOAM are always in international system in this order: kilogram, meter, second, Kelvin, mole, ampere and candela

When simulating a turbulent flow with *compressionfluxFoam*, six fields or variables are needed, the volume fraction (alpha.sluge), the field velocity (U), the pressure ($p_r$gh), the parameters for the turbulent model, in this case (k and ϵ) and the turbulent viscosity (nut).

1. *alpha.sludge*. One must set the value of the initial volume fraction at the inlet or internal field. The volume fraction is calculated through equation 2.6. This is a dimensionless variable.

2. *epsilon*. If the k-epsilon turbulence model is chosen, the rate at which the turbulence kinetic energy is converted into thermal internal energy (epsilon) initial condition is needed. Units are $m^2.s^{-3}$.

```
/*--------------------------------*- C++ -*----------------------------------*\
| =========                 |                                                 |
| \\      /  F ield         | OpenFOAM: The Open Source CFD Toolbox           |
|  \\    /   O peration     | Version:  3.0.1                                 |
|   \\  /    A nd           | Web:      www.OpenFOAM.org                      |
|    \\/     M anipulation  |                                                 |
\*---------------------------------------------------------------------------*/
FoamFile
{
    version     2.0;
    format      ascii;
    class       volScalarField;
    location    "0";
    object      epsilon;
}
// * * * * * * * * * * * * * * * * * * * * * * * * * * * * * * * * * * * * //

dimensions      [ 0 2 -3 0 0 0 0 ];

internalField   uniform 2.9972291E-07;

boundaryField
{
    back
    {
        type            wedge;
    }
    baffleExt
    {
        type            epsilonWallFunction;
        value           $internalField;
        Cmu             0.09;
        kappa           0.41;
        E               9.8;
    }
    baffleInt
    {
        type            epsilonWallFunction;
        value           $internalField;
        Cmu             0.09;
        kappa           0.41;
        E               9.8;
    }
    freeSurface1
    {
        type            symmetry;
    }
```

FIGURE A.3: Initial conditions for the epsilon file, dimensions, internalField and boundaryField shall be filled to start a case

3. *k*. The kinetic energy generated by the fluid is set up in this file. It has $m^2.s^{-2}$ units.

4. *nut*. Stands for the turbulent viscosity field used for the turbulence model. The units are $m^2.s^{-1}$.

5. p$_r$gh. The pressure equation is solved for p_rgh, which is the dynamic pressure, and is equal to the total pressure minus the hydro static pressure (ρ*gh). It has the pressure unities of $kg.m^{-1}.s^{-2}$.

6. *nut*. Velocity field is a vector, therefore 3 components (x, y and z) and the sense (positive or negative) should be filled. If the value of velocity is set to 0 for the walls it indicates that a no slip condition is imposed. Velocity units are $m.s^{-1}$

There exist a large variety of boundary conditions according to the field and the related patch, but they will be explained in chapter for4 when the main case is set up.

A.2 The constant directory

The directory contains the physical properties and constants used for the different models: rheology, sedimentation and turbulence and the boundaries for the mesh (figure A.4).

The description of each file/directory within the folder is as follows:

```
freeSurface3
{
    type            symmetry;
    inGroups        1(symmetry);
    nFaces          6;
    startFace       20891;
}
front
{
    type            wedge;
    inGroups        1(wedge);
    nFaces          6914;
    startFace       20897;
}
inlet
{
    type            patch;
    inGroups        1(patch);
    nFaces          15;
    startFace       27811;
}
intWall1
{
    type            wall;
    inGroups        1(wall);
    nFaces          97;
    startFace       27826;
}
```

FIGURE A.4: Extract from the boundary file showing the different types of boundaries and names for the mesh

1. *polyMesh*. Eight different files are included in the directory. The declaration of the limits of the mesh is done in the boundary file. The names of the limits (inlet, outlet, wall, free surfaces...) and the type of boundary (patch, wall, empty, wedge or symmetry) shall be the same as the ones used for the initial conditions in the zero directory. OpenFOAM make difference between capital and small letters. The rest of the files contains the number of points, cells and faces of the unstructured mesh.

2. *transportProperties*. The file contains basically the parameters for the rheology model and the settling velocity model. The rheology model for the activated sludge can be chosen between Plastic or Bingham. The velocity settling model can be chosen among Vesilind, Takacs or Diehl equations for hindered settling. For compression settling the inputs are the values of alpha for effective solids stress and the critical concentration. See Figure A.5.

3. *turbulenceProperties*. The turbulence model (RANS, LES or laminar) is declared in this file. CompressionFluxFoam suggest the using of the buoyant k-epsilon model, since a density gradient may be created by a variation in the composition of the mixture. According to OpenFOAM manual the 1/Prt coefficient is replaced by Cg to provide control of the model.

4. *g*. This corresponds to the value of the gravity (9.81 $m.s^{-1}$). The sense and the direction of the gravity force according to the mesh orientation must be indicated.

```
relativeVelocityModel diehl;

"(vesilind|takacs|diehl)Coeffs"
{
    V0              (0 -0.00199 0);
    a               308.35012;
    a1              5217.369;
    residualAlpha   0;
    q               8.468426;
    x               0.003063;

}
alphaComp       alphaComp [ 0 2 -2 0 0 0 0 ] 1.35;
criticalalpha   criticalalpha [ 0 0 0 0 0 0 0 ] 0.00495; //divided by rho sludge
```

Parameters for the hindered settling model

Parameters for the compression settling model

FIGURE A.5: Illustration of how to set the parameters for the settling velocity model

A.3 The system directory

The system directory contains three main files (controlDict, fvSchemes and fvOptions) that will be discussed next. However, it can contain also pre and postprocessing tools for extracting points, velocity or pressure profiles, refining or editing meshes among other functions. Refer to the OpenFOAM manual for more details in the different postProcessing tools.

1. *controlDict*. The input for the simulation time and data writing is defined in this file (figure A.6). Start and stop time must be set. One advantage in OpenFOAM is that if a simulation is stopped before the ending time it can be restarted in the last written time step by using the latestTime option.

   The data results are written into csv format and the written time can be set in the writeInterval option. A new directory will be created for each time Step and the values of the variables introduced in the time 0 directory and new variables, such as Udm, dComp and sigma, will be written.

2. *fvSchemes*.The numerical schemes are specified for the first and second time derivatives, gradient normal to a cell face, gradient, divergent, Laplacian, and interpolations terms. When the word "default" is used, OpenFOAM uses the specified numerical method for all variables. If a variable should be solved with a different scheme, then it can be specified as in figure A.7.

   Interpolations in the variables are made from point to point of the unstructured mesh is made from cell centre to face centre in OpenFOAM. The surface normal gradient is evaluated at the cell face from two adjacent cells.

   For more details of the different numerical schemes please refer to OpenFOAM manual.

3. *fvSolution*. The solutions, tolerances and algorithms are set in within the fvSolution file. Other sub-sections can be found in the file are solvers, relaxationFactors and PIMPLE.

In the section solver the linear solver for each discretised equation for each variable (alpha.sludge, U, $p_r gh$, k, epsilon) is defined. Different solvers can be used, Preconditioned (bi-)conjugate gradient (PCG), Stabilized Preconditioned (bi-) conjugate gradient (PBiCGStab), smoother, generalized geometric-algebraic multi-grid (GAMG) and diagonal. Refer to OpenFOAM manual for more information about the solver usage. The tolerances are an indicator of the accuracy of the simulation, they assure that the residual is small enough and they must be specified for each solver.

The relaxation factors improve stability in simulation. The Under-relaxation (alpha) limits how a variable changes from one iteration to the next. The choice in the value of alpha, ranging from 0 to 1, should be high enough to move quickly into the next iteration but low enough to ensure stability into the iterative process.

The PIMPLE algorithm combines the PISO and SIMPLE algorithm, *i.e.*, it looks for the steady-state in each time step, after this, the outer correction loops ensure that explicit parts of the equations are converged. If the tolerance criterion is reached within the steady-state calculation, the outer correction loop is left and the computation moves on until the end time of the simulation. Large courant numbers ($\gg 1$) can be used and therefore time step highly increase. Refer to Holzmann, 2016 book for further details about the PIMPLE algorithm.

A.4   Processing

Just after setting up all the variables and boundary conditions in the 0 directory, the parameters in the constant directory, and the time controls and numerical schemes, one just must type *compressionFluxFoam* in a terminal to run the case.

Further, OpenFOAM provides the option to run in parallel in order to reduce the computational time. A file called *decomposeParDict* has to be integrated into the system directory indicating the number of the processors one wants to employ.

Then in a terminal one first types *decomposePar* and then *mpirun -np X compressionFluxFoam -parallel* where X corresponds to the number of processors indicated in the decomposeParDict file.

CompressionFluxFoam is a derivation of driftFluxFoam, thus the PIMPLE Algorithm is used. To assure the converge of the simulations the residuals of the variables are monitored, the smallest value is, the more accurate the solution.

The advantage of the PIMPLE Algorithm is that higher Courant Numbers can be used without compromising the accuracy and convergence of the simulation. Figure A.8 shows a results of the residuals monitored during the simulation. This can be done by using *foamMonitor -l postprocessing/residuals/0/residuals.dat*.

```
/*--------------------------------*- C++ -*----------------------------------*\
| =========                 |                                                 |
| \\      /  F ield         | OpenFOAM: The Open Source CFD Toolbox           |
|  \\    /   O peration     | Version:  2.3.1                                 |
|   \\  /    A nd           | Web:      www.OpenFOAM.org                      |
|    \\/     M anipulation  |                                                 |
\*---------------------------------------------------------------------------*/
FoamFile
{
    version     2.0;
    format      ascii;
    class       dictionary;
    location    "system";
    object      controlDict;
}
// * * * * * * * * * * * * * * * * * * * * * * * * * * * * * * * * * * * * * //

application     compressionDriftFluxFoam;

startFrom       latestTime;

startTime       0;

stopAt          endTime;

endTime         9000;

deltaT          0.001;

writeControl    adjustableRunTime;

writeInterval   900;

purgeWrite      0;

writeFormat     ascii;

writePrecision  8;

writeCompression uncompressed;

timeFormat      general;

timePrecision   8;

runTimeModifiable yes;

adjustTimeStep  on;

maxCo           0.9;

maxDeltaT       1;
```

Time Step control

Data file control

Courant number control

FIGURE A.6: Extract from a controlDict file and the different inputs.

```
gradSchemes
{
    default           Gauss linear;
    grad(alpha.sludge)  cellLimited Gauss linear 1;
}
```

FIGURE A.7: Specified numerical scheme for the gradient of alpha.sludge.
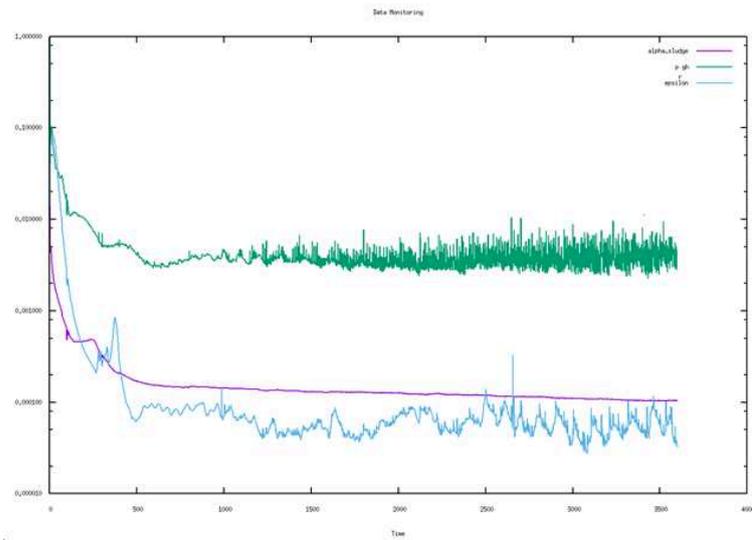
FIGURE A.8: Specified numerical scheme for the gradient of alpha.sludge.

A.5   Post-Processing

For the postprocessing data view or analysis there are different tools one can use, the main one is the graphical interface (figure A.9) called Paraview and the user can access by just typing paraFoam in a terminal. Paraview offers a large set of options where one can see the velocity fields, extract information about data points and values of variables in each cell, make different cuts of the geometry to analyze a specific part of the geometry, obtain velocity, pressure or volume fraction profiles, get the evolution of the variables in time, etc.
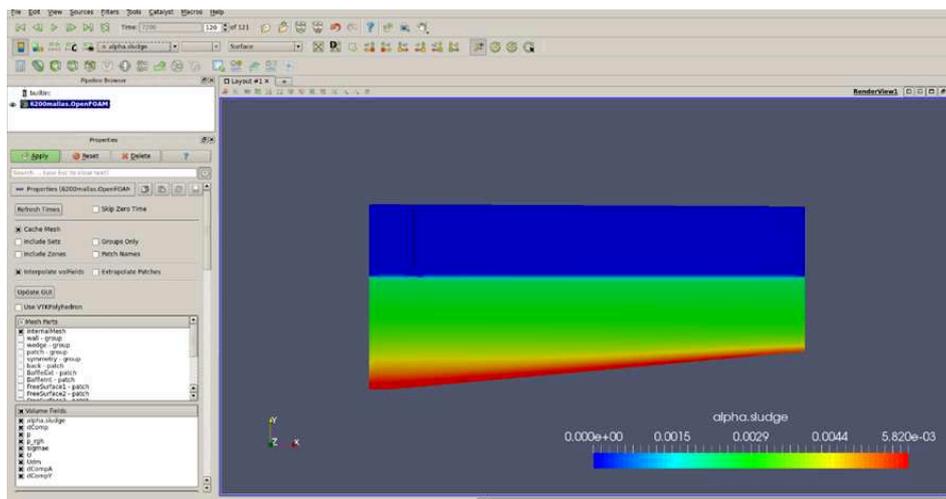
FIGURE A.9: Paraview graphical interphase.

Bibliography

Abda, F. et al. (2009). "Ultrasonic device for real-time sewage velocity and suspended particles concentration measurements". en. In: *Water Science and Technology* 60.1, pp. 117–125. ISSN: 0273-1223. DOI: `10.2166/wst.2009.281`. URL: `/wst/article/60/1/117/15850/Ultrasonic-device-for-real-time-sewage-velocity` (visited on 07/03/2019).

Adams, B.M. et al. (2014). *Dakota, A Multilevel Parallel Object-Oriented Framework for Design Optimization, Parameter Estimation, Uncertainty Quantification, and Sensitivity Analysis: Version 6.0 User's Manual*. Vol. Version 6.3. Sandia Technical Report SAND2014-4633,

Ahmed, S. R., G. Ramm, and G. Faltin (1984). "Some Salient Features Of The Time-Averaged Ground Vehicle Wake". In: *SAE Technical Paper*. SAE International. DOI: `10.4271/840300`. URL: `https://doi.org/10.4271/840300`.

Al-Sammarraee, M. and A. Chan (2009). "Large-eddy simulations of particle sedimentation in a longitudinal sedimentation basin of a water treatment plant. Part 2: The effects of baffles". In: *Chemical Engineering Journal* 152.2–3, pp. 315–321. ISSN: 1385-8947. DOI: `10.1016/j.cej.2009.01.052`. URL: `https://www.sciencedirect.com/science/article/pii/S1385894709000667` (visited on 01/27/2017).

Anderson, Norval E. and R. H. Gould (1945). "Design of Final Settling Tanks for Activated Sludge [with Discussion]". In: *Sewage Works Journal* 17.1, pp. 50–65. ISSN: 00969362. URL: `http://www.jstor.org/stable/25029971`.

Aziz, A. A. et al. (2000). "The characterisation of slurry dewatering". en. In: *Water Science and Technology* 41.8, pp. 9–16. ISSN: 0273-1223, 1996-9732. DOI: `10.2166/wst.2000.0136`. URL: `https://iwaponline.com/wst/article/41/8/9/8836/The-characterisation-of-slurry-dewatering` (visited on 10/02/2019).

Biggs, C.A., P. Lant, and M. J. Hounslow (2003). "Modelling the effect of shear history on activated sludge flocculation". In: *Water Science & Technology* 11, pp. 251–257.

Bingham, E. C. (1916). "An investigation of the laws of plastic flow". en. In: *Bulletin of the Bureau of Standards* 13.2, p. 309. ISSN: 0096-8579. DOI: `10.6028/bulletin.304`. URL: `https://nvlpubs.nist.gov/nistpubs/bulletin/13/nbsbulletinv13n2p309_A2b.pdf` (visited on 10/12/2019).

Bokil, S.D. and J.K. Bewtra (1972). "Influence of mechani-cal blending on aerobic digestion of waste activated sludge." In:

Boller, Markus (1997). "Small wastewater treatment plants - a challenge to wastewater engineers". en. In: *Water Science and Technology* 35.6, pp. 1–12. ISSN: 0273-1223,

168

1996-9732. DOI: 10.2166/wst.1997.0237. URL: https://iwaponline.com/wst/article/35/6/1-12/5868 (visited on 10/19/2019).

Bratby, J and G.V.R. Marais (1976). "A Guide for the Design of Dissolved air (Pressure) Flotation Systems for Activated Sludge Processes." In: *Water SA, 2 (2),* pp. 86–100.

Brennan, D. (2001). *The Numerical Simulation of Two Phase Flows in Settling Tanks.* University of London. URL: https://books.google.fr/books?id=nWw-nQEACAAJ.

Brouckaert, C. J. and C. A. Buckley (1999). "The use of Computational Fluid Dynamics for improving the design and operation of water and wastewater treatment plants". In: *Water Science and Technology* 40.4–5, pp. 81–89. ISSN: 0273-1223. DOI: 10.1016/S0273-1223(99)00488-6. URL: https://www.sciencedirect.com/science/article/pii/S0273122399004886 (visited on 01/27/2017).

Burckbuchler, Marie and Stephan Fischer (2017). "A miniature UVP hardware applied to environmental monitoring". In: *HydroSenSoft Symposium Proceedings.*

Buscall, Richard and Lee R. White (1987). "The consolidation of concentrated suspensions. Part 1.—The theory of sedimentation". In: *Journal of the Chemical Society, Faraday Transactions 1: Physical Chemistry in Condensed Phases* 83.3, pp. 873–891.

Bürger, R., W.l. Wendland, and F. Concha (2000). "Model Equations for Gravitational Sedimentation-Consolidation Processes". en. In: *ZAMM - Journal of Applied Mathematics and Mechanics / Zeitschrift für Angewandte Mathematik und Mechanik* 80.2, pp. 79–92. ISSN: 1521-4001. DOI: 10.1002/(SICI)1521-4001(200002)80:2<79::AID-ZAMM79>3.0.CO;2-Y. URL: http://onlinelibrary.wiley.com/doi/10.1002/(SICI)1521-4001(200002)80:2<79::AID-ZAMM79>3.0.CO;2-Y/abstract (visited on 01/27/2017).

Bürger, Raimund, Julio Careaga, and Stefan Diehl (2017). "A simulation model for settling tanks with varying cross-sectional area". en. In: *Chemical Engineering Communications* 204.11, pp. 1270–1281. ISSN: 0098-6445, 1563-5201. DOI: 10.1080/00986445.2017.1360871. URL: https://www.tandfonline.com/doi/full/10.1080/00986445.2017.1360871 (visited on 10/13/2019).

Bürger, Raimund, Stefan Diehl, and Ingmar Nopens (2011). "A consistent modelling methodology for secondary settling tanks in wastewater treatment". In: *Water Research* 45.6, pp. 2247–2260. ISSN: 0043-1354. DOI: 10.1016/j.watres.2011.01.020. URL: https://www.sciencedirect.com/science/article/pii/S0043135411000352 (visited on 01/27/2017).

Bürger, Raimund, Kenneth H. Karlsen, and John D. Towers (2005). "A Model of Continuous Sedimentation of Flocculated Suspensions in Clarifier-Thickener Units". In: *SIAM Journal on Applied Mathematics* 65.3, pp. 882–940. ISSN: 0036-1399. URL: https://www.jstor.org/stable/4096201 (visited on 05/22/2019).

Bürger, Raimund, Ricardo Ruiz-Baier, and Héctor Torres (2012). "A Stabilized Finite Volume Element Formulation for Sedimentation-Consolidation Processes". en. In: *SIAM Journal on Scientific Computing* 34.3, B265–B289. ISSN: 1064-8275, 1095-7197.

DOI: 10.1137/110836559. URL: http://epubs.siam.org/doi/10.1137/110836559 (visited on 10/12/2019).

Bürger, Raimund et al. (2012). "On reliable and unreliable numerical methods for the simulation of secondary settling tanks in wastewater treatment". In: *Computers & Chemical Engineering* 41, pp. 93–105. ISSN: 0098-1354. DOI: 10.1016/j.compchemeng.2012.02.016. URL: https://www.sciencedirect.com/science/article/pii/S0098135412000725 (visited on 01/27/2017).

Bürger, Raimund et al. (2013). "A consistent modelling methodology for secondary settling tanks: a reliable numerical method". en. In: *Water Science & Technology* 68.1, p. 192. ISSN: 0273-1223. DOI: 10.2166/wst.2013.239. URL: http://wst.iwaponline.com/cgi/doi/10.2166/wst.2013.239 (visited on 10/31/2017).

Cacossa, Kenneth F. and David A. Vaccari (1994). "Calibration of a compressive gravity thickening model from a single batch settling curve". en. In: *Water Science and Technology* 30.8, pp. 107–116. ISSN: 0273-1223, 1996-9732. DOI: 10.2166/wst.1994.0392. URL: https://iwaponline.com/wst/article/30/8/107-116/27982 (visited on 10/13/2019).

Carlsson, Bengt (1998). "An introduction to sedimentation theory in wastewater treatment". en. In: *Systems and Control Group* Uppsala University, p. 7.

Cho, S. H. et al. (1993). "Settling velocity model of activated sludge". In: *Water Research* 27.7, pp. 1237–1242. ISSN: 0043-1354. DOI: 10.1016/0043-1354(93)90016-B. URL: http://www.sciencedirect.com/science/article/pii/004313549390016B (visited on 01/27/2017).

Cole, R.F. (1968). *Experimental Evaluation of the Kynch Theory*. University of North Carolina at Chapel Hill. URL: https://books.google.fr/books?id=K4PLoQEACAAJ.

Concha, F. and M. C. Bustos (1991). "Settling velocities of particulate systems, 6. Kynch sedimentation processes: batch settling". In: *International Journal of Mineral Processing* 32.3, pp. 193–212. ISSN: 0301-7516. DOI: 10.1016/0301-7516(91)90068-T. URL: http://www.sciencedirect.com/science/article/pii/030175169190068T (visited on 07/31/2019).

Copp, J.B. (2001). *The COST Simulation Benchmark: Description and Simulator Manual*.

Dahl, Claus (1993). *Numerical modelling of flow and settling in secondary settling tanks*. Aalborg University, Department of Civil Engineering.

Das, Shankhadeep et al. (2016). "Improving the performance of industrial clarifiers using three-dimensional computational fluid dynamics". In: *Engineering Applications of Computational Fluid Mechanics* 10.1, pp. 130–144. ISSN: 1994-2060. DOI: 10.1080/19942060.2015.1121518. URL: http://dx.doi.org/10.1080/19942060.2015.1121518 (visited on 01/27/2017).

De Clercq, B. (2003). *Computational Fluid Dynamics of Settling Tanks: Development of Experiments and Rheological, Settling, and Scraper Submodels*. Belgium: Dept. Applied Mathematics, Biometrics and Process Control, Ghent University. URL: https://books.google.fr/books?id=-cACtwAACAAJ.

De Clercq, Jeriffa (2006). "Batch and continuous settling of activated sludge: in-depth monitoring and 1D compression modelling". eng. PhD thesis. Ghent University. URL: `http://lib.ugent.be/fulltxt/RUG01/001/376/220/RUG01-001376220_2010_0001_AC.pdf`.

De Clercq, Jeriffa et al. (2005). "Detailed spatio-temporal solids concentration profiling during batch settling of activated sludge using a radiotracer". In: *Water Research* 39.10, pp. 2125–2135. ISSN: 0043-1354. DOI: `10.1016/j.watres.2005.03.023`. URL: `https://www.sciencedirect.com/science/article/pii/S0043135405001193` (visited on 01/27/2017).

De Clercq, Jeriffa et al. (2008). "Extending and calibrating a mechanistic hindered and compression settling model for activated sludge using in-depth batch experiments". In: 42, pp. 781–791. DOI: `10.1016/j.watres.2007.08.040`.

Derlon, Nicolas et al. (2017). "Batch settling curve registration via image data modeling". en. In: *Water Research* 114, pp. 327–337. ISSN: 00431354. DOI: `10.1016/j.watres.2017.01.049`. URL: `https://linkinghub.elsevier.com/retrieve/pii/S0043135417300568` (visited on 10/14/2019).

Dick, Richard I. and Ben B. Ewing (1967). "The Rheology of Activated Sludge". In: *Journal (Water Pollution Control Federation)* 39.4, pp. 543–560. ISSN: 0043-1303. URL: `https://www.jstor.org/stable/25035907` (visited on 10/10/2018).

Diehl, S. (2015). "Numerical identification of constitutive functions in scalar nonlinear convection–diffusion equations with application to batch sedimentation". In: *Applied Numerical Mathematics*. Fourth Chilean Workshop on Numerical Analysis of Partial Differential Equations (WONAPDE 2013) 95, pp. 154–172. ISSN: 0168-9274. DOI: `10.1016/j.apnum.2014.04.002`. URL: `https://www.sciencedirect.com/science/article/pii/S0168927414000531` (visited on 01/27/2017).

Ding, A., M.J. Hounslow, and C.A. Biggs (2006). "Population balance modelling of activated sludge flocculation: Investigating the size dependence of aggregation, breakage and collision efficiency". en. In: *Chemical Engineering Science* 61.1, pp. 63–74. ISSN: 00092509. DOI: `10.1016/j.ces.2005.02.074`. URL: `https://linkinghub.elsevier.com/retrieve/pii/S0009250905004410` (visited on 10/13/2019).

Eikelboom, Dick H. (2000). *Process Control of Activated Sludge Plants by Microscopic Investigation*. en. Google-Books-ID: wE8C7SVySbMC. IWA Publishing. ISBN: 978-1-900222-29-7.

Ekama, G. A. and P. Marais (2004). "Assessing the applicability of the 1D flux theory to full-scale secondary settling tank design with a 2D hydrodynamic model". In: *Water Research* 38.3, pp. 495–506. ISSN: 0043-1354. DOI: `10.1016/j.watres.2003.10.026`. URL: `https://www.sciencedirect.com/science/article/pii/S0043135403005797` (visited on 01/27/2017).

Ekama, GA (1986). "Sludge settleability and secondary settling tank design procedures". In: *Wat. Pollut. Control* 85, pp. 101–113.

Ekama, G.A. et al. (1997). *Secondary Settling Tanks: Theory, Modelling, Design and Operation.* Vol. 6. Richmond, UK: International Association on Water Quality, STR.

Flamant, O. et al. (2004). "Experimental Analysis and Simulation of Settling Process". In: *Process Safety and Environmental Protection* 82.4, pp. 312–318. ISSN: 0957-5820. DOI: 10.1205/095758204323162337. URL: https://www.sciencedirect.com/science/article/pii/S0957582004711787 (visited on 01/27/2017).

François, Pierre et al. (2016). "Experimental study of activated sludge batch settling velocity profile". In: *Flow Measurement and Instrumentation* 48, pp. 112–117. ISSN: 0955-5986. DOI: 10.1016/j.flowmeasinst.2015.08.009. URL: https://www.sciencedirect.com/science/article/pii/S0955598615300091 (visited on 01/27/2017).

Fuchs, Andreas and Gernot Staudinger (1999). "Characterising the clarification of the supernatant of activated sludges". In: *Water Research* 33.11, pp. 2527–2534. ISSN: 0043-1354. DOI: 10.1016/S0043-1354(98)00491-6. URL: http://www.sciencedirect.com/science/article/pii/S0043135498004916 (visited on 08/01/2019).

G. Chebbo Ph.D. and M.-C. Gromaire, Ph.D. (2009). "VICAS—An Operating Protocol to Measure the Distributions of Suspended Solid Settling Velocities within Urban Drainage Samples". In: *Journal of Environmental Engineering* 135.9. DOI: 10.1061/(ASCE)0733-9372(2009)135:9(768). URL: http://ascelibrary.org/doi/abs/10.1061/%28ASCE%290733-9372%282009%29135%3A9%28768%29 (visited on 01/27/2017).

Gao, Haiwen and M. K. Stenstrom (2018). "Evaluation of three turbulence models in predicting the steady state hydrodynamics of a secondary sedimentation tank". In: *Water Research* 143, pp. 445 –456. ISSN: 0043-1354. DOI: https://doi.org/10.1016/j.watres.2018.06.067. URL: http://www.sciencedirect.com/science/article/pii/S004313541830527X.

Ghawi, Ali and J. Kriš (2012). "Improvement performance of secondary clarifiers by a computational fluid dynamics model". In: *Slovak Journal of Civil Engineering* 19.4, pp. 1–11. ISSN: 1210-3896. DOI: 10.2478/v10189-011-0017-9. URL: https://www.degruyter.com/view/j/sjce.2011.xix.issue-4/v10189-011-0017-9/v10189-011-0017-9.xml (visited on 01/27/2017).

Gong, M. et al. (2011). "Development of a flocculation sub-model for a 3-D CFD model based on rectangular settling tanks". en. In: *Water Science and Technology* 63.2, pp. 213–219. ISSN: 0273-1223, 1996-9732. DOI: 10.2166/wst.2011.035. URL: https://iwaponline.com/wst/article/63/2/213/13783/Development-of-a-flocculation-submodel-for-a-3D (visited on 10/13/2019).

Goula, Athanasia M. et al. (2008). "A CFD methodology for the design of sedimentation tanks in potable water treatment: Case study: The influence of a feed flow control baffle". In: *Chemical Engineering Journal* 140.1–3, pp. 110–121. ISSN: 1385-8947. DOI: 10.1016/j.cej.2007.09.022. URL: https://www.sciencedirect.com/science/article/pii/S1385894707006250 (visited on 01/27/2017).

Greenshields, Chris (2017). *OpenFOAM User Guide*. OpenFOAM. URL: https://cfd.direct/openfoam/user-guide/.

Griborio, Alonso (2004). "Secondary Clarifier Modeling: A Multi-Process Approach". PhD thesis. University of New Orleans Theses and Dissertations.

Griborio, Alonso and Alex J. McCorquodale (2006). "Optimum Design of your Center Well: Use of a CFD Model to understand the Balance between Flocculation and improved Hydrodynamics". en. In: *Proceedings of the Water Environment Federation* 2006.13, pp. 263–280. ISSN: 1938-6478. DOI: 10.2175/193864706783710587. URL: http://www.ingentaconnect.com/content/10.2175/193864706783710587 (visited on 10/13/2019).

Grijspeerdt, Koen, Peter Vanrolleghem, and Willy Verstraete (1995). "Selection of one-dimensional sedimentation: Models for on-line use". en. In: *Water Science and Technology*. Modelling and Control of Activated Sludge Processes 31.2, pp. 193–204. ISSN: 0273-1223. DOI: 10.1016/0273-1223(95)00192-P. URL: http://www.sciencedirect.com/science/article/pii/027312239500192P (visited on 10/18/2019).

Guo, Lisha et al. (2009). "An experimental study of low concentration sludge settling velocity under turbulent condition". In: *Water Research* 43.9, pp. 2383–2390. ISSN: 0043-1354. DOI: 10.1016/j.watres.2009.02.032. URL: https://www.sciencedirect.com/science/article/pii/S0043135409001353 (visited on 01/27/2017).

Gupta, Hoshin V. et al. (2009). "Decomposition of the mean squared error and NSE performance criteria: Implications for improving hydrological modelling". en. In: *Journal of Hydrology* 377.1-2, pp. 80–91. ISSN: 00221694. DOI: 10.1016/j.jhydrol.2009.08.003. URL: http://linkinghub.elsevier.com/retrieve/pii/S0022169409004843 (visited on 09/10/2018).

Holzmann, Tobias (2016). *Mathematics, Numerics, Derivations and OpenFOAM®*. en. Holzmann CFD. DOI: 10.13140/RG.2.2.27193.36960. URL: http://rgdoi.net/10.13140/RG.2.2.27193.36960 (visited on 03/20/2019).

Hreiz, Rainier et al. (2019). "CFD Investigation of the effects of bubble aerator layouts on hydrodynamics of an activated sludge channel reactor". en. In: *Environmental Technology* 40.20, pp. 2657–2670. ISSN: 0959-3330, 1479-487X. DOI: 10.1080/09593330.2018.1448001. URL: https://www.tandfonline.com/doi/full/10.1080/09593330.2018.1448001 (visited on 10/18/2019).

Härtel, L. and H. J. Pöpel (1992). "A Dynamic Secondary Clarifier Model including Processes of Sludge Thickening". en. In: *Water Science and Technology* 25.6, pp. 267–284. ISSN: 0273-1223, 1996-9732. DOI: 10.2166/wst.1992.0128. URL: https://iwaponline.com/wst/article/25/6/267-284/27799 (visited on 10/18/2019).

Isenmann, Gilles (2016). "Approche Euler-Lagrange pour la modélisation du transport solide dans les ouvrages de décantation". fr. In: URL: https://tel.archives-ouvertes.fr/tel-01490384 (visited on 10/09/2019).

Ishii, M. and K. Mishima (1984). "Two-fluid model and hydrodynamic constitutive relations". In: *Nuclear Engineering and Design* 82.2–3, pp. 107–126. ISSN: 0029-5493. DOI: 10.1016/0029-5493(84)90207-3. URL: https://www.sciencedirect.com/science/article/pii/0029549384902073 (visited on 01/27/2017).

Ishii, Mamoru and Takashi Hibiki (1975). *Thermo-fluid Dynamics of Two-Phase Flow*. en. Springer US. ISBN: 978-0-387-28321-0. URL: https://www.springer.com/gp/book/9780387283210 (visited on 03/27/2019).

Jareteg, Adam, Alejandro Lopez, and Olivier Petit. "Coupling of Dakota and Open-FOAM for automatic parameterized optimization". en. In: p. 22.

Jimenez, Jose et al. (2015). "High-rate activated sludge system for carbon management – Evaluation of crucial process mechanisms and design parameters". en. In: *Water Research* 87, pp. 476–482. ISSN: 00431354. DOI: 10.1016/j.watres.2015.07.032. URL: https://linkinghub.elsevier.com/retrieve/pii/S0043135415301342 (visited on 10/10/2019).

Judd, S.J. and C. Judd (2011). *The MBR Book*. URL: https://www.scopus.com/inward/record.uri?eid=2-s2.0-84949176564&partnerID=40&md5=f0059fe0a2915fe12c94ead73ff6c47e.

Kahane, R, T Nguyen, and M.P Schwarz (2002). "CFD modelling of thickeners at Worsley Alumina Pty Ltd". en. In: *Applied Mathematical Modelling* 26.2, pp. 281–296. ISSN: 0307904X. DOI: 10.1016/S0307-904X(01)00061-0. URL: https://linkinghub.elsevier.com/retrieve/pii/S0307904X01000610 (visited on 10/12/2019).

Kahane, R.B., M. P Schwarz, and R.M. Johnston (1997). *Proceedings of the Computational Fluid Dynamics in Minerals and Metal Processing and Power Generation, CSIRO*. Melbourne, Australia. URL: http://www.cfd.com.au/cfd_conf97/papers/kah020.pdf.

Khalili-Garakani, Amirhossein et al. (2011). "Comparison between different models for rheological characterization of activated sludge". In: *Iranian Journal of Environmental Health Science & Engineering* 8, pp. 255–264.

Kim, H. S. et al. (2005). "Study of flow characteristics in a secondary clarifier by numerical simulation and radioisotope tracer technique". In: *Applied Radiation and Isotopes* 63.4, pp. 519–526. ISSN: 0969-8043. DOI: 10.1016/j.apradiso.2005.03.016. URL: https://www.sciencedirect.com/science/article/pii/S0969804305000916 (visited on 01/27/2017).

Kinnear, D.J. and K. Deines (2001). "Acoustic Doppler current profiler: clarifier velocity measurement. Atlanta, USA." In: *Proceedings WEFTEC 2001,*

Koopman, Ben and Keith Cadee (1983). "Prediction of thickening capacity using diluted sludge volume index". en. In: *Water Research* 17.10, pp. 1427–1431. ISSN: 00431354. DOI: 10.1016/0043-1354(83)90274-9. URL: https://linkinghub.elsevier.com/retrieve/pii/0043135483902749 (visited on 10/18/2019).

Krebs, Peter et al. (1996). "Influence of inlet and outlet configuration on the flow in secondary clarifiers". In: *Water Science and Technology*. Water Quality International '96 Part 3: Modelling of Activated Sludge Processes; Microorganisms in Activated Sludge and Biofilm Processes; Anareobic Biological Treatment; Biofouling 34.5, pp. 1–9. ISSN: 0273-1223. DOI: 10.1016/0273-1223(96)00622-1. URL: http://www.sciencedirect.com/science/article/pii/0273122396006221 (visited on 08/01/2019).

Kynch, G. J. (1952). "A theory of sedimentation". en. In: *Transactions of the Faraday Society* 48.0, pp. 166–176. ISSN: 0014-7672. DOI: `10.1039/TF9524800166`. URL: `https://pubs.rsc.org/en/content/articlelanding/1952/tf/tf9524800166` (visited on 07/31/2019).

Lakehal, Djamel et al. (1999). "Computing shear flow and sludge blanket in secondary clarifiers". In: *Journal of Hydraulic Engineering* 125.3, pp. 253–262. URL: `http://ascelibrary.org/doi/abs/10.1061/(ASCE)0733-9429(1999)125:3(253)` (visited on 03/24/2017).

Larsen, P (1977). *On the Hydraulics of Rectangular Settling Basins.* Tech. rep. Lund, Sweden.: Dept of Water Res. Engrg. Lind University.

Laurent, J. et al. (2014). "A protocol for the use of computational fluid dynamics as a supportive tool for wastewater treatment plant modelling". en. In: *Water Science and Technology* 70.10, pp. 1575–1584. ISSN: 0273-1223, 1996-9732. DOI: `10.2166/wst.2014.425`. URL: `http://wst.iwaponline.com/content/70/10/1575` (visited on 01/27/2017).

Li, Ben and M. K. Stenstrom (2014). "Research advances and challenges in one-dimensional modeling of secondary settling Tanks – A critical review". In: *Water Research* 65, pp. 40–63. ISSN: 0043-1354. DOI: `10.1016/j.watres.2014.07.007`. URL: `https://www.sciencedirect.com/science/article/pii/S004313541400503X` (visited on 01/27/2017).

Locatelli, F. et al. (2015). "Detailed Velocity and Concentration Profiles Measurement During Activated Sludge Batch Settling Using an Ultrasonic Transducer". In: *Separation Science and Technology* 50.7, pp. 1059–1065. ISSN: 0149-6395. DOI: `10.1080/01496395.2014.980002`. URL: `http://dx.doi.org/10.1080/01496395.2014.980002` (visited on 01/27/2017).

Locatelli, Florent (2015). "Activated sludge batch settling : from experimental investigation using an ultrasonic transducer to 1D modelling, sensitivity analysis and parameter identification". Theses. Université de Strasbourg. URL: `https://tel.archives-ouvertes.fr/tel-01404066`.

Locatelli, Florent et al. (2013). "Impact de la loi de comportement rhéologique sur la sédimentation en batch de boues activées : approche expérimentale et numérique". fr. In: *La Houille Blanche* 4, pp. 31–36. ISSN: 0018-6368, 1958-5551. DOI: `10.1051/lhb/2013030`. URL: `http://dx.doi.org/10.1051/lhb/2013030` (visited on 01/27/2017).

Mancell-Egala, William A. S. K. et al. (2016). "Limit of stokesian settling concentration characterizes sludge settling velocity". In: *Water Research* 90, pp. 100–110. ISSN: 0043-1354. DOI: `10.1016/j.watres.2015.12.007`. URL: `https://www.sciencedirect.com/science/article/pii/S00043135415304073` (visited on 01/27/2017).

Mancell-Egala, William A. S. K. et al. (2017). "Settling regimen transitions quantify solid separation limitations through correlation with floc size and shape". In: *Water Research* 109, pp. 54–68. ISSN: 0043-1354. DOI: `10.1016/j.watres.`

2016.10.080. URL: `https://www.sciencedirect.com/science/article/pii/S0043135416308399` (visited on 01/27/2017).

Manninen, Mikko, Veikko Taivassalo, and Sirpa Kallio (1996). "On the mixture model for multiphase flow". en. In: *VTT Publications*. Espoo Technical Research Centre of Finland, 288. 67 p. URL: `https://docs.google.com/document/d/185xhiG3cKxMz2IDOdADQlDFMEz5ZuGirS edit?usp=drive_web&ouid=105725106488157656131&usp=embed_facebook` (visited on 03/27/2019).

Marchisio, D.L. Fox (2013). "Computational Models for Polydisperse Particulate and Multiphase Systems". In:

Matko, T. et al. (1996). "Recent Progress in the Numerical Modelling of Wastewater Sedimentation Tanks". In: *Process Safety and Environmental Protection* 74.4, pp. 245–258. ISSN: 0957-5820. DOI: `10.1205/095758296528590`. URL: `http://www.sciencedirect.com/science/article/pii/S0957582096706274` (visited on 01/27/2017).

McCorquodale, J.A. (1976). *Hydraulic study of the circular settling tanks at the West Windsor Pollution Control Plant.* Windsor, Ontario, Canada.: Rep., University of Windsor,

Moriasi D. N. et al. (2015). "Hydrologic and Water Quality Models: Performance Measures and Evaluation Criteria". In: *Transactions of the ASABE* 6, pp. 1763–1785. ISSN: 21510032, 21510040. DOI: `10.13031/trans.58.10715`. URL: `http://elibrary.asabe.org/abstract.asp?aid=46548&t=3&dabs=Y&redir=&redirType=` (visited on 08/23/2018).

Moukalled, F., L. Mangani, and M. Darwish (2016). *The Finite Volume Method in Computational Fluid Dynamics*. Vol. 113. Fluid Mechanics and Its Applications. Cham: Springer International Publishing. ISBN: 978-3-319-16873-9 978-3-319-16874-6. DOI: `10.1007/978-3-319-16874-6`. URL: `http://link.springer.com/10.1007/978-3-319-16874-6` (visited on 04/18/2018).

Márquez Damián, Santiago (2013). "An extended mixture model for the simultaneous treatment of short and long scale interfaces". eng. In: URL: `https://bibliotecavirtual.unl.edu.ar/tesis//handle/11185/489` (visited on 10/12/2019).

Nopens, Ingmar (2005). "Modelling the activated sludge flocculation process: a population balance approach". nl. OCLC: 66401508. PhD thesis. S.l.: s.n.]

Nopens, Ingmar et al. (2015). "Population balance models: a useful complementary modelling framework for future WWTP modelling". en. In: *Water Science and Technology* 71.2, pp. 159–167. ISSN: 0273-1223, 1996-9732. DOI: `10.2166/wst.2014.500`. URL: `https://iwaponline.com/wst/article/71/2/159/18775/Population-balance-models-a-useful-complementary` (visited on 10/13/2019).

Otterpohl, R. and M. Freund (1992). "Dynamic Models for Clarifiers of Activated Sludge Plants with Dry and Wet Weather Flows". en. In: *Water Science and Technology* 26.5-6, pp. 1391–1400. ISSN: 0273-1223, 1996-9732. DOI: `10.2166/wst.1992.0582`. URL: `https://iwaponline.com/wst/article/26/5-6/1391-1400/26988` (visited on 10/13/2019).

Pallares, A. et al. (2017). "Suspended Sediment Monitoring: Comparison between Optical and Acoustical Turbidity". In: *International Conference on Urban Drainage*.

Parker, D. S., D. J. Kinnear, and E. J. Wahlberg (2001). "Review of Folklore in Design and Operation of Secondary Clarifiers". en. In: *Journal of Environmental Engineering* 127.6, pp. 476–484. ISSN: 0733-9372, 1943-7870. DOI: 10.1061/(ASCE)0733-9372(2001)127:6(476). URL: http://ascelibrary.org/doi/10.1061/%28ASCE%290733-9372%282001%29127%3A6%28476%29 (visited on 10/18/2019).

Parker, Denny S., Warren J. Kaufman, and David Jenkins (1972). "Floc Breakup in Turbulent Flocculation Processes". eng. In: *Journal of the Sanitary Engineering Division* 98.1, pp. 79–99. URL: https://cedb.asce.org/CEDBsearch/record.jsp?dockey=0127407 (visited on 10/13/2019).

Patziger, M. (2016). "Computational fluid dynamics investigation of shallow circular secondary settling tanks: Inlet geometry and performance indicators". In: *Chemical Engineering Research and Design* 112, pp. 122–131. ISSN: 0263-8762. DOI: 10.1016/j.cherd.2016.06.018. URL: https://www.sciencedirect.com/science/article/pii/S0263876216301502 (visited on 01/27/2017).

Patziger, M. et al. (2012). "Influence of secondary settling tank performance on suspended solids mass balance in activated sludge systems". In: *Water Research* 46.7, pp. 2415–2424. ISSN: 0043-1354. DOI: 10.1016/j.watres.2012.02.007. URL: http://www.sciencedirect.com/science/article/pii/S0043135412000954 (visited on 10/03/2019).

Phillips, O. M. (1957). "On the generation of waves by turbulent wind". en. In: *Journal of Fluid Mechanics* 2.05, p. 417. ISSN: 0022-1120, 1469-7645. DOI: 10.1017/S0022112057000233. URL: http://www.journals.cambridge.org/abstract_S0022112057000233 (visited on 07/31/2019).

Pitman, AR (1984). "Operation of biological nutrient removal plants". In: *Theory, Design and Operation of Nutrient Removal Activated Sludge Processes* 11.111, p. 16.

Plósz, Benedek Gy. et al. (2007). "One-dimensional modelling of the secondary clarifier-factors affecting simulation in the clarification zone and the assessment of the thickening flow dependence". en. In: *Water Research* 41.15, pp. 3359–3371. ISSN: 00431354. DOI: 10.1016/j.watres.2007.03.007. URL: http://linkinghub.elsevier.com/retrieve/pii/S0043135407001820 (visited on 03/24/2017).

Ramalingam, K. et al. (2009). "Development and Validation of a 3-Dimensional Computational Fluid Dynamics (CFD) Model for Rectangular Settling Tanks in New York City Water Pollution Control Plants". In: *Water Practice and Technology* 4.1, wpt2009015. URL: http://wpt.iwaponline.com/content/4/1/wpt2009015.abstract (visited on 07/25/2017).

Ramin, Elham et al. (2014a). "A new settling velocity model to describe secondary sedimentation". In: *Water Research* 66, pp. 447–458. ISSN: 0043-1354. DOI: 10.1016/j.watres.2014.08.034. URL: https://www.sciencedirect.com/science/article/pii/S0043135414006010 (visited on 01/27/2017).

Ramin, Elham et al. (2014b). "Modelling of secondary sedimentation under wet-weather and filamentous bulking conditions". PhD thesis. DTU Environment.

Ramkrishna, D (2000). *Population Balances: Theory and Applications to Particulate Systems in Engineering*. London, U.K.: Academic Press.

Rao, M. Anandha (2014). *Rheology of Fluid, Semisolid, and Solid Foods*. Food Engineering Series. Boston, MA: Springer US. ISBN: 978-1-4614-9229-0 978-1-4614-9230-6. DOI: 10.1007/978-1-4614-9230-6. URL: http://link.springer.com/10.1007/978-1-4614-9230-6 (visited on 10/18/2019).

Ratkovich, N. et al. (2013). "Activated sludge rheology: A critical review on data collection and modelling". In: *Water Research* 47.2, pp. 463–482. ISSN: 0043-1354. DOI: 10.1016/j.watres.2012.11.021. URL: https://www.sciencedirect.com/science/article/pii/S0043135412008330 (visited on 01/27/2017).

Sagnella, G.A. (1985). "Model fitting, parameter estimation, linear and non-linear regression". en. In: *Trends in Biochemical Sciences* 10.3, pp. 100–103. ISSN: 09680004. DOI: 10.1016/0968-0004(85)90261-0. URL: https://linkinghub.elsevier.com/retrieve/pii/0968000485902610 (visited on 09/07/2019).

Samstag, R. W. et al. (2016). "CFD for wastewater treatment: an overview". In: *Water Science and Technology* 74.3, pp. 549–563. ISSN: 0273-1223. DOI: 10.2166/wst.2016.249. URL: http://wst.iwaponline.com/content/74/3/549.

Samstag, Randal W. et al. (2012). "Field and CFD Analysis of Jet Aeration and Mixing". en. In: *Proceedings of the Water Environment Federation* 2012.12, pp. 4113–4139. ISSN: 19386478. DOI: 10.2175/193864712811708301. URL: http://openurl.ingenta.com/content/xref?genre=article&issn=1938-6478&volume=2012&issue=12&spage=4113 (visited on 10/09/2019).

Sari Erkan, Hanife, Nouha Bakaraki Turan, and Güleda Önkal Engin (2018). "Chapter Five - Membrane Bioreactors for Wastewater Treatment". In: *Comprehensive Analytical Chemistry*. Ed. by Dotse Selali Chormey et al. Vol. 81. Fundamentals of Quorum Sensing, Analytical Methods and Applications in Membrane Bioreactors. Elsevier, pp. 151–200. DOI: 10.1016/bs.coac.2018.02.002. URL: http://www.sciencedirect.com/science/article/pii/S0166526X18300035 (visited on 07/23/2019).

Smethurst, G (1992). *Basic Water Treatment for Application Worldwide*. Second. Thomas Telford.

Stamou, Anastasios and Anthoula Gkesouli (2015). "Modeling settling tanks for water treatment using computational fluid dynamics". In: pp. 745–762. DOI: 10.2166/hydro.2015.069.

Stricker, A.-E., I. Takács, and A. Marquot (2007). "Hindered and compression settling: parameter measurement and modelling". en. In: *Water Science & Technology* 56.12, p. 101. ISSN: 0273-1223. DOI: 10.2166/wst.2007.786. URL: http://wst.iwaponline.com/cgi/doi/10.2166/wst.2007.786 (visited on 10/31/2017).

Sweeney, Dennis J., Thomas A. Williams, and David R. Anderson (2019). *Statistics - Experimental design*. en. URL: https://www.britannica.com/science/statistics (visited on 04/30/2019).

Taebi-Harandy, Amir and Edward D. Schroeder (2000). "Formation of density currents in secondary clarifier". In: *Water Research* 34.4, pp. 1225–1232. ISSN: 0043-1354. DOI: 10.1016/S0043-1354(99)00261-4. URL: http://www.sciencedirect.com/science/article/pii/S0043135499002614 (visited on 07/31/2019).

Takács, I., G. G. Patry, and D. Nolasco (1991). "A dynamic model of the clarification-thickening process". In: *Water Research* 25.10, pp. 1263–1271. ISSN: 0043-1354. DOI: 10.1016/0043-1354(91)90066-Y. URL: http://www.sciencedirect.com/science/article/pii/004313549190066Y (visited on 04/23/2018).

Tamayol, A., B. Firoozabadi, and M. A. Ashjari (2010). "Hydrodynamics of Secondary Settling Tanks and Increasing Their Performance Using Baffles". en. In: *Journal of Environmental Engineering* 136.1, pp. 32–39. ISSN: 0733-9372, 1943-7870. DOI: 10.1061/(ASCE)EE.1943-7870.0000126. URL: http://ascelibrary.org/doi/10.1061/%28ASCE%29EE.1943-7870.0000126 (visited on 03/09/2019).

Tao, Junjie et al. (2012). "Composition of Waste Sludge from Municipal Wastewater Treatment Plant". In: *Procedia Environmental Sciences*. 2011 International Conference of Environmental Science and Engineering 12, pp. 964–971. ISSN: 1878-0296. DOI: 10.1016/j.proenv.2012.01.372. URL: http://www.sciencedirect.com/science/article/pii/S1878029612003738 (visited on 07/24/2019).

Tarpagkou, Roza and Asterios Pantokratoras (2013). "CFD methodology for sedimentation tanks: The effect of secondary phase on fluid phase using DPM coupled calculations". en. In: *Applied Mathematical Modelling* 37.5, pp. 3478–3494. ISSN: 0307904X. DOI: 10.1016/j.apm.2012.08.011. URL: https://linkinghub.elsevier.com/retrieve/pii/S0307904X12004672 (visited on 10/18/2019).

Tchobanoglous, G, F Burton, and D Stensel (2003). *Wastewater Engineering: Treatment and Resource*. 4th ed. Metcalf & Eddy, Inc. New York, N.Y.: McGraw-Hill.

Tebbutt, T. H. Y. (2001). *Fundamentos de control de la calidad del agua*. es. Google-Books-ID: q49iPAAACAAJ. Limusa. ISBN: 978-968-18-3317-6.

Thorne, P.D. and Hanes (2002). "A review of acoustic measurement of small-scalesediment processes." In: *Continental shelf research,* 22(4), pp. 603–632.

Torfs, E. et al. (2015a). "Impact on sludge inventory and control strategies using the benchmark simulation model no. 1 with the Bürger-Diehl settler model". eng. In: *Water Science and Technology: A Journal of the International Association on Water Pollution Research* 71.10, pp. 1524–1535. ISSN: 0273-1223. DOI: 10.2166/wst.2015.122.

Torfs, Elena et al. (2013). "Towards improved 1-D settler modelling: calibration of the Bürger model and case study". eng. In: URL: http://lup.lub.lu.se/record/4174878 (visited on 07/03/2019).

Torfs, Elena et al. (2015b). "Impact of the flocculation state on hindered and compression settling: experimental evidence and overview of available modelling frameworks". eng. In: *Systems Analysis and Integrated Assessment, 9th IWA Symposium, Papers*. Gold Coast, QLD, Australia: International Water Association (IWA), p. 4.

Torfs, Elena et al. (2016). "Concentration-driven models revisited: towards a unified framework to model settling tanks in water resource recovery facilities". en. In: *Water Science and Technology*, wst2016485. ISSN: 0273-1223, 1996-9732. DOI: 10.2166/wst.2016.485. URL: http://wst.iwaponline.com/content/early/2016/10/20/wst.2016.485 (visited on 01/27/2017).

Torfs, Elena et al. (2017). "On constitutive functions for hindered settling velocity in 1-D settler models: Selection of appropriate model structure". In: *Water Research* 110, pp. 38–47. ISSN: 0043-1354. DOI: 10.1016/j.watres.2016.11.067. URL: https://www.sciencedirect.com/science/article/pii/S0043135416309290 (visited on 01/27/2017).

Ueberl, Judith (1995). *Verbesserung der Absetzwirkung von Nachklärbecken*. Deutsch. Zurich.

Ungarish, Marius (1995). "Hydrodynamics of Suspensions." en. In: *Springer-Verlag* 290, pp. 406–408. ISSN: 1469-7645, 0022-1120. DOI: 10.1017/S0022112095212576. URL: https://www.cambridge.org/core/journals/journal-of-fluid-mechanics/article/hydrodynamics-of-suspensions-by-m-ungarish-springer-1993-322-pp-dm-138/A9CEDC1EA5F9554CD524C365C50DD4DC (visited on 10/12/2019).

Vahedi, Arman and Beata Gorczyca (2012). "Predicting the settling velocity of flocs formed in water treatment using multiple fractal dimensions". In: *Water Research* 46.13, pp. 4188–4194. ISSN: 0043-1354. DOI: 10.1016/j.watres.2012.04.031. URL: https://www.sciencedirect.com/science/article/pii/S0043135412002862 (visited on 01/27/2017).

– (2014). "Settling velocities of multifractal flocs formed in chemical coagulation process". en. In: *Water Research* 53, pp. 322–328. ISSN: 00431354. DOI: 10.1016/j.watres.2014.01.008. URL: https://linkinghub.elsevier.com/retrieve/pii/S004313541400030X (visited on 10/14/2019).

Valle Medina, M.E. and J. Laurent (2020). "Incorporation of a compression term in a CFD model based on the mixture approach to simulate activated sludge sedimentation". en. In: *Applied Mathematical Modelling* 77, pp. 848–860. ISSN: 0307904X. DOI: 10.1016/j.apm.2019.08.008. URL: https://linkinghub.elsevier.com/retrieve/pii/S0307904X19304962 (visited on 10/07/2019).

Van Marle, C. and C. Kranenburg (1994). "Effects of Gravity Currents in Circular Secondary Clarifiers". en. In: *Journal of Environmental Engineering* 120.4, pp. 943–960. ISSN: 0733-9372, 1943-7870. DOI: 10.1061/(ASCE)0733-9372(1994)120:4(943). URL: http://ascelibrary.org/doi/10.1061/%28ASCE%290733-9372%281994%29120%3A4%28943%29 (visited on 08/01/2019).

Vanderhasselt, A. et al. (1999). *Sludge Settling Characterisation With An Automated Settlometer*.

180

Verloop, W. C. (1995). "The inertial coupling force". In: *International Journal of Multiphase Flow* 21.5, pp. 929 –933. ISSN: 0301-9322. DOI: https://doi.org/10.1016/0301-9322(95)00029-W. URL: http://www.sciencedirect.com/science/article/pii/030193229500029W.

Versteeg, H.K. and W. Malalasekera (2007). *An Introduction to Computational Fluid Dynamics: The Finite Volume Approach*. Longman Scientific & Technical. ISBN: 978-0-582-21884-0. URL: https://books.google.fr/books?id=7UynjgEACAAJ.

Vesilind, P. A. (1968). "Theoretical considerations: Design of prototype thickeners from batch settling tests." In: *Water & Sewage Works*, pp. 115–302.

Von Sperling, Marcos (2007). *Activated sludge and aerobic biofilm reactors*. en. Biological wastewater treatment series Marcos von Sperling ; Vol. 5. OCLC: 255801712. London: IWA Publ. ISBN: 978-1-84339-165-4.

Voutchkov, Nikolay (2005). *Settling Tank Design – Let's settle the matter*. en. 10.1002/047147844X.mw506. URL: https://www.researchgate.net/publication/284774604_The_activated_sludge_process_Part_1_-_Steady_state_behaviour (visited on 07/23/2019).

Weiss, Michael et al. (2007). "Suction-lift sludge removal and non-Newtonian flow behaviour in circular secondary clarifiers: Numerical modelling and measurements". In: *Chemical Engineering Journal* 132.1–3, pp. 241–255. ISSN: 1385-8947. DOI: 10.1016/j.cej.2007.01.004. URL: https://www.sciencedirect.com/science/article/pii/S1385894707000101 (visited on 01/27/2017).

Wells, Scott A. and David M. LaLiberte (1998). "Winter temperature gradients in circular clarifiers". en. In: *Water Environment Research* 70.7, pp. 1274–1279. ISSN: 10614303. DOI: 10.2175/106143098X123642. URL: http://doi.wiley.com/10.2175/106143098X123642 (visited on 08/01/2019).

Wicklein, Edward et al. (2015). "Good modelling practice in applying computational fluid dynamics for WWTP modelling". en. In: *Water Science and Technology*, wst2015565. ISSN: 0273-1223, 1996-9732. DOI: 10.2166/wst.2015.565. URL: https://iwaponline.com/wst/article/73/5/969-982/18977 (visited on 10/09/2019).

Wicklein, Edward A. and Randal W. Samstag (2009). "Comparing Commercial and Transport CFD Models for Secondary Sedimentation". en. In: *Proceedings of the Water Environment Federation* 2009.10, pp. 6066–6081. ISSN: 1938-6478. DOI: 10.2175/193864709793952765. URL: http://www.ingentaconnect.com/content/10.2175/193864709793952765 (visited on 10/09/2019).

Wilson, T.E. (1996). "A new approach to interpreting settling data." In: *Proceeding of the 69th Annual WEF Conference and Exposition*. WEF Alexandria, Virginia 1, pp. 491–497.

Xanthos, S. et al. (2013). "Implementation of CFD modeling in the performance assessment and optimization of secondary clarifiers: the PVSC case study". en. In: *Water Science & Technology* 68.9, p. 1901. ISSN: 0273-1223. DOI: 10.2166/wst.2013.280. URL: http://wst.iwaponline.com/cgi/doi/10.2166/wst.2013.280 (visited on 07/25/2017).

Xanthos, Savvas et al. (2011). "Performance Assessment of Secondary Settling Tanks Using CFD Modeling". en. In: *Water Resources Management* 25.4, pp. 1169–1182. ISSN: 0920-4741, 1573-1650. DOI: 10.1007/s11269-010-9620-1. URL: http://link.springer.com/article/10.1007/s11269-010-9620-1 (visited on 01/27/2017).

Xie, Hao et al. (2014). "Simulation of flow field and sludge settling in a full-scale oxidation ditch by using a two-phase flow CFD model". In: *Chemical Engineering Science* 109, pp. 296–305.

Xu, Shuang et al. (2018). "Analysis of Bacterial Community Structure of Activated Sludge from Wastewater Treatment Plants in Winter". In: *BioMed Research International* 2018. ISSN: 2314-6133. DOI: 10.1155/2018/8278970. URL: https://www.ncbi.nlm.nih.gov/pmc/articles/PMC5863335/ (visited on 07/24/2019).

Yang, Fei et al. (2009). "Yield stress and rheological characteristics of activated sludge in an airlift membrane bioreactor". English. In: *Journal of Membrane Science* 334.1-2, pp. 83–90. DOI: 10.1016/j.memsci.2009.02.022.

Zhang, Daijun et al. (2006). "A method for characterizing the complete settling process of activated sludge". In: *Water Research* 40.14, pp. 2637–2644. ISSN: 0043-1354. DOI: 10.1016/j.watres.2006.05.017. URL: https://www.sciencedirect.com/science/article/pii/S0043135406003034 (visited on 01/27/2017).

Zhiyin, Yang (2015). "Large-eddy simulation: Past, present and the future". In: *Chinese Journal of Aeronautics* 28.1, pp. 11–24. ISSN: 1000-9361. DOI: 10.1016/j.cja.2014.12.007. URL: https://www.sciencedirect.com/science/article/pii/S1000936114002064 (visited on 01/27/2017).

Zhou, Siping, J. A. McCorquodale, and A. M. Godo (1994). "Short Circuiting and Density Interface in Primary Clarifiers". en. In: *Journal of Hydraulic Engineering* 120.9, pp. 1060–1080. ISSN: 0733-9429, 1943-7900. DOI: 10.1061/(ASCE)0733-9429(1994)120:9(1060). URL: http://ascelibrary.org/doi/10.1061/%28ASCE%290733-9429%281994%29120%3A9%281060%29 (visited on 08/01/2019).

Zhou, Siping, J. A. McCorquodale, and Z. Vitasovic (1992). "Influences of Density on Circular Clarifiers with Baffles". en. In: *Journal of Environmental Engineering* 118.6, pp. 829–847. ISSN: 0733-9372, 1943-7870. DOI: 10.1061/(ASCE)0733-9372(1992)118:6(829). URL: http://ascelibrary.org/doi/10.1061/%28ASCE%290733-9372%281992%29118%3A6%28829%29 (visited on 10/09/2019).

Zhou, Siping and John A. McCorquodale (1992). "Influence of skirt radius on performance of circular clarifier with density stratification". en. In: *International Journal for Numerical Methods in Fluids* 14.8, pp. 919–934. ISSN: 0271-2091, 1097-0363. DOI: 10.1002/fld.1650140804. URL: http://doi.wiley.com/10.1002/fld.1650140804 (visited on 10/09/2019).

María Elena VALLE MEDINA

Modélisation des décanteurs secondaires : Etude en mécanique des fluides numériques de la dynamique de la sédimentation des boues activées

Résumé

Le procédé à boues activées conventionnel est le plus utilisé pour traiter les eaux usées urbaines. La biomasse (boues activées) croît et forme des flocs biologiques qui doivent être séparés de l'eau traitée. Cette opération s'effectue généralement par gravité dans un clarificateur. Les particules de boues activées sont sujettes à différents comportements de décantation, selon leurs propriétés. La simulation des clarificateurs est probablement le domaine d'application le plus développé de la mécanique des fluides numérique appliquée au traitement des eaux usées. Cependant, l'ensemble des mécanismes de sédimentation ne sont pas toujours représentés de manière complète. Le présent travail a consisté dans un premier temps en l'ajout du mécanisme de compression en tant que terme de second ordre dans l'équation différentielle aux dérivées partielles décrivant la sédimentation de la boue. Les paramètres du modèle ainsi modifié ont fait l'objet d'une identification basée sur des données expérimentales acquises en système fermé. Ensuite, des simulations d'un clarificateur à taille réelle ont permis de valider le modèle sur la base des hauteurs de voiles de boues mesurées et des profils de vitesse des particules. Les petites installations de traitement sont caractérisées par des conditions d'entrée très dynamiques (variations de débits, cycles de marche/arrêt). Ainsi, le modèle validé a été utilisé pour simuler ces conditions particulières de fonctionnement.

MOTS-CLÉ : Décanteurs secondaires, Mécanique des Fluides Numérique, Compression, Comportement dynamique des décanteurs, vitesse de sédimentation des particules, OpenFOAM, DAKOTA.

Abstract

The conventional activated sludge process is the most widely used process for treating urban wastewater. Biomass (activated sludge) grows and forms biological flocs that must be separated from the treated water. This is usually performed by gravity in a clarifier. Activated sludge particles are subject to different settling processes, depending on their properties. Clarifier simulation is probably the most developed field of application for computational fluid dynamics applied to wastewater treatment. However, all sedimentation mechanisms are not always fully represented. This work began by adding the compression mechanism as a second-order term in the partial differential equation describing sludge sedimentation. The parameters of the modified model were identified based on experimental data from a closed system. Then, simulations of a full-scale clarifier allowed the model to be validated based on the measured sludge blanket height and particle velocity profiles. Small treatment plants are characterized by very dynamic inlet conditions (flow variations, on/off cycles). Thus, the validated model was used to simulate these operating conditions.

KEY WORDS: Secondary clarifiers, Computational Fluids Dynamics, Compression, Dynamic behavior of clarifiers, small WRRF, particle settling velocity, OpenFOAM, DAKOTA

Resumen

El proceso de lodos activados convencional para el tratamiento del agua residual es el más usado para remover los contaminantes del agua residual urbana. La biomasa (lodo activado) crece y forma flocs biológicos que deben ser separados del agua tratada. Normalmente esta acción se realiza por medio de la gravedad en un sedimentador. Las partículas de lodo activado pueden someterse a diferentes comportamientos de sedimentación dependiendo de sus propiedades. La simulación de los clarificadores secundarios es probablemente el área más desarrollada para la aplicación de la mecánica de fluidos computacional en el tratamiento del agua residual. Sin embargo, no todos los mecanismos de sedimentación están siempre representados en un modelo. Este trabajo presenta la adición de la compresión como un término de segundo orden en una ecuación diferencial parcial que describe la sedimentación del lodo. La identificación de los parámetros del modelo se realizó a través de experimentos realizados en un sistema cerrado. Luego, simulaciones en un clarificador a escala real permitieron validar el modelo basándose en la medición de la altura del manto de lodos y los perfiles de velocidad de las partículas. Estaciones depurados de pequeña capacidad se caracterizan por una dinámica discontinua de las condiciones de entrada (variaciones en el caudal, ciclos de encendido/apagado). Así el modelo validado se usó para simular estas condiciones operacionales.

PALABRAS CLAVE: Sedimentadores secundarios, Mecánica de fluidos computacional, Compresión, Comportamiento dinámico de sedimentadores, velocidad de sedimentación de partículas, OpenFOAM, DAKOTA.